Strategies For Increasing Frataxin Expression in Friedreich's Ataxia: Modulation of the Epigenome and Proteome

Robert Quinlan
Jesus College
University of Oxford
Trinity Term 2021

A Thesis Submitted in Partial Fulfilment of the Requirements of the Degree of Doctor of Philosophy

ABSTRACT

Friedreich's ataxia is a rare and fatal childhood neurodegenerative disease that causes shrinkage of the spinocerebellar tracts and the progressive loss of neurons in the dorsal root ganglia. This leads to awkward, unsteady movements and impaired sensory function, leaving sufferers wheelchair bound. It is caused by the expansion of a trinucleotide repeat region within the first intron of the *FXN* gene, leading to reduced production of the essential mitochondrial protein frataxin. The average life expectancy of sufferers is 37 years old, and there is currently no available treatment.

Reduced frataxin production is thought to be the result of a host of epigenetic changes at the *FXN* locus that cause heterochromatin-induced gene silencing. Recently, the histone lysine methyltransferase SUV4-20 has been implicated in heterochromatin formation. Pharmacological inhibition with SUV4-20 chemical probe **A-196** leads to an increase in frataxin production, however its substantial metabolic instability precludes its use *in vivo*. This thesis describes attempts to design and synthesise analogues of **A-196** with improved metabolic stability, enabling their testing in animal disease models and continued preclinical development. It also examines the development of a novel approach to disease treatment through the use of a heterobifunctional molecule to induce frataxin stabilisation.

Chapter 1 evaluates the challenges facing drug discoverers in the context of rare disease treatment and provides an overview of Friedreich's ataxia. It also examines key pharmacokinetic concepts and strategies for their modulation. Chapter 2 describes the design and synthesis of analogues of **A-196**, culminating in the development of a compound with a nine-fold improvement in stability that will permit its evaluation *in vivo*. Chapter 3 describes the conceptualisation and efforts towards the development of a novel, heterobifunctional small molecule for induced frataxin stabilisation via deubiquitination.

ACKNOWLEDGEMENTS

I would initially like to say thank you to all the colleagues and collaborators I have worked with over the past couple of years. First and foremost, Gabriela, whose dedication and hard work has been key to the success of the project. Alongside her, the help of Professor Richard Wade-Martins, Professor Masoud Vedadi, Dr Fengling Li, Saumya Maheshwari, Ewa Wieczorek, and Roberta Mazzone has been invaluable. I'd also like to thank Amber Truepenny and Professor Benedikt Kessler for all their hard work and support.

I have been lucky enough to have been helped along my journey to Oxford and the DPhil by some excellent mentors. I'd like to say thank you to Professor Guy Lloyd-Jones, Professor Ben Davis, and Professor Jim Naismith for their inspiration and guidance, but most importantly to Dr Nicolas Blanchard, whose kindness and support had the most profound impact on me during my time in France, and without which I definitely would not have pursued a DPhil. Merci Nico!

My friends from home and from Edinburgh have been an incalculable source of joy throughout my time in Oxford. I've sometimes found it difficult being so removed (at least geographically) from your lives, but you've never made me feel excluded and I've loved always being able to drop in on you at a moment's notice. So, to Lyall, Mansfield, Baxter, RDB, Russell, Mike, Cammy, Kenny, Ed, Hanks, Cheese, Webby, Baz, Fala, Fi, Alex, Emily, Cat, Ellie, and Jess, thanks so much for everything over the years and here's to many more great memories.

A DPhil can at times feel somewhat lonely and isolating, but throughout my time I have been surrounded by a group of excellent friends and role models within the Brennan Group. In no particular order, I'd like to say thank you to Mark McLaughlin, Vinnie Fagan, Stephane de Cesco, Carmen Jimenez Antunez, Josh Almond-Thynne, Katherine England, Anna Cederbalk, Thomas Grimes, Andrew Thompson, Laura Ortega-Varga, Alice di Pasquale, Janine Gray, Milan Fowkes, Mia Callens, Amber Truepenny, Yining Yang, Loane Serrano and Kathryn Pugh. It's been an honour

to work alongside you all and I look forward to remaining firm friends in the future. I'd like to single out Gian-Filippo Ruda, Tamas Szommer, Saleta Vazquez-Rodriguez, Raina Seupel, Tryfon Zarganis-Tzitzikas, Moses Moustakim, and Miranda Wright, in order to say thank you for all your guidance, support, and friendship throughout my DPhil. I undoubtedly would not have reached this point without you all and I hope this goes some way to show the immense amount of respect, admiration, and gratitude I feel for you all.

More broadly, I'd like to thank some of the people with whom I have shared the NDMRB over the past few years and who have made it a great environment to work in. In no particular order, Andrew Lewis, Jenny Ward, James Bennett, Franziska Guenther, Chris Dodd, Ross Macrae, Darren Blase, and Omar Rivas Rosiles. I would also like to thank the Synthesis for Biology and Medicine CDT and partners for all their support, in particular Dr Lara Lourenço Venda, Dr Maitane Fernandez Chento, and Laura Thomas for all their hard work and support during my time in Oxford. I would also like to thank Jesus College for all the wonderful experiences over the past few years.

Outside of the lab I have met some truly remarkable people during my time at Oxford, and the length of a DPhil seems far too short a time to spend amongst such a group. To list you all would likely take the same length as the thesis itself, so suffice to say I hope to be able to tell you in person one day. There are some people I must mention however: firstly Ronan, one of my oldest friends here whose generosity of spirit has shaped my time in the city. I'm looking forward to when we finally master the art of cigar smoking. To Maurice, what is there to say? I could only hope to aspire to your levels of humour, kindness, and intelligence. Thanks for everything and I hope our friendship lasts for years to come, not least because of the amount of incriminating evidence you have which could derail any future career of mine. To Seb, Stilo, Poz, Jacko, GWarr, CK, Aaron, and Cal, you've quite literally run me into the ground, but have been wonderful friends and given me some of my fondest memories. Long may it continue! To Fez, thanks for your

unfailing sunny disposition and always being on hand to give me some much needed perspective. To Oli, Marral, and Hamish, although I initially resented you for making me trek to St Anthony's, I'm so glad you did because it was the beginning of a wonderful friendship. I'm looking forward to catching up properly once we're all back together. To Shobhan, thanks for putting up with my thesis writing neuroses and always being on hand for a coffee (or tea). Hopefully I can repay you I kind when you get to the same stage. Duncan, I'm so glad you came to Oxford, and even gladder you moved into the building next door! I do have some issues with the fact your research is far cooler than mine but I'm willing to overlook that. Thanks for all the lunches and keeping me up to date with the latest gossip. To Jamie, I'm glad our shared love of pizza brought us together and thanks for roughing it through lockdown with me – I'll forever cherish the memory of Top Chef. To Audi, I'm glad the allure of London was too much for you to resist because you've been an amazing friend these past few years and I think I'd be a bit lost if you headed back stateside. Looking forward to sipping a white claw or two with you in the big smoke. To Humbo, having you to share the highs and lows of the DPhil/Oxford experience with has been invaluable and I can't thank you enough for your support, insight, and friendship throughout. If I can offer you a fraction of the same when you come to write-up then you'll breeze through, although you're an incredibly tough act to follow! To Dylan, we've come a long way from you being mean to me at preseason but I'm so glad we have. It's rare to meet someone as generous as you, much less get to be in their company for as long as I've had the pleasure of yours. Thanks for everything and I'm looking forward to the next steps! Tress, even though you jumped ship halfway through to follow the money, the time you were here was truly special. You've been an unfailing friend and confidant through some of my toughest times at Oxford, and I've been lucky enough to spend some of my best times with you as well. Thanks for all the laughs, dancing, support, advice, and song recommendations. I'll see you on the RnB floor. Finally, to Lucy: you've had to bear as much of my stress around the DPhil as anyone and you've been an absolute superstar throughout. If I had

a fraction of your ability and intelligence, then that stress would have been much lessened! Truly, thank you for everything you are and everything you do. How lucky I am to have been able to spend this time with someone as special as you.

My family have always shown me the most incredible amount of love, support, and encouragement. They have been my biggest cheerleaders throughout my life, and particularly during my DPhil. I can't really express how much this has meant, nor how much it has helped me throughout my time. To Jac, Michelle, and Robin, thank you for everything and for how much joy you bring to all our lives. In particular, thank you to Michelle for the visits and support with my research, which have made all the difference. I hope I've done Barry proud! To Shaun, thanks for the fascinating discussions, the knowledge shared, and all the support and encouragement around sport and everything else. It means a lot! To the Cousins, Katherine, Tom, Joe, Luke, Sophie, Craig, Alex, Ali, and Greg: it would be rare to find such a wonderful group of people anywhere in the world, let alone all in one family. I hope you know just how much you all inspire me and how much you mean to me. To James and Caitlin, you have both carved out such impressive paths that I feel wholly inadequate sitting between you. Thank you for not just being great siblings but also great friends; I love you both dearly and hopefully this means we can now put the tennis court incident behind us. To Rachel, it's been such a joy welcoming you to the family and I've loved being able to share some of Oxford with you. Thank you to you and James for bringing the overwhelming joy that is Lydia into our lives. Finally, I'd like to thank my grandparents, who sadly won't get to read this but who have shaped me into the person I am today. I hope I've made you proud.

Perhaps the person who has had the most profound impact on me at Oxford has been my supervisor, Paul. Very few of the experiences I've had or friends I've made at Oxford would have been possible without his encouragement to enjoy everything that life at the University has to offer. As a mentor, he has always supported independent, creative thought and the pursuit of the

ideas that result. Alongside this, he has fostered an environment within the research group that enables everyone to flourish and feel empowered to reach their potential. Finally, his humility belies an intelligence makes him an incredible teacher from whom I have learned an enormous amount. I have done my best to secure him a coveted College fellowship by introducing him to various bigwigs, but when the time comes to schmooze them, he is inevitably speaking to a young postgraduate student about their research, which I think is a testament to his dedication to his students. His generosity knows no bounds, extending from offering opportunities within academia and industry, to fixing my bike in his back room. In my experience, supervisors like Paul are incredible rare and it's difficult to truly sum up the impact he has had on me and countless others, so suffice to say thank you for everything and I hope to repay you one day.

Finally, I would like to say thank you to my parents. This thesis is as much yours to claim as it is mine, and I would like to dedicate it to you both as thanks for the limitless love, support, and encouragement you have shown me throughout my life. You have always empowered and enabled me to pursue my own interests with no conditions or pressures, providing nothing but comfort and guidance through difficult times, and always celebrating and delighting in my successes. Mum, you will sometimes quote a line from a notorious Philip Larkin poem about parenting, the irony being that both you and Dad are complete exceptions to it. I have been incredibly lucky to have been so completely loved by such wonderful people as you both, and I hope to have made you proud, although you always ensure that I already know you are. As I move onto the next stage of my life, I don't feel daunted but excited, and safe in the knowledge that you have gifted me all the tools I need to succeed. Thank you for everything.

DECLARATION

The work described in this thesis is entirely my own except:

Figure 1.12: German translation was carried out with the aid of Lucy Burgin, University of Oxford.

Table 2.1: Microsomal stability assays were carried out by Cyprotex.

Figure 2.1: Metabolite identification studies were carried out by Sygnature Discovery.

Table 2.2: IC_{50} determinations were carried out by Dr Fengling Li and Professor Masoud Vedadi of the University of Toronto.

Table 2.3: IC_{50} determinations were carried out by Dr Fengling Li and Professor Masoud Vedadi of the University of Toronto. Compounds **23**, **24**, and **25** were synthesised with the aid of Roberta Mazzone (University of Oxford) as part of a supervised internship.

Table 2.4: IC_{50} determinations were carried out by Dr Fengling Li and Professor Masoud Vedadi of the University of Toronto.

Table 2.5: IC_{50} determinations were carried out by Dr Fengling Li and Professor Masoud Vedadi of the University of Toronto. Compounds **50** and **53** were synthesised with the aid of Ewa Wieczorek (University of Oxford) as part of a supervised internship.

Table 2.6: IC_{50} determinations were carried out by Dr Fengling Li and Professor Masoud Vedadi of the University of Toronto.

Table 2.7: IC_{50} determinations were carried out by Dr Fengling Li and Professor Masoud Vedadi of the University of Toronto.

Table 2.8: IC_{50} determinations were carried out by Dr Fengling Li and Professor Masoud Vedadi of the University of Toronto.

Figure 2.10: Frataxin-luciferase expression assays were carried out by Dr Gabriela Vilema-Enriquez and Saumya Maheshwari of the Department of Physiology, Anatomy, and Genetics, University of Oxford.

Figure 2.11 Frataxin-luciferase expression assays were carried out by Dr Gabriela Vilema-Enriquez and Saumya Maheshwari of the Department of Physiology, Anatomy, and Genetics, University of Oxford.

Figure 2.12: Frataxin-luciferase expression assays were carried out by Dr Gabriela Vilema-Enriquez and Saumya Maheshwari of the Department of Physiology, Anatomy, and Genetics, University of Oxford.

Figure 2.13: Frataxin-luciferase expression dose-response assays were carried out by Dr Gabriela Vilema-Enriquez and Saumya Maheshwari of the Department of Physiology, Anatomy, and Genetics, University of Oxford.

Figure 2.14: Frataxin-luciferase expression assays were carried out by Dr Gabriela Vilema-Enriquez and Saumya Maheshwari of the Department of Physiology, Anatomy, and Genetics, University of Oxford.

Table 2.9: Hepatocyte stability assays were carried out by Sygnature Discovery.

Table 2.10: *In vivo* PK assessment was carried out by Pharmidex Pharmaceutical Services Ltd.

Table 2.11: CNS MPO scores were calculated with the aid of Tamas Szommer at the Target Discovery Institute, University of Oxford.

Figure 3.1: The premise of a DUBTAC was conceived by the author alongside Dr Moses Moustakim and Amber Truepenny (University of Oxford).

Table 3.1: BLI experiments were carried out by the author with the aid of Dr James Bennett, Dr Franziska Guenther, and Amber Truepenny at the Target Discovery Institute, University of Oxford.

Table 3.2: BLI experiments were carried out by the author with the aid of Dr James Bennett, Dr Franziska Guenther, and Amber Truepenny at the Target Discovery Institute, University of Oxford.

Supplementary Table 2.1: Microsomal stability assays were carried out by Cyprotex.

Supplementary Table 2.1: Hepatocyte stability assays were carried out by Sygnature Discovery.

Supplementary Figure 2.1: *In vivo* PK assessment was carried out by Pharmidex Pharmaceutical Services Ltd.

Supplementary Figure 3.1: BLI experiments were carried out by the author with the aid of Dr James Bennett, Dr Franziska Guenther, and Amber Truepenny at the Target Discovery Institute, University of Oxford.

Supplementary Figure 3.2: BLI experiments were carried out by the author with the aid of Dr James Bennett, Dr Franziska Guenther, and Amber Truepenny at the Target Discovery Institute, University of Oxford.

Supplementary Figure 3.3: BLI experiments were carried out by the author with the aid of Dr James Bennett, Dr Franziska Guenther, and Amber Truepenny at the Target Discovery Institute, University of Oxford.

I confirm that appropriate credit has been given within the thesis where reference has been made to the work of others.

Robert Quinlan

University of Oxford, Trinity Term 2021.

TABLE OF CONTENTS

LIST OF FIGURES

LIST OF SCHEMES

LIST OF TABLES

LIST OF EQUATIONS

LIST OF ABBREVIATIONS

AB	Apical to basolateral
Ac	Acetyl
AceTAG	Acetylation tagging system
AD	Alzheimer's disease
ADME	Absorption, distribution, metabolism, and excretion
ADP	Adenine dinucleotide phosphate
ANOVA	Analysis of Variance
AO	Aldehyde oxidase
ASO	Antisense oligonucleotide
AUC_{last}	Area under the plasma concentration-time curve from time zero to the time of the last measurable concentration
AUTAC	Autophagy targeting chimera
BA	Basolateral to apical
BAG3	BCL2-associated athanogene 3
BBB	Blood Brain Barrier
BCL2	B-cell lymphoma 2
BD	Bromodomain
BET	Bromodomain and Extra Terminal
BLI	Biolayer interferometry
Boc	*tert*-Butyloxycarbonyl
BRD4	Bromodomain containing protein 4
$C_{ss,av,u}$	Steady state unbound concentration
C_{max}	Maximum plasma concentration
cAMP	Cyclic adenosine monophosphate
CB1/CB2	Cannabinoid receptor type 1 and 2

CBP	cAMP responsive element binding (CREB) protein
CFTR	Cystic fibrosis transmembrane regulator
CIV	Continuous intravenous
CL	Clearance
$CL_{int,u}$	Intrinsic clearance independent of blood flow or drug binding
clogD	Calculated pH-dependent distribution constant
clogP	Calculated octanol-water partition coefficient
CNS	Central nervous system
CREB	cAMP responsive element binding
CRISPR	Clustered regularly interspersed short palindromic repeats
CYLD	Cylindromatosis
CYP	Cytochrome P450
CYP2C	Cytochrome P450 2C
CYP2D	Cytochrome P450 2D
CYP3A4	Cytochrome P450 3A4
CV	Coefficient of variation
DAST	Diethylaminosulfur trifluoride
DCM	Dichloromethane
DIC	*N-N'*-diisopropylcarbodiimide
DIPEA	Diisopropylethylamine
DMSO	Dimethylsulfoxide
DNA	Deoxyribonucleic acid
DNMT	DNA methyltransferase
DORA	Dual orexin receptor antagonist
DOT1L	Disruptor of telomeric silencing 1-like
DPP	Dipeptidyl peptidase

dsRNA	Double stranded RNA
DUB	Deubiquitinase
DUBTAC	Deubiquitinase targeting chimera
EC_{50}	Half-maximal effective concentration
enDUB	Engineered deubiquitinase
EZH2	Enhancer of zeste homologue 2
F_a	Fraction absorbed
F_g	Fraction escaping gut wall extraction
FARS	Friedreich's Ataxia Rating Scale
FDA	Food and Drug Administration
Fmoc	Fluorenylmethyloxycarbonyl
FRDA	Friedreich's ataxia
fu	Fraction unbound
fu_p	Fraction unbound in plasma
fu_t	Fraction unbound in tissues
GeneTAC	Gene targeting chimera
GFR	Glomerular filtration rate
GI	Gastrointestinal
GLP1	Glucagon-like peptide 1
GMP	Guanosine monophosphate
GMPS	GMP-synthetase
GPCR	G-protein coupled receptor
GWAS	Genome wide association studies
H3K4	Lysine 4 on histone 3
H3K9	Lysine 9 on histone 3
H3K27	Lysine 27 on histone 3

H3K36	Lysine 36 on histone 3
H3K79	Lysine 79 on histone 3
H4K20	Lysine 20 on histone 4
HAT	Histone acetyltransferase
HBD	Hydrogen bond donor
HDAC	Histone deacetylase
HDACi	Histone deacetylase inhibitor
HDR	Homology directed repair
hERG	Human ether-à-go-go related gene
HEK293	Human embryonic kidney 293
HER2	Human epidermal growth factor 2
HLM	Human liver microsomes
HOBt	Hydroxybenzotriazole
HSV-1	Herpes simplex virus type-1
HTS	High throughput screen
IC_{50}	Half-maximal inhibitory concentration
ICP0	Infected cell protein 0
iPSC	Induced pluripotent stem cell
ISCU	Iron-sulfur cluster assembly
ITC	Isothermal titration calorimetry
JAMM	JAB1, MPN, MOV34 metalloenzymes
JMJD3	Jumonji domain-containing protein D3
k_a	Rate of absorption
k_m	Rate of movement away from site of absorption
KDM	Lysine demethylase
Keap1	Kelch-like ECH-associated protein 1

KMT	Lysine methyltransferase
KMT1A/B	Lysine methyltransferase 1A/B
KMT1C	Lysine methyltransferase 1C
logD	pH-dependent distribution constant
logP	Octanol-water partition coefficient
Luc	Luciferase
LYTAC	Lysosome targeting chimera
Me1	Monomethyl
Me2	Dimethyl
Me3	Trimethyl
Met	Methionine
MetAP-2	Methionine aminopeptidase-2
MDM2	Mouse double minute 2 homologue
MINDY	Motif-interacting with ubiquitin-containing novel DUB family
MLL	Mixed lineage leukaemia
MLM	Mouse liver microsomes
MPO	Multiparameter optimisation
mRNA	Messenger RNA
MTS	Mitochondrial targeting sequence
MW	Molecular weight
NAD	Nicotinamide adenine dinucleotide
NDA	New Drug Application
NF-κB	Nuclear factor-κB
NHEJ	Non-homologous end joining
Nrf2	Nuclear factor (erythroid-derived 2)-like 2
ODA	Orphan Drug Act

OTUB1	OTU Domain-containing ubiquitin aldehyde-binding protein 1
OUT	Ovarian tumour proteases
OX_1R	Orexin receptor-1
OX_2R	Orexin receptor-2
p27	Tumour protein p27
p53	Tumour protein p53
PAH	Phenylalanine hydroxylase
PB1	Polybromo Protein-1
pBac	Baculovirus transfer plasmid
PBMCs	Peripheral blood mononuclear cells
PC-3	Prostate cancer cell line
PD	Pharmacodynamic
PEG	Polyethylene glycol
PEV	Position-effect variegation
P-gp	Permeability glycoprotein
PHD	Plant homeodomain
Phe	Phenylalanine
PK	Pharmacokinetic
PO	Oral administration (Per Os)
POI	Protein of interest
PPB	Plasma protein binding
PPI	Protein-protein interaction
PhoRC	Phosphatase recruiting chimera
PHOTAC	Photochemically targeting chimera
PROTAC	Proteolysis targeting chimera
PRC2	Polycomb repressive complex 2

PRMT	Protein arginine methyltransferase
PR-SET7	PR/SET-domain containing protein 7
PSA	Polar surface area
p-TEFb	Positive transcription elongation factor b
PTM	Post-translational modification
Q_H	Hepatic blood flow
RIBOTACS	Ribonuclease targeting chimeras
RING	Really interesting new gene
RNA	Ribonucleic acid
RNAi	RNA inhibition
RNF126	RING finger protein 126
ROS	Reactive oxygen species
RT	Room temperature
SAM	*S*-adenosylmethionine
SAR	Structure-activity relationship
SC	Subcutaneous
SCF	Skp1-Cullin-F box complex containing Hrt1
SE	Standard error
SEM	Standard error of mean
Ser	Serine
SET	Suppressor of variegation 3-9, Enhancer of zeste, and Trithorax
SGC	Structural Genomics Consortium
siRNA	Small interfering RNA
SLC	Solute carrier
Smad7	Mothers against decapentaplegic homologue 7

SMYD2	SET (Suppressor of variegation, Enhancer of Zeste, Trithorax) and MYND (Myeloid-Nervy-DEAF1) domain-containing protein 2
S_NAr	Nucleophilic aromatic substitution
SPA	Scintillation proximity assay
SPPS	Solid-phase peptide synthesis
SUV4-20H1	Suppressor of variegation 4-20 homologue 1
SUV4-20H2	Suppressor of variegation 4-20 homologue 2
Syn-TEF	Synthetic transcription elongation factor
$t_{1/2}$	Half-life
TAT	Trans-activator of transcription
TET	Ten-eleven translocation
TGF-β	Transforming growth factor-β
THF	Tetrahydrofuran
TPP	Target product profile
tPSA	Topological polar surface area
TRAF	Tumour necrosis factor receptor–associated factor
Trp	Tryptophan
U2OS	Human bone osteosarcoma epithelial cells
UBL	Ubiquitin-like domain
UCH	Ubiquitin carboxy-terminal hydrolase
UPS	Ubiquitin-proteasome system
US	United States
USP	Ubiquitin-specific peptidase
USP7	Ubiquitin-specific peptidase 7
V_p	Physiological volume of plasma
V_{ss}	Volume of distribution at steady state

$V_{ss,u}$	Volume of distribution at steady state corrected for fraction unbound in plasma
V_t	Physiological volume of tissues
YFP	Yellow fluorescent protein

1 INTRODUCTION

1.1 SELDOM SILENT, NEVER HEARD – THE ORPHAN DRUG ACT OF 1983

Jack Klugman may be better remembered as Dr R. Quincy, the crack medical examiner that graced television screens in *Quincy, M. E.* in the late 1970s and early '80s.[1] Perhaps lesser known is the role he played in passing a piece of legislation that has transformed the landscape of drug development and disease treatment since its inception.[2] During the '70s, patient groups had been lobbying members of the US Congress to take notice of the plight of people suffering from rare diseases that had no available treatments, such as Huntington's disease.[3] These efforts compelled the then Senator for Massachusetts, Edward Kennedy, to introduce a measure in his Drug Regulation Reform bill of 1978 to establish a National Centre for Clinical Pharmacology that would, amongst other things, attempt to research and develop "drugs of limited commercial value".[3]

The bill failed twice, once in 1978 and again in 1979, however prompted the Food and Drug Administration (FDA) to set up an Interagency Task Force that commissioned a report examining the experience of people suffering from these rare diseases.[3,4] The report, entitled "Significant Drugs of Limited Commercial Value",[5] described a situation whereby patients suffering from uncommon but serious diseases did not have access to treatment because drugs developed for these disorders would be limited in their applicability and thus represented a poor return on investment for pharmaceutical companies. The report recommended that the FDA offer economic incentives, such as grants and financial support for clinical trials, to research institutions and pharmaceutical companies to encourage the development of drugs for these disorders.[5]

The recommendations were picked up by Elizabeth Holtzman, member of Congress for New York's 16th congressional district, at the request of researchers and patients at Mount Sinai Hospital who had been trying to develop a treatment for a rare neurological disorder.[3,6] Holtzman introduced a bill in 1980 to "assist in the development of drugs for diseases and conditions of low incidence",[3] which was supported by the then chair of the House Subcommittee on Health and the Environment, Henry Waxman. Despite this support, the bill failed to pass the US House of Representatives at its hearing. Enter, Jack Klugman.

A write-up of the hearing published in *The Los Angeles Times* caught the attention of Maurice Klugman, brother of Jack and a producer on *Quincy, M.E.*, who himself was suffering from a rare form of cancer.[7] Together, he and Jack wrote an episode of the show called "Seldom Silent, Never Heard", that told the story of a young patient suffering from Tourette's syndrome who couldn't obtain treatment for his disorder in the US.[8] The episode brought national attention to the issue, and is widely credited as inspiring a new, concerted effort to address the problem. The bill was reintroduced in 1981 and Jack Klugman was invited to testify in support of it before Congress, where he spoke on the need for "orphan drugs".[9] The bill recommended measures that would not only lower the regulatory hurdles for the approval of existing drugs for rare conditions but also offer considerable incentives for companies that brought novel drugs to market, for example tax credits and exclusive marketing rights.[3] It passed through the house but met opposition in the Senate, where it was stripped of the tax credits at the behest of Orrin Hatch, the senator for Utah. In response the Klugman brothers wrote a second *Quincy* episode, "Give Me Your Weak", that saw Quincy confront a cold-hearted senator who was preventing the passage of an Orphan Drug Act.[1] The pressure that mounted as a result caused Hatch to relent. The tax credits were reintroduced,

and the Orphan Drug Act (ODA, Figure 1.1) was signed into law by President Ronald Reagan in January 1983.[3]

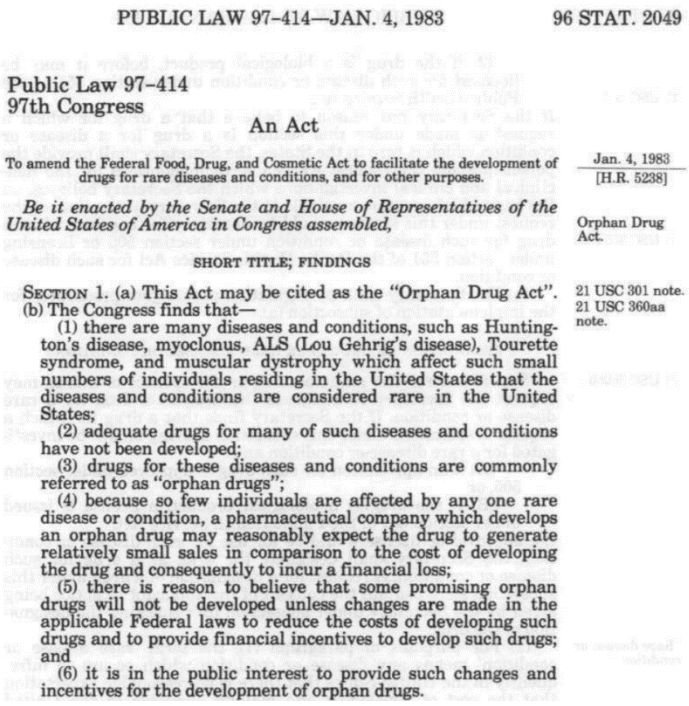

PUBLIC LAW 97-414—JAN. 4, 1983 96 STAT. 2049

Public Law 97-414
97th Congress

An Act

To amend the Federal Food, Drug, and Cosmetic Act to facilitate the development of drugs for rare diseases and conditions, and for other purposes.

Jan. 4, 1983
[H.R. 5238]

Be it enacted by the Senate and House of Representatives of the United States of America in Congress assembled,

Orphan Drug Act.

SHORT TITLE; FINDINGS

SECTION 1. (a) This Act may be cited as the "Orphan Drug Act". 21 USC 301 note.
(b) The Congress finds that— 21 USC 360aa note.

(1) there are many diseases and conditions, such as Huntington's disease, myoclonus, ALS (Lou Gehrig's disease), Tourette syndrome, and muscular dystrophy which affect such small numbers of individuals residing in the United States that the diseases and conditions are considered rare in the United States;

(2) adequate drugs for many of such diseases and conditions have not been developed;

(3) drugs for these diseases and conditions are commonly referred to as "orphan drugs";

(4) because so few individuals are affected by any one rare disease or condition, a pharmaceutical company which develops an orphan drug may reasonably expect the drug to generate relatively small sales in comparison to the cost of developing the drug and consequently to incur a financial loss;

(5) there is reason to believe that some promising orphan drugs will not be developed unless changes are made in the applicable Federal laws to reduce the costs of developing such drugs and to provide financial incentives to develop such drugs; and

(6) it is in the public interest to provide such changes and incentives for the development of orphan drugs.

Figure 1.1. The Orphan Drug Act of 1983

The ODA provides support for the development of so-called "orphan drugs", defined as a drug developed for a disease or condition that affects fewer than 200,000 people, or a drug whose sales will not offset the costs of its development or marketing in the United States.[10] In its current form, it offers New Drug Application (NDA) fee waivers, tax credits for clinical trials of orphan drugs, grant funding for rare disease research, and market exclusivity for seven years post-approval.[11] The act inspired similar pieces of legislation across the globe, such as in Europe and Japan, after policy makers observed the effect it had on the growth of the US biotechnology industry.[3] To date, more than 500 drugs have been approved for use in the treatment of rare diseases by the FDA, compared to just ten in the decade preceding 1983.[2,3]

Perhaps most importantly, the legacy of the ODA is that of the empowerment of rare disease patients, and the promise of hope in the face of disabling and potentially fatal conditions.[3,12]

1.2 Rare Diseases: Challenges and Progress in Drug Development

The ODA has undoubtedly played a significant role in encouraging diverse research efforts into the underlying causes of rare diseases and the discovery of treatments for them.[13–15] However, despite the large increase in drug approvals precipitated by the ODA, the majority of the approximately 7000 rare diseases still have no specific therapy.[16,17] Even though the diseases themselves are of low prevalence, around 350 million people are affected by a rare disease globally, the vast majority of whom have no recourse to treatment.[16] The "translation gap" also continues to grow: whilst advances in pharmacogenomics and next-generation sequencing have accelerated the discovery of the underlying genetic causes of rare diseases,[18,19] this knowledge is not being translated into new therapies at the same rate.[16]

Why is the "translation gap" increasing? Rare diseases are of course not insulated from the traditional challenges of drug discovery: high attrition rates as drugs move through the development pipeline mean that only 10% of drugs that reach phase I for any indication eventually go on to be approved for use.[20] Even before phase I, a 2015 study analysing the failure rates of drugs from four large pharmaceutical companies found that just over 50% of candidates advanced to the clinic following preclinical development.[21] This translation from basic to clinical research is known as "the valley of death" (Figure 1.2) due to these high failure rates and the challenges faced by drug discoverers.[22,23]

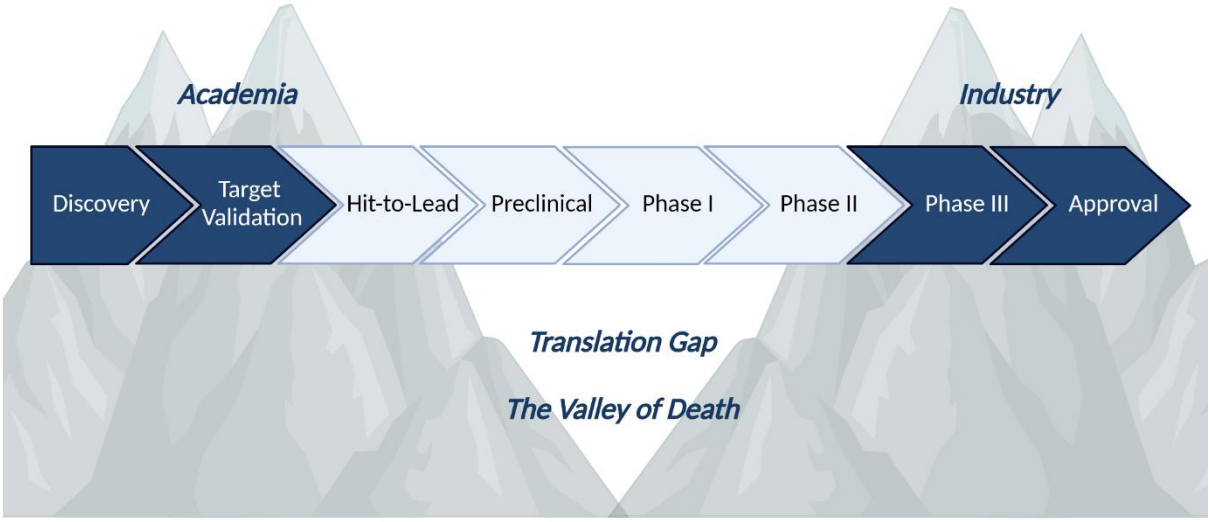

Figure 1.2. Drug development pipeline and the "valley of death".

The main cause of candidate failure prior to entering the clinic is overwhelmingly non-clinical toxicology, and once a drug reaches phase I this is mirrored in high failure rates due to clinical safety concerns.[21] Pharmaceutical companies have attempted to address these issues in a variety of ways, including linking physiochemical properties such as logP and topological polar surface area (tPSA) to toxicology in order to guide preliminary medicinal chemistry efforts.[24–26] For example, analysis of a set of clinical compounds by researchers at Pfizer found that those with a logP > 3 and a tPSA < 75 Å^2 were more than twice as likely to exhibit toxicity,[24] findings that were supported following a similar study by scientists at Eli Lilly.[25] Whilst an attractive prospect, such an absolute approach to limiting toxicity is perhaps misguided:[27] toxicity concerns must be viewed within the context of the therapy itself, for example considering the risk-benefit ratio in the disease setting, the therapeutic index of the drug, and the severity of the effect.[21] Similarly, the profile of a "safe" drug may change should the necessary efficacious dose prove to be toxic during human dose escalation, or if a toxicity concern thought to be manageable proves not to be when in the clinic.[28] Finally, it is sometimes impossible to predict certain toxicity outcomes: for example, the cannabinoid

receptor antagonist rimonabant was withdrawn from the clinic for the treatment of obesity after it was associated with an increased risk of depression and suicidal ideation.[29] Despite tremendous advances, the ability to fully predict the safety profile of a drug candidate remains a challenge.[30] The continued development of predictors of required doses that can then be investigated in the clinic, as well as predictive safety markers, are of key importance, however this area remains a significant challenge for drug discoverers.

Whilst safety issues remain, the primary reason compounds do not advance beyond phase II is a lack of clinical efficacy.[21,28,31] These instances of failure led Pfizer to establish their "three pillars of survival", essential data needed to establish whether a compound has the necessary qualities to elicit the desired pharmacological effect and thus validate their target hypothesis *in vivo.*[32] These were evidence that the compound achieved sufficient target exposure, occupancy, and functional modulation, key pharmacokinetic (PK) and pharmacodynamic (PD) parameters that would indicate the likelihood of a compound progressing to phase III. Hand in hand with these pillars is the knowledge of suitable biomarkers to demonstrate proper target engagement.[33,34] Without these, it would be difficult to discern whether a lack of efficacy was due to poor target selection or just inadequate pharmacological activity.[32] That being said, poor target selection is often a cause of failure:[35] analysis by AstraZeneca found that their confidence in the disease role of a drug target did not increase as the drug advanced through the clinic,[28] suggesting the root cause of failures at this stage is simply insufficiently robust target validation strategies.[31] As well as this, whilst animal disease models remain a major source of information at the early stage of drug development, they often do not adequately replicate the disease in humans and are limited by poor translatability in a clinical setting.[36,37]

Rare disease drug discovery also brings its own unique challenges. Before the drug development process can begin, identification of a suitable drug target poses a significant challenge due to the so called "n > 1 plateau":[38] the rarity of these diseases, as well as misdiagnosis due to the overlap of symptoms with others, leads to difficulty when attempting to identify pathogenic variations in the same gene across individuals. As a result, there often exists a lack of knowledge about the natural progression of the disease, meaning validated clinical end-points are scarce.[39] This has implications for clinical trial design, compounded by difficulties in identifying and recruiting suitably large patient cohorts along with practitioners who possess adequate knowledge and expertise.[39,40] That being said, advances in next-generation sequencing technology have enabled increased identification of important rare disease genes,[18,38] and the help of patient advocacy groups has been essential in recruiting participants for multicentre trials.[40] In addition, improvements in therapeutic modalities beyond small molecules, such as enzyme replacement, anti-sense oligonucleotide, and biological therapies,[16,41] have expanded the arsenal at our disposal for the treatment of these rare diseases. Despite this, the vast majority of rare disease sufferers have no recourse to treatment, and even an increase of 500-600 new orphan drugs over the next decade would still leave almost 90% of sufferers without an approved therapy.[38]

1.3 The Promise of Chemical Probes in Drug Development

This section is adapted from the following paper:

> **R. B. A. Quinlan,** P. E. Brennan, Chemogenomics for Drug Discovery: Clinical Molecules from Open Access Chemical Probes, *RSC Chem. Biol.*, **2021,** *2*, 759-795

As described above, a main cause of failure for compounds entering the clinic is a lack of efficacy deriving from poor target validation strategies.[28,31] This is despite rapid progress in

next-generation sequencing and genome wide association studies (GWAS) that have enabled the identification of key genes influencing disease progression.[35] Advances in countering this disconnect could be achieved through the development and subsequent use of readily available pharmacological modulators for proteins of interest, which would enable functional studies and evaluation of a protein's potential as a therapeutic target.[42] In recent years, chemical probes have emerged as valuable tools in this respect, enabling specific and non-destructive means of investigating the role of a protein in cellular and disease processes.[43]

Chemical probes are small molecules defined by four main criteria:[44–46]

1. A minimal *in vitro* potency of 100 nM.
2. Greater than 30-fold selectivity over sequence related proteins.
3. Profiled against an industry standard of pharmacologically relevant proteins.
4. On-target cellular effects at less than 1 μM.

With respect to drug discovery, chemical probes have proven very useful in preclinical research, impacting studies of target viability, safety, and translation.[47,48] The most common application of probes is their use determining the tractability of a particular target, that is its ability to modulate a phenotype, enabling a "Go/No-Go" decision. One example is the use of probes in differentiating between cannabinoid receptor type 1 (CB1) and type 2 (CB2) agonism in order to investigate the potential of CB2 as a target for the treatment of chronic pain.[49–51] It was hypothesised that selective CB2 agonism could induce the desired analgesia whilst avoiding the neurological effects associated with CB1 agonism. Distinct chemical probes based on imidazopyridine and decahydroquinoline scaffolds (compounds **1, 2, 3,** and **4**, Figure 1.3) were developed that were highly selective for CB2 over CB1 (**2** and **4**), along with structurally similar compounds that maintained residual CB1 activity (**1** and **3**).[50,51]

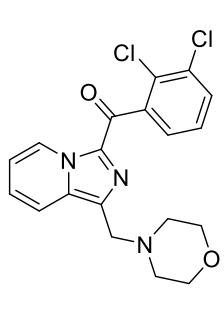

1

CB2 IC_{50} = 11 nM

CB1 IC_{50} = 1068 nM

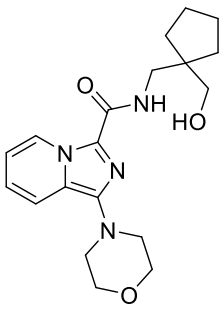

2

CB2 IC_{50} = 58 nM

CB1 IC_{50} = >17,000 nM

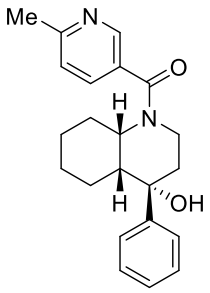

3

CB2 IC_{50} = 6.3 nM

CB1 IC_{50} = 1887 nM

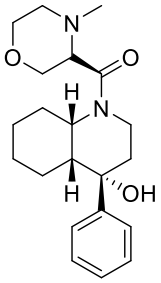

4

CB2 IC_{50} = 81 nM

CB1 IC_{50} = >17,000 nM

Figure 1.3. Imidazopyridine and decahydroquinoline probe series' that enabled target validation studies of CB2 agonism for chronic pain.

Through the use of these probes, it was found that analgesic effects were only observed for compounds that maintained residual CB1 agonist activity, indicating CB2 agonism alone was insufficient.[47,50,51] This directly informed the eventual decision to discontinue investigations into the targeting of CB2 for chronic pain.

Another area in which probes have found use is the investigation of on-target safety,[47] the leading cause of compound failure in the clinic.[21] Of particular use are probes selective for individual members of a family of proteins, as was observed in the development of dipeptidyl peptidase IV (DPP-4) inhibitors for the treatment of diabetes.[52] DPP-4 inhibition had been demonstrated to be a viable strategy to improve the levels of circulating glucagon-like peptide 1 (GLP1), which is essential for insulin secretion.[53] However, compounds thought to be DPP-4 specific induced severe toxicities in animal safety studies.[52] The discovery of the related DPP-8 and -9 proteins, and the observed activity of the compounds against them, led to the development of selective chemical probes for these family members in order to assess whether the toxicity was a result of off-target effects. The same toxicities were induced with a selective, dual DPP-8/9 inhibitor however not with a selective DPP-4 probe (compounds **5**

and **6**, respectively, Figure 1.4), providing a route forward for DPP-4 selective compounds. This paved the way for the discovery of **sitagliptin** for the treatment of type 2 diabetes.[52]

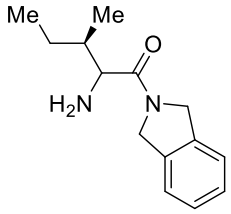

5

DPP-4 IC_{50} = >30,000 nM

DPP-8 IC_{50} = 38 nM

DPP-9 IC_{50} = 55 nM

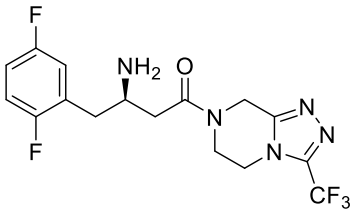

6

DPP-4 IC_{50} = 27 nM

DPP-8 IC_{50} = 69,000 nM

DPP-9 IC_{50} = >100,000 nM

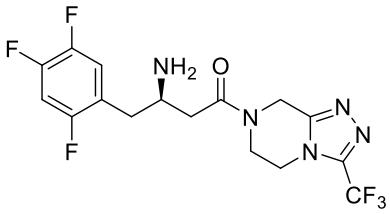

Sitagliptin

DPP-4 IC_{50} = 18 nM

DPP-8 IC_{50} = 48,000 nM

DPP-9 IC_{50} = >100,000 nM

Figure 1.4. DPP-8/9 and DPP-4 selective probes, alongside the eventually approved drug **sitagliptin**.[54]

Establishing a relationship between the PK and PD of a compound enables the validation of target engagement biomarkers and is essential for translating preclinical findings into humans.[47] Probes can be developed alongside lead optimisation efforts, often with structures distinct from the final clinical candidate but with selectivity and toxicity profiles that enable their evaluation in higher order species as translatable models. Scientists at Merck made use of chemical probes in this way in the development of **suvorexant** as a treatment for insomnia.[55] When the dysfunction in the orexin system was found to be associated with sleep disorders,[56–58] orexin receptors 1 and 2 (OX_1R and OX_2R, respectively) were identified as potential targets for small molecules in the treatment of insomnia. The development of a dual orexin receptor antagonist (**DORA-1**, Figure 1.5) that had good physiochemical, PK, and brain penetrant properties allowed for its evaluation in first a rat and then a monkey model of insomnia.[55,59] As a result, scientists were able to validate the target and also establish a relationship between PK, PD, and measured sleep parameters as biomarkers. Whilst **DORA-1**

is structurally distinct from the eventually approved **suvorexant**, it was an essential part of its development.

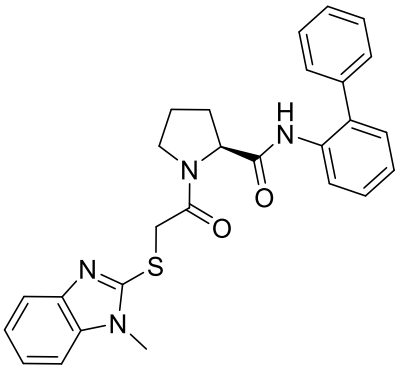

DORA-1

OX_1R IC_{50} = 17 nM

OX_2R IC_{50} = 4 nM

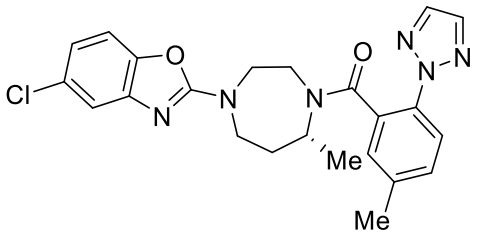

Suvorexant

OX_1R IC_{50} = 50 nM

OX_2R IC_{50} = 56 nM

Figure 1.5. Dual orexin antagonist probe **DORA-1** and the approved insomnia drug **suvorexant**.

Finally, whilst probes are not designed with drug-like qualities (for example absorption, distribution, metabolism, and excretion (ADME) properties) in mind, they can act as small-molecule starting points for drugs, inspiring lead optimisation efforts around a scaffold.[43,48] Indeed, this is an often cited advantage of probes, and one that is evident in the number of clinical molecules that derive obvious structural features from probes for the same target. This application of chemical probes was reviewed extensively in a 2021 publication,[48] and some examples are highlighted in the following paragraphs. Given the scope of this thesis, the chosen examples focus on probes that target lysine methyltransferases (KMTs), a class of epigenetic writer protein that will be described in greater detail in a later section (1.4.2).

EPZ004777 and **SGC0946**[60,61] (Figure 1.6) are structurally related probes targeting the KMT disruptor of telomeric silencing 1-like (DOT1L), which is responsible for the methylation of lysine 79 on histone 3 (H3K79).[62,63] Di- (me2) and tri- (me3) methylation of H3K79 is thought

to prevent the formation of certain transcriptionally repressive lysine methylation marks,[64] and is thus associated with euchromatin formation and transcriptional activation.[62,65] In a subset of leukaemias that involve a chromosomal translocation of the mixed lineage leukaemia (MLL) gene,[66,67] DOT1L is implicated in the transcription of a variety of pro-leukaemogenic genes.[68–70] **EPZ004777** and **SGC0946** have proved incredibly useful in further elucidating the role of DOT1L in these cancers, highlighting its potential as a therapeutic target.[71–75] Analogues of *S*-adenosylmethionine (SAM), they are potent inhibitors of DOT1L but lack the necessary physiochemical properties that would permit their clinical development.[61,71] As a result, scientists at Epizyme developed **pinometostat** (Figure 1.6), a DOT1L inhibitor directly derived from **EPZ004777** and **SGC0946** but with vastly improved physiochemical properties.[76,77] Continuous intravenous (CIV) administration of **pinometostat** in a rat xenograft model of MLL-rearranged leukaemia led to complete tumour regression after 14 days,[76] which, coupled with favourable PK properties, led to its advancement to the clinic for the treatment of adult and paediatric MLL-rearranged acute leukaemias.[78,79] It is currently under evaluation as part of a combination therapy in two phase Ib/II trials (NCT03701295 and NCT03724084).[80]

Polycomb repressive complex 2 (PRC2) containing the catalytic subunit enhancer of zeste homologue 2 (EZH2) mediates H3K27 di- and tri-methylation,[81–83] a transcriptionally repressive mark implicated in a variety of cancers.[84] GSK and Epizyme concurrently reported the development of probes for this target, **GSK126** and **EPZ005687** (Figure 1.7), disclosing structures that were both based on the same pyridone pharmacophore.[85–87] Both probes induced a reduction in H3K27me3 levels, as well as cell death in both solid and haematologic tumour cell lines.[85,88] The promise of PRC2-EZH2 as a target for cancer treatment led to the

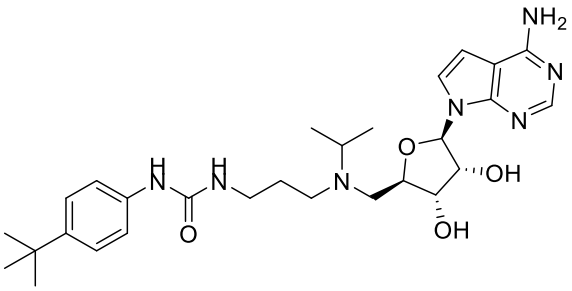

EPZ004777
DOT1L K_i = 0.3 nM

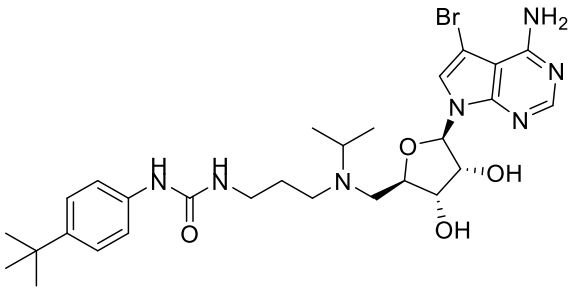

SGC0946
DOT1L K_i = 0.06 nM

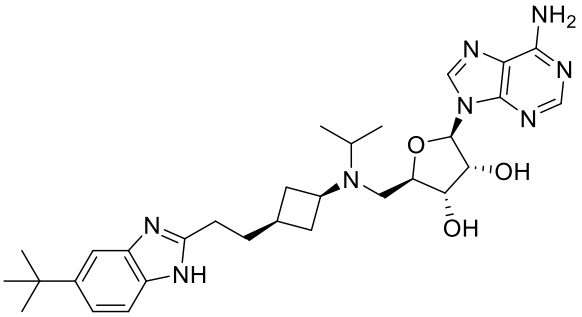

Pinometostat
DOT1L K_i = 0.08 nM

Figure 1.6. **EPZ004777** and **SGC0946**, probes for the KMT DOT1L. Alongside is **pinometostat**, structurally derived from the probes and currently under evaluation in the clinic.

development of a variety of clinical molecules whose structures derived from the pyridone-based probes, the most successful of which has proved to be **tazemetostat** (Figure 1.7).[86,89,90] Approved in 2020 for the treatment of follicular lymphoma and epithelioid sarcoma,[91,92] it is a direct derivative of **EPZ005687** with improved potency against EZH2 and importantly vastly superior PK properties.[90,93]

Chemical probes have thus proven to be invaluable tools in numerous target-based drug discovery efforts, enabling studies of target validation, safety, and translation, as well as providing small-molecule starting points for drug development.

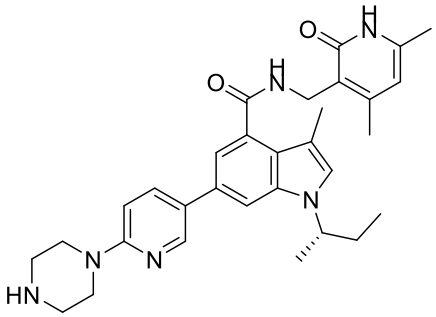

GSK126
EZH2 (WT) IC_{50} = 9.9 nM

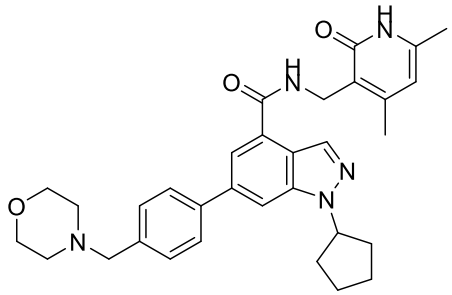

EPZ005687
EZH2 (WT) IC_{50} = 54 nM

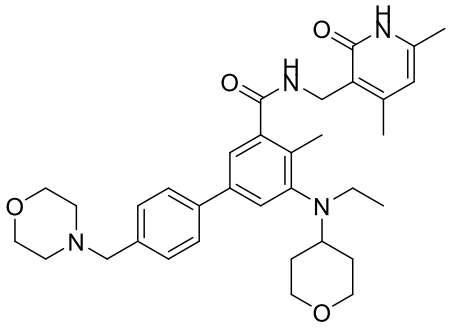

Tazemetostat
EZH2 (WT) IC_{50} = 11 nM

Figure 1.7. **GSK126** and **EPZ005687**, chemical probes for EZH2, and approved drug **Tazemetostat**.

1.3.1 Chemogenomic Library Screening for Novel Disease Targets

The aforementioned advances in genomics and disease understanding have made target-based drug discovery a cornerstone of the pharmaceutical industry.[94] However, many consider the attrition rate in drug discovery to be a direct result of this, with poor target selection precipitating a decline in pharmaceutical R&D efficiency.[31,95–97] Whilst chemical probes are of use in this arena, if a target is invalidated then the drug discovery process grinds to a halt. An alternative to target-based discovery is to screen molecules against a biologically relevant system in a target agnostic manner, with defined functional end points enabling hit identification (Figure 1.8).[96,98] This phenotypic drug discovery approach is thought to better mitigate the risks associated with target validation, as compound selection is based on activity

in relevant disease models. That being said, a phenotypic screening approach still suffers from drawbacks, such as the difficulty in generating compound structure-activity relationships (SAR), insufficiently robust disease models or assays, and the complexity of eventual target deconvolution.[96]

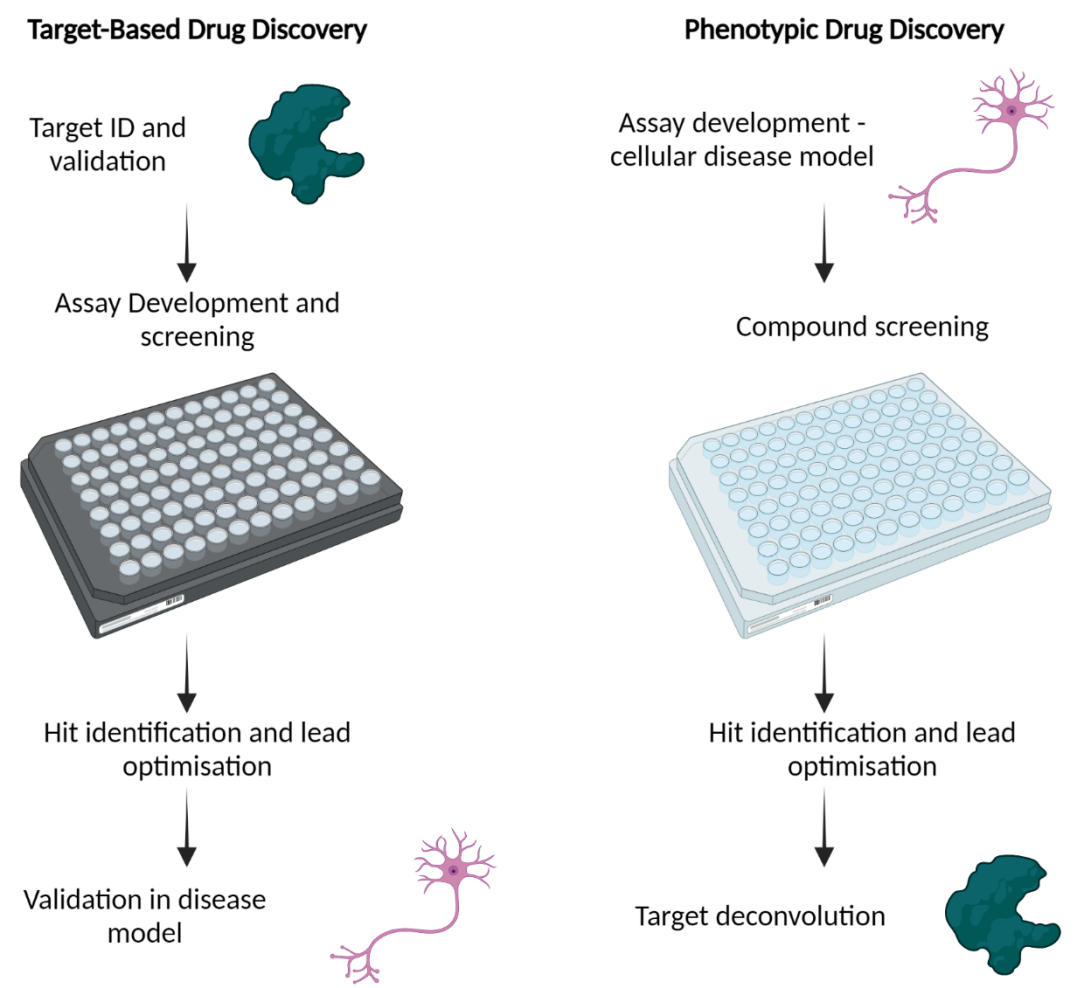

Figure 1.8. Target based drug discovery vs phenotypic drug discovery.

Over the past two decades, the use of chemogenomic libraries as phenotypic screening tools has emerged as an attractive means of circumventing some of these problems.[95,99–101] Chemogenomics is defined as the study of the genomic response of a biological system to chemical perturbation and has come to describe interrogating the genomic response with chemistry through the use of libraries of compounds with defined pharmacological activities

in cell-based assays to accelerate drug discovery.[99,100] A chemogenomic library is usually a set of compounds that are potent and selective for a variety of targets across the human proteome, however they can also be targeted to particular protein families and target classes.[99] For example, the Pfizer chemogenomic library contains 2,984 compounds across 1,043 biological targets, whereas the GSK Published Kinase Inhibitor set includes 367 compounds across 24 kinases (although in reality the number of targets is far higher due to the polypharmacology of these compounds).[102] Chemical probe collections are ideally suited for chemogenomic library screening: their requirements for both on target and cellular potency, as well as selectivity, makes target deconvolution far more straightforward. Probe collections often contain multiple, structurally distinct probes for the same target, along with negative controls, increasing the confidence that any observed phenotype is not due to off-target polypharmacology.[99] The target can then be validated using complementary techniques such as RNA inhibition (RNAi) or CRISPR-Cas9 gene editing.[103] The SAR around probes and their targets is also well defined, accelerating lead compound development.

One such collection is the epigenetic chemical probe library compiled by the Structural Genomics Consortium (SGC).[104–106] It currently comprises 55 probes across 42 different epigenetic targets, along with negative controls for the majority. Epigenetic regulation of gene expression is a dynamic process that contributes to the maintenance of normal cellular phenotypes, but when dysregulated can cause disease.[107] This regulation typically involves covalent modifications to DNA or to the histone proteins around which DNA is packed (Figure 1.9), although epigenetics is broadly defined as changes in gene expression that are not a result of the underlying DNA sequence. The probes contained in the collection target a variety of proteins involved in epigenetic regulation as a result of covalent histone modifications, so-called writer, reader, and eraser proteins.[108] Writers are responsible for adding these post-

translational modifications (PTMs) and include lysine methyltransferases (KMTs), arginine methyltransferases (PRMTs), and histone acetyltransferases (HATs). Reader proteins recognise and bind to the modifications in order to mediate their cellular effects and include bromodomains (BD) and plant homeodomains (PHDs). Finally, erasers catalyse the removal of the histone PTMs and include histone deacetylases (HDACs) and lysine demethylases (KDMs).

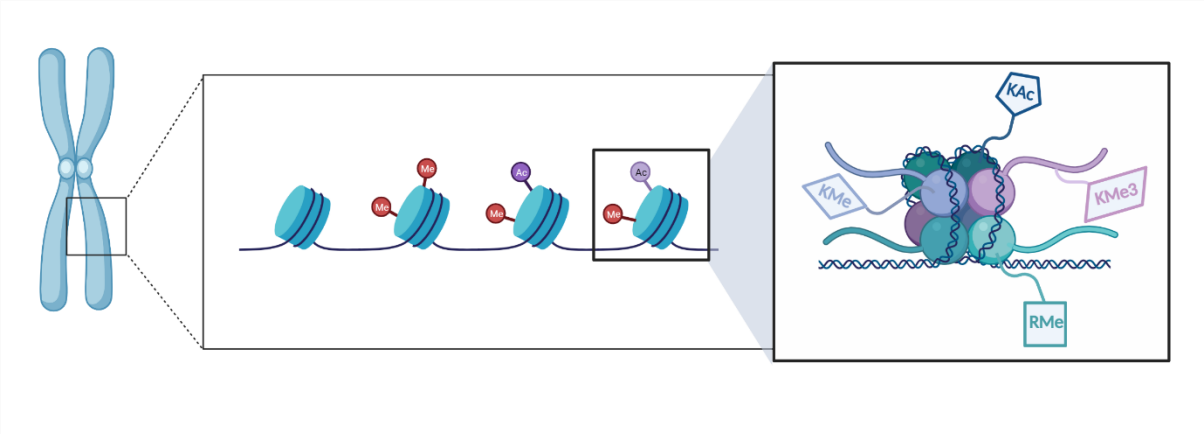

Figure 1.9. Histone modifications that affect gene expression

1.3.2 Epigenetic Compound Library Screening for Drug Discovery

Epigenetic modifications have emerged as key players in various disease pathologies, including cancer,[109] inflammatory disease,[110,111] and endocrine[112] and neurological disorders.[113] As a result, there is increasing interest in screening epigenetic probe libraries against various disease models in an attempt to discover novel therapeutic targets,[107] and this approach has proved fruitful in a number of disease areas.

Researchers at the University of Oxford studying the fibrotic disease Dupuytren's contracture hypothesised that the environmental risk factors associated with the disease indicated some epigenetic involvement.[114] Dupuytren's is characterised by the thickening of connective tissue

in the palm of the hand that eventually prevents the extension of one or more of the fingers, with surgical intervention the only available therapy.[115] The Oxford team screened a library of 39 epigenetic probes to evaluate their effect on the expression of pro-fibrotic genes, identifying cAMP responsive element binding (CREB) protein (CBP) and the closely related p300 as key regulators of the disease phenotype in patient derived myofibroblasts.[114] Two structurally distinct CBP/p300 bromodomain inhibitors induced similar effects on gene expression, and the target was further validated with the use of small interfering RNA (siRNA), highlighting the complementarity of the techniques. One of the chemical probes used in the screen, **CBP-30** (Figure 1.10),[116,117] has already directly inspired the discovery of a CBP/p300 inhibitor (**CCS1477,** Figure 1.10) for the treatment of haematologic malignancies and solid tumours,[118,119] and could now also inspire the translation of CBP/p300 inhibition into a topical treatment for Dupuytren's contracture.

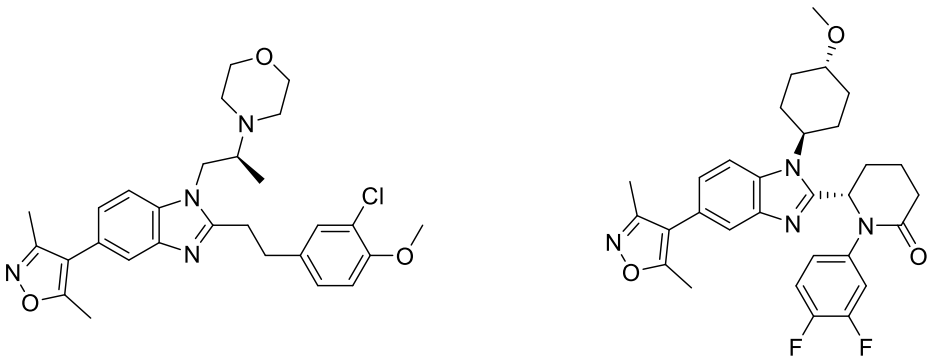

CBP-30
CBP K_i = 21 nM
BRD4 K_i = 850 nM

CCS1477
CBP K_i = 1.3 nM
BRD4 K_i = 222 nM

Figure 1.10. **CBP30** and **CCS1477**

Adopting a similar approach, a team from the University of Toronto evaluated a library of epigenetic modulators against several patient-derived glioblastoma cell lines.[120] Glioblastoma is the most aggressive form of adult brain cancer and is inevitably fatal.[121] Treatment options

include surgical resection and radiation therapy however all patients invariably relapse into the disease, and as such new treatment options are of vital importance. Evaluation of 24 epigenetic probes found three EZH2 probes, including **UNC1999** which is structurally similar to the pyridone-based **GSK-A** and **EPZ005687** (Figure 1.7), potently inhibited the proliferation of glioblastoma lines *in vitro*.[120] A combination of **UNC1999** and the corticosteroid **dexamethasone** was found to work synergistically, highlighting the potential of using EZH2 inhibitors as part of a combination therapy for glioblastoma. Achieving targeted EZH2 inhibition in glioblastoma is challenging due to the inability of reported inhibitors to cross the blood-brain barrier (BBB),[122] however the relevance of the target as demonstrated through epigenetic library screening will hopefully inspire efforts to develop CNS-penetrant compounds.[120]

Outside of non-communicable diseases, epigenetic library screens have also identified potential therapeutic targets for bacterial,[123] viral,[124] and parasitic infections.[125] In the case of the latter, 37 epigenetic probes were screened against the *Schistosoma mansoni* parasite that causes schistosomiasis,[125] a tropical disease resulting from contact with fresh water contaminated with the parasites.[126] Inflammatory immune responses to the parasites and their eggs can cause intestinal, hepatic, and urogenital disease, which if left untreated can prove fatal. Evidence for the role of epigenetic processes in regulating the parasite life-cycle led researchers across the Universities of Aberystwyth and Cardiff to evaluate an epigenetic compound library for anti-schistosomal activity.[125,127,128] Two probes for the protein methyltransferase SMYD2 (**LLY-507** and **BAY-598**, Figure 1.11) and another for the demethylase JMJD3 (**GSK-J1**, Figure 1.11) demonstrated significant activity, highlighting a key role for protein methylation homeostasis in the schistosome life-cycle and identifying potential therapeutic targets for anthelmintic development.

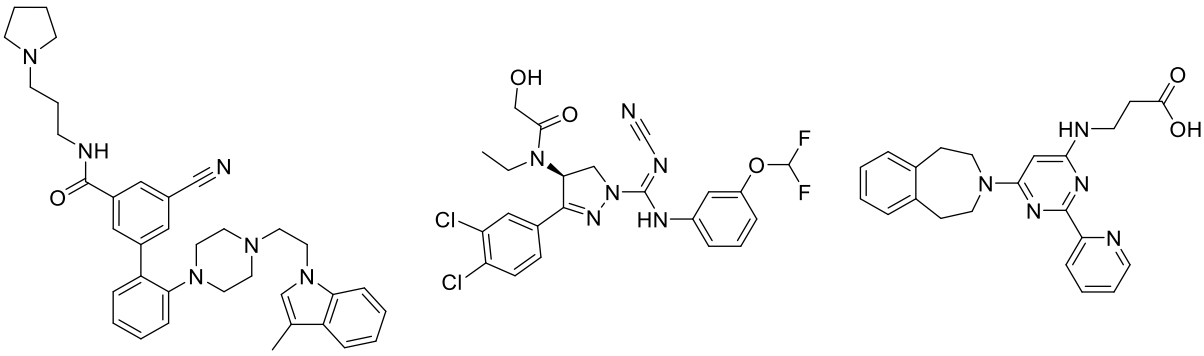

LLY-507
SMYD2 IC_{50} = <15 nM

BAY-598
SMYD2 IC_{50} = 27 nM

GSK-J1
JMJD3 IC_{50} = 60 nM

Figure 1.11. **LLY-507**, **BAY-598**, and **GSK-J1**.

The use of chemogenomic libraries represents an attractive solution to the issue of attrition as a result of poor target validation strategies.[96,98] Whilst there are benefits to target-based approaches, such as superior screening capacity and the ability to rationalise discovery programs, often the narrow target focus ignores the wider role of the target in complex physiological processes.[129] Chemical probes are ideally placed to bridge the gap between these two approaches: rationally designed in a "disease-agnostic" manner, with high importance placed on having well-defined potency, selectivity, and SAR, they can rapidly accelerate target deconvolution when used in "target-agnostic" screens. Within the context of rare diseases, this is of critical importance in cases where relevant disease targets have been difficult to identify.

As greater scrutiny is placed on both the quality of chemical probes and the availability of multiple structurally distinct probes for the same target to avoid off-target pharmacology, probe collections enable increased confidence in this target selection.[43] One limitation is the availability of probes for a broad enough section of the proteome, as probe development has tended to focus on the druggable genome.[99] However, there has recently been an increased focus on moving beyond this and developing probes to cover the entire proteome. With the

advent of collaborative projects such as the Target 2035 initiative, great strides will hopefully be made towards achieving this goal in the near future.[42] Such a collection of compounds could unite the target-based and phenotypic approaches and usher in a new era of drug development.

This approach to rare disease drug discovery forms the basis of the work described in this thesis. Researchers in the Department of Physiology, Anatomy, and Genetics at the University of Oxford screened the SGC epigenetic probe collection against a cell model of the rare neurodegenerative disease Friedreich's ataxia (FRDA), identifying a novel epigenetic disease target and accompanying chemical probe that have formed the basis of an ongoing drug discovery effort.[130]

1.4 Friedreich's Ataxia – A Brief History

Nikolaus Friedreich (1825-1882) was a Professor of Medicine in Heidelberg who observed the clinical features of a previously undescribed hereditary illness in the children of three different families.[131] In a series of five papers spanning the years from 1863-1877, he described a disease that started around puberty and caused ataxia (lack of voluntary coordination of movement), dysarthria (slurred speech), sensory loss, muscle weakness, scoliosis, foot deformity, and cardiac symptoms.[132–136] The early history of FRDA is somewhat muddled: Friedreich ignored several key physiological symptoms that are now known to be characteristic of the disease, ascribing their cause to other diseases.[137–139] The prevalence of neurosyphilis and the associated tabes dorsalis (demyelination of the neural tracts), may go some way to explain this as the disorders shared many similar symptoms.[137,139]

The name “Friedreich’s illness” was coined in 1882, the same year Friedreich died.[140,141] Several similar hereditary motor and sensory neuropathies were beginning to be described contemporaneously, such as Charcot-Marie-Tooth disease and the associated Roussy-Lévy syndrome.[131] This added significantly to the ambiguity surrounding the disease, leading to numerous probable misdiagnoses.[142,143] The lack of a complete picture of the neurological basis of the disease contributed to this: although incredibly detailed, the anatomical studies conducted by Friedreich at the time drove the impression that FRDA was a disease of the spinal cord, with no cerebellar involvement (Figure 1.12).[138,139] However, a cerebellar component was established in 1907,[144] along with the lesion of the dentate nucleus, both of which are now known to be characteristic of the disease.[145–147]

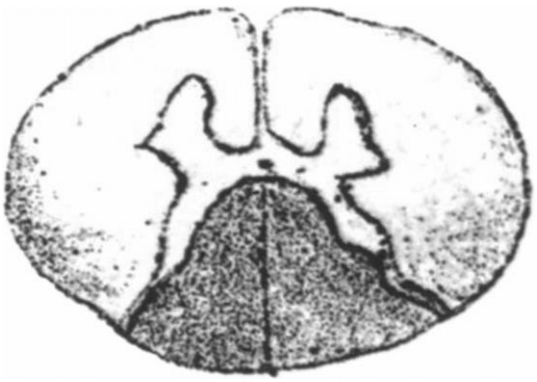

Figure 1.12. One of Friedreich’s original drawings of the spinal column of an FRDA patient. Black shading indicates haematoxylin staining of degenerated tissues (adapted from Friedreich, 1877).[136]

Even though a clearer physiological picture was beginning to slowly emerge, debate still raged over the distinctions between FRDA and other forms of hereditary ataxia.[131] Despite clinical evidence, the cerebellar component was largely ignored until 1957,[145] but by that point interest in the disease had begun to subside and few clinical studies were being conducted.[131] This confusion meant that establishing a biochemical basis for the disease was challenging, a

consequence of the lack of a clearly defined patient cohort. In 1974, a group of Québécois clinicians established "The Quebec Cooperative Study of Friedreich's Ataxia" and set out to delineate a distinct set of clinical criteria for a diagnosis of Friedreich's Ataxia in order to provide such a group for study.[148,149] They described a set of seven symptoms that they deemed "obligatory for diagnosis":

1. Onset before the age of puberty and never after age 20.
2. Ataxia of gait.
3. Progression of ataxia within last two years.
4. Dysarthria.
5. Proprioceptive sensory loss.
6. Muscle weakness.
7. Deep tendon areflexia.

Whilst subsequent studies supported the majority of these assertions,[131,150,151] the genetic homogeneity of the studied patient cohort from Quebec was criticised as it would mean the clinical criteria might not be broadly applicable to patients everywhere.[131] On the other hand, the Cooperative argued that the availability of a genetically isolated cohort descended from single ancestor offered an unparalleled opportunity to study the genetic basis for the disease.[149] However, the Cooperative were unable to elucidate the molecular underpinnings of FRDA. They had hoped to find some defect in a metabolic pathway however could establish no single specific enzyme deficiency that accounted for the disease.[149]

It had been just over 100 years since Friedreich's initial description of the disease. Despite having no knowledge of the cerebellar involvement, his detailed observations of the effect of the diseases on the spinal column and medulla oblongata remain both accurate and

remarkable given the apparatus at his disposal.[137] Another valuable contribution was his descriptions of the effect on the heart, where he correctly identified the presence of a hypertrophic cardiomyopathy, although attributed it to typhoid fever.[132] Whilst the neurological features of the disease were studied in detail, any cardiac involvement was largely written off as the result of sclerosis of the vagus nerve causing greater sympathetic stimulation.[152] It wasn't until 1946 that myocarditis associated with the disease was found to be independent of any vagal degeneration, and thus deemed to be part of the disease pathology. The study concluded:

"*The myocarditis is of toxic origin, and, in view of the known association between the nervous and cardiac disorders in Friedreich's Ataxia, it is probable that the same agent is responsible for both legions*".[152]

The recognition that cardiac involvement was part of disease pathology began to take deeper root, and soon an electrocardiogram was recommended to differentiate between Friedreich's and other forms of ataxia.[153,154]

The toxins responsible remained elusive; numerous new theories emerged, with coronary artery disease the most popular.[155,156] In an attempt to unify the two theories, it was suggested that occluded coronary arteries caused the myocardium to degenerate, releasing antigens that induced an autoimmune response causing further degeneration.[157] These antigens acted as the long sought after "toxins". However, numerous cases of FRDA patients dying from cardiac issues were observed with no coronary artery blockages.[152,158–160]

In 1950, Manning proposed that the association between a familial link and the abnormal cardiac changes were caused by "*the inheritance of a lethal gene which affects both the heart and the central nervous system*".[160] A 1962 study supported this assertion, further suggesting

that the cause of FRDA was a genetic abnormality in a metabolic pathway, affecting both cardiac and neural tissues.[155] More research was emerging showing just how widespread cardiac issues were in sufferers of the disease.[161] Approximately 50% of patients were dying due to heart failure, with 75% having some cardiac dysfunction over the course of their life. The root cause of these issues was still unknown.

A novel finding emerged in 1976 that the heart muscle cells of a FRDA sufferer contained granular deposits of calcium and iron (Figure 1.13).[156] The authors postulated that this was the result of metabolic changes occurring during cellular degeneration, but also suggested the possibility that it may bear a more direct relationship to the disease pathology. These findings were supported by another report in 1980 that described iron deposits in the hypertrophic myocardium of FRDA sufferers.[162] Unbeknownst to them, these researchers had stumbled across a big clue as to the underlying cause of FRDA.

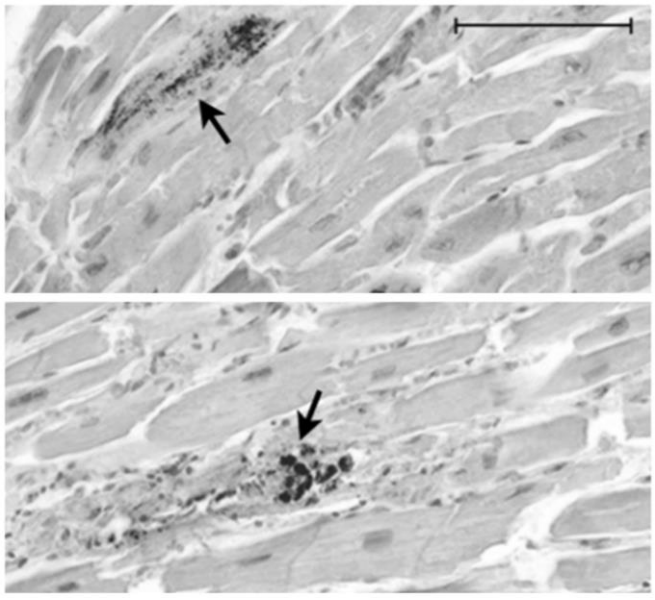

Figure 1.13. Iron deposits in the myocardium of an FRDA sufferer (adapted from Michael *et al*).[163]

1.4.1 Frataxin

Even though the Quebec cooperative were ultimately unsuccessful in their attempt to find the cause of FRDA,[149] their work in defining diagnostic criteria was to eventually prove crucial to efforts that uncovered the genetic basis of the disease.[164–167] A mutation was initially tracked to chromosome 9, with work in the following years narrowing down the specific locus.

In 1996, over 120 years after Friedreich first published his studies on the disease, the cause was discovered: a region on chromosome 9 coding for a 210-amino acid long protein subsequently named frataxin.[166] The gene, *X25*, contained a GAA trinucleotide repeat sequence in its first intron. This region was massively expanded in sufferers, increasing from around 20 repeat units in healthy individuals to 700-800 units in FRDA patients.[166] The discovery of *X25*, later called the *FXN* or *FRDA* gene,[143,168] was a landmark moment for disease diagnosis and research.

The discovery of frataxin preceded the rapid growth of the FRDA field and disease-defining discoveries.[169] In the two and a half decades since, understanding of disease pathology and molecular genetics has greatly advanced. Friedreich's ataxia is now known to be an autosomal recessive neurodegenerative disorder affecting the central and peripheral nervous systems.[138] It is the most common inherited ataxia,[143] with an incidence debated to be between 1:29,000 and 1:50,000, and a carrier incidence of around 1:90.[170–172]

FRDA is typically a disease of adolescence, with the average age of onset around 15.[173] The initial presentation is gait ataxia, however some present with scoliosis first, and patients are confined to a wheelchair within approximately ten years. Symptoms progress to include dysarthria, areflexia, proprioceptive deficits with loss of vibrational sense, and extensor plantar reflexes, amongst others.[131,173] Cardiac symptoms also emerge, with over half of

patients displaying hypertrophic cardiomyopathy.[174,175] Sufferers also show an increased frequency of diabetes and glucose intolerance.[176] FRDA is eventually lethal, with the average age of death around 37 years old due to the associated heart problems.[131]

The neurological symptoms arise due to shrinkage of the dorsal root ganglia, alongside degeneration of peripheral sensory nerve fibres, the posterior columns of the spinal cord, and the dentate nucleus (Figure 1.14).[177,178] The underlying cause of these symptoms is the reduced production of frataxin caused by expansion of the GAA trinucleotide repeat region in the first intron of the *FXN* gene.[166] The length of the expansion is directly related to the severity and inversely related to the age of onset of the disease.[173]

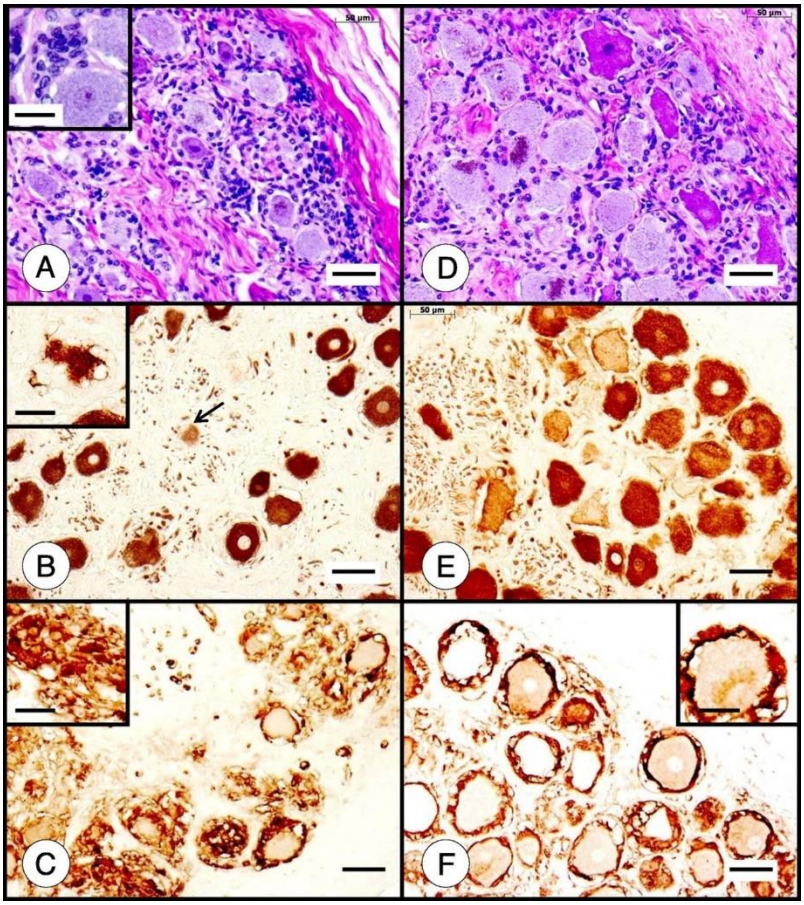

Figure 1.14. Evidence of the shrinkage of the dorsal root ganglion of FRDA sufferers (**A-C**) when compared to healthy controls (**D-F**) (adapted from Koeppen *et al.*)[138]

Frataxin is an evolutionarily conserved small protein that is localised to the mitochondrial matrix.[179–182] It has been shown to be an essential allosteric modulator of iron-sulfur (Fe-S) cluster formation,[183–185] inorganic cofactors essential for a variety of cellular processes such as electron transfer, radical generation, and protein stabilisation.[186] In eukaryotes, Fe-S cluster synthesis is localised to the mitochondrial matrix and requires a core complex of proteins that act to generate the components from cofactors and scaffold their assembly, prior to their downstream delivery to various targets.[183,186–188]

Frataxin binds at the interface of two proteins in this core complex, causing a conformational change that displaces an inhibitory Zn^{2+} ion (Figure 1.15).[183,189] Upon binding, Zn^{2+} sequesters a catalytic cysteine, preventing the sulfur transfer necessary for Fe-S cluster formation. A lack of frataxin leads to a strong decrease in Fe-S cluster biosynthesis,[185] leading to the toxic accumulation of iron within the mitochondria as well as deficits in the electron transport chain and increased sensitivity to oxidative stress.[190–193] This mitochondrial dysfunction is the basis for the disease pathology.

1.4.2 FXN-gene Silencing

The molecular mechanism of gene silencing has not yet been definitively established, however there are two prevailing theories.[168] The first concerns the formation of abnormal, higher order DNA structures composed of the GAA·TCC repeat regions. The tract of DNA comprising the repeat regions contains only purines (R) on one strand, and pyrimidines (Y) on the other.[177,194] These R·Y sequences can adopt a three-stranded structure, whereby an R or a Y strand folds back to interact with itself, forming an R·R·Y or Y·Y·R structure and leaving an unpaired segment of a Y or R strand, respectively (Figure 1.16).[194,195]

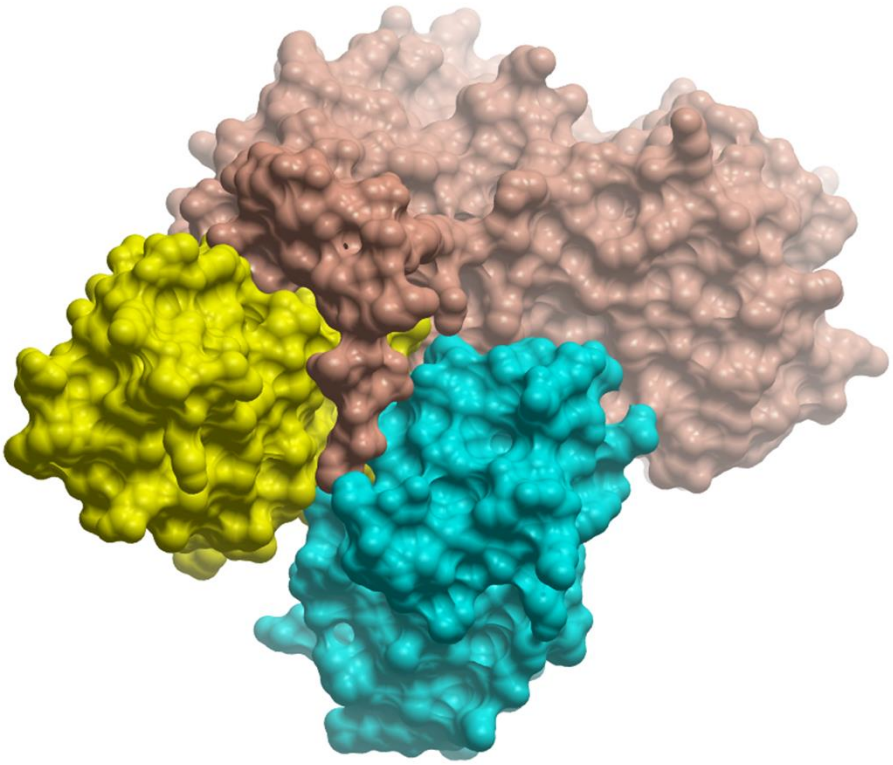

Figure 1.15. Frataxin (blue) at the interface of the NFS1 cysteine desulfurase (pink) and the iron-sulfur cluster assembly (ISCU) scaffold protein (yellow), two proteins in the core complex essential for Fe-S cluster formation (PDB: 6NZU)

Two triplexes can interact through exchange of an R or Y strand, forming an "intermolecular bitriplex" that has been termed "sticky DNA".[194,196] Sticky DNA has been shown to strongly inhibit transcription *in vitro*, providing an explanation for the gene silencing associated with the repeat region.[194–196] However, it has not yet been proven that this process occurs in the nucleus, where DNA interacts with proteins and is packaged into other higher-order structures that may preclude the formation of these R·R·Y or Y·Y·R structures.[177]

The second hypothesis concerns a variety of epigenetic changes that occur in the vicinity of the *FXN* locus.[168] Evidence suggests that the epigenetic changes involved in FRDA result in a

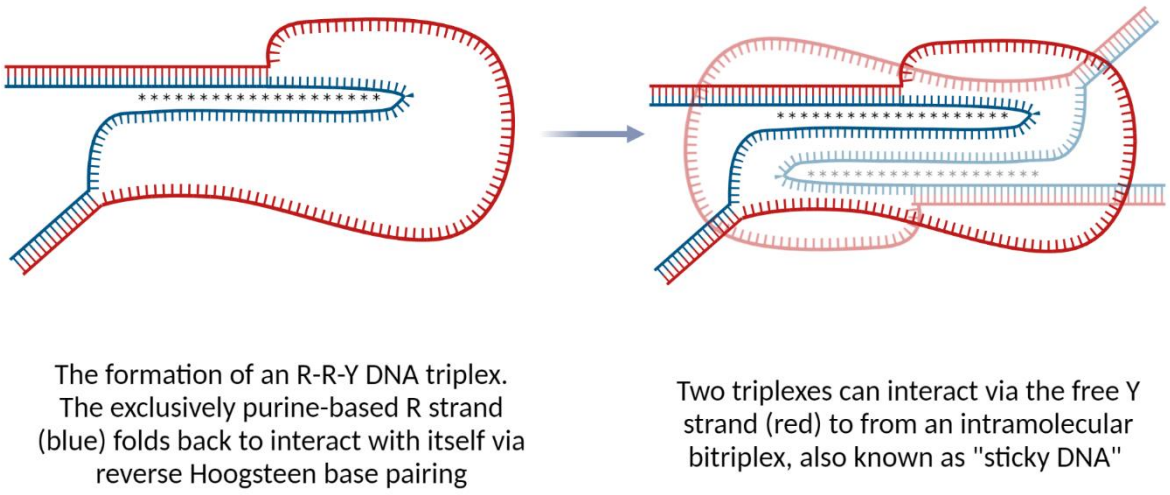

Figure 1.16. Triplex formation in GAA·TCC repeat regions.

phenomenon known as position-effect variegation (PEV), which has been demonstrated to be associated with long GAA triplet repeat regions.[197] PEV occurs when a gene is located near a region of heterochromatin, a highly condensed form of chromatin that is inaccessible to transcriptional machinery and is thus transcriptionally silent.[198] This proximity induces silencing in the affected gene.[197] The chromatin changes themselves are thought to be induced by the formation of an RNA-loop (R-loop) between the expanded intronic RNA and chromosomal DNA, which may also act to impede transcription itself.[199,200]

Heterochromatin is characterised by a number of distinct covalent modifications to both DNA and histones.[168] DNA methylation is one of the most common mammalian epigenetic changes, arising through the action of DNA methyltransferases (DNMTs) on cytosine bases contained within cytosine-guanine dinucleotide sequences, so-called CpG islands.[201,202] DNA methylation converts cytosine to 5'-methylcytosine (5mC)[201] and is associated with a variety of cellular processes, not least of which transcriptional repression.[203,204] This is thought to be a result of a reduced affinity of transcription factors for these methylated regions.[205]

Compared to healthy individuals, FRDA patients have been found to have increased CpG methylation at specific sites upstream of the repeat region.[206,207] The extent of this methylation has also been shown to be correlated to the length of the expansion and inversely correlated with the age of disease onset and *FXN* expression levels.[208,209] Alongside 5mC, another modification, 5'-hydroxymethylcytosine (5hmC), exists which was initially thought to be an intermediate in DNA demethylation processes.[210] Conversion of 5mC to 5hmC is carried out by ten-eleven translocation (TET) proteins,[211] and as knowledge of this modification has increased its role in epigenetic signalling has begun to emerge.[212] In FRDA patients, one of the affected CpG sites upstream of the repeat region comprises mainly 5hmC as opposed to 5mC, indicating that DNA hydroxymethylation may also play a role in disease pathology.[213]

Alongside DNA methylation, a number of histone post-translational modifications are observed, which alter the accessibility of the genetic loci to transcriptional machinery.[214] The landscape of histone modifications around the *FXN* locus is dramatically different in FRDA patients, with several changes associated with heterochromatin formation and transcriptional silencing observed.[168]

Histone acetylation involves the transfer of an acetyl group to a lysine residue. This tends to be a mark for open, transcriptionally active chromatin (euchromatin), as acetylation neutralises the positive charge of the basic lysine and weakens the interaction between the histone and the negatively charged DNA phosphate backbone.[214,215] Acetylation of histones is regulated by two classes of enzymes, HATs and HDACs.[216] HATs catalyse the transfer of an acetyl group using acetyl-coenzyme A as a cofactor,[217] whilst HDACs catalyse the reverse process, removing acetyl groups from lysine residues.[216] In unaffected individuals, the global

FXN chromatin architecture includes H3K9ac, a mark for euchromatin and active transcription.[216] By comparison, FRDA sufferers exhibit significant hypoacetylation of residues on H3 and H4 at the *FXN* locus, typically a mark for heterochromatin and gene silencing.[216,218,219]

Alongside changes in histone lysine acetylation, histone lysine methylation levels also differ significantly between healthy individuals and FRDA sufferers.[216,220–222] Histone lysine methylation is a tightly regulated process that determines cell fate, genomic stability, and, depending on the degree and site of methylation, can have varying effects on transcription.[223–225] KMTs display a high degree of specificity for both the site and degree of methylation.[223] For example, KMT1C (also known as G9a) induces H3K9 dimethylation (H3K9me2) from a monomethylated state, whereas KMT1A/B induces H3K9 trimethylation (H3K9me3) from the monomethylated state.[226,227] KDMs show a similar degree of specificity for the site and extent of methylation.[223]

Whilst histone acetylation has a more defined effect on chromatin structure,[214] the variability of histone lysine methylation states paints a more complex picture of its role in the regulation of chromatin environments.[223,225] Given each lysine residue can exist in one of four methylation states (naked, mono-, di-, and trimethylated), it is perhaps unsurprising that genome-wide studies have identified up to 51 different chromatin states in human cells that can be defined by their pattern of lysine methylation.[228] These differing states can have marked effects on transcription and chromatin signalling.[228–230]

In the context of FRDA, changes in the histone lysine methylation landscape play a crucial role in the transition from euchromatin to heterochromatin. In healthy individuals, alongside H3K9ac, chromatin at the *FXN* locus contains H3K4me3 and H3K36me3 at the promoter, and

H3K79me2 and H3K36me3 downstream. These are marks for a more open chromatin state, and specifically for transcription initiation and elongation.[216] By comparison, sufferers show a marked decrease in the levels of H3K79me2 and H3K36me3 downstream of the promoter, where the methylation landscape remains largely the same.[216] This would suggest that there is a defect in transcription elongation as opposed to initiation, which is further supported by the presence of the transcriptionally repressive H3K9me3, H3K27me3, and H4K20me3 marks at the regions downstream of the promoter and upstream of the repeat expansion.[216,231–234] Taken together, the evidence would suggest that the reduction in frataxin expression is a result of a host of repeat expansion-induced epigenetic changes (Figure 1.17), leading to heterochromatin formation and induced transcriptional silencing through position effect variegation.

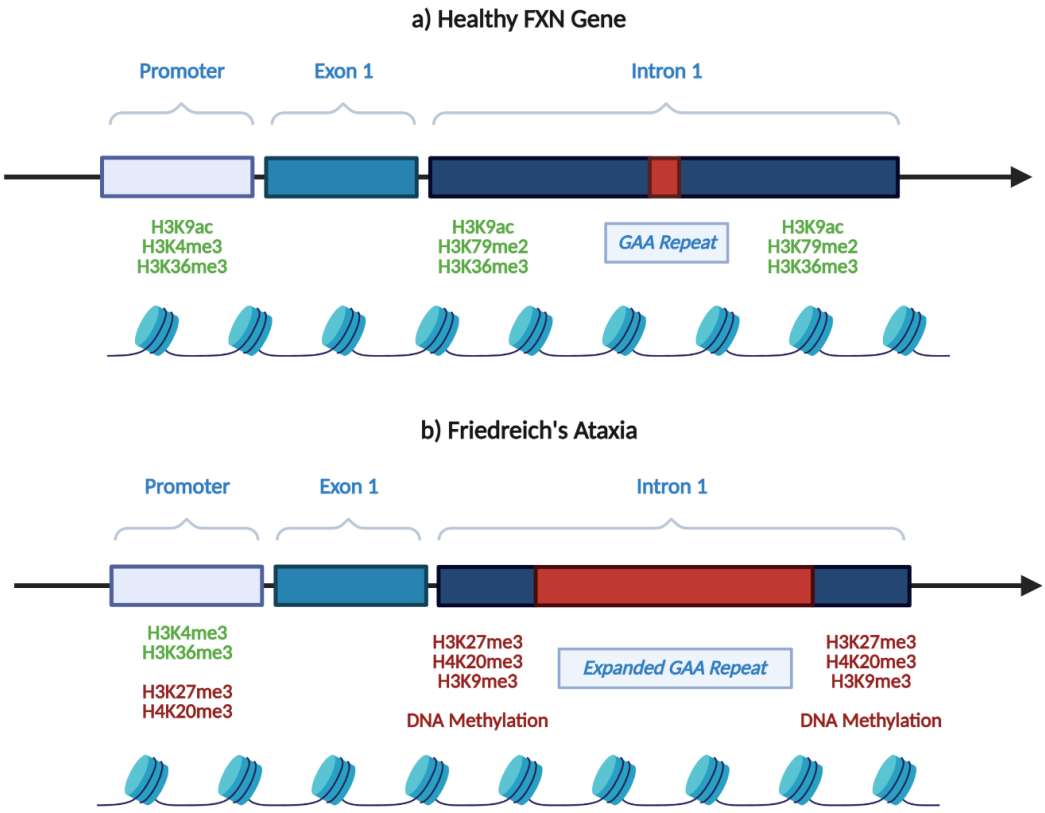

Figure 1.17. Epigenetic changes associated with FRDA and the *FXN* gene.

1.4.3 Current Approaches to the Treatment of Friedreich's Ataxia

At present, there exists no approved treatment or cure for FRDA.[235] Several drugs are currently at various stages of development,[236] targeting three main areas: increasing *FXN* expression, targeting impaired mitochondrial dysfunction, and increasing frataxin levels through replacement therapy.[237] Summarised below (Figure 1.18) are the most advanced potential therapies, and in the following sections some select examples will be highlighted.

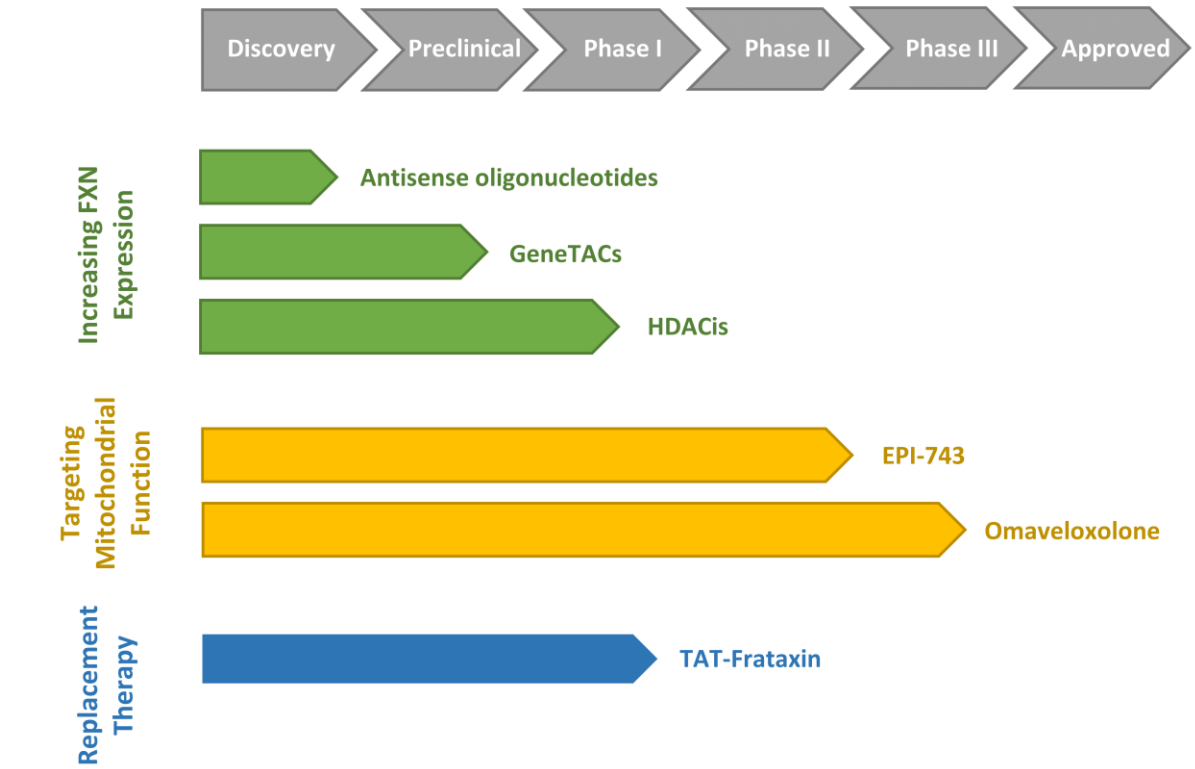

Figure 1.18. Pipeline of FRDA therapies (adapted from curefa.org).[236]

1.4.3.1 Increasing FXN Expression

Given the pathological basis for the disease is the transcriptional silencing of the *FXN* gene, increasing its expression to improve frataxin levels would seem the obvious approach to treatment. Heterozygous carriers of the disease produce approximately 50% of the levels of frataxin of unaffected individuals and yet remain asymptomatic, suggesting that only modest

improvements are required for therapeutic efficacy.[237] At the chromatin level, HDAC inhibitors (HDACis) have been shown to reverse *FXN* gene silencing induced partly by histone hypoacetylation at the gene locus.[238] Two different classes of HDACis induced sustained frataxin up-regulation in both patient-derived cells and mouse models of the disease, leading to their progression to the clinic.[239–241] The first phase I study published evaluated the effect of nicotinamide (vitamin B3), and found that it induced a dose-dependent increase in frataxin expression in peripheral blood mononuclear cells (PBMCs) with a concurrent decrease in heterochromatin-associated epigenetic marks.[242] Despite this, frataxin levels in the CNS and heart were not measured, and due to the short length of the study no improvements in patients' clinical features of ataxia were reported. Furthermore, the dose required to induce these changes was incredibly high and led to nausea and vomiting in almost all patients, limiting its utility for chronic treatment. A second HDACi, **RG2833**, was evaluated in FRDA patients after having been shown to increase *FXN* expression in induced pluripotent stem cell (iPSC)-derived neuronal cells, along with patient-derived PBMCs.[243] In patients, histone acetylation and *FXN* mRNA expression were induced in a dose-dependent manner, however this was not matched by an appreciable increase in frataxin levels, attributed to the short duration of dosing. Alongside this, **RG2833** was poorly CNS penetrant, formed toxic metabolites *in vivo*, and inhibited the human ether-a-go-go related gene (hERG) ion channel to a degree that was high-risk for inducing QTc prolongation. As a result, it progressed no further in the clinic.

Whilst HDACis seem a promising avenue for the treatment of FRDA, preclinical work to establish the role of HDAC selectivity in increasing *FXN* expression showed that it was necessary to inhibit three different HDACs (HDAC1, 2, and 3) in order to reverse the gene silencing.[243] Alongside this, two separate studies reported approximately two-fold changes in

gene expression in 655 and 822 genes, respectively.[244,245] Given the chronic nature of the disease and the necessity for long-term dosing of any drug, such a lack of specificity leading to extensive off-target effects could prove to be incredibly harmful over long periods of time.

A novel approach to increasing frataxin expression involves the use of heterobifunctional molecules that recruit transcriptional machinery to the repeat expansion region of the *FXN* gene.[246] Initially named "synthetic transcription elongation factors (Syn-TEFs)", they have since been rebranded as Gene Targeted Chimeras (GeneTACs) to fit the current vogue for heterobifunctional molecules.[247] Polyamides that target the repeat region were tethered to **JQ1**, a small molecule Bromodomain and Extra Terminal motif (BET) bromodomain inhibitor.[248] **JQ1** was chosen as it binds to BRD4, which recognises acetylated histones and engages positive transcription elongation factor b (P-TEFb), a multiprotein complex that is essential for facilitating productive transcription elongation by RNA polymerase II.[249] The GeneTAC induces the proximity of transcription elongation machinery to the repeat region (Figure 1.19), leading to robust *FXN* expression in a variety of patient-derived, disease relevant cell types at concentrations of 1 μM.[246]

The technology is now in preclinical development for the treatment of FRDA, and also being applied to other repeat-expansion disorders such as Fragile X syndrome and Huntington's disease. As the technology progresses, it remains to be seen if some of the issues traditionally associated with heterobifunctional small molecules, such as poor permeability and ADME properties, will also affect GeneTACs.[250,251] As well as this, whether any off-target effects will be observed due to the metabolism-induced release of the P-TEFb recruiting ligand, be it **JQ1** or a different epigenetic probe. Many of these compounds are cytotoxic,[48] and whilst

genome-wide BRD4 binding was not perturbed by the GeneTAC, it was by free **JQ1,** which could be problematic for chronic dosing.[246]

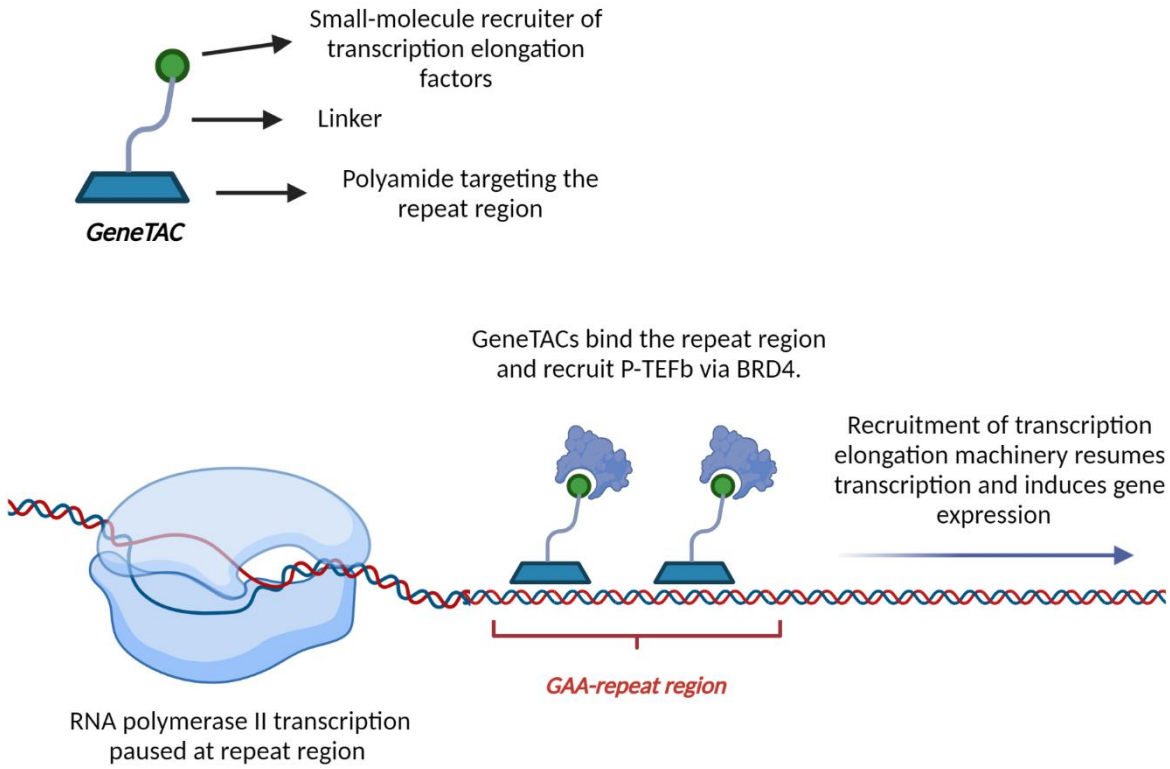

Figure 1.19. Functional premise of a GeneTAC

Another approach involves targeting the higher order R-loop structures that arise as a result of expanded intronic RNA hybridising to the genomic DNA.[252–254] The use of double stranded RNA (dsRNA) and antisense oligonucleotides (ASOs) complementary to the GAA repeat region was shown to increase frataxin production in patient-derived cells with nanomolar potencies. These synthetic nucleic acids bind to the expanded intronic RNA and prevent its interaction with the complementary region of chromosomal DNA, inhibiting R-loop formation and re-starting gene transcription (Figure 1.20). The increase in *FXN* expression was also associated with a reversal of the epigenetic changes associated with the repeat expansion,[222] such as an increase in histone acetylation and changes in histone methylation levels throughout the gene.[252]

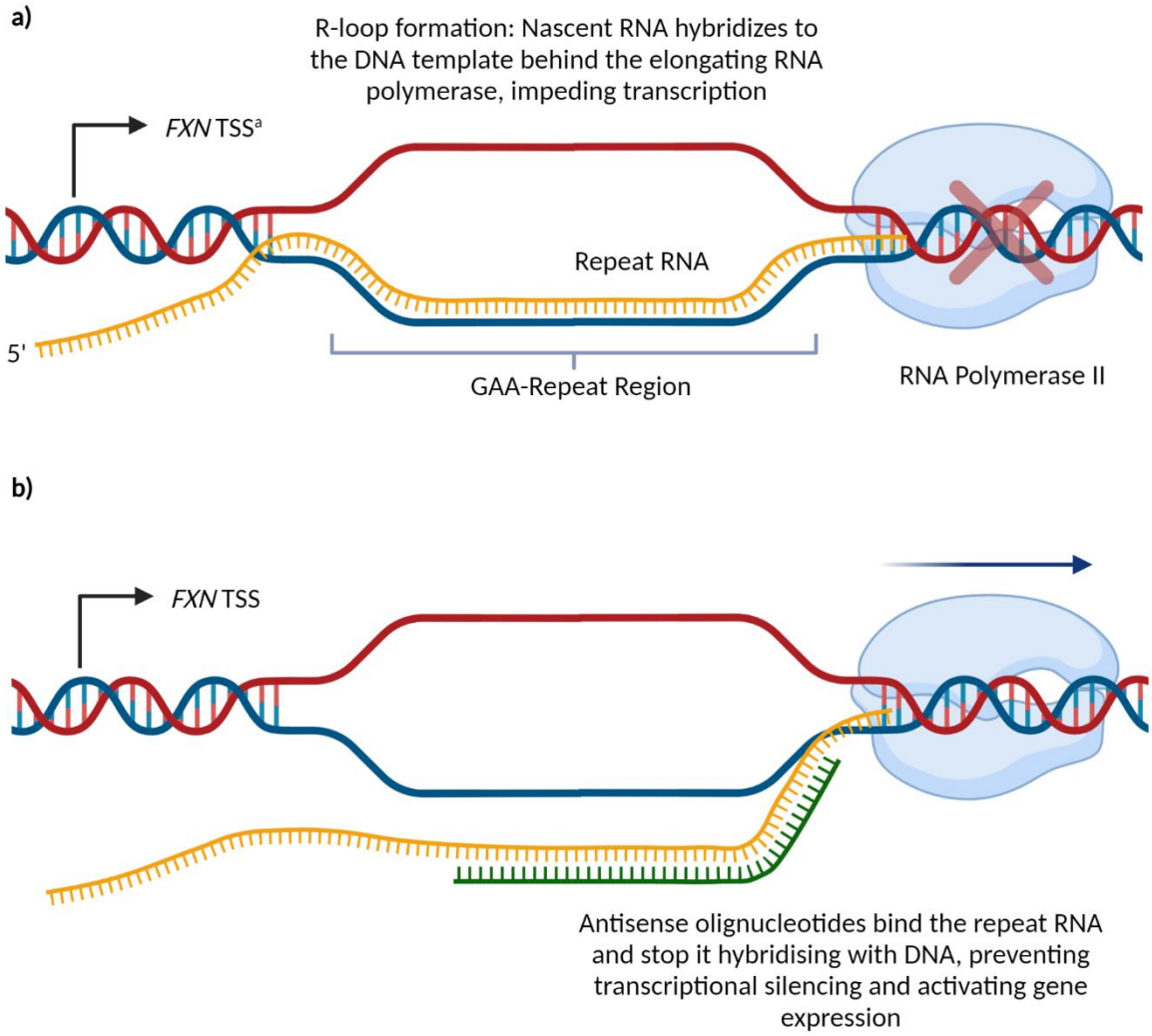

Figure 1.20. **a)** The mechanism of R-loop formation following transcription of the GAA-repeat region. **b)** Inhibition of R-loop formation by an ASO.

Both the dsRNAs and ASOs need to be further evaluated in animal models of the disease to investigate efficacy and potential off-target effects, however they are a promising approach to increasing frataxin expression. Their clinical application remains some way off, particularly given the difficulties associated with administering these therapies to the CNS,[253] however the recent success of **Spinraza**, the ASO-based therapy for spinal muscular atrophy,[255] provides some considerable encouragement for the approach.

1.4.3.2 Targeting Impaired Mitochondrial Function

The pathogenic downstream effects of reduced frataxin expression are the target of several therapeutic approaches which seek to alleviate mitochondrial defects and the resulting increased sensitivity to oxidative stress due to impaired iron-sulfur cluster formation. Several studies have evaluated the effect of antioxidants such as idebenone, vitamin E, and coenzyme Q_{10}, finding that they may have a modest benefit in improving both cardiac and neurological symptoms however to no degree of significance.[235,256] Researchers at Edison Pharmaceuticals posited that a more readily bioavailable antioxidant might display improved efficacy, developing **EPI-743** (Figure 1.21), a *para*-benzoquinone-based structural analogue of idebenone and coenzyme Q_{10}.[257,258] **EPI-743** targets various oxidoreductases essential for redox control of metabolism, and has been shown to potently protect patient-derived cells from oxidative stress, as well as induce neuronal recovery in an *in vitro* frataxin knock-out model.[259,260] It was evaluated over 24 months in a phase II trial using the Friedreich's Ataxia Rating Scale (FARS), which comprises a measure of ataxia, an activities of daily living subscale, and a neurological subscale.[261] **EPI-743** was well tolerated and induced a statistically significant improvement in patient outcome over 24 months, with a mean decrease (improvement) in FARS score of 1.8 points, compared to a mean increase (worsening) in FARS score of 4.8 points in untreated patients.[258,260] It has since been granted orphan drug designation by the FDA and is currently under evaluation in phase III trials for the treatment of FRDA (NCT04577352), with results expected to be reported in July 2023.

The promise of small molecule antioxidants for the treatment of FRDA led to the investigation of the role of endogenous antioxidant and reactive oxygen species (ROS) scavenging pathways in the disease. A key regulator of these responses is Nuclear factor (erythroid-derived 2)-like 2 (Nrf2), a transcription factor that induces the transcription of a number of antioxidant genes

and also plays a role in metabolism and mitochondrial function.[262] The translocation of Nrf2 from the cytosol to the nucleus has been shown to be defective in FRDA, leading to increased susceptibility to oxidative stress.[263] **Omavexolone** (Figure 1.21) is a small molecule Nrf2-inducer that acts to inhibit Nrf2 ubiquitination by Kelch-like ECH-associated protein 1 (Keap1), increasing its levels by preventing proteasomal degradation.[264] Initially developed for the treatment of solid tumours,[265] **omavexolone** was shown to protect patient-derived fibroblasts from oxidative stress caused by ROS and increased lipid peroxidation.[264] It was also protective against mitochondrial membrane depolarisation and cell death induced by hydrogen peroxide, which suggested it may be an effective therapy for FRDA. Patients treated in a phase II trial experienced a statistically significant mean improvement in FARS score of 2.4 points compared to a placebo after 48 weeks of treatment.[266,267] Despite this, several patients experienced elevated liver aminotransferase levels, leading to the discontinuation of treatment. As a result, an open-label extension study was carried out to evaluate the long term safety and efficacy of **omavexolone,** which showed that the patients who switched from the placebo to the drug displayed a parallel trajectory of improvement (as measured by FARS score) to those who stayed on the drug, an indication of true disease-modifying activity.[268] A second pivotal study is due to start in late 2021.

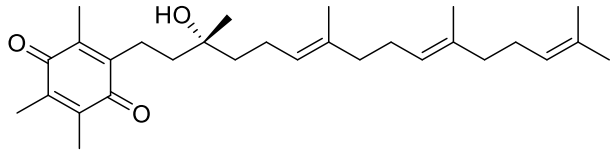

EPI-743

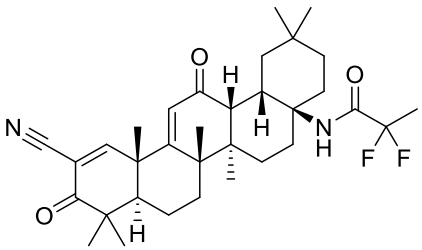

Omaveloxolone

Figure 1.21. **EPI-743** and **Omavexolone**

1.4.3.3 Increasing Frataxin Levels Through Replacement Therapy

Whilst approaches to re-initiating transcription of the *FXN* gene have shown promise, another means of increasing frataxin levels is direct exogenous replacement of the protein. Researchers from the University of Indiana fused recombinant precursor frataxin protein to a short cationic peptide called a trans-activator of transcription (TAT), which enables efficient delivery of a protein to a variety of tissues.[269] The precursor protein contains a mitochondrial targeting sequence (MTS) that, along with the TAT protein, is cleaved by matrix processing peptidases when the TAT-frataxin is delivered to the mitochondria, leaving replacement frataxin in the mitochondrial matrix. FRDA fibroblasts treated with TAT-frataxin showed reduced susceptibility to oxidative stress, and *FXN*-knockout mice showed improved lifespan and cardiac function when treated. As well as this, frataxin-depleted neurons derived from dorsal root ganglia treated with TAT-frataxin showed a decrease in apoptotic markers and improved survival.[270] In addition, TAT-frataxin was shown to cross the BBB in a study evaluating its effect in protecting dopaminergic neurons from oxidative stress in a mouse model of Parkinson's disease.[271] As a result, it was progressed to phase I trials as **CTI-1601** (NCT04519567), where subcutaneous (SC) dosing has been shown to increase frataxin levels in skin and buccal cells, as well as platelets in a dose-dependent manner.[272] However, the FDA has recently put a clinical hold on the trial after it was reported that higher doses of **CTI-1601** led to mortalities in non-human primate toxicology studies.[273] This may be a result of an unwanted immune reaction to higher doses of the TAT-frataxin, but begs the question if this is a viable approach if lower doses cannot achieve the requisite increase in frataxin levels in the necessary tissues.

1.5 A New Approach - Targeting SUV4-20 and H4K20 Methylation to Restore Frataxin Expression

None of the above approaches are without their limitations. Despite their promise and clinical progression, there remain both efficacy and safety concerns associated with all of the treatments. Given the disease affects multiple tissue types including the CNS, a small molecule that can enter the systemic circulation as well as cross the BBB seems to hold the most promise for an effective therapy. Targeting mitochondrial function has yielded some positive results, however they seem only modestly efficacious and there are concerns with toxicity given the need for long-term, chronic dosing. As well as this, these therapies do not target the primary pathology of the disease, meaning the deficit in frataxin will remain. ASO and dsRNA therapies have demonstrated efficacy in ameliorating this deficit, however they have not yet reached the clinic and would require invasive routes of administration, for example intrathecally.[255] HDACis fit the need for small molecules that restore the frataxin deficit, however their lack of specificity and broad effect on gene expression make them unsuitable as therapies. A more targeted approach to reversing the epigenetic changes associated with the repeat expansion could prove to be a viable means of increasing frataxin expression whilst avoiding global changes in gene expression.

As a means of initiating drug discovery efforts, an epigenetic probe library screen could therefore prove very useful. To this end, the SGC epigenetic probe collection was screened against an FRDA cell model containing a repeat expanded *FXN*-Luciferase (*FXN*-Luc) fusion construct, enabling relative luciferase intensity to be used as a proxy for frataxin expression.[130] This identified **A-196** (Figure 1.22), a potent and selective probe for the homologous histone methyltransferases Suppressor of variegation 4-20 (SUV4-20) H1 and H2,

as an inducer of *FXN* expression.[274] The two SUV4-20 homologues are responsible for the di- and tri-methylation of H4K20.[275] In patient-derived fibroblasts, knockdown of both homologues induced an approximate 1.5-fold increase in frataxin expression. Treatment with **A-196** induced a decrease in H4K20me2/3 and a concurrent increase in frataxin levels in both patient fibroblasts and PBMCs of 1.5-fold and 2-fold, respectively.[130] Global transcriptome profiling found that at the highest concentration (10 µM), treatment with **A-196** induced a change in expression of 1098 genes, compared to 3478 genes in cells that were treated with **RG2833** at 5 µM.[276] The absolute magnitude of the change in expression was also lower, at 67% compared to 94%.[130] At a concentration of 1 µM, **A-196** was observed to have perturbed 193 genes whilst still inducing frataxin expression, highlighting the specificity of this approach compared to broad HDAC inhibition.

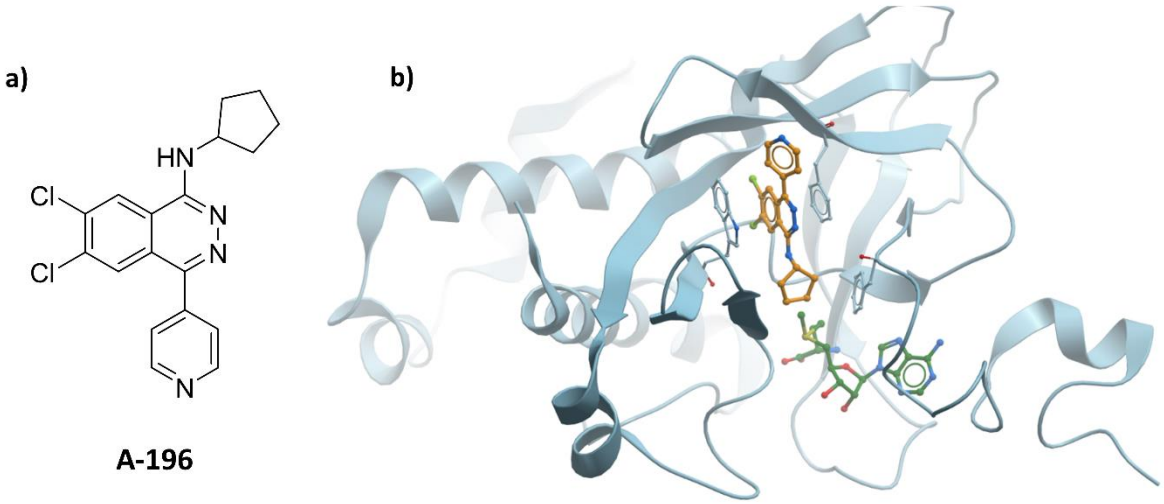

Figure 1.22. **a) A-196; b)** SUV4-20 in complex with **A-196** (yellow) and ***S*-adenosylmethionine** (green) (PDB: 5CPR)

1.5.1 The Role of SUV4-20 and H4K20 Methylation

The SUV4-20 family of methyltransferases form part of a wider group of KMTs that all contain a common, evolutionarily conserved domain.[274] The Suppressor of variegation 3-9, Enhancer of zeste, and Trithorax (SET)-domain catalyses the transfer of a methyl group to the ε-amino group of lysine residues, using *S*-adenosyl methionine (SAM) as a co-factor (Figure 1.23).[277] Given lysine residues can exist in multiple methylation states, the SET-domain containing proteins are responsible for the regulation of diverse cellular processes and biological responses.[278]

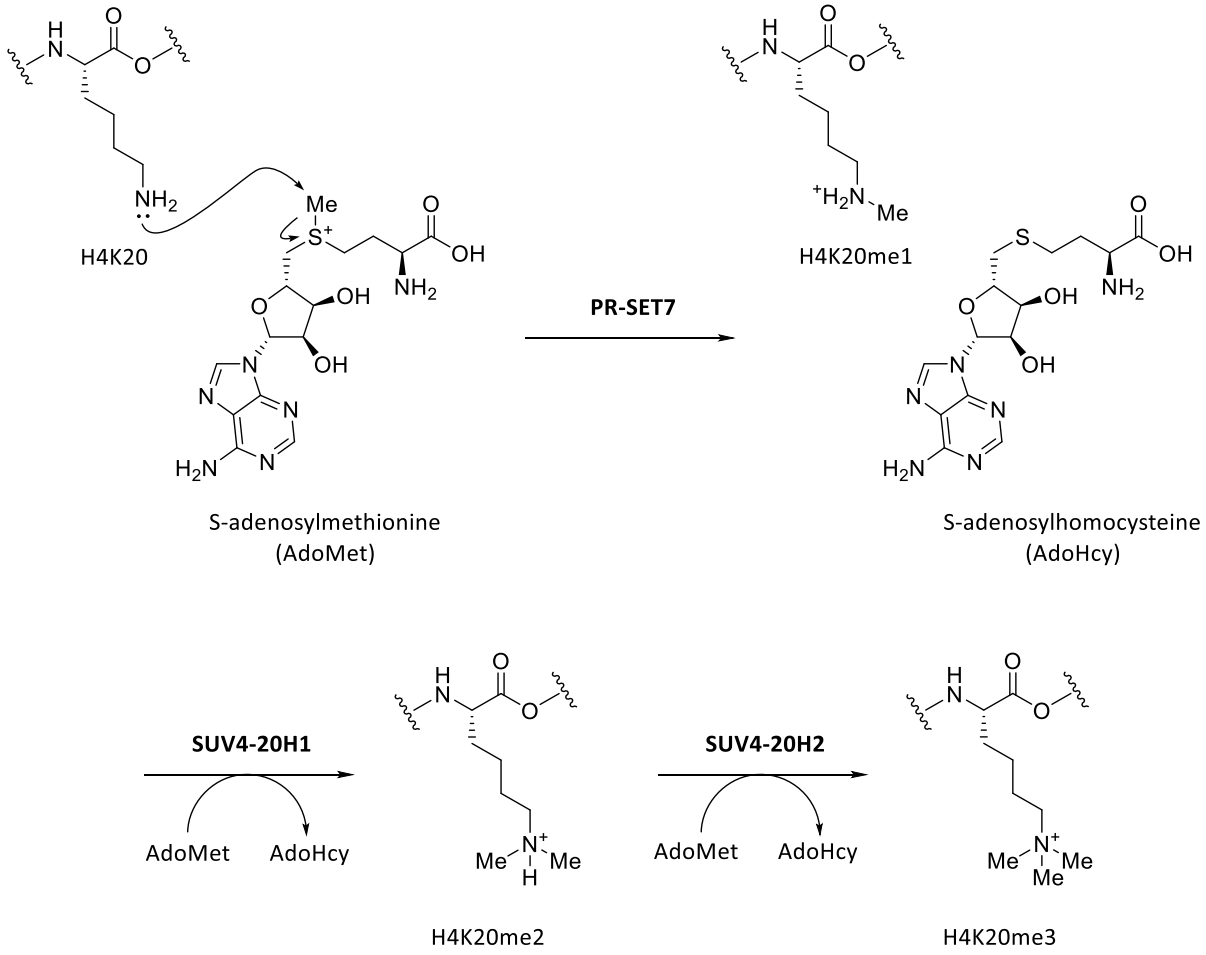

Figure 1.23. Mechanism for the methylation of H4K20 using SAM, and the role of the SUV4-20 proteins.

Methylation of H4K20 plays a key role in processes that ensure genomic integrity, for example DNA damage repair, chromatin structuring, and DNA replication.[275,279] H4K20me1 is controlled by PR-SET7 (also known as SET8) and is essential for the proper regulation of cell cycle progression.[280] Genetic ablation of PR-SET7 is lethal in both flies and mice,[275] and in mouse embryonic stem cells causes defects in cellular proliferation along with severe DNA damage.[279,280] H4K20me1 and PR-SET7 activity has been shown to be crucial for maintaining a threshold of chromatin compaction during the transition between different phases of the cell cycle.[281] The loss of chromatin compaction in the absence of H4K20me1 causes aberrant and excessive recruitment of licensing factors, resulting in DNA damage and leading to the formation of single stranded DNA.

The di- and tri-methylation of H4K20 is mediated by SUV4-20H1 and SUV4-20H2, respectively.[275] SUV4-20H1 is expressed throughout murine embryogenesis and adult homeostasis, and genetic ablation leads to impaired development and perinatal lethality.[282] By contrast, SUV4-20H2 is far less ubiquitous during development and its knockout leads to no apparent defects. Double knockout of both homologues causes perinatal lethality and a genome-wide accumulation of H4K20me1, leading to increased sensitivity to DNA damage and defective repair which reveals an important role for H4K20me2 in the DNA damage response pathways. p53 binding protein 1 (53BP1) directs non-homologous end joining (NHEJ) DNA repair and is recruited to sites of DNA damage by H4K20me2; in its absence, 53BP1 accumulation at these sites is significantly delayed, leading to increased sensitivity to exogenous stress. The restricted expression of SUV4-20H2 and the impact of its ablation suggests that H4K20me3 plays little to no role in the mediation of cell cycle progression and DNA repair.[275] Despite this, H4K20me3 has been identified as a hallmark of constitutive heterochromatin enriched at centromeres, thus playing an important role in the maintenance

of genomic integrity through the silencing of transposable elements.[283,284] As well as this, SUV4-20H2 has been shown to be a dominant suppressor of PEV, indicating the potential of H4K20me3 to induce heterochromatin-mediated gene silencing in euchromatic regions. As described previously, this is theorised to be the cause of the *FXN* gene silencing observed in FRDA.[168,197]

1.5.2 The Effect of Pharmacological Inhibition of SUV4-20H1 and H2

In pursuing the SUV4-20 homologues as therapeutic targets for FRDA, the effects of their genetic ablation are of particular concern with respect to chemical inhibition. One advantage of chemical probes over RNAi or CRISPR knockout is the potential for non-destructive inhibition, which permits the evaluation of any extra-catalytic protein activity, for example scaffolding or as molecular chaperones.[48] It may be the case that the defects observed in the double-null model are the result of structural deficits caused by the loss of SUV4-20, as opposed to solely H4K20me2/me3. As well as this, it is essential to make sure any compound is highly selective to avoid any unwanted off-target effects that may lead to toxicity.

A-196 is a highly potent and selective inhibitor of SUV4-20H1 (IC_{50} = 25 ± 5 nM) and H2 (IC_{50} = 114 ± 21 nM).[274] It is inactive against other KMTs at 10 µM, as well as against a panel of PRMTs and DNMTs. It also shows no activity against a range of epigenetic and non-epigenetic targets, including chromatin binders, kinases, and G-protein coupled receptors (GPCRs). It was shown to induce robust decreases in the levels of H4K20me2/me3 in human osteosarcoma (U20S) and prostate adenocarcinoma (PC-3) cell lines along with a concurrent increase in H4K20me1 but did not impair the association of SUV4-20 with chromatin. In addition, despite inducing changes in the H4K20 methylation state during the cell cycle, it was found to be non-toxic and had no effect on cellular proliferation. Treatment with **A-196** markedly inhibited 53BP1

recruitment to sites of DNA damage and greatly impaired NHEJ-mediated repair processes, however importantly had no effect on homology directed repair (HDR).[274] U2OS cells treated with **A-196** were only mildly sensitive to DNA damaging agents which is in stark contrast to SUV4-20 double-null cells, suggesting SUV4-20 may have an extra-catalytic role as a scaffolding protein that further mediates the DNA damage response. With no overt toxicity observed, and the maintenance of crucial pathways that are lost as a result of knockout, pharmacological inhibition of SUV4-20 would seem a viable route to reversing H4K20me3-induced gene silencing.

1.6 The Importance of Pharmacokinetics in Drug Design – Strategies for Optimisation

Successful library screening and target validation efforts are by no means the end of the drug discovery process; indeed, of equal importance is the modulation of the PK properties of a compound. Pharmacokinetics is defined as the time-course of a drug within the body, which involves the absorption, distribution, metabolism, and excretion of a molecule, and can be the difference between a lead compound and eventual successful drug.[285,286] Poor PK properties are a major cause of attrition in the drug discovery process, and pharmaceutical companies have broadly recognised that these need to be addressed early in the discovery process. For example, Pfizer's "three pillars of survival",[32] or Lipinski's rule of 5, a qualitative absorption and permeability predictor that states that a compound is likely to be poorly bioavailable when the molecular weight (MW) is > 500, clogP is > 5, number of H-bond donors is > 5, and the number of H-bond acceptors is > 10.[287] The finding that PK can be related to physiochemical properties allows the medicinal chemist to approach drug design with these parameters in mind and manipulate them in order to improve ADME properties.[286] Below is a

discussion of factors affecting the ADME properties of a compound and how they can be improved through structural modification.

1.6.1 Absorption

For reasons of ease and patient compliance, oral delivery of a drug is often the preferred route of administration. Good absorption of an oral drug is broadly dependent on two processes: the dissolution of the drug in the GI tract and its subsequent transfer across the membrane (Figure 1.24).[285,286]

Figure 1.24. Simplified schematic of the drug absorption process.

Dissolution of a compound depends on the surface area of the dissolving solid and the solubility of the solid at that surface.[285] The former is largely contingent on manufacturing practices, for example micronization or formulation with disintegrants, however the latter is mainly due to the structure of the drug and thus can be manipulated to be improved. Solubility is generally inversely proportional to the lipophilicity of a compound and can be enhanced by the incorporation of an ionisable centre, for example an amine functionality.[286] The transfer of a substance across a membrane is driven by its concentration in solution, and so even if the formulation can be improved low solubility will still cause problems for absorption. This may not be an issue if a compound is highly potent, as it can still achieve effective concentrations even with poor solubility.

Once in solution, compounds must then traverse the membrane of the gastrointestinal (GI) tract. While active transport processes do occur, these are usually limited to nutrient molecules and thus not particularly relevant for drug absorption.[286] There are two principal routes for the passive transfer of drugs: diffusion across the lipid membranes of cells (transcellular absorption) and diffusion through the aqueous pores at the tight junctions between cells (paracellular absorption). The latter, paracellular route of absorption is less common and of more importance for hydrophilic molecules. Given absorption via aqueous pores depends on their diameter and relatively low surface area, the molecular size is of great importance when considering the ability of polar molecules to be absorbed paracellularly. Additionally, this route is only available in the small intestine as opposed to the whole length of the GI tract, meaning the window for absorption is much smaller. The amount of drug absorbed (F_a) depends on the rate of absorption (k_a) and the rate of movement of the drug away from the site of absorption (k_m) (equation 1):[285]

$$F_a = \frac{k_a}{(k_a + k_m)} \qquad \textit{Eq. 1}$$

The paracellular pathway leads to low k_a due to the small surface area of the aqueous pores.[285] As well as this, k_m is greater due to the smaller absorption window in the small intestine. As a result, compounds that are absorbed paracellularly tend to show incomplete absorption and low F_a.

Transcellular absorption is the primary route of absorption for lipophilic molecules through the GI tract.[286] Compounds absorbed via this pathway tend to have high k_a due to good distribution into lipid membranes and a low k_m as the compound can be absorbed throughout the tract.[285] The limits of chemical space within which medicinal chemists can work to achieve good transcellular absorption are broadly defined by Lipinski's rule of 5 (*vide supra)*.[287] High

logP (>5) impacts solubility and is inherently linked to high molecular weight (>500), with heavier compounds tending towards higher logP. The hydrogen bond donor and acceptor count (>5 and >10, respectively), is related to PSA, the upper limit of which represents the point at which desolvation of the molecule to allow for membrane transfer becomes energetically unfavourable.[285] Molecular structures can be optimised with these properties in mind in order to improve transcellular absorption.

1.6.1.1 Barriers to Membrane Transfer

Within the gut epithelium are expressed various proteins that act to prevent the absorption of and thus protect the body from toxins in the diet.[286] Consequently, they can also limit the oral absorption of drug molecules through the action of metabolic enzymes and efflux transporters.[288] Glucoronyl and sulfotransferases, along with cytochrome P450 (CYP) enzymes, can metabolise substrates crossing the gut wall rapidly enough to effect F_a.[285,288] Strategies to attenuate this will be discussed in a later section (1.6.3). The efflux transporter P-glycoprotein (P-gp) acts to actively transport compounds out of the gut epithelium back into the GI tract, and due to a large overlap in their substrates is thought to work in synergy with CYP enzymes to limit oral absorption.[286,288] The recycling of substrates by P-gp back into the gut leads to repeated interactions with CYP enzymes as they subsequently re-transfer back into the epithelium. The conformational flexibility of P-gp means it can interact with a broad range of substrates;[289] it has been proposed that the number and strength of hydrogen bonding groups in a molecule can impact P-gp binding, and that introducing intramolecular hydrogen bonds can act to mask problematic groups that may subsequently be required for target engagement,[290] but the lack of clearly defined SAR means it is difficult to design molecules without substrate characteristics.[286]

Considering P-gp is a membrane transporter, any rate of efflux is intrinsically linked to the rate of passive transfer.[285] A compound that is highly membrane permeable will have a low rate of efflux, as the rate of passive transfer will be equal to or greater than the rate of transport back into the tract. The lack of P-gp recycling means the action of metabolic enzymes in the gut epithelium will also be reduced, leading to a greater degree of absorption. As a result, poorly permeable compounds tend to be better substrates for P-gp and thus suffer from a greater degree of metabolism, leading to poor absorption.[286] With this is mind, the strategies outlined above for improving membrane permeation are also of importance in avoiding these barriers to membrane transfer: modulation of lipophilicity, molecular size, and PSA.

1.6.2 Distribution

Following oral administration, and after absorption via the intestinal lumen and through the portal vein and liver, drugs then reach the systemic circulation before being further distributed into various tissues and organs via the vasculature. Distribution can be thought of as essentially another passive transfer process, and thus the same properties that affect absorption also affect distribution.[291] The body can be considered as being made up of a number of pharmacokinetically distinct “compartments”, which permits the modelling of drug transport actively occurring across membranes between organs and tissues via blood vessels.[292] Post-administration, if a drug is rapidly distributed throughout the body then the body is represented as a single, pharmacokinetically homogenous compartment. This single compartment model assumes immediate distribution to tissues and an equilibrium establishing constant concentration ratios between the plasma and tissues. This means the

rate of change in tissue concentration of a drug is directly related to the change in plasma concentration, which will show a linear, monophasic decline a on a semilogarithmic scale.

If a drug is less rapidly distributed to certain tissues, then the body can be considered in terms of a multicompartment model: a central compartment representing the plasma and highly perfused organs and tissues; and a peripheral compartment representing weakly perfused organs and tissues.[292] It is assumed that a drug will be distributed much faster to highly perfused organs such as the liver, lungs, or kidneys compared to weakly perfused tissues such as muscle or bone. As a result, the plasma concentration of a drug will show a multiphasic decline on a semilogarithmic scale dependent on the number of compartments in the model, for example biphasic decline in a two-compartment model.[292] In this instance, the initial phase represents the distribution of the drug into the tissues and the latter stage the elimination from the body. The concentration of the drug in tissues increases during the distribution phase before the distribution equilibrium is reached where the ratios between plasma and tissue concentrations become constant, and levels of the drug in the tissue decrease at the same rate as the plasma (Figure 1.25).[293]

1.6.2.1 Volume of Distribution

The volume of distribution at steady state (V_{ss}) represents the apparent volume a drug is distributed into based on its measured concentration in the plasma and the administered dose.[293] It is a theoretical value that assumes that the drug is in equal concentrations in the plasma and the tissue, and thus represents what volume of tissue is required to give the concentration measured in the plasma based on the dose.[291] The V_{ss} values of drugs are typically compared to the volumes of various physiological compartments, for example the plasma, total body water, and tissues (Figure 1.26). For a drug, the theoretical value gives

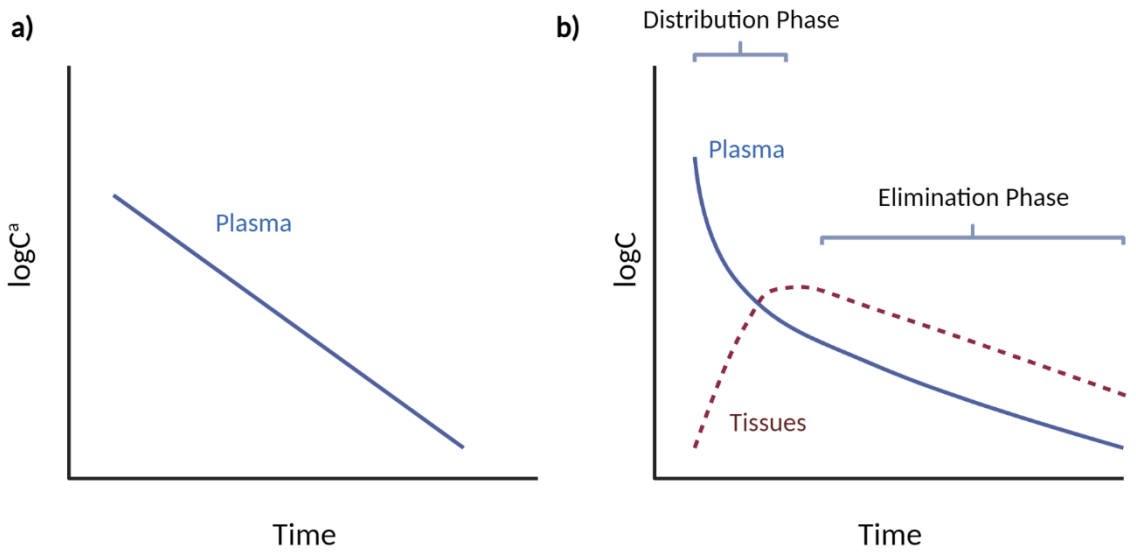

Figure 1.25. Change in drug concentration over time in plasma and tissues considering both single- and multi-compartment modelling. In the single-compartment model (**a**), the drug is instantaneously distributed to the tissues once in enters systemic circulation, and concentration ratios immediately reach equilibrium between the plasma and the tissue. In the multi-compartment model (**b**), the drug is slowly distributed to the tissues and the initial decline in plasma concentration is matched by an increase in tissue concentration. Once the distribution equilibrium is reached, the concentrations decline at the same rate.

some indication as to where it is mainly distributed within the body; for example a V_{ss} of 2 L/kg would suggest a compound is highly distributed to the tissues.

The basis for the V_{ss} of a compound derives from equation 2, relating the physiological volumes of the plasma (V_p) and tissues (V_t) to the relative unbound fraction of the drug in each (fu_p and fu_t, respectively).[293]

$$V_{ss} = V_p + \left(\frac{fu_p}{fu_t}\right) V_t \qquad \textit{Eq.2}$$

The dependence on the fu_t term is the reason why some drugs exhibit a theoretical V_{ss} that is far higher than any known physiological volume.[293] The extent of tissue binding largely tracks

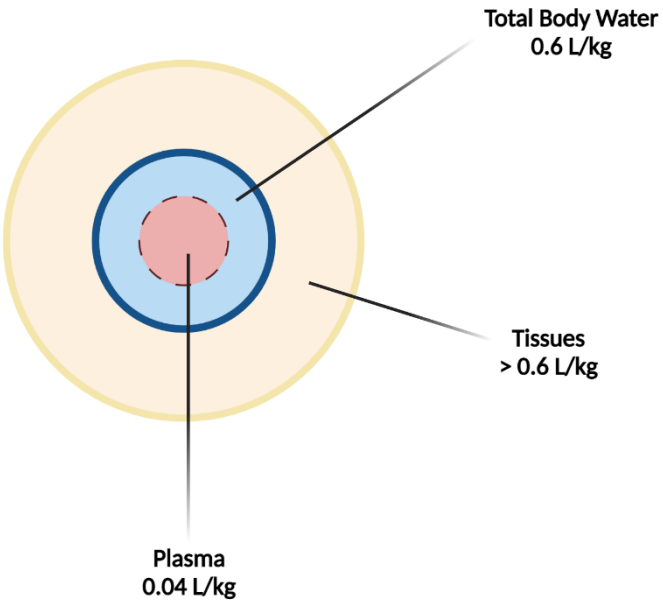

Figure 1.26. The physiological volumes of body compartments in humans (body weight 70kg, adapted from Smith *et al.).*[293]

with lipophilicity, however the greatest determinant of volume of distribution is the acidic or basic character of the molecule. Acidic compounds are negatively charged at physiological pH and thus interact with lysine-rich albumin in the plasma, leading to high plasma protein binding (low fu_p). As well as this, they do not interact with the negatively charged phospholipid head groups of tissue membranes (high fu_t). As a result, acids tend to have low volumes of distribution in the range of 0.1-0.4 L/kg. By contrast, basic compounds are positively charged at physiological pH and so accumulate in phospholipid membranes due to charge interactions with the head groups (low fu_t). Similarly, they display a low degree of plasma protein binding (high fu_p) leading to high volumes of distribution in the range of 1-25 L/kg.[293] Neutral molecules partition into membranes as a function of their lipophilicity and thus display volumes of distribution in the range of 0.7-4 L/kg.

The importance of V_{ss} is not in determining whether a drug will reach its site of action: low V_{ss} does not mean that a drug will remain in the plasma and not enter the tissues, and similarly

high V_{ss} does not necessarily mean a drug will be more active at target sites in the tissues.[293] The high dependence of V_{ss} on tissue and plasma protein binding means differences in values between compounds bear almost no relation to their relative unbound aqueous concentrations. Indeed, when corrected for the fraction unbound in the plasma ($V_{ss,u}$, equation 3), the volumes of distribution show that compounds with equivalent unbound aqueous concentrations show the same ability to partition into tissues, regardless of differences in V_{ss}. As a result, a compound will interact with its target based on dose, clearance of the drug from the circulation, and its pharmacology at the site of action.[292,293]

$$V_{ss,u} = \frac{V_{ss}}{fu_p} \qquad \textit{Eq.3}$$

Where V_{ss} is critical in drug design is in determining the duration of action of a compound through its relationship to half-life ($t_{1/2}$).[293,294] Half-life is the time taken for the concentration of a drug to fall to half of its original value, when the concentration is in simple exponential decline. It is a key parameter to consider when deciding the dosing frequency of a drug as it will determine the duration of action. When considered in the context of the single compartment model (*vide supra*), half-life can be related to the volume of distribution through equation 4, where CL is the clearance of the drug, defined as the irreversible removal of a drug from the measured matrix.[295]

$$t_{1/2} = \ln(2)\left(\frac{V_{ss}}{CL}\right) \qquad \textit{Eq. 4}$$

Half-life is thus directly proportional to the volume of distribution, and so the duration of action can be directly influenced by modulation of V_{ss}. In the context of a multi-compartment model, the picture becomes a little murkier due to the multiphasic nature of the decline in concentration (Figure 1.25). As a result, half-life becomes a function of the terminal

elimination rate (β, equation 5), which is the rate of decline following distribution equilibrium (for example the second phase of decline in a biphasic model).[294] Despite the increased complexity in determining β, it still closely approximates to CL/V_{ss}, and thus the relationship of volume of distribution to half-life remains largely the same as in the single compartment model (equation 5):

$$t_{1/2} = \frac{\ln(2)}{\beta} \qquad \textit{Eq. 5}$$

As described above, V_{ss} is largely a measure of tissue binding and so is most heavily influenced by the degree of acidic or basic character.[293] Increasing V_{ss} will lead to an increase in half-life as shown by equation 4, and so the introduction of a basic functionality can be used as a strategy to improve duration of action through an increase in V_{ss}. This strategy is famously exemplified in the design of the calcium channel blocker **amlodipine** (Figure 1.27), which was derived from an earlier drug **nifedipine** (Figure 1.27).[296,297] The introduction of the basic amine centre vastly increased the V_{ss} of **amlodipine** over **nifedipine**, which led to a far higher terminal half-life despite no change in rate of clearance. This allows **amlodipine** to be dosed once daily, compared to four times a day for **nifedipine**.[293] An attractive strategy for improving half-life, it will also bring improvements in aqueous solubility. However, it may lead to a loss of selectivity and an increased affinity for ion channels which could lead to toxicity, for example in the case of binding to the hERG channel.

A second means of increasing V_{ss} is through modulation of lipophilicity.[293] Whilst an increase in logP tends to increase V_{ss}, it can also increase CL which will negate any gains in duration of action. The strategy of blocking sites of metabolism to reduce clearance will be discussed in a later section (1.6.3), however the deliberate use of particular functional groups can achieve this whilst also increasing V_{ss}. Specifically, the introduction of a methylcyclopropyl group as in

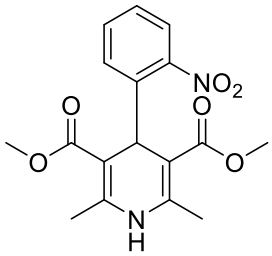

Nifedipine

$\mathbf{V_{ss}}$ = 0.79 L/kg
CL = 7.3 mL min^{-1} kg^{-1}
$\mathbf{t_{1/2}}$ = 1.9 hrs

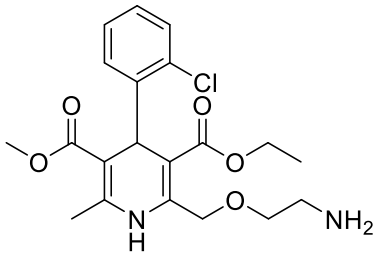

Amlodipine

$\mathbf{V_{ss}}$ = 17 L/kg
CL = 7.0 mL min^{-1} kg^{-1}
$\mathbf{t_{1/2}}$ = 34 hrs

Figure 1.27. **Nifedipine** and **amlodipine** and their respective PK parameters, highlighting the effect of introducing a basic centre in increasing V_{ss} and terminal half-life.

the case of β-blocker **betaxolol** (Figure 1.28) has the effect of both blocking metabolism (reducing CL) whilst increasing lipophilicity and thus V_{ss}.[293,298] This leads to an approximately four-fold increase in half-life over the related **metoprolol** (Figure 1.28).

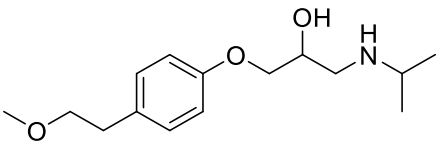

Metoprolol

$\mathbf{V_{ss}}$ = 3.1 L/kg
CL = 13 mL min^{-1} kg^{-1}
$\mathbf{t_{1/2}}$ = 3.6 hrs

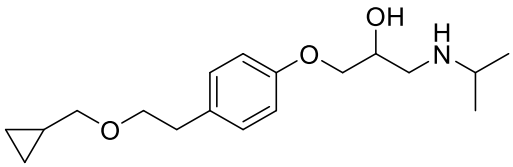

Betaxolol

$\mathbf{V_{ss}}$ = 4.8 L/kg
CL = 3.4 mL min^{-1} kg^{-1}
$\mathbf{t_{1/2}}$ = 17 hrs

Figure 1.28. Substitution of the methyl group in **metoprolol** with the methylcyclopropyl of **betaxolol** leads to an increase in V_{ss} and an accompanying decrease in CL, leading to improved duration of action.

Although of critical importance as a pharmacokinetic parameter, and integral in determining duration of drug action, modulation of volume of distribution is not typically the first resort

when attempting to improve half-life.[286,293,294] Structural modifications that induce the greatest changes in V_{ss} (e.g., introducing a basic functionality) tend to be accompanied by changes in other parameters such as selectivity and potency. Despite this, intelligent design of molecules to exploit changes in V_{ss} can be of great use to the medicinal chemist where changes in duration of action are required.

1.6.2.2 Achieving CNS Penetrance - Crossing the Blood Brain Barrier

The BBB is a term used to describe the structure of the vasculature associated with the CNS.[299,300] It tightly controls the movement of molecules and ions into and out of the CNS and is essential in maintaining CNS homeostasis, providing a stable environment for neural function. The BBB consists of a physical barrier and a transport barrier:[300] the physical barrier is formed by extremely tight junctions between endothelial cells that surround the capillaries - these tight junctions effectively prevent the paracellular absorption of compounds and block the diffusion of ions and other polar molecules into the CNS. The transport barrier, similar to that of the gut, involves the action of efflux transporters (such as P-gp) that actively pump molecules out of the brain capillary endothelium and CNS. Conversely, there are a large number of solute carriers (SLCs) in the endothelium that act to transport essential, polar molecules (such as amino acids and glucose) into the CNS that would otherwise be blocked due to the barrier to paracellular absorption.

The ability of molecules to cross the BBB and distribute into the CNS is of crucial importance to the medicinal chemist. For non-CNS disorders, a drug that crosses the BBB can induce unwanted CNS side-effects, for example in the case of some lipophilic β-blockers.[301] For CNS disorders such as FRDA, it is of crucial importance that a drug can cross the BBB in order to exert its effect at the desired site of action. In order to better identify compounds that would

distribute into the CNS, scientists at Pfizer developed a CNS multiparameter optimisation (MPO) score to enable a flexible approach to drug design based on six key physiochemical properties.[302,303] Through analysis of a set of marketed CNS drugs and various internal CNS candidates, they identified the optimal ranges for CNS-penetrant compounds of clogP, clogD, molecular weight (MW), tPSA, number of hydrogen bond donors (HBD), and the pK_a of the most basic centre (Table 1.1).[303] These were all assigned equal weight and a score between 0 and 1, giving compounds an additive score between 0 and 6, with higher scores indicating a higher likelihood of CNS penetrance. As might be expected given the factors affecting volume of distribution described above, greater weight is given to lipophilicity (clogP and clogD), and basicity (pK_a and clogD). As a result, the medicinal chemist can tailor the design of their molecules in order to find the best alignment of these properties in order to enable (or prevent) sufficient CNS penetrance for drug action.

Table 1.1. The optimal ranges for CNS penetrance of six properties identified as part of a CNS MPO score (adapted from Wager *et al.*)[303]

Property	***Desirable Range***	***Undesirable Range***
clogP	≤ 3	> 5
clogD	≤ 2	> 4
MW	≤ 360	> 500
tPSA	40 < TPSA ≤ 90	TPSA ≤ 20; TPSA > 120
HBD	≤ 0.5	> 3.5
pK_a	≤ 8	> 10

1.6.3 Clearance

Clearance is perhaps the most important of the PK parameters to consider in drug design and concerns the final two ADME processes: metabolism and excretion. As described above, clearance is defined as the irreversible removal of a compound from a measured matrix, whether by structural modification or complete elimination from the body.[295] Clearance links the rate of elimination of a drug to its measured concentration and is given in units of volume per time which reflects the volume of matrix (e.g., blood or plasma) that is effectively cleared of a drug per unit time. It is of critical importance in determining the half-life of a compound (equation 4), and to assess the availability and predict the steady state concentration of a compound following a particular route of administration.[304]

The liver and kidneys are the two major organs concerned with this process, with hepatic clearance playing a key role.[295] Before entering the systemic circulation compounds absorbed via the GI tract first pass through the highly perfused liver, where they can be immediately cleared via the "first-pass effect".[304,305] This is the elimination of a drug following initial absorption and perfusion into the liver, and it can have a significant effect on the oral bioavailability of a compound (Figure 1.29).

Quantification of this process relies on the "well-stirred" model of drug clearance, which assumes that the liver (or organ of clearance) is a single, well-stirred compartment where the concentration of unbound drug is in equilibrium with that of the blood.[304] Another important assumption of this model, and for clearance generally, is that only unbound drug can traverse membranes and thus only unbound drug is available for clearance. This model relates clearance (CL) to the blood flow to the organ (Q), the unbound fraction available for clearance (f_u), and the intrinsic ability of the organ to clear drug independent of flow or binding

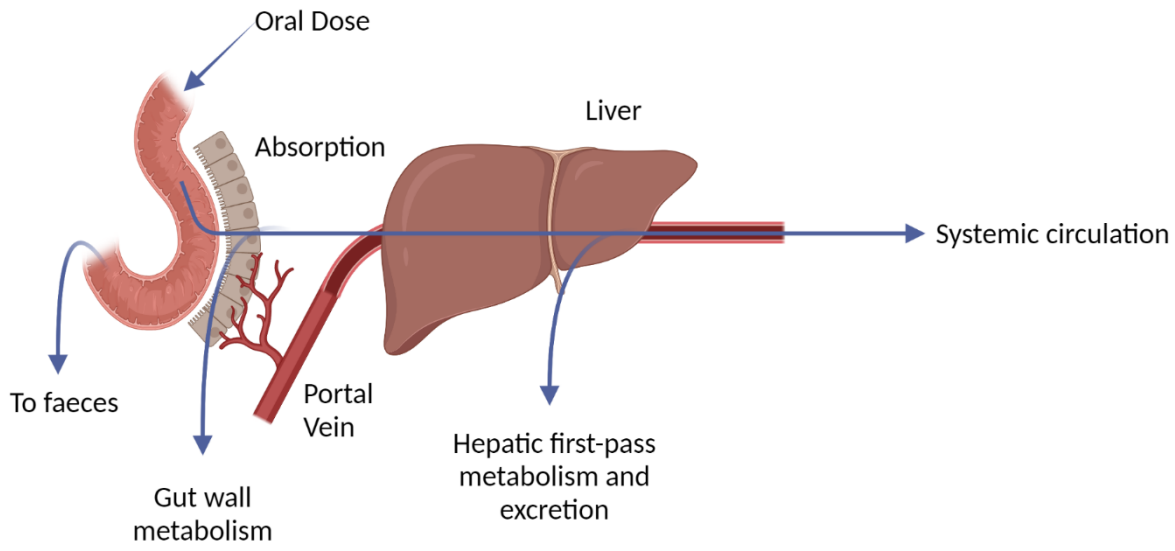

Figure 1.29. The first-pass effect: drugs are absorbed via the GI tract where they pass via the portal vein to the liver. A proportion of the dose absorbed is immediately eliminated as a result of first-pass extraction.

limitations ($CL_{int,u}$) (equation 6).

$$CL = \frac{(Q \times f_u \times CL_{int,u})}{(Q + f_u \times CL_{int,u})} \qquad \textit{Eq. 6}$$

This model can be combined with factors affecting oral bioavailability in order to derive an equation that describes how clearance affects dosing (equation 7).[295] It relates the steady state unbound concentration ($C_{ss,av,u}$), unbound intrinsic clearance ($CL_{int,u}$), dosing interval (τ), fraction absorbed (F_a) and the fraction that escapes gut wall extraction (F_g):

$$dose = \frac{C_{ss,av,u} \times CL_{int,u} \times \tau}{F_a \times F_g} \qquad \textit{Eq.7}$$

Considering equations 4 and 7, of critical importance for the medicinal chemist in drug design is a focus on reducing clearance to improve half-life and lower the required dose. Understanding the processes involved in drug clearance is thus important in order to guide strategies aimed at achieving this.

1.6.3.1 Metabolism

Drug metabolism is a biotransformative process that increases the polarity of a molecule to permit its excretion via the urine or bile.[306] Conventionally, metabolism is separated into two, chronologically distinct process. Phase I metabolism involves oxidative processes that introduce a functional handle which is subsequently employed in conjugative, phase II reactions to introduce a polar substituent that enables excretion. This is not definitive, as many compounds undergo phase II metabolism without any need for prior oxidative processes, however phase I reactions occupy a pivotal role in the metabolism of drugs.[306]

The aforementioned CYP family of enzymes play a central role in regulating phase I metabolism and are present in both the gut wall and the liver.[306] A heme containing superfamily, they catalyse the insertion of an oxygen atom into a drug molecule across a range of substrates, with varying degrees of selectivity between isoenzymes. A formal $(FeO)^{3+}$ species mediates a one-electron oxidation via the abstraction of protons or electrons, followed by the combination of the substrate radical with an hydroxyl radical to form the oxidised metabolite.[307] Of the main isoforms involved in oxidative metabolism, CYP3A4 is responsible for the metabolism of approximately 45% of known drugs.[308] The factors that govern interactions with CYP3A4, and CYP enzymes generally, are broadly the same factors important for permeability, namely increased lipophilicity correlates with increased metabolism and clearance.[295] As a result, a global reduction in logP can lead to reduced clearance, however given the similarly positive correlation between lipophilicity and potency at a target this may be at the expense of efficacy.

More targeted strategies are available to the medicinal chemist. The main approach to preventing metabolism and lowering clearance involves incorporating stable functional

groups at metabolically labile sites in order to block oxidation reactions.[309,310] The position of these so-called metabolic "soft-spots" is largely determined by the ease of proton or electron abstraction, and the stability of the resulting radical.[306] Benzylic and allylic positions, as well as the *para*-position of aromatic rings, are particularly prone to oxidation, and heteroatoms will commonly undergo dealkylation reactions (Figure 1.30). Attempting to prevent these reactions can be difficult as the SAR at the CYP enzyme has to also be considered in the context of the SAR at the target. The use of bioisosteres as replacements for certain labile moieties enables the effective modulation of metabolism whilst maintaining potency.[311] Bioisosteres are defined as compounds that elicit the same biological effect, and in recent years the development of novel bioisosteres has seen widespread application in medicinal chemistry.

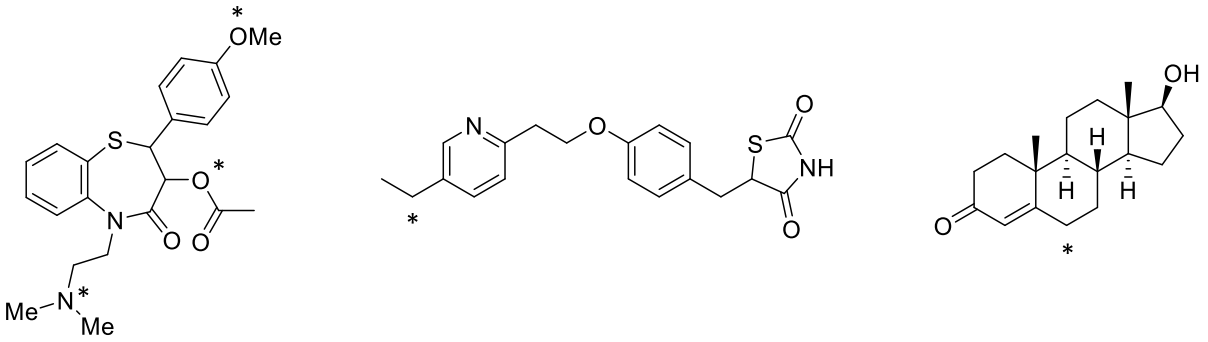

Dilitazem **Pioglitazone** **Testosterone**

Figure 1.30. Known drug molecules and their metabolic "soft-spots" (asterisked).

Perhaps the most classic example of bioisosteric replacement is the substitution of hydrogen with fluorine, exploiting the strength of the C—F bond to achieve metabolic stability.[312] The electronegativity of fluorine can also be used to modulate the basicity (or acidity) of neighbouring sites, particularly in instances where pK_a modulation can induce changes in PK, for example in CNS penetrance.[311] Finally, the polarity of the C—F bond can induce conformational changes, for example through intramolecular electrostatic interactions, that

constrain the molecule in such a way that it does not effectively bind to the active site of metabolic enzymes.

The ways in which fluorine modulates metabolism are largely the main focus of other strategies: blocking metabolically labile positions with stronger bonds; the introduction of heteroatoms to modulate the electronics and lipophilicity of a substrate rendering it less susceptible to oxidation; and introducing steric or conformational changes that constrain the molecule in a way that is unfavourable to metabolic pathways, for example chirality or bicyclic, three-dimensional structures.[309]

Drug design to modulate phase II metabolic processes is somewhat more difficult as they primarily follow phase I processes and therefore cannot be affected. However, in cases where conjugative reactions take place initially, there are strategies to avoid this. The main conjugative enzymes are the glucuronosyl transferases and the sulfotransferases, which catalyse the addition of a glucuronide or sulfo group respectively.[306] To facilitate this process, a nucleophilic functionality is required in the substrate, typically a phenol or other hydroxyl component, and conjugation usually renders the compound inactive. As a result, strategies to prevent this involve removing the nucleophilic component unless essential for activity. If essential, it may be possible to replace the hydroxyl group with another H-bond donor that is not susceptible to conjugation, to introduce neighbouring functionalities that modulate the nucleophilicity, or to again constrain the molecule in a way that is unfavourable to the enzymes.[306,309]

1.6.3.2 Excretion

Drug excretion refers to the removal of the drug from the body.[313] As described above, compounds usually undergo biotransformation via metabolic processes in order to render

them more hydrophilic to enable effective excretion. If a compound is sufficiently hydrophilic then it may undergo direct excretion into the urine as the unchanged parent molecule.

Whilst the liver is the primary organ of clearance, hepatobiliary excretion is not the major route of drug removal.[295,305] It tends to be an active process, whereby transporter proteins recognise poorly permeable compounds and promote their uptake into hepatocytes. Once inside, bile canicular transporters then act to secrete the compound into the bile following which it returns to the gut and can be excreted in the faeces.[314] Compounds that can passively cross membranes tend to be exclusively cleared by metabolism, and although are sometimes secreted into the bile they are largely removed to the blood for excretion in urine.[295] Biliary excretion can lead to a process called enterohepatic recirculation, whereby a compound that has been secreted into the bile and passed back into the GI tract can be reabsorbed via the intestine and re-enter the systemic circulation.[315] This can significantly impact measures of bioavailability and clearance, and may prolong the pharmacological effect of certain compounds.

The primary route of excretion, either for a parent compound or its metabolite, is renally via the urine.[316] After a compound is absorbed into the systemic circulation, or a drug metabolite is removed from the liver into the blood, blood is filtered at the glomerulus of the kidney in the first step of urine formation, and any unbound compound present will enter the proximal convoluted tubule before passing into the bladder. Once in the tubule however, lipophilic compounds can be almost fully passively reabsorbed back into the blood and will experience little to no immediate renal clearance. On the other hand, poorly permeable polar molecules ($\log D < 0$) will experience a large degree of renal clearance at rates approaching that of the blood flow to the glomeruli (glomerular filtration rate, GFR), which is approximately 1-2 mL

min^{-1} kg^{-1}.[305] Compounds can also be actively transported into the tubules, which can lead to clearance rates higher than that of GFR.

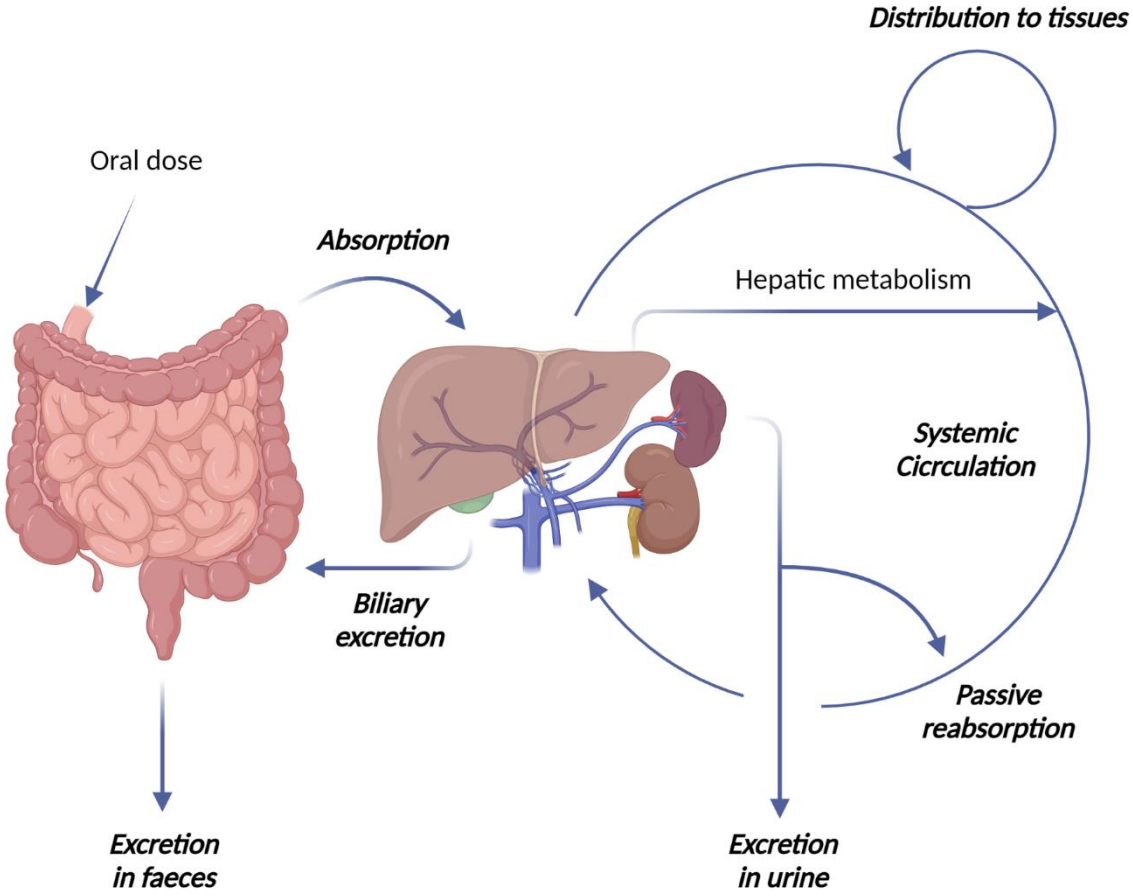

Figure 1.31. ADME processes within the body

Given clearance is of critical importance, it would seem advantageous to design hydrophilic compounds and drive them towards renal excretion pathways, where rates tend not to exceed the GFR. This is far lower than the rates that can be observed with metabolic clearance pathways that predominate as lipophilicity increases.[305] However, a decrease in lipophilicity has implications for both pharmacodynamics and the PK parameters described above, namely: low passive permeability can lead to a decrease in potency due to poor access to intracellular targets; absorption will rely heavily on the paracellular pathway which can lead to incomplete absorption and low F_a (equation 1); V_{ss} will decrease which will lead to a shorter

elimination half-life (equation 4); and finally, as PSA increases, active transport processes play a more prominent role in clearance which can increase CL and thus decrease half-life as well (equation 4). However, the converse approach does not necessarily solve the problem: favouring more lipophilic molecules to improve potency will invariably also cause issues for various PK parameters such as clearance, as well as reducing solubility and thus absorption.[305] It is clear that drug design must focus on the interplay of all these properties and attempt to develop an SAR that balances absorption, distribution, clearance, and potency (Figure 1.31).

1.7 THESIS AIMS

The objective of the work presented in this thesis was to develop small molecule modulators of frataxin expression as potential treatments for Friedreich's ataxia (FRDA). Two strategies were employed in approaching this challenge: firstly, manipulation of the epigenome. **A-196** provides an excellent small-molecule starting point for hit-to-lead optimisation aimed at the development of a therapeutic. The first section of this thesis describes efforts to improve the PK characteristics of **A-196**, primarily its metabolic stability in a manner outlined above, in order to carry out *in vivo* efficacy studies.

The second part of the thesis concerns the conceptualisation of and initial efforts towards the development of a heterobifunctional molecule for the targeted stabilisation of frataxin. Inducing the proximity of a deubiquitinase to frataxin will lead to its deubiquitination and prevent its degradation by the proteasome, leading to increased intracellular levels. Initial attempts to develop a deubiquitinase recruiting ligand are described as well as future prospects for the technology.

2 INCREASING FRATAXIN EXPRESSION THROUGH MODULATION OF THE EPIGENOME – TOWARDS AN *IN VIVO* SUV420 INHIBITOR

2.1 PROJECT ORIGIN – THE PROMISE OF A CHEMICAL PROBE

The use of a "target-agnostic" epigenetic library screen against a cell model of FRDA is an excellent example of how this strategy can accelerate the drug discovery process. **A-196** was found to be a potent up-regulator of frataxin expression,[130] and due to its well defined pharmacology SUV4-20 was identified a potential therapeutic target.[274] Knockdown experiments that showed that the decrease in H4K20 di- and tri-methylation induced by SUV4-20 abrogation led to a concomitant increase in frataxin expression, further validating the choice of target.[130]

The promise of **A-196** as a potential therapeutic prompted evaluation of its PK properties to assess its suitability for *in vivo* studies. In mouse liver microsomes (MLM), **A-196** was highly cleared at a rate of 240 µL min^{-1} mg $protein^{-1}$, with a half-life of 6 minutes (Table 2.1). A similarly high rate of clearance was observed in human liver microsomes (HLM), 190 µL min^{-1} mg $protein^{-1}$, along with a half-life of 7 minutes (Table 2.1). The substantial metabolic instability of **A-196** precludes its use *in vivo*; although highly potent and selective, it would be challenging to achieve a high enough dose to ensure a sufficient circulating concentration. For a compound to be suitable for *in vivo* efficacy studies it would preferably possess the target product profile (TPP) outlined in Table 2.1, derived as a means of ensuring compound potency and ADME properties that would enable a low enough dose to avoid off-target toxicity whilst maintaining on-target activity. Given the desired TPP, the primary aim of this project was to improve the metabolic stability of **A-196** to enable its use *in vivo*. In addition, to improve its on-target and cellular potency whilst maintaining a high degree of selectivity over other

methyltransferases. Finally, to develop a compound with suitable physiochemical properties to enable oral dosing.

Table 2.1. The required target product profile (TPP) of an *in vivo* SUV4-20 inhibitor compared to the profile of **A-196.** [a]Measurement of the rate of apical to basolateral (AB) transfer across a monolayer of Caco-2 cells; [b]Assessment of transport in both directions (apical to basolateral (AB) and basolateral to apical (BA)) across a Caco-2 cell monolayer to calculate an efflux ratio (BA/AB) and indicate whether a compound undergoes active efflux; [c]Oral bioavailability; [d]Hepatic blood flow rate; [e]Minimum ratio of compound concentration in the brain vs plasma; [f]Minimum desired unbound concentration in the brain.

Potency and Selectivity	**TPP**	**A-196**
SUV4-20 IC_{50} (nM)	20	25 (H1) 144 (H2)
SUV4-20 cellular IC_{50} (nM)	100	262 (H1) 370 (H2)
FXN Expression EC_{50} (nM)	100	5200
Methyltransferase selectivity	50x	50x
In Vitro ADME		
HLM $t_{1/2}$ (min)	60	7.3
CL_{Int} (µL min^{-1} mg $protein^{-1}$)	1	191
MLM $t_{1/2}$ (min)	60	5.8
CL_{Int} (µL min^{-1} mg $protein^{-1}$)	1	239
Caco-2 AB (10 nm/s)[a]	4	
Caco-2 BA/AB[b]	2.5	
Solubility	sufficient for *in vivo* use	
***In Vivo* PK (rodent)**		
F%[c]	50%	
Cl (ml/min/kg)	25% Q_H[d]	
$T_{1/2}$ (h)	6	
C_{brain}/C_{plasma}[e]	1	
$C_{min}(brain_u)$[f]	3x FXN-Luc reporter EC_{50}	

2.2 Improving the Metabolic Stability of A-196

At first glance, the obvious metabolic liability of **A-196** is the lipophilic cyclopentyl moiety which would likely be a substrate for CYP-mediated oxidative metabolism. Secondly, the pyridyl moiety may be subject to oxidation by aldehyde oxidase (AO) *ortho* to the nitrogen.[317] Finally, the 6,7-dichloro substituted planar aromatic core, coupled with the cyclopentane ring, contributes to an overall high clogP which will drive up clearance. Metabolite profiling of **A-196** found that 17% of the parent compound remained after 60 minutes, with four major metabolites identified (Figure 2.1). Metabolite 1 (**M1**) and metabolite 2 (**M2**) corresponded to hydroxylation products on the cyclopentane ring, with metabolite 3 (**M3**) the product of further oxidation to the ketone. Metabolite 4 (**M4**) was the product of pyridyl transformation however not due to AO. Interestingly, an adduct was observed to have formed between the pyridine nitrogen and the ribose ring of adenine dinucleotide phosphate (ADP)-ribose. This transformation has previously been reported with the protein tyrosine kinase inhibitor **imatinib**, although it was noted that this primarily occurred after incubation with rat liver microsomes and in human microsomes only trace levels were detected.[318] Nevertheless, the transfer of ADP-ribose to various acceptors has been shown to be an important step in the regulation of intracellular Ca^{2+} release, and is controlled by a class of enzyme called nicotinamide adenine dinucleotide (NAD^+) glycohydrolases.[319] These catalyse the conversion of NAD^+ into nicotinamide and ADP-ribose, the latter of which can then be transferred to acceptors such as water, methanol, and pyridine. In this case, **A-196** may be interacting with a glycohydrolase and intercepting this pathway, leading to its clearance. However, the transformation seems to be a result of assessment in rat microsomes, and so whilst worthy of consideration, will remain a secondary focus of the approach to reducing metabolism.

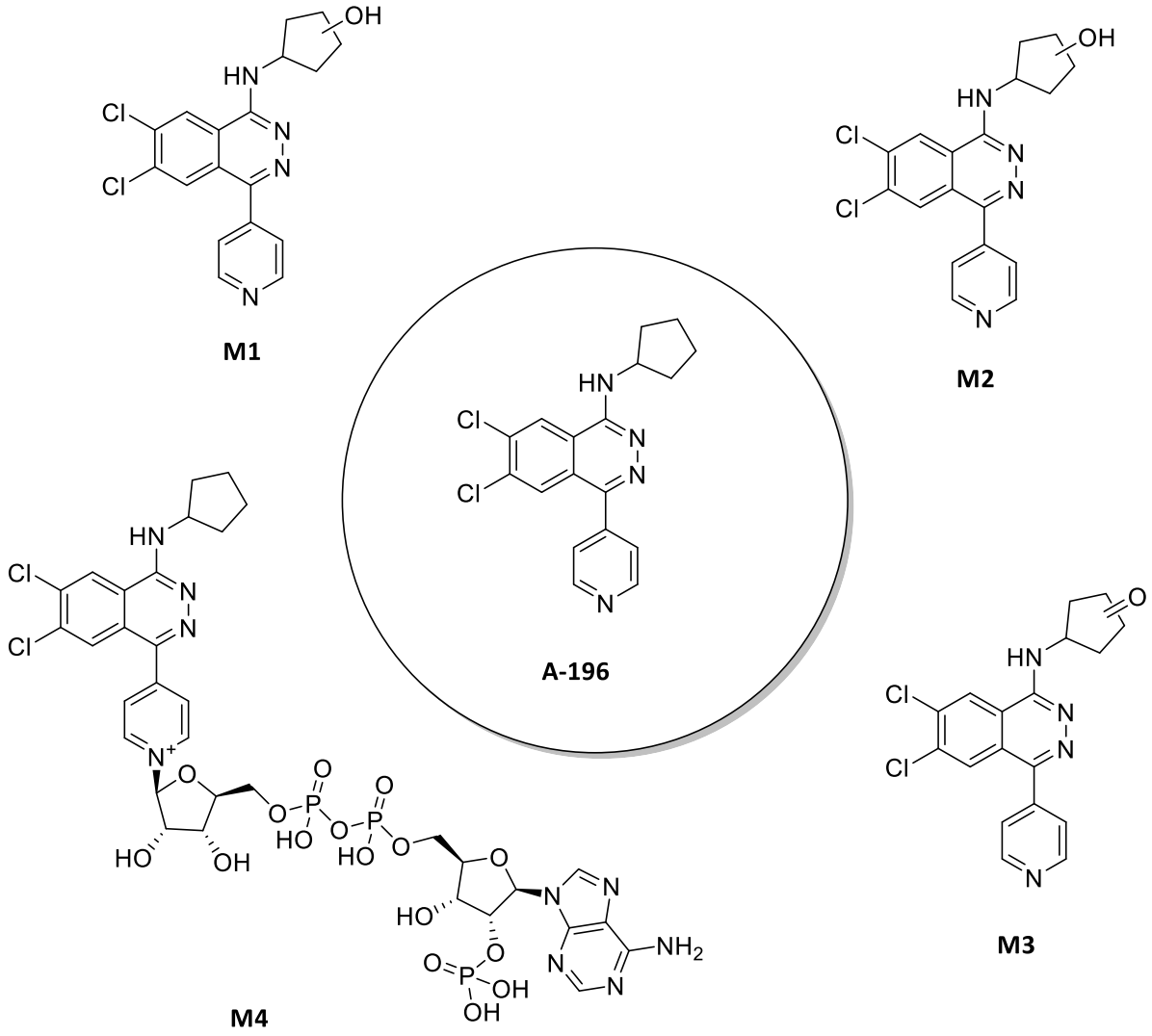

Figure 2.1. Metabolite profiling identified the cyclopentyl group of **A-196** as the primary site of oxidative metabolism (**M1, M2, M3**), as well as the formation of an adenine dinucleotide phosphate (ADP)-ribose conjugate between the pyridine nitrogen of **A-196** and the ribose of ADP (**M4**).

2.2.1 A-196 Structure-Activity Relationship

The three main stated aims of the project were: improving the metabolic stability of **A-196**; improving its on-target and cellular potency; and developing a compound with suitable physiochemical properties to enable oral dosing. An understanding of the SAR around **A-196** would therefore be crucial to achieving this and guiding analogue design. Its discovery stemmed from a quinoline-based high throughput screen (HTS) hit **7**, which inhibited SUV4-

20 H1 and H2 with IC_{50}s of 5.9 μM and 4.8 μM, respectively.[274] The introduction of a second chlorine atom led to a ten-fold jump in potency against SUV4-20H1 (**8**), before changing the central core to a phthalazine and introducing a pyridyl substituent yielded **A-196** (Figure 2.2.)

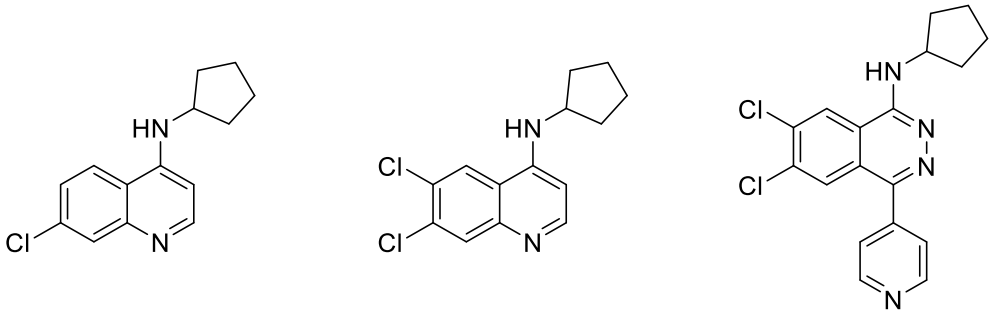

7	**8**	**A-196**
SUV4-20H1 IC_{50} = 5.9 μM	SUV4-20H1 IC_{50} = 0.59 μM	SUV4-20H1 IC_{50} = 0.025 μM
SUV4-20H1 IC_{50} = 4.8 μM	SUV4-20H1 IC_{50} = 1.2 μM	SUV4-20H1 IC_{50} = 0.144 μM

Figure 2.2. The discovery of **A-196** from initial quinoline hit.

A-196 is a substrate competitive inhibitor and binds to the histone H4-peptide binding groove of SUV4-20.[274] The key interaction is a hydrogen bond between the amine of **A-196** and an active site water molecule that is simultaneously hydrogen bonded to the catalytic serine (Ser251) (Figure 2.3). This occupies the position where the nitrogen of the methylated lysine would lie and blocks access to the residue. Methylation of the amine nitrogen leads to a complete loss of activity and forms the inactive control (**SGC2043**, Figure 2.4). Met253 rotates out of the binding site to accommodate the cyclopentane ring which engages in various van der Waals interactions with the surrounding hydrophobic residues. The phthalazine core sits in a π-sandwich between Trp264 and Phe281, a result of Trp264 and Ile231 rotating to form a binding pocket that the backbone chlorines tightly fill. Finally, the pyridyl nitrogen forms a hydrogen bond to another water molecule and is somewhat solvent exposed.

Analysis of the patent literature surrounding **A-196** paints a limited picture of its SAR.[320] Excluding the brief description of its discovery by Bromberg *et al.,*[274] there is no data available concerning modification of the cyclopentyl (R1, Figure 2.4) or chloro (R2 and R3, Figure 2.4) substituents, nor is there any information regarding changes to the phthalazine core. Only changes to the pyridyl substituent (R4, Figure 2.4) have been extensively characterised, although the SAR around these changes is difficult to distil.

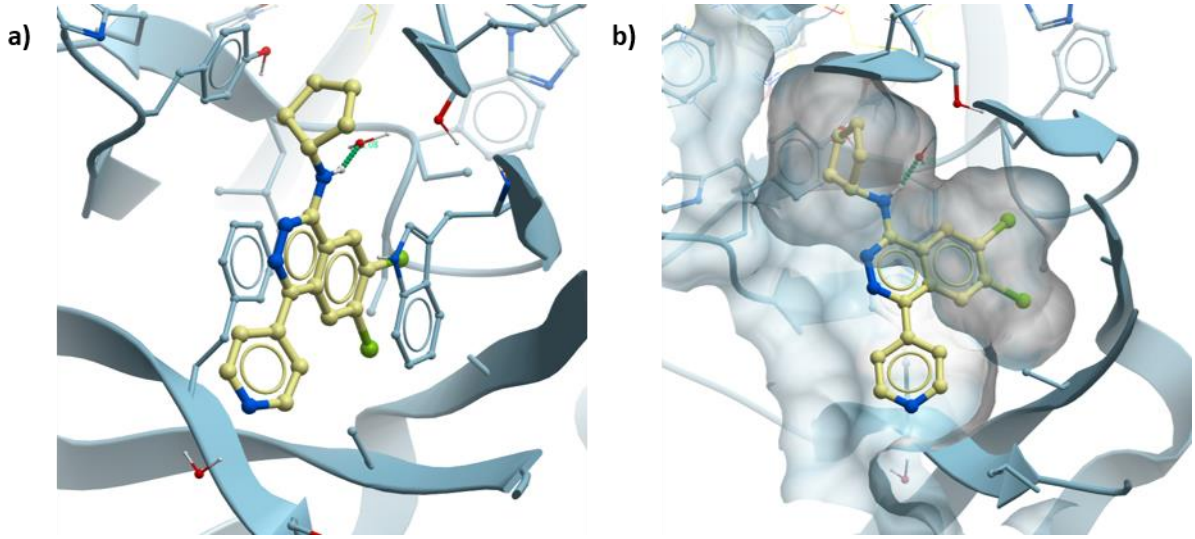

Figure 2.3. Crystal structures showing the binding mode of **A-196** to SUV4-20: **a) A-196** sits between Trp264 and Phe281, with the amine nitrogen forming a hydrogen bond with an active site water; **b)** The binding pocket occupancy of **A-196**: The cyclopentyl ring sits in a hydrophobic pocket whilst the pyridine is solvent exposed. The two chlorine substituents tightly occupy a hydrophobic region at the back of the pocket (PDB: 5CPR).

Largely, heterocycles such as thiopene, pyrazole, and various substituted pyridines are well tolerated. Pyrrolidine and morpholine-based substituents are poorly tolerated, whilst piperidines and piperazines show good potencies. Smaller aryl substituents with a hydrogen

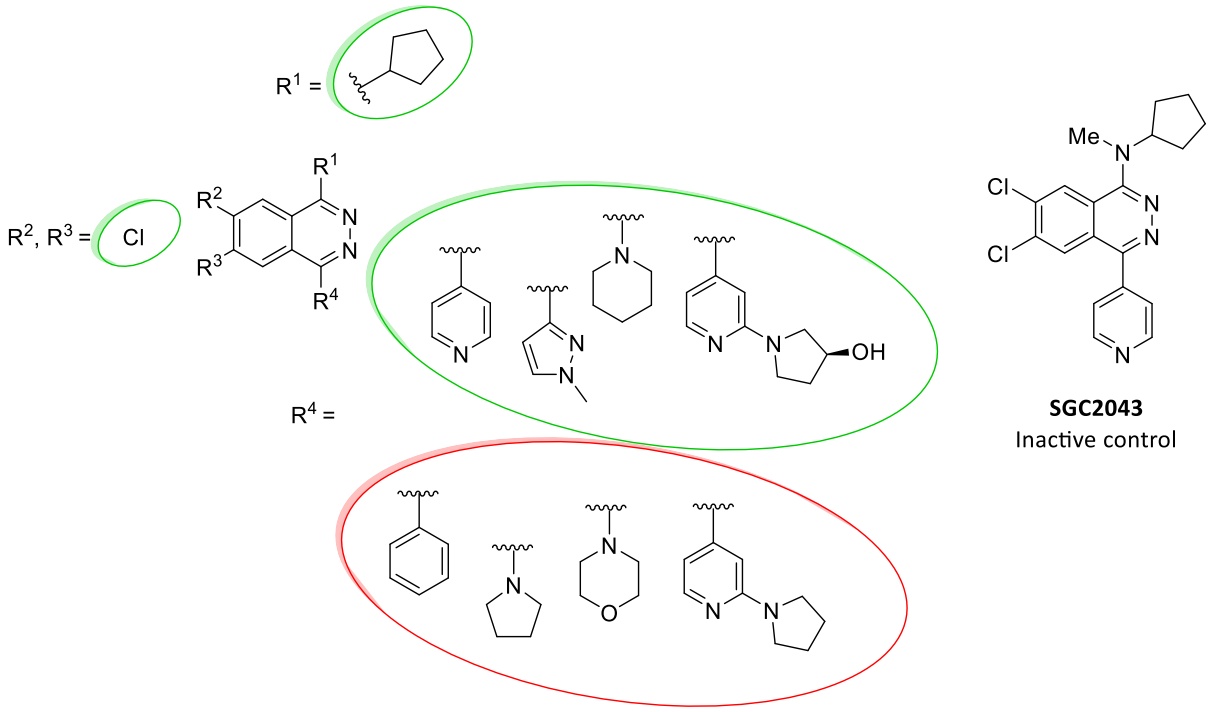

Figure 2.4. SAR around the **A-196** scaffold. Well-tolerated substituents are highlighted in green and poorly tolerated substituents in red. The inactive control **SGC2043** is also shown.

Bond donor are the most potent however extended systems, for example *N*-substituted pyrazoles and piperidines, and 2-substituted pyridines, also show reasonable potencies. In these cases, the presence of a hydrogen bond donor or acceptor on the substituent seems to be necessary. The degree to which the donor or acceptor influences potency appears to depend to some extent on both a conformational (i.e., free or constrained, e.g., linear vs cyclic) and directional component.

2.2.2 Analogue Design and Synthesis

Some of the results in this section have been reported in the following publication:

G. Vilema-Enriquez, **R. Quinlan**, P. Kilfeather, R. Mazzone, S. Saqlain, I. Del Molino Del Barrio, A. Donato, G. Corda, F. Li, M. Vedadi, A. H. Németh, P. E. Brennan and R. Wade-Martins, *J. Biol. Chem.*, **2020**, *295*, 17973-17985

On-target IC_{50}s were determined by **Dr Fengling Li** and **Professor Masoud Vedadi** at the University of Toronto.

The lack of clearly defined SAR around the cyclopentyl group and the phthalazine core meant analogue design took a two-pronged approach: modifications aimed at improving the immediate metabolic stability and clearance; and modifications exploring SAR in an attempt to improve potency and potentially find other means of improving the stability. The structure of **A-196** lends itself to three key disconnections that would allow extensive R group modification through straightforward chemistry (Scheme 2.1).

Starting from a phthalic anhydride would allow the incorporation of different groups at R^2 and R^3, before conversion to the corresponding dichlorophthalazine (Scheme 2.1, Table 2.1). A nucleophilic aromatic substitution (S_NAr) could be used to install various amine substituents at R^1, which would be followed by a Suzuki reaction to incorporate different aryl boronic acids at R^4. Alternatively, a second S_NAr could be used at R^4 to incorporate saturated heteroaryl substituents, for example piperidines or piperazines.

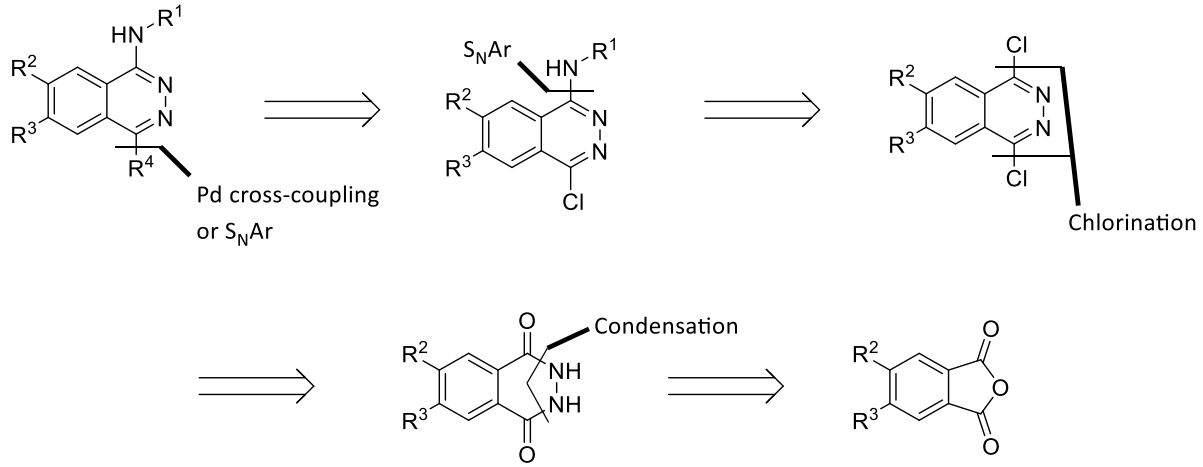

Scheme 2.1. Disconnections and synthetic routes to **A-196** analogues.

2.2.2.1 Cyclopentyl Modification

The focus on improving metabolic stability began with attempting to block sites of oxidation on the cyclopentyl ring through isosteric replacement. Amine **9** was synthesised following reaction of the corresponding ketone with diethylaminosulfur trifluoride (DAST) to yield the *gem*-diflurorocyclopentylamine (Scheme 2.2). As discussed in the introduction, the stronger C—F bond is less labile to oxidative metabolism, however the increased van der Waals radius and polarity may impact hydrophobic interactions in the binding pocket, and so initially only substitution at a single carbon was evaluated. Given the physiochemical differences between hydrogen and fluorine, a convenient alternative is the use of deuterium.[321] The C—D bond is virtually indistinguishable from the C—H bond in terms of the above properties, however the increased stability of the C—D bond as a result of the kinetic isotope effect can lower the rates of metabolism by 6-10 fold when bond breaking is the rate determining step.[322] Amine **10** was synthesised by deuteration of the corresponding cyclopentene to yield D_2-cyclopentylamine (Scheme 2.3). Initially the D_2-analogue was chosen to test the viability of this approach with respect to potency prior to pursuing the less synthetically trivial perdeuterated compound. The amines were incorporated into compounds **11** and **12** (Table 2.1) respectively.

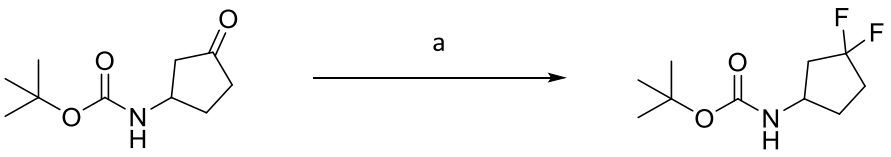

9

Scheme 2.2. Synthesis of *tert*-butyl (3,3-difluorocyclopentyl)carbamate **9**. Reagents and conditions: a) Diethylaminosulfur trifluoride (1.6 eq.), DCM, 0 °C to RT, 24h, 61%.

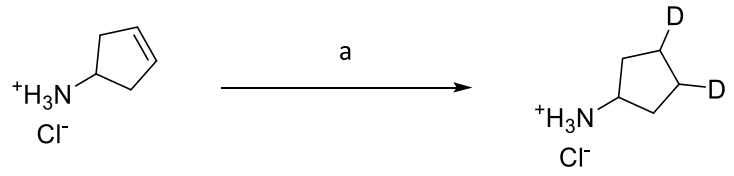

10

Scheme 2.3. Synthesis of cyclopentan-3,4-d_2-1-aminium chloride **10**. Reagents and conditions: a) D_2 (1 atm.), Pd/C (10%), CD_3OD, RT, 16h, quant.

The second approach to improving stability involved incorporating heteroatoms into the cyclopentane ring in order to lower lipophilicity and modulate its electronics so as to be less susceptible to oxidation. This could also introduce chirality into the molecule, which can induce further changes in rates of metabolism depending on the chiral environment of the enzyme.[323] Racemic tetrahydrofuran (THF) analogue **13** was synthesised along with both *R*- and *S*-enantiomers (**14** and **15**, respectively), as well as the pyrrolidine analogue **16**. The Boc-protected intermediate **17** was also evaluated for activity (Table 2.2).

The final approach involved incorporating conformationally constrained bicycles and functionalities known to be resistant to metabolism. Compounds **18** and **19** incorporate a methyl- and ethyl cyclopropyl group respectively, which should have the concerted effect of lowering clearance whilst also maintaining or increasing volume of distribution. The bicyclopentane and norbornane-based analogues **20** and **21** were synthesised in the hope that the constrained scaffolds would be unfavourable to metabolic pathways (Table 2.2). Beginning from the 1,4,6,7-tetrachlorophthalazine, the amines were installed via S_NAr, which was followed by a Suzuki reaction with 4-pyridinylboronic acid to furnish the desired analogues.

Table 2.2. Analogues with modifications of the cyclopentane ring aimed at improving metabolic stability alongside their potency against SUV4-20H1 and H2. [a]IC_{50} determined by scintillation proximity assay (SPA).

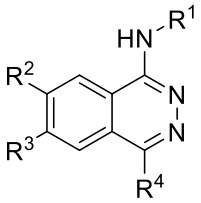

Compound	R^1	R^2	R^3	R^4	SUV4-20H1 IC_{50} (µM)	SUV4-20H2 IC_{50} (µM)
A-196	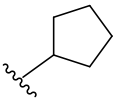	Cl	Cl	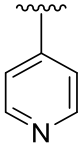	0.025	0.144
11	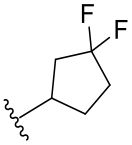	Cl	Cl	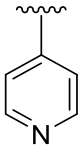	4	9
12	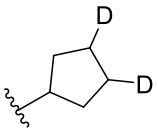	Cl	Cl	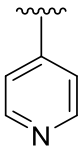	0.05	0.14
13	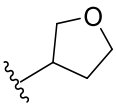	Cl	Cl	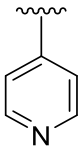	0.90	0.70
14	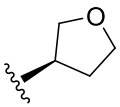	Cl	Cl	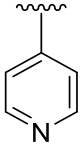	0.22	0.33
15	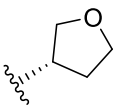	Cl	Cl	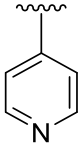	1.80	1.80
16	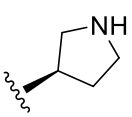	Cl	Cl	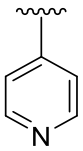	1.40	2.40

Compound	R^1	R^2	R^3	R^4	SUV4-20H1 IC_{50} (μM)	SUV4-20H2 IC_{50} (μM)
17	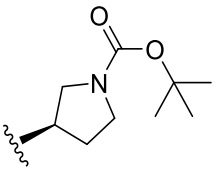	Cl	Cl	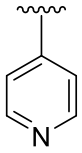	2.00	1.30
18	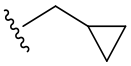	Cl	Cl	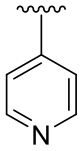	0.50	0.60
19	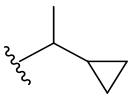	Cl	Cl	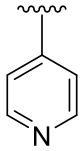	0.80	0.80
20		Cl	Cl	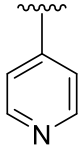	0.30	0.40
21	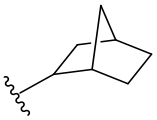	Cl	Cl	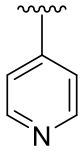	0.16	0.17

Fluorination (**11**) led to a 100-fold drop in potency compared to **A-196**, suggesting the binding pocket may be very sensitive to the introduction of polarity or changes in size given the almost double van der Waals volume of fluorine compared to hydrogen.[321] As expected deuteration (**12**) had no effect on potency, so this may be a viable strategy moving forward if a fully deuterated cyclopentane ring can be synthesised. Of the heterocycle analogues, **14** had reasonable potency which was significantly reduced when switching to the epimer **15**, indicating a degree of chirality to the binding pocket. The equivalent pyrrolidine enantiomer was approximately ten-fold less potent than **14**, suggesting a preference for a hydrogen bond acceptor over a donor in the ring. Finally, of the conformational changes the introduction of the norbornane (**21**) was the best tolerated, followed by the bicyclopentane of **20**, although no substitution maintained the potency of **A-196**.

Beyond modifications to improve metabolic stability, changes were also made to the scaffold following the synthetic route described above in an attempt to better understand the SAR around the cyclopentyl moiety (Table 2.3). The changes centred on varying the steric bulk at the cyclopentyl moiety and attempting to extend its vector in order to examine the limitations of the binding pocket.

Table 2.3. Analogues with modifications of the cyclopentane ring aimed at exploring the limitations of the binding pocket.

Compound	R^1	R^2	R^3	R^4	SUV4-20H1 IC_{50} (µM)	SUV4-20H2 IC_{50} (µM)
22	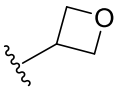	Cl	Cl	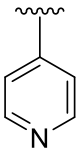	24	>50
23	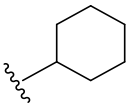	Cl	Cl	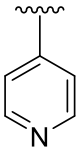	1.50	>50
24	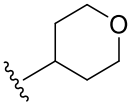	Cl	Cl	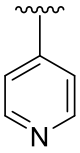	13	8
25	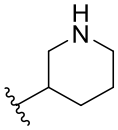	Cl	Cl	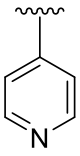	17	17
26	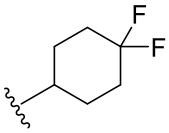	Cl	Cl	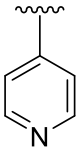	>10	>10
27	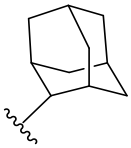	Cl	Cl	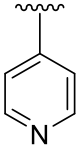	4.80	5.20
28	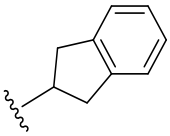	Cl	Cl	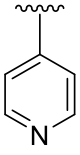	0.90	5.00

Compound	R^1	R^2	R^3	R^4	SUV4-20H1 IC_{50} (μM)	SUV4-20H2 IC_{50} (μM)
29	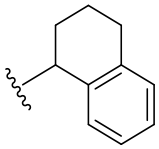	Cl	Cl	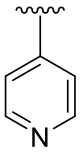	6	8
30	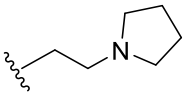	Cl	Cl	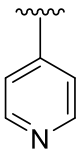	12	12
31	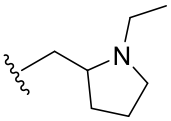	Cl	Cl	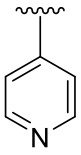	10	13
32	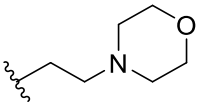	Cl	Cl	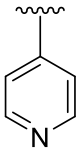	10	8
33	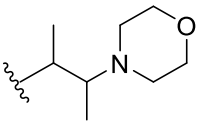	Cl	Cl	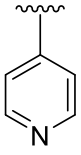	17	18
34	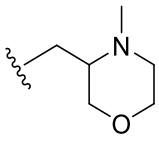	Cl	Cl	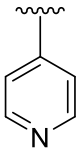	14	15
35	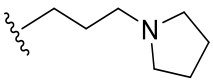	Cl	Cl	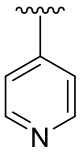	17	16

It is immediately clear that the strength of binding is very sensitive to changes in ring size at the amine substituent. Potency was lost completely with the introduction of a four-membered oxetane ring (**22)**, and an approximate 36-fold drop was observed for SUV4-20H1 following substitution of the cyclopentane for cyclohexane (**23**). Interestingly, the drop was far more extreme for SUV4-20H2, almost ten-fold greater than that for the H1 isoform. Pyran (**24**) and piperidine (**25**) substituents were not tolerated, nor was the *gem*-difluorocyclohexyl

group of **26** or the adamantane of **27**. **28** retained sub-micromolar activity against H1 although suffered a large loss of potency compared to **A-196**. Similarly to **23**, the increased bulk of the indane led to a far greater drop in potency against H2. This has two implications: firstly, whilst steric bulk at the amine substituent is a factor, so is the conformation. For example, switching from the norbornane of **21** to the cyclohexane of **23** leads to an almost ten-fold drop in potency, and the increased but planar bulk of **28** retains sub-micromolar activity. Secondly, the cyclopentyl binding pocket of H2 is less accommodating to changes in steric bulk than that of H1, which may be a potential route to achieving selectivity. Disappointingly, all of the other attempts to extend further into the binding pocket led to substantial losses of potency.

One further strategy attempted was mimicking the methylated histone peptide in the binding pocket. This has previously been shown to be a viable strategy for increasing potency against KMTs, for example in the development of **A-366**, a chemical probe for the H3K9 methyltransferase G9a.[48] Overlaying the binding modes of **A-196** and the peptide (Figure 2.5) suggests that alkylation of the amine with a methylated lysine mimic could eliminate the active site water and directly engage the active site serine, leading to increased potency. The introduction of a basic centre would also improve volume of distribution whilst lowering logP.

36 was synthesised following deprotonation of **A-196** and alkylation with 2-chloro-*N,N*-dimethylethylamine. Although there was a substantial drop in potency (Table 2.4), considering methylation of the amine nitrogen forms the inactive control **SGC2043** (Figure 2.4) compound **36** still retains reasonable activity. Mimicking the monomethyl lysine as opposed to dimethyl may prove more fruitful in terms of engaging the active site serine, whilst varying the linker length could allow fine-tuning of the potency.

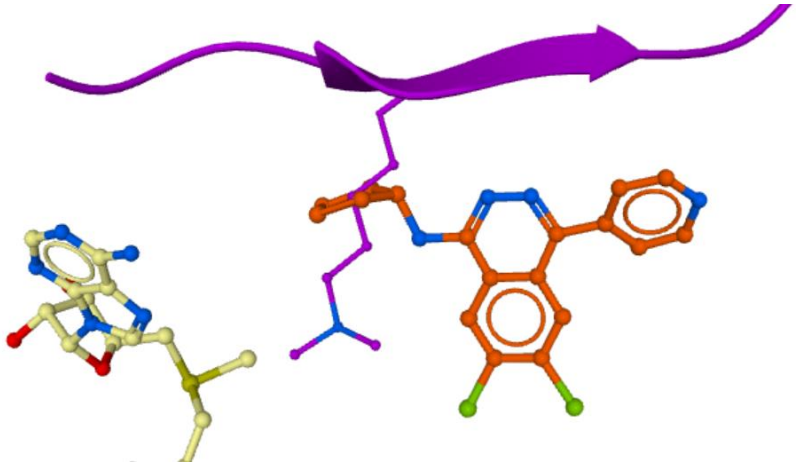

Figure 2.5. Overlaid binding modes of **A-196** (orange), SAM (yellow) and the histone 4 peptide (purple). H4K20me2 extends into the vector occupied by the amine of **A-196**.

Table 2.4. Mimicking the histone 4 peptide through alkylation of the amine nitrogen of **A-196**.

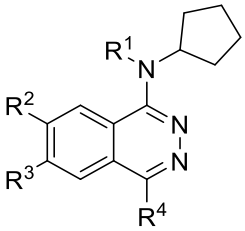

Compound	R^1	R^2	R^3	R^4	SUV4-20H1 IC_{50} (µM)	SUV4-20H2 IC_{50} (µM)
36	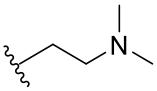	Cl	Cl	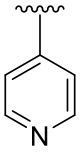	3.2	5.6

Taken together, these results suggested that the best route to improving stability was through the conformational changes induced by the introduction of the norbornane (**20**) and bicyclopentane (**21**).

2.2.2.2 Pyridyl Modification

As the SAR around the bottom half of **A-196** had been extensively probed, it provided a rich source of analogues that could potentially improve metabolic stability. The ease of synthesis from compound **37** (Scheme 2.4) meant that a library of boronic esters and nucleophiles could also be evaluated to expand the SAR.

Of immediate interest were pyrazole-based derivatives, due to their relative metabolic stability compared to other heterocycles as well as the analogues' comparable potency to **A-196**. **38** was initially chosen for evaluation given its previously reported superior potency and prompted the design of **39**, in the hope that the difluoromethyl group would more productively engage in hydrogen bonding with the active site water at the solvent exposed region (Figure 2.3). **40** was synthesised in order to probe the dependence of potency on the substitution pattern around the pyrazole ring. Beyond the pyrazoles, the main focus of derivatisation at this position was to improve compound potency through stronger hydrogen bonding interactions (Table 2.5).

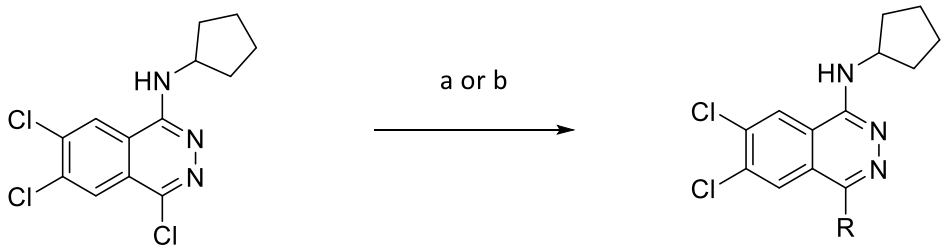

37

Scheme 2.4. Synthetic route to derivatives via compound **37**. Reagents and conditions: a) R-B$(OH)_2$ (1.2 eq.), Pd(dppf)Cl_2 (0.1 eq.), Na_2CO_3 (3 eq.), dioxane:water (4:1), 75 °C, 52-91%; b) R_2NH (1.0 eq.), DIPEA (1.2 eq.), DMSO, 80 °C, 63-65%.

Table 2.5. Analogues with modifications of the pyridine substituent aimed at improving metabolic stability and potency.

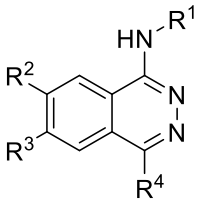

Compound	R^1	R^2	R^3	R^4	SUV4-20H1 IC_{50} (μM)	SUV4-20H2 IC_{50} (μM)
38	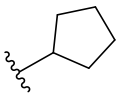	Cl	Cl	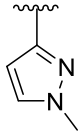	0.06	0.13
39	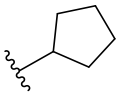	Cl	Cl	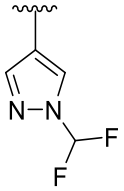	0.015	0.043
40	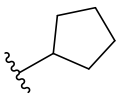	Cl	Cl	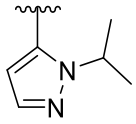	1.50	1.00
41	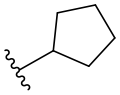	Cl	Cl	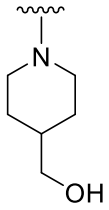	1.20	1.50
42	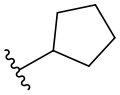	Cl	Cl	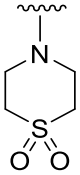	1.20	1.40
43	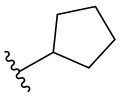	Cl	Cl	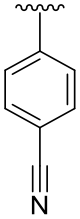	0.045	0.092

Compound	R^1	R^2	R^3	R^4	SUV4-20H1 IC_{50} (μM)	SUV4-20H2 IC_{50} (μM)
44	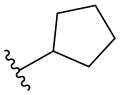	Cl	Cl	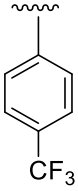	0.70	0.60
45	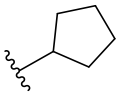	Cl	Cl	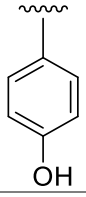	0.094	0.136
46	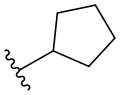	Cl	Cl	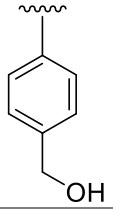	0.035	0.077
47	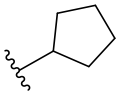	Cl	Cl	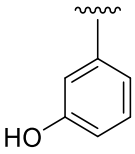	0.044	0.089
48	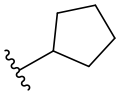	Cl	Cl	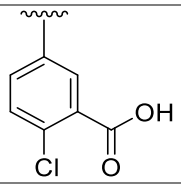	0.07	0.15
49	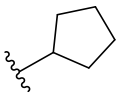	Cl	Cl	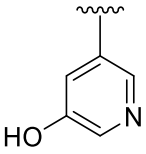	0.037	0.042
50	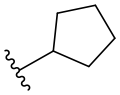	Cl	Cl	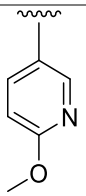	1.10	6.00
51	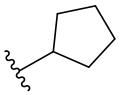	Cl	Cl	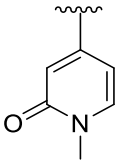	0.10	0.149
52	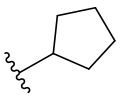	Cl	Cl	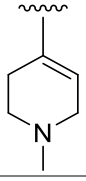	0.40	0.60

Compound	R^1	R^2	R^3	R^4	SUV4-20H1 IC_{50} (μM)	SUV4-20H2 IC_{50} (μM)
53	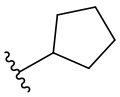	Cl	Cl	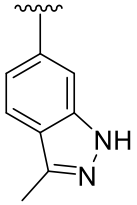	0.50	2.00
54	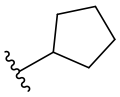	Cl	Cl	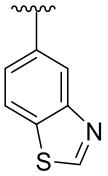	0.079	0.106
55	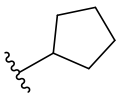	Cl	Cl	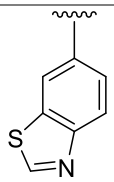	0.079	0.141
56	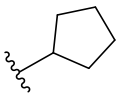	Cl	Cl	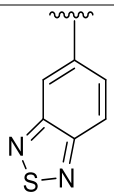	0.189	0.198
57	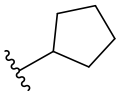	Cl	Cl	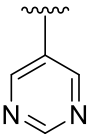	1.20	1.50

As can be seen above, pursuing a stronger hydrogen bond via the pyridyl vector was a largely successful venture. *N*-methylated pyrazole **38** recapitulated the reported high potency and pleasingly the *N*-difluoromethylated analogue **39** showed improved potency over **A-196**, vindicating this strategy. The nitrile of **43** led to high potency as did the phenol of **45**, although to a minimally lesser extent. This is perhaps due to the slightly shorter extension towards the water molecule, and a one-carbon homologation to give **46** seems to solve this issue. Compounds **47**, **48**, and **49** all have hydrogen bond donors extending towards the vector that would be occupied by the 2-position of the pyridyl group. Despite the high dependence of hydrogen bonding on directionality, they maintain high potencies which suggests a different interaction. Closer inspection of the binding pocket reveals a second water molecule along

that vector which they may be productively engaging. Alternatively, in the original crystal structure the pyridyl moiety is twisted slightly out of plane with the phthalazine ring; a greater degree of orthogonality for these aryl groups could potentially lead to hydrogen bonding with the backbone of SUV4-20. **51** has a hydrogen bond acceptor along this vector which displays a slightly lower potency, perhaps indicating a preference for donors at this position. As more metabolically stable surrogates for the phenolic analogues, benzothiazoles **54** and **55** retained high potency, as did benzothiadiazole **56**. By comparison, indazole **53** was far less potent, which is perhaps due to unfavourable hydrophobic interactions with the methyl substituent. Introduction of the tetrahydropyridine of **52** led to a loss of potency, however the compound displayed improved potency compared to other reported tetrahydropyridine analogues.[320]

Whilst not leading to huge drops in potency, the relatively unsuccessful approaches seem to be a result of loss of the appropriate vector along which to engage in hydrogen bonding. Compare for example the 3-, 4-, and 5-substituted pyrazole analogues **38**, **39**, and **40** respectively, with the 5-substitution pattern leading to a loss of potency. Binding may also be hampered by the hydrophobic isopropyl group, in a similar fashion to **53**. The piperidine analogues **41** and **42** have strong hydrogen bond donor and acceptor capability and yet show relatively low potency. This is perhaps due to the axial and equatorial distribution of the substituents around the piperidine ring, which would place the hydroxyl and sulfoxide oxygens along the wrong vectors to engage with the water molecules. The low potency of **50** is surprising given the methoxy group was expected to be a strong hydrogen bond acceptor, however the methyl group may be interfering in some way with the interaction. Finally, the low potency of pyrimidine **57** is again presumably a result of poor extension along the proper vectors for hydrogen bonding.

Although the above approach has yielded several highly potent compounds, some contain potential metabolic liabilities such as nucleophilic hydroxyl groups (**45**, **46**, **47**, and **49**) and unsubstituted aryl rings. Strategies for circumventing this, for example the use of non-conjugable hydrogen bond donors (*vide supra* section 1.6.3.1) like benzothiazoles **54** and **55**, gave comparable potencies however raised concerns about the solubility of the final compound. The pyrazole-based analogues (**38** and **39**) provide the best balance in terms of potential metabolic stability and potency, with **39** achieving the aim of improving the on-target potency of **A-196**. As well as this, the nitrile containing **43** has high potency and may show increased stability given the metabolic robustness of the functionality.[324] Finally, the benzoic acid of **48** may be interesting to pursue with respect to improving some physiochemical properties, although it would likely impact the ability of the molecule to cross the BBB. As well as this, the acidic functionality would decrease the volume of distribution and be detrimental to half-life, however this could possibly be negated by lower clearance as a result of the metabolically susceptible *para*-position of the aryl ring being blocked.

2.2.2.3 Backbone Modification

The SAR around the phthalazine ring is limited to the effect of mono- and di-chlorination of the backbone and switching from a quinoline to a phthalazine.[274] As the phthalazine ring itself is not of great concern with respect to metabolic stability, and in fact should aid solubility, the main focus of derivatisation was the backbone chlorine atoms. They sit in a tight hydrophobic pocket (Figure 2.3) which presents two key challenges: achieving a reduction in lipophilicity without losing potency; and making modifications that are tolerated with respect to steric constraints.

Introducing a second chlorine substituent to the backbone had a dramatic effect on the potency of **A-196** which suggests the di-substituted pattern needs to be maintained. Methoxy groups act as isosteres of chlorine and offer a means of lowering lipophilicity whilst maintaining hydrophobic interactions with the pocket, although are potential sites of metabolic instability due to *O*-demethylation reactions. A means of circumventing this would be to append a heterocycle to the phthalazine in the form of a methylenedioxy group (Scheme 2.5), which could be further stabilised by difluorination of the methylene bridge. Synthetically, installing these modifications required building the phthalazine ring from the related benzoic acid via a palladium-catalysed *ortho*-alkylation.[325]

The synthesis of isobenzofuranones **58**, **59**, and **60** was non-trivial, requiring extended reaction times at high temperatures in a sealed tube. The subsequent steps were straightforward however the final chlorination was low yielding, meaning it was not possible to isolate enough of either **68** or **69** to continue with analogue synthesis. Despite this, **70** was synthesised from **67** which permitted evaluation of its potency against SUV4-20H1 and H2 (Table 2.6).

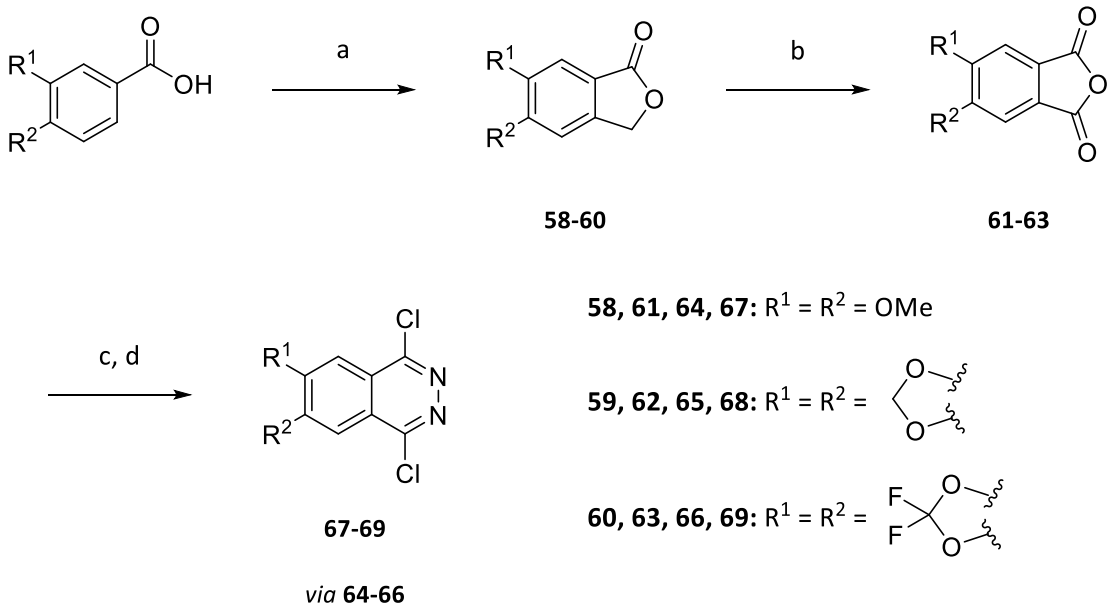

Scheme 2.5. Synthetic route to the modified phthalazine core of **A-196**. Reagents and conditions: a) $Pd(OAc)_2$ (0.1 eq.), K_2HPO_4 (2.5 eq.), CH_2Br_2, 140 °C, 48 hrs, 32-67%; b) i) NaOH (3 eq.), $KMnO_4$ (2.2 eq.), H_2O, RT, 12 hrs, quant.; ii) Ac_2O, reflux, 12 hrs, quant.; c) N_2H_4 (1.2 eq), AcOH, 70 °C, 24 hrs, quant.; d) $POCl_3$ (10 eq.), DIPEA (2.4 eq.), 130 °C, 24 hrs, 7-43%.

Table 2.6. Potency of compound **70** against SUV4-20H1 and H2.

Compound	R^1	R^2	R^3	R^4	SUV4-20H1 IC_{50} (μM)	SUV4-20H2 IC_{50} (μM)
70	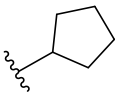	OMe	OMe	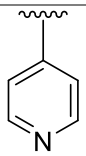	>10	>10

The dimethoxy substitution was very poorly tolerated, with only 15% inhibition of SUV4-20H1 observed at 10 μM. This may be because to occupy the same pocket as the chlorine atoms

the methoxy substituents of **70** would have to adopt a gauche conformation, whereas *ortho*-dimethoxybenzenes of this type almost exclusively adopt a planar conformation to maximise conjugation of the oxygen lone pair with the aromatic ring (Figure 2.6).[326] Both the methylenedioxy-based analogues (derived from **68** and **69**) would likely avoid this issue, and so efforts are ongoing to complete their synthesis.

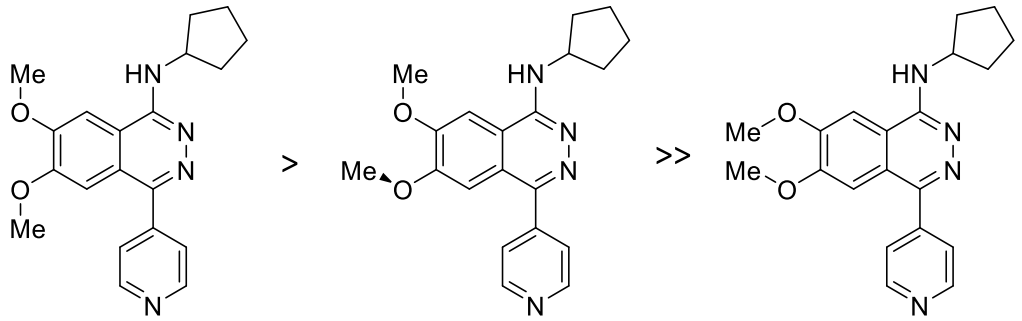

Figure 2.6. Potential conformations of the *ortho*-dimethoxy substituents of **70** in order of decreasing stability. Bonds in bold represent a deviation from planarity.

2.2.2.4 Combined Modifications

Modifications that were tolerated with respect to potency and potentially more metabolically stable and were then combined to try and achieve the greatest increase in stability. Knowing that racemic **13** was reasonably potent and enantiomer **14** would give increased potency, the *rac*-THF was chosen for further evaluation. As well as this, both the methyl- and ethylcyclopropyl analogues **18** and **19** were chosen alongside the bicyclopentane of **20**. Of the pyridyl modifications, the pyrazole analogues **38** and **39** were chosen together with the phenyl analogue **46** and the indazole **53** (Table 2.7). Once again, the amines were installed via S_NAr of the 1,4,6,7-tetrachlorophthalazine, followed by Suzuki reaction with the requisite boronic acid to yield the desired analogues.

Whilst it had been hoped that the SAR around the scaffold of **A-196** would be additive, in most instances this wasn't the case and the analogues showed large drops in potency compared to their parent structures. **71** retained potency and would be expected to be more potent when the single enantiomer is tested, which may form the basis for future efforts.

Table 2.7. Combined modifications of **A-196** aimed at improving metabolic stability whilst maintaining potency.

Compound	R^1	R^2	R^3	R^4	SUV4-20H1 IC_{50} (μM)	SUV4-20H2 IC_{50} (μM)
71	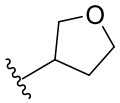	Cl	Cl	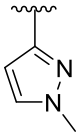	0.87	0.97
72	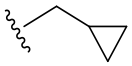	Cl	Cl	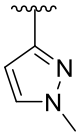	1.00	0.90
73	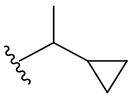	Cl	Cl	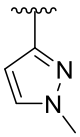	1.10	0.90
74	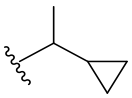	Cl	Cl	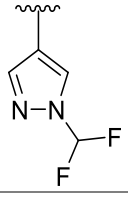	1.00	0.70
75	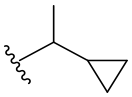	Cl	Cl	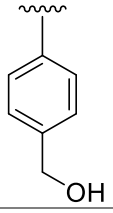	2.40	1.60
76		Cl	Cl	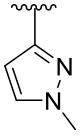	0.40	0.60
77		Cl	Cl	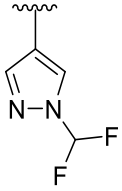	0.30	0.70

Compound	R^1	R^2	R^3	R^4	SUV4-20H1 IC_{50} (μM)	SUV4-20H2 IC_{50} (μM)
78		Cl	Cl	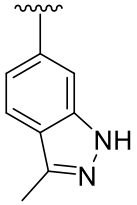	3.2	3.7

76 and **77** also remained reasonably potent and combine the functionalities previously identified as most likely to improve the metabolic stability.

2.2.3 Scaffold Diversification – Second Compound Series

During the course of the work around **A-196** a crystal structure of SUV4-20 with a new, structurally distinct inhibitor bound was disclosed (Figure 2.7, compound **79**, PDB: 5WBV). **79** occupies the histone binding pocket of SUV4-20 in a very similar manner to that of **A-196**: the pyrazolopyrone core is sandwiched between Trp264 and Phe281 with the carbonyl occupying the same vector as one of the chlorines; the phenyl ring occupies the cyclopentyl pocket; and the chlorobenzoic acid sits in the same solvent exposed region as the pyridine, the chlorine overlapping with the pyridyl nitrogen. In the absence of a hydrogen bond donor, the active site water is excluded from the pocket by the interaction of the phenyl ring and the methyl substituent on the pyrone.

The potency of **79** against SUV4-20 was not disclosed, however if highly active the pyrazolopyrone core offers an attractive, less lipophilic alternative to the dichlorophthalazine of **A-196**. It was envisaged that combining features of the two structures could yield a new class of inhibitors with enhanced metabolic stability. **79** could be accessed following consecutive condensations of 2-chloro-5-hydrazinylbenzoic acid with ethyl benzoylacetate then ethyl acetoacetate (Scheme 2.6). Initially, synthetic efforts focused on exploring the SAR around the scaffold of **79** and attempting to engage certain residues in the binding pocket in

order to improve its potency (Table 2.8). Sequential condensations of various aryl hydrazines with β-keto esters afforded expedient access to a range of analogues.

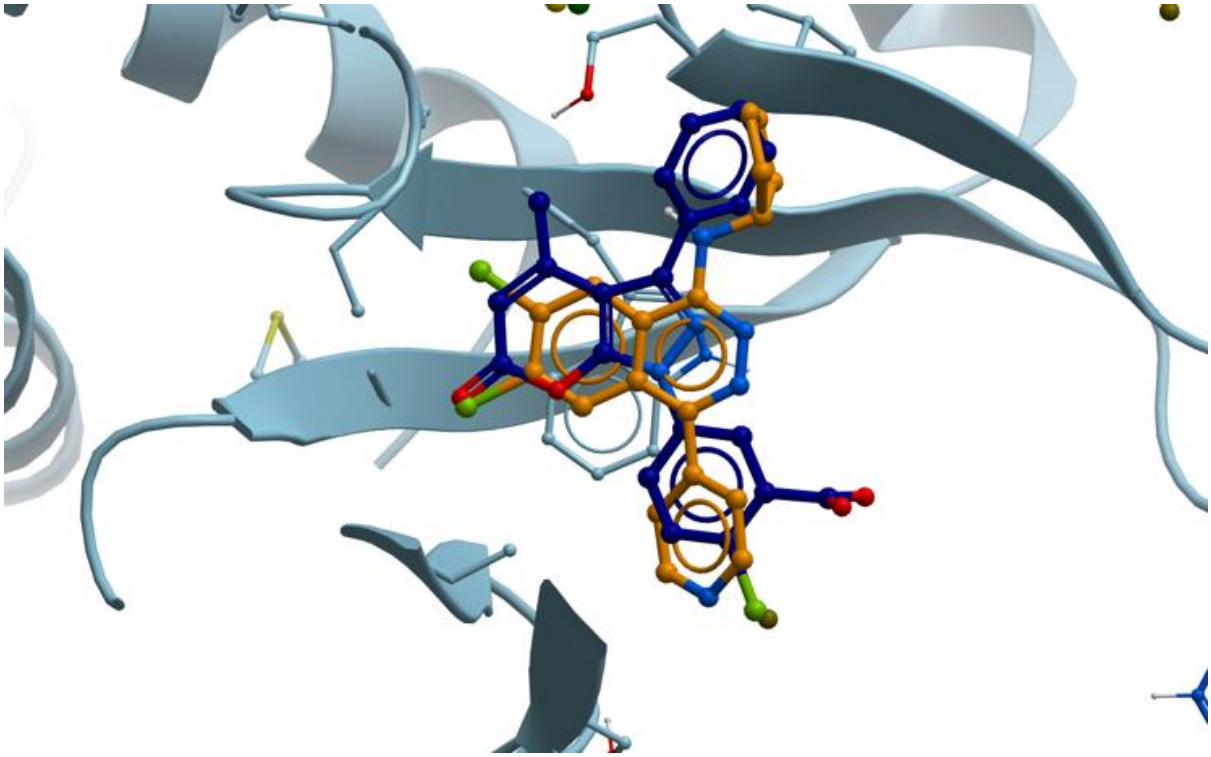

Figure 2.7. Crystal structure of SUV4-20 in complex with **A-196** (orange) overlaid with the structure in complex with **79** (blue) (PDB: 5CPR, 5WBV).

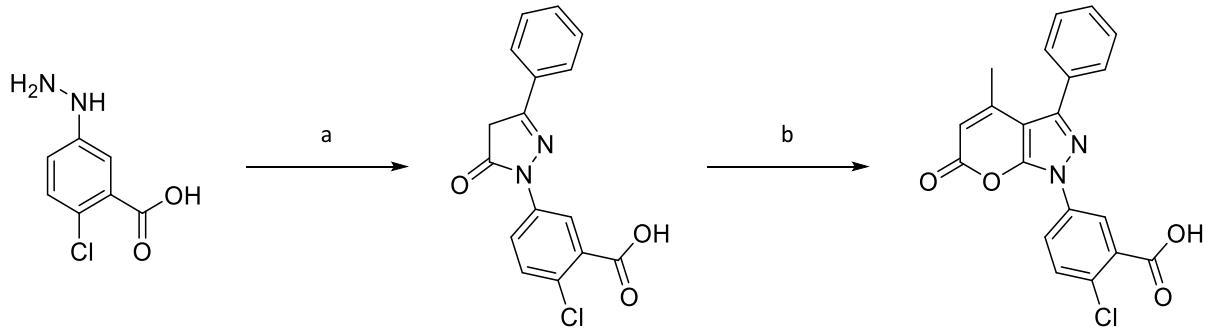

79

Scheme 2.6. Synthesis of **79.** Reagents and conditions: a) Ethyl benzoylacetate (1.0 eq.), EtOH, 60 °C, 12h, quant.; b) Ethyl acetoacetate (10.0 eq.), reflux, 12h, 82%.

Table 2.8. Analogues of reported SUV4-20 inhibitor, **79**, and their activity against SUV4-20H1 and H2.

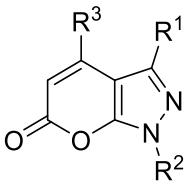

Compound	R^1	R^2	R^3	SUV4-20H1 IC_{50} (μM)	SUV4-20H2 IC_{50} (μM)
79	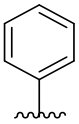	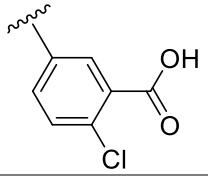	CH_3	5.00	8.50
80	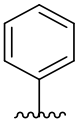	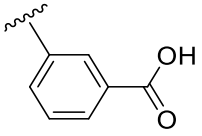	CH_3	5.60	8.60
81	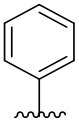	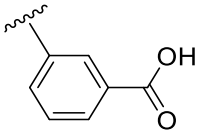	CF_3	>10	>10
82	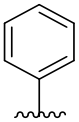	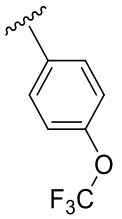	CH_3	>10	>10
83	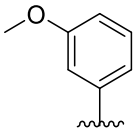	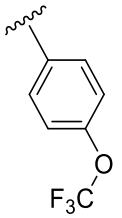	CH_3	>10	>10
84	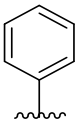	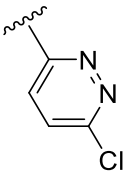	CH_3	>10	>10
85	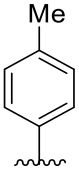	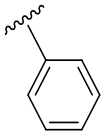	CH_3	>10	>10

Compound	R^1	R^2	R^3	SUV4-20H1 IC_{50} (μM)	SUV4-20H2 IC_{50} (μM)
86	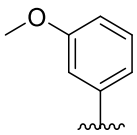	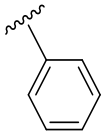	CH_3	>10	>10

Compound **79** was revealed to be a relatively weak inhibitor of both isoforms of SUV4-20, and no derivative tested showed improved potency. Loss of the chlorine (**80**) caused a slight drop in potency, however the carboxylic acid moiety proved to be crucial for maintaining some degree of activity (see compounds **82**, **83**, **84**, **85**, **86**). Attempts to place hydrogen bond donors along the R^2 vector in order to engage the active site water (**82** and **83**) analogous to the pyridyl of **A-196**, proved fruitless. Similarly, introducing hydrogen bond donors along R^1 to interact with Ser251 yielded no gains in potency. It is worth noting that this strategy was not attempted with the chlorobenzoic acid at R^2 due to the availability of the starting aryl hydrazine, however it may yield better results if attempted in future. Finally, compound **81** was designed to investigate stabilising the potentially metabolically labile vinylic methyl group, however the introduction of the trifluoromethyl was not tolerated.

Despite the low potency of **79** and its analogues, there remains the possibility that the pyrazolopyrone core could be a suitable isostere for the phthalazine. As a result, efforts are ongoing to synthesise compounds based on the pyrazolopyrone core of **79** that incorporate a cyclopentylamine and pyridyl component (**87**, Figure 2.8). Further derivatives comprising the more metabolically stable and more potent substituents (**88** and **89**) could then be synthesised should the combination retain the potency of **A-196**.

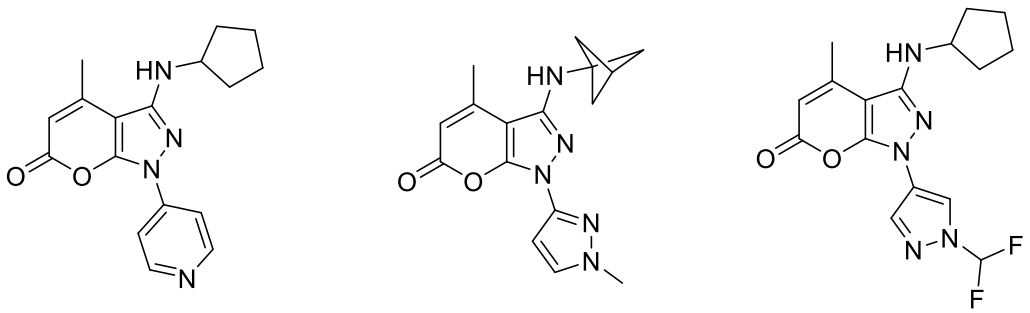

87 **88** **89**

Figure 2.8. Envisaged combinations of **79**, **A-196**, and other analogues**.**

2.3 INCREASING FRATAXIN EXPRESSION

Determination of frataxin-luciferase expression was carried out by **Dr Gabriela Vilema-Enriquez** and **Saumya Maheshwari** at the Department of Physiology, Anatomy, and Genetics, University of Oxford.

2.3.1 GAA-Repeat Expansion Reporter Model of FRDA

The FRDA cell model that was the basis of the initial discovery of **A-196** (section 1.5) was also essential in identifying those analogues that induced an equivalent or improved up-regulation of *FXN* expression. The model allows the direct comparison of frataxin expression between a normal and diseased *FXN* gene containing an expanded repeat region.[327] A vector containing a promoter sequence, the *FXN* locus containing six GAA repeats, and a downstream sequence was fused with a firefly luciferase gene at exon 5a immediately before the stop codon (pBAC-*FXN*-*Luc* vector, Figure 2.9). To mimic the genomic changes associated with FRDA, a second vector was designed with a GAA region 310 repeats long inserted into intron 1 of the *FXN* locus, in order to replace the six GAA repeats and mimic the changes associated with FRDA (pBAC-*FXN*-GAA-*Luc*, Figure 2.9).

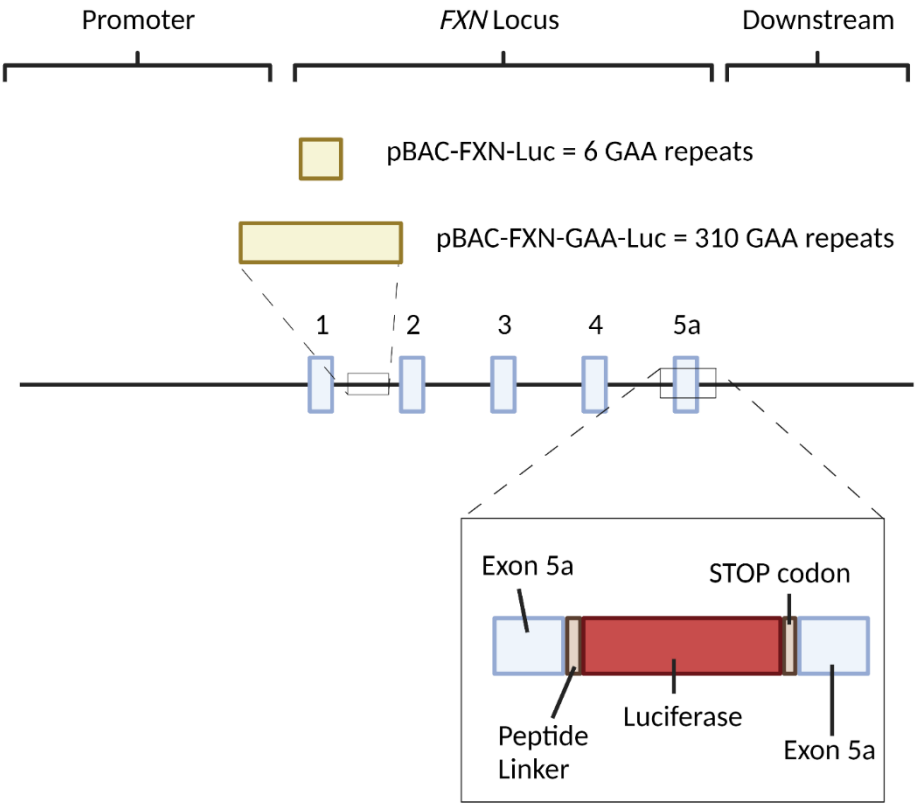

Figure 2.9. Schematic representation of the pBAC-*FXN-Luc* vector (6 GAA repeats) and pBAC-*FXN*-GAA-*Luc* vector (310 GAA repeats). The vectors contain approximately 38 kb of promoter region, the 80 kb FXN locus and 17 kb of downstream sequence. Exon 5a contains a luciferase sequence preceded by a peptide linker at the 5' end and followed immediately before the stop codon.

HEK293 cells transformed with both vectors expressed a frataxin-luciferase fusion protein of the expected size, which could be measured using relative luciferase expression as proxy.[327] The presence of the repeat expansion led to a 37% decrease in *FXN-Luc* mRNA levels, and a 42% decrease in levels of the frataxin-luciferase protein, recapitulating the phenotype observed in FRDA patient cells. Importantly, the presence of the repeat region in the vector induced the same epigenetic changes observed around the *FXN* locus in FRDA patients: global histone hypoacetylation; an increase in repressive histone methylation marks; and an increase in CpG methylation.

HEK293 cells bearing the pBAC-*FXN*-GAA-*Luc* vector were treated with the **A-196** analogues for six days at 5 µM. Frataxin-luciferase expression in these cells was compared to a DMSO vehicle control and HEK293 cells transfected with the healthy pBAC-*FXN-Luc* vector.

2.3.2 Effect on Frataxin Expression – Reporter Model

2.3.2.1 Cyclopentyl Modifications

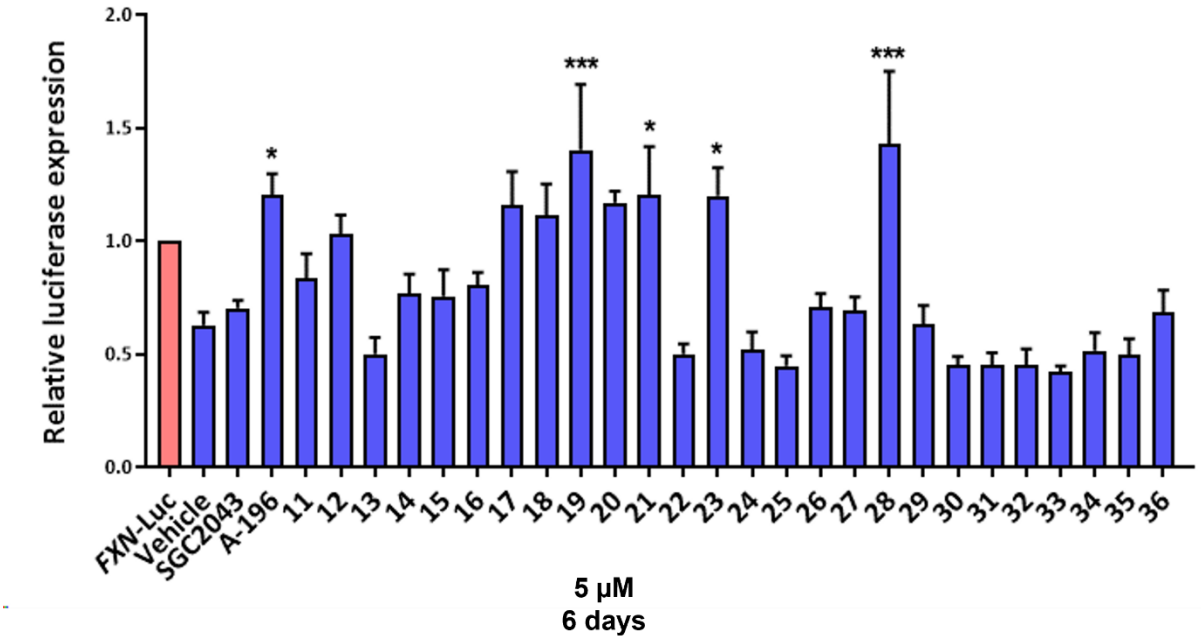

Figure 2.10. Effect of compounds **11-36** on *FXN* expression in a reporter cell model of FRDA. *FXN*-Luc represents a reporter model of healthy *FXN* expression. The vehicle control is DMSO and **SGC2043** acts as a negative control. Cells were treated with compounds at 5 µM for 6 days. Results are the average of three experiments each with three biological replicates. The data are relative to the vehicle and are presented as means ± SEM (one-way ANOVA followed by Bonferroni test): * = $p < 0.05$; ** = $p < 0.01$; *** = $p < 0.001$; **** = $p < 0.0001$

Four compounds (**19**, **21**, **23**, and **28**) induced a significant increase in *FXN* expression to levels comparable to or above that of **A-196** (Figure 2.10). Within error, all these increases were to the level of expression observed in the healthy control. Several others (**12**, **17**, **18**, and **20**)

also induced an increase in expression however not to a degree of statistical significance. Interestingly, **13** and its enantiomer **14** showed no appreciable increase in *FXN* expression, despite being equally if not more potent against SUV4-20H1 than **23** and **28**, respectively. **14** is also more potent than both **18** and **20**, so the reason for this lack of efficacy is not immediately apparent. It may be a result of decreased cellular permeability, as the introduction of the THF ring in place of the cyclopentane will lead to a drop in ClogP, however it would not be expected to be to such an extent as to prevent cell penetrance. Unique to **23** and **28** is a high degree of selectivity for SUV4-20H1 over H2, such that little to no H2 inhibition would be expected upon treatment of cells with these compounds. **13** and **28** display the same potency against H1, but **13** is actually marginally more selective for H2 over H1, which could play some role in the observed efficacy of the compounds. The potential mechanism underpinning this is unclear; SUV4-20H2 inhibition may be in some way antagonistic to H1 inhibition in the context of *FXN* expression. SUV4-20H1 knockout cells could be treated with **A-196** to see if H2 inhibition reverses the increase in *FXN* expression induced by knockdown to test this hypothesis. However, if this were the case, some effect would be expected after treatment at 5 µM with those more potent compounds, such as **A-196**, which is not observed. As such, it is more likely a result of poor permeability or solubility.

2.3.2.2 Pyridyl Modifications

Many of these analogues were potent inhibitors of SUV4-20, which is reflected in the fact that the vast majority induced a significant increase in *FXN* expression, and many to a level above that of the healthy control and **A-196** (Figure 2.11). However, several analogues with IC_{50}s of less than 5 µM did not induce a significant increase in *FXN* expression, including some of the more potent analogues yet synthesised. This again may be explained by issues with cell

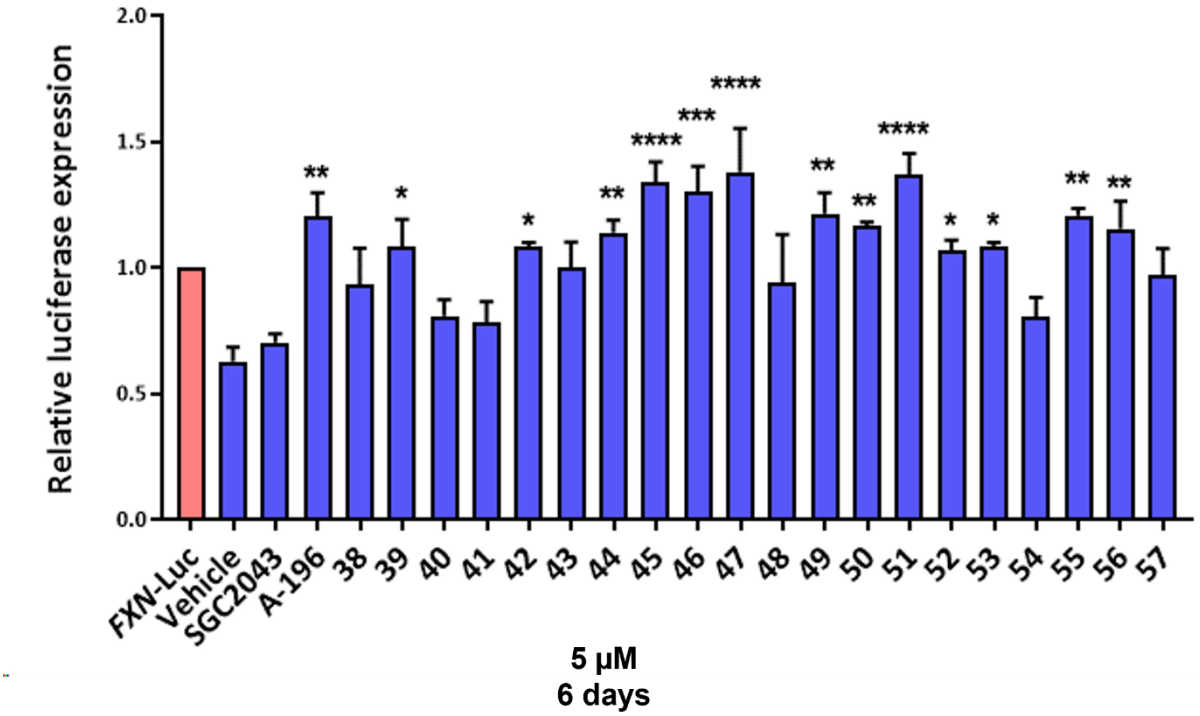

Figure 2.11. Effect of compounds **38**-**57** on *FXN* expression in a reporter cell model of FRDA. *FXN*-Luc represents a reporter model of healthy *FXN* expression. The vehicle control is DMSO and **SGC2043** acts as a negative control. Cells were treated with compounds at 5 µM for 6 days. Results are the average of three experiments each with three biological replicates. The data are relative to the vehicle and are presented as means ± SEM (one-way ANOVA followed by Bonferroni test): * = $p < 0.05$; ** = $p < 0.01$; *** = $p < 0.001$; **** = $p < 0.0001$

permeability: for example, **48** has an IC_{50} of 70 nM against SUV4-20H1 however the benzoic acid functionality would likely render it ionised under assay conditions and thus poorly permeable. More puzzling however is the difference in cellular effect between equipotent compounds (e.g., **42** vs **41**, or **47** vs **43**), and between near structurally identical compounds (e.g., **54**, **55**, and **56**). The latter examples suggest that this isn't an issue with either permeability or solubility, and neither can it be attributed to increased potency against SUV4-20H2 over H1. Previous CRISPR knockout studies[130] and the efficacy of **A-196** provide

conclusive support for target selection, and so the differences could be due to experimental inconsistencies. However, the results are the average of nine biological replicates with a relatively small standard error (SE) per compound. Mass spectrometry suggests there are no issues with compound degradation, and so it may be that there are problems with the reproducibility and fidelity of the *FXN* reporter model.

2.3.2.3 Combined Modifications

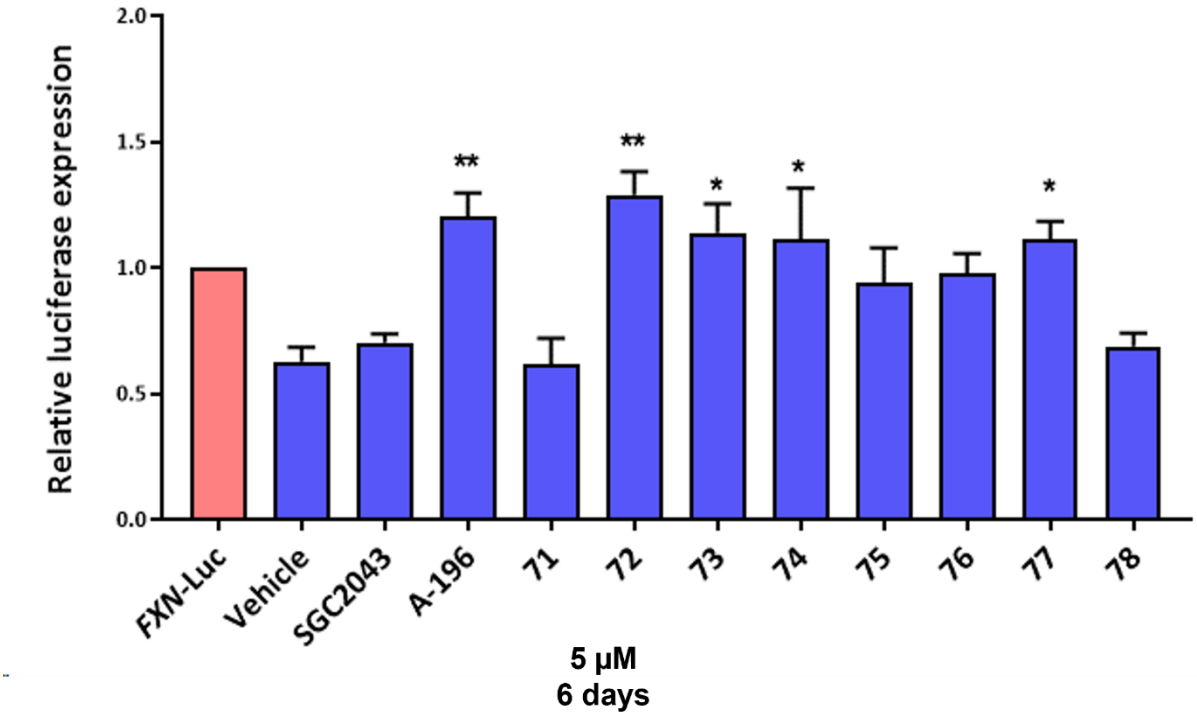

Figure 2.12. Effect of compounds **71-78** on *FXN* expression in a reporter cell model of FRDA. *FXN*-Luc represents a reporter model of healthy *FXN* expression. The vehicle control is DMSO and **SGC2043** acts as a negative control. Cells were treated with compounds at 5 µM for 6 days. Results are the average of three experiments each with three biological replicates. The data are relative to the vehicle and are presented as means ± SEM (one-way ANOVA followed by Bonferroni test): * = $p < 0.05$; ** = $p < 0.01$; *** = $p < 0.001$; **** = $p < 0.0001$

Of those analogues that combined modifications aimed at boosting metabolic stability, **72**, **73**, **74** and **77** induced an increase in *FXN* expression to a degree of significance compared to the vehicle. **75** and **76** also increase *FXN* expression to the level of the healthy control (Figure 2.12). Interestingly, **71** had no effect on *FXN* expression despite having sub-micromolar potency against SUV4-20, replicating the results observed for the structurally similar compounds **13** and **14**. Poor cellular permeability may be a feature of the THF containing analogues, and it would be worth assessing this in future experiments. **76** combines structural features that should improve metabolic stability, and so it is heartening that the potency against SUV4-20 is matched by good efficacy in the reporter model. The lack of statistical significance is likely due to the highly conservative nature of the Bonferroni correction for multiple comparisons. Dose-response experiments calculated the cellular EC_{50} of **76** for inducing *FXN* expression at 3.3 µM (Figure 2.13). The plateau of the curve was not reached which may affect the accuracy of this measurement, and so the experiment will be repeated in future. Nevertheless, the calculated EC_{50} remains relatively high and would need to be optimised with further analogue design in order to improve the eventual *in vivo* dose.

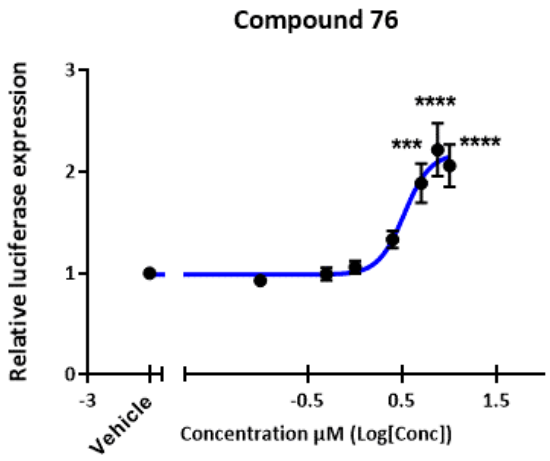

Figure 2.13. Dose-response of **76** in the reporter model of *FXN* expression

2.3.2.4 *Second Compound Series*

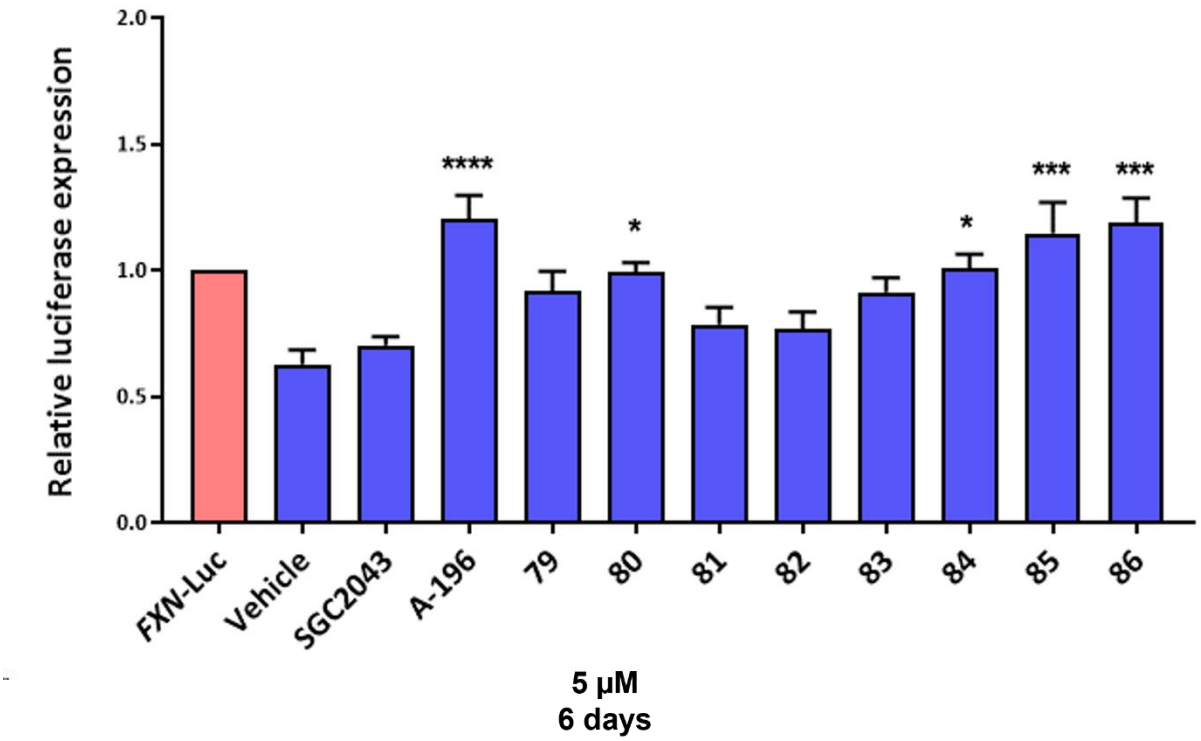

Figure 2.14. Effect of compounds **79-86** on *FXN* expression in a reporter cell model of FRDA. *FXN*-Luc represents a reporter model of healthy *FXN* expression. The vehicle control is DMSO and **SGC2043** acts as a negative control. Cells were treated with compounds at 5 µM for 6 days. Results are the average of three experiments each with three biological replicates. The data are relative to the vehicle and are presented as means ± SEM (one-way ANOVA followed by Bonferroni test): * = $p < 0.05$; ** = $p < 0.01$; *** = $p < 0.001$; **** = $p < 0.0001$

Despite little to no observed potency against the SUV4-20 homologues, four compounds of the pyrazolopyrone series induced a significant increase in *FXN* expression relative to the vehicle (Figure 2.14). This would suggest an increase via a separate mechanism to SUV4-20 inhibition, perhaps some interaction with nascent RNA to prevent R-loop formation. Literature analysis revealed structurally similar compounds that acted as inhibitors of the bromodomains of Polybromo Protein-1 (PB1), which has been implicated in various forms of cancer (**PB1-10** and **PB1-11,** Figure 2.15).[328] This compound series may be interacting with

these domains, however given the histone hypoacetylation characteristic of the FRDA *FXN* locus the mechanism by which this would induce gene expression remains unclear. As such, before further compound characterisation can take place these contentions remain purely speculative. Another possibility, as described previously, is issues with the fidelity of the reporter cell assay. Although the response of cells to the vectors has been extensively characterised,[327] the repeat length of the pBAC-*FXN*-GAA-*Luc* vector is relatively short (310 repeats) compared to what is observed in sufferers (700-800 repeats).[166] This may lead to an inconsistent *FXN* expression profile across cells, with some exhibiting the disease phenotype where others do not. It may also lead to inconsistencies across the epigenome of cells, which may explain why some potent compounds do not induce expression whilst others do.

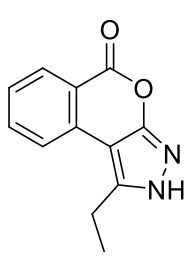

PB1-10
PB1 K_D = 3.4 μM

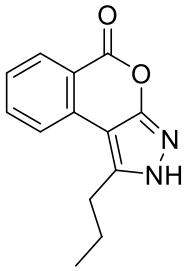

PB1-11
PB1 K_D = 3.3 μM

Figure 2.15. Isochromeno[3,4-*c*]pyrazol-5(2*H*)-one-based PB-1 inhibitors, **PB1-10** and **PB1-11**

2.4 PHARMACOKINETICS

Hepatocyte stability studies were carried out by **Sygnature Discovery**. *In vivo* PK assessment was carried out by **Pharmidex Pharmaceutical Services Ltd**.

2.4.1 *In Vitro* PK

Microsomal stability assays are valuable for determining the clearance of compounds that are substrates for phase I enzymes, however hepatocytes are thought to be closer to a model for the whole liver as they comprise cell membranes and the physiological concentrations of enzymes and cofactors.[329] As such, they are more useful for predicting *in vivo* clearance. Therefore, looking ahead to *in vivo* studies hepatocytes were chosen as a more relevant system for metabolic stability assessment. **A-196** was incubated with mouse and human hepatocytes and displayed a high rate of clearance and relatively short half-life in both (Table 2.8). A longer half-life than that observed after incubation with MLM and HLM may indicate that the uptake of **A-196** into hepatocytes is rate-limiting, suggesting a relatively low degree of passive permeability compared to a high rate of metabolism.[330]

Of the analogues synthesised, compounds **76** and **77** combined structural features envisaged to give the greatest increase in stability with good potency against SUV4-20. Alongside this, they displayed good efficacy in the FRDA reporter model, inducing robust expression of frataxin back to healthy levels. The compounds were incubated with mouse and human hepatocytes, where they displayed stark differences in metabolic stability between species (Table 2.9). Pleasingly, both **76** and **77** displayed vastly improved clearances and half-lives in human hepatocytes compared to **A-196**. In particular, **76** had a half-life of almost three hours, a 9-fold improvement over **A-196**, with an 8-fold reduction in clearance. Although clearance is significantly reduced, it would still ideally be lower as per the target-product profile. The introduction of the *N*-difluoromethyl substituent of **77** led to an increase in potency over **A-196** and it was hoped this would be coupled with an increase in stability relative to **76**, but it displayed a far shorter half-life. In mouse hepatocytes, **76** showed slight improvements in

clearance and half-life over **A-196** however to a far smaller extent than those observed in human hepatocytes. By comparison, **77** showed far worse stability in mouse hepatocytes than in human, and even when compared to **A-196**. Compound **39** was subsequently incubated with mouse and human hepatocytes to investigate the effect on stability of introducing the *N*-difluoromethyl pyrazole.

Table 2.9. Stability in mouse and human hepatocytes of **A-196** and compounds **39**, **76** and **77.**

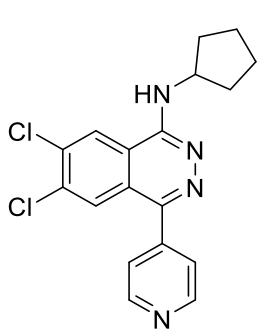

A-196

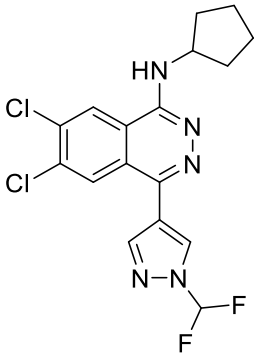

39

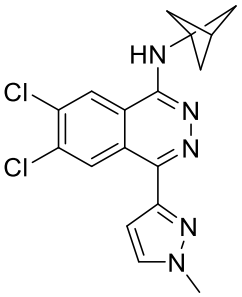

76

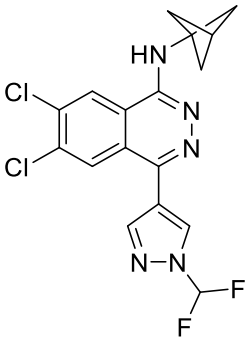

77

Species (hepatocytes)	Compound	CL_{int} (µL/min/x10^6 cells)	$t_{1/2}$ (mins)
Mouse	**A-196**	60	23
	39	248	6
	76	41	34
	77	193	7
Human	**A-196**	72	19
	39	56	25
	76	9	179
	77	13	103

39 displayed comparable stability to **A-196** in human hepatocytes however was cleared at a four-fold higher rate by mouse hepatocytes. This difference may be explained by an increase in the passive permeability of **39** meaning hepatic uptake is no longer rate-limiting, however

this would be expected to be observed in human hepatocytes as well, where instead there is a slight improvement in clearance and half-life. It is more likely that species differences between mice and humans are the cause: for example, mice have a far larger and more complex CYP2C and CYP2D families of enzymes for which these compounds may be substrates.[331]

2.4.2 *In Vivo* PK

The improved stability of **76** in hepatocytes prompted its evaluation *in vivo* to assess its suitability for dosing in a mouse model of FRDA. Subcutaneous (SC) dosing was chosen as the route of administration in order to prolong exposure as much as possible, and because it lends itself to drugs that need chronic dosing as an epigenetic modulator would.[332] The study was carried out in two arms: firstly, dosing exclusively with **76**; and secondly, co-dosing **76** with the CYP3A4 inhibitor **ritonavir** in an attempt to artificially increase half-life further.

The plasma concentration of **76** was assessed at multiple time points following SC dosing at 1 mg/kg. As shown in Table 2.10, in the first arm plasma concentrations peaked at 30 minutes and then dropped to below the limit of quantification after 8 hours, with a half-life of 1.9 hours. In the second arm, the mice were dosed with ritonavir at 12.5 mg/kg orally (PO) 30 minutes prior to receiving an SC dose of **76** at 1 mg/kg. The specific CYP3A4 inhibitor made little to no difference to the half-life of **76**, further supporting the idea that members of the CYP2C and CYP2D families may be responsible for its metabolism. This is a limitation of the study design and perhaps should have been recognised sooner; future studies will evaluate **76** alongside a pan-CYP inhibitor such as **aminobenzotriazole**, or perhaps a CYP2C specific inhibitor like **sulfaphenazole**.

Table 2.10. *In vivo* pharmacokinetic assessment of **76**. Arm 1: **76** (1 mg/kg SC); arm 2: **76** (1 mg/kg SC) + **ritonavir** (12.5 mg/kg PO). [a]Time to reach peak plasma concentration following administration; [b]Maximum plasma concentration; [c]Area under the plasma concentration-time curve from time zero to the time of the last measurable concentration.

Arm	$t_{1/2}$ (hr)	t_{max}[a] (hr)	C_{max}[b] (μM)	AUC_{last}[c] (μM·hr)
1	1.9	0.5	0.299	0.625
2	2.2	0.5	0.295	0.495

Despite this, at 1 mg/kg SC **76** caused no adverse effects and displayed a reasonable half-life. It did not reach plasma concentrations greater than cellular EC_{50} at this dose however, even before the extent of plasma protein binding (PPB) and thus the fraction unbound has been calculated. As a result, the dose would need to be substantially increased in order to achieve efficacy *in vivo* for a prolonged period of time.

2.4.3 CNS MPO Score

To establish the probability that **76** will cross the BBB when tested *in vivo*, it was evaluated against the CNS MPO criteria outlined in section 1.6.2.2 (Table 2.11). A score of 4.78 indicates that **76** will likely cross the BBB and enter the CNS,[302] which is of critical importance for FRDA. Both clogP and clogD remain too high, and further efforts to lower these will aid both clearance and the CNS MPO score.

Table 2.11. Individual calculated CNS MPO component parameter values, their scores, and total MPO score for compound **76**.

	clogP	clogD	MW	tPSA	HBD	pK_a	MPO Total
76	3.53	3.53	360.24	55.63	1	2.29	
MPO Score	0.73	0.23	1	1	0.83	1	**4.79**

2.5 Conclusions and Future Work

At the beginning of this chapter, a set of pharmacokinetic and pharmacodynamic criteria necessary for an *in vivo* SUV4-20 inhibitor to induce *FXN* expression was established (Table 2.1). It was immediately obvious that the reported inhibitor **A-196**, despite excellent *in vitro* activity, would not be suitable as an *in vivo* tool due to its significant metabolic instability. The highly lipophilic cyclopentyl moiety was identified as the principal site of CYP-mediated oxidation, and it became the focus of efforts aimed at developing a new SUV4-20 inhibitor with improved PK and PD properties.

With limited knowledge of the SAR surrounding the molecule, a series of over 70 analogues were synthesised in order to identify potential structural modifications that would improve both clearance and half-life whilst maintaining potency and selectivity. It became apparent that the H4 binding pocket of SUV4-20 was incredibly sensitive to steric factors, with any change in the size of the cyclopentyl ring leading to sharp drops in potency. Traditional strategies, such as the blocking of metabolically labile positions, or the introduction of heteroatoms, were also not tolerated. A means of constraining the molecule in such a way as to be unfavourable to metabolic enzymes without incurring too heavy a steric penalty was found through the introduction of bicycles, with bicyclopentane and norbornane analogues retaining nanomolar potency. Gains in potency were achieved through modification of the

pyridyl substituent, with pyrazole analogues displaying comparable and in one case improved potency over the parent compound. Eventually, combining the modifications resulted in compound **76**, which retained good potency against SUV4-20, induced robust expression of the *FXN* gene in an FRDA reporter cell model, and had vastly improved metabolic stability when assessed both *in vitro* and *in vivo*.

Despite progress having been made, there remain significant issues that need to be addressed in order to meet the requirements of the target product profile. Both on-target and cellular potency need to be improved, and a more suitable alternative to the metabolically unstable cyclopentyl moiety found. Although it was hoped that the selectivity of the analogues compared to **A-196** would not have been greatly affected given the structural similarities, this also needs to be assessed to ensure off-target effects are limited at higher doses. With respect to eventual *in vivo* studies, the extent of PPB needs to be calculated in order to inform the dose needed to increase the circulating unbound concentration to above cellular EC_{50}. The metabolic stability has been substantially improved; however, a relatively high clearance is still contributing to a short half-life. Efforts are ongoing to address this: lowering the logP through substitution on the core (**90**); further improving the stability of **76** by blocking metabolically labile sites (**91**); and scaffold modification to create novel compound series with improved stability (**92**, Figure 2.17). Finally, although MPO calculations suggests it would be CNS-penetrant, this, and other physiochemical properties such as permeability and solubility, needs to be assessed.

Beyond the compound itself, discrepancies between on-target potency and effect in the reporter assay have hampered progress. As can be seen in Figure 2.16, there are a large number of compounds that are potent inhibitors of SUV4-20 but induce no change in *FXN*

expression in the reporter cell model. Similarly, several compounds with no observed potency against SUV4-20 induce an increase in frataxin levels. It may be prudent to repeat the characterisation of the *FXN*-Luc fusion vectors in order to investigate if there are any inconsistencies in both frataxin expression and the changes to the epigenome due to the reduced number of GAA repeats. The various analogues, and in particular the second compound series, will be evaluated in selectivity assays to investigate the potential that *FXN* expression is being increased via a separate pathway to SUV4-20 inhibition. Moving forward, the effect on cellular *FXN* expression will be evaluated in terms of compound EC_{50} as opposed to single point measurements to give a more accurate picture of cellular efficacy. This would also allow the development of an SAR that combines both cellular EC_{50}s and on-target IC_{50}s.

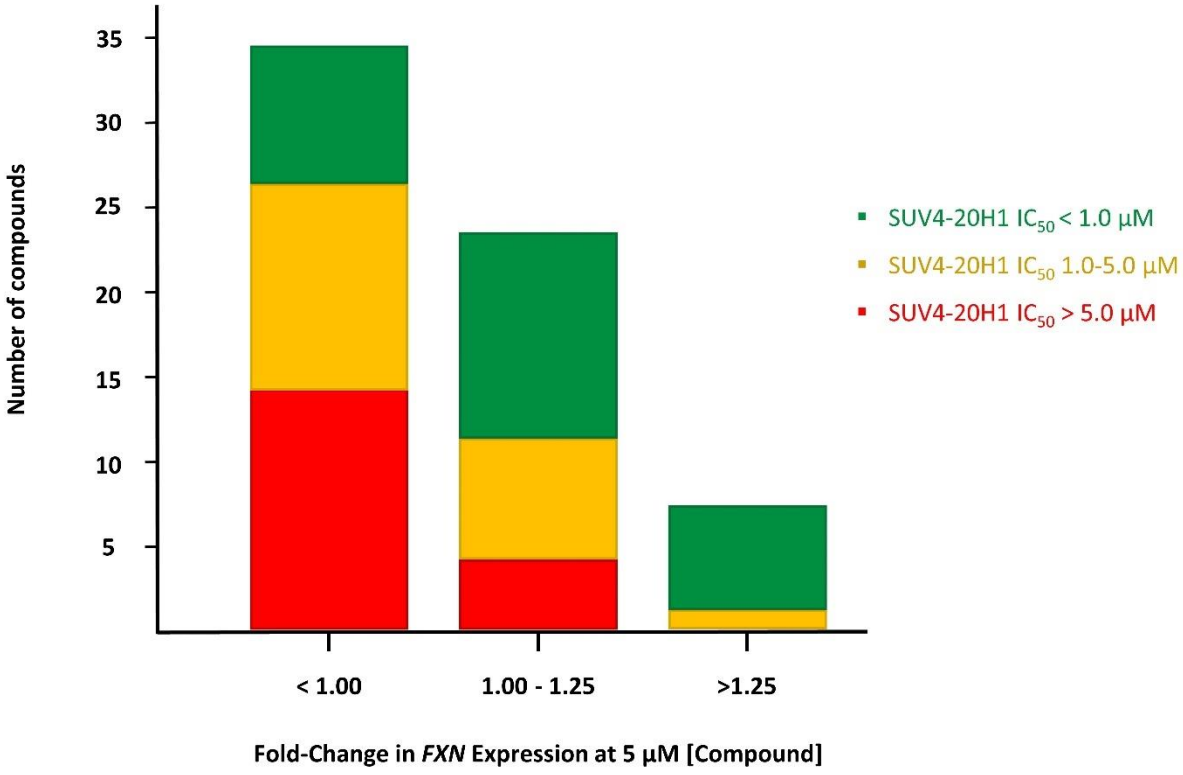

Figure 2.16. Histogram showing the number of compounds with SUV4-20 IC_{50} < 1.0 µM (green), 1.0-5.0 µM (amber), and > 5.0 µM (red), and the fold-change in *FXN* expression they induce in the reporter cell model of FRDA.

Nevertheless, the main goal of this work was to improve the metabolic stability of **A-196** whilst maintaining activity, and great strides have been made towards this. With a nine-fold improvement in half-life from 19 minutes to almost three hours achieved with compound **76**, the stage is set for the *in vivo* assessment of SUV4-20 inhibition for the treatment of FRDA in the near future. Any study will have to be designed with certain factors in mind, for example: appropriate biomarkers for compound efficacy; subcutaneous administration to prolong exposure and enable chronic dosing; potential co-dosing with a specific or broad-spectrum CYP inhibitor; and finally correct choice of animal model given the potential for species differences in metabolism. Should SUV4-20 prove to be an unviable therapeutic target for FRDA, it is hoped that a potent and selective *in vivo* tool will also allow for the interrogation of the target in the pathology of other diseases.

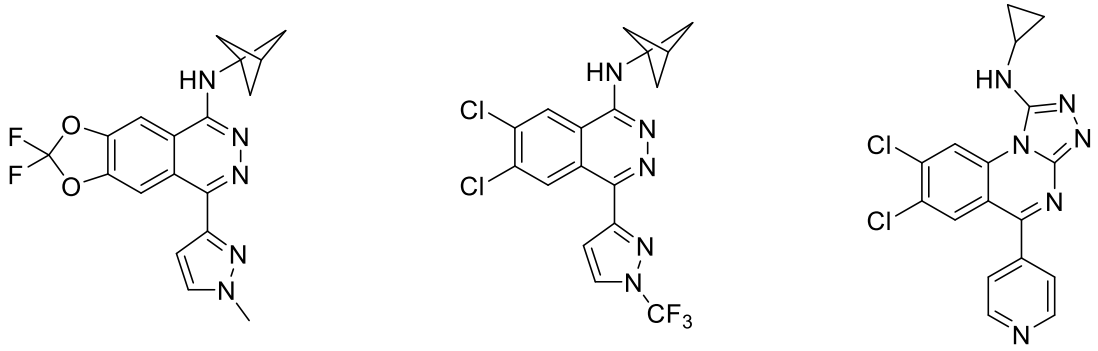

90 **91** **92**

Figure 2.17. Next steps in analogue design towards an *in vivo* SUV4-20 inhibitor.

3 Increasing Frataxin Expression Through Modulation of Proteome – Deubiquitinase Targeting Chimeras

3.1 Project Origin – Induced Protein Stabilisation

In 2001, collaborative work between researchers at the California Institute of Technology and Yale University was published describing a novel method for the conditional inactivation of proteins.[333] A chimeric molecule was synthesised that covalently bound to methionine aminopeptidase-2 (MetAP-2) at one end, and at the other recruited the ubiquitin ligase complex Skp1-Cullin-F box complex containing Hrt1 (SCF). The induced proximity of MetAP-2 to SCF led to its ubiquitination and subsequent degradation by the proteasome, and thus the first proteolysis targeting chimera (PROTAC) was born. This heralded the start of a new era for drug discovery, and since then the field of chimeric (or heterobifunctional) small molecules has exploded.[334]

The key role of a PROTAC is to drive the formation of a ternary complex between a protein of interest (POI), the PROTAC itself, and an E3 ligase that can catalyse the ubiquitination process.[335] This means of promoting protein-protein interactions (PPIs) has inspired a host of novel heterobifunctional molecules, an example of which has already been discussed, the GeneTAC.[246] Other examples include: lysosome targeting chimeras (LYTACs), that bind extracellular and membrane proteins along with a cell-surface lysosome-shuttling receptor to target them for degradation by the lysosome;[336] ribonuclease targeting chimeras (RIBOTACS), which promote the degradation of RNA by ribonucleases;[337] phosphatase recruiting chimeras (PhoRCs), that induce the dephosphorylation of target proteins;[338] autophagy targeting chimeras (AUTACs) which target proteins for degradation by autophagosomes;[339] photochemically targeting chimeras (PHOTACs), which enable optical control of PROTAC

action;[340] and most recently the acetylation tagging system (AceTAG) which induces protein acetylation.[341] Through induction of post-translational modifications (PTMs), these technologies enable the control of protein function, fate, localisation, and can massively impact cellular signalling.

One example described, PhoRCs, are an interesting new addition to the field of heterobifunctionals in that they are the first to describe the removal of a PTM.[338] Whilst inducing the degradation of proteins through ubiquitination has broad applications in disease treatment,[335] the reverse process could also be of great value in diseases that require protein stabilisation. The deubiquitinases (DUBs) are a superfamily of isopeptidases that cleave ubiquitin chains in a manner specific to the degree and internal site of ubiquitination.[342] A chimeric molecule that recruits a DUB to a POI and induces its deubiquitination to prevent degradation could be a ground-breaking addition to the toolbox of heterobifunctionals. It is estimated that 80-90% of cellular proteins are degraded by the ubiquitin-proteasome system (UPS), highlighting the potentially vast applications of this technology.[343] Frataxin is one of these proteins: it is ubiquitinated by the really interesting new gene (RING) finger protein 126 (RNF126) whose genetic ablation leads to the accumulation of frataxin within the cell.[344] A deubiquitinase targeting chimera (DUBTAC) for frataxin could achieve the same effect (Figure 3.1).

3.1.1 Recruiting a Deubiquitinase – USP7

The human genome encodes over 100 DUBs which can be subdivided into six, structurally distinct families:[345] ubiquitin-specific peptidases (USPs); ubiquitin carboxy-terminal hydrolases (UCHs); Machado–Josephin domain-containing proteases (MJDs); ovarian tumour proteases (OTUs); motif-interacting with ubiquitin-containing novel DUB family (MINDYs);

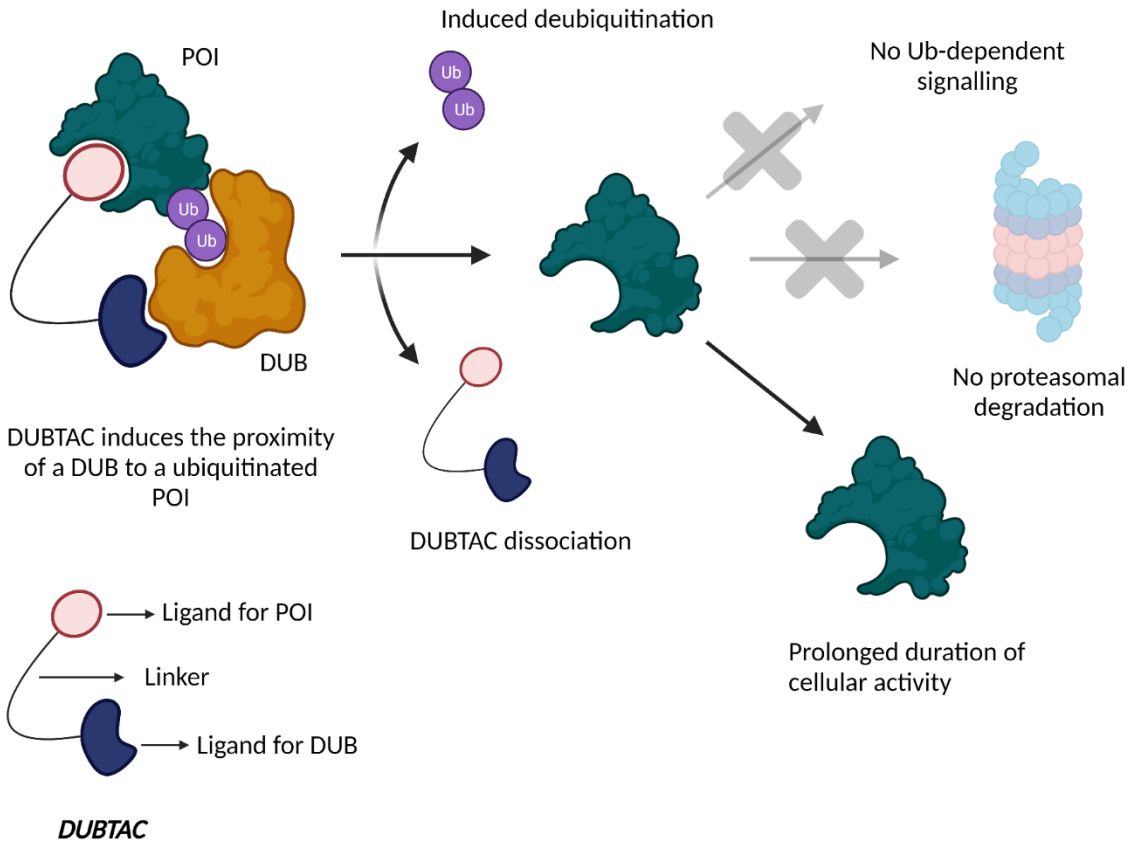

Figure 3.1. The premise of a DUBTAC.

and JAB1, MPN, MOV34 metalloenzymes (JAMMs).[346] They perform three key functions across the cell in relation to deubiquitination: generating free ubiquitin following its translation by the ribosome; shortening polyubiquitin chains to edit the PTM; and finally removing ubiquitin from a protein to reverse ubiquitin signalling or prevent its degradation.[342] Of the myriad ubiquitination types, mono-, K48-linked and K63-linked are the most abundant.[345] K48-linked polyubiquitination is the cellular signal for proteasomal degradation, and so a DUBTAC for induced protein stabilisation would have to recruit a DUB that targets these ubiquitin chains. The USP subfamily of DUBs is by far the largest of the six, and the majority of USPs remove ubiquitin from their substrates regardless of linkage type,[345] making them an ideal family within which to find a suitable DUB. An appropriate ligand will need to

be allosteric, binding to a domain functionally distinct from the catalytic USP domain so as not to inhibit DUB activity.

USP7 targets multiple proteins and has been extensively studied for its role in the deubiquitination of the oncogenic E3 ligase MDM2, which is a key player in the degradation of the tumour suppressor p53.[347,348] It is a 135 kDa protein comprising seven domains: an N-terminal tumor necrosis factor receptor–associated factor (TRAF)-like domain; the catalytic USP domain; and five C-terminal ubiquitin-like domains, UBL1-5 (Figure 3.2).[348] The TRAF-like domain is crucial for substrate recognition via a shallow groove on its surface. The catalytic USP domain contains the conserved fold typical for the USP family of enzymes, along with a catalytic triad comprising residues C223, H464 and D481. USP7 is somewhat unique amongst the USPs in that its catalytic domain remains in the inactive conformation until it binds its ubiquitin substrate or UBL4-5 interact with its "switching loop".[349]

USP7 was initially discovered as a result of its strong interaction with the herpes simplex virus type-1 (HSV-1) encoded E3 ligase, infected cell protein 0 (ICP0).[350,351] ICP0 mediates the proteasomal degradation of a number of cellular targets central to host immune responses, and recruits USP7 to prevent autoubiquitination and stabilise it *in vivo*,[352] akin to a natural DUBTAC. ICP0 binds to USP7 at the interface of UBL1-2, in a similar manner to other known USP7 UBL binders such as GMP-synthetase (GMPS), which allosterically promotes the interaction of UBL4-5 with the catalytic domain to form the active state.[349,353] These proteins interact with the negatively charged surface of UBL2 via a shared *KxxxK* motif, with the two lysine residues forming direct contacts with D762 and D764 of UBL2 (Figure 3.3).[354] Analogous to the first reported PROTAC,[333] a peptide containing this *KxxxK* motif that mimics the allosteric interaction of ICP0 with USP7 could from one end of a prototype DUBTAC. Recruiting

USP7 in this fashion would have the added benefit of promoting the interaction of UBL4-5 with the catalytic domain and increasing its catalytic activity.

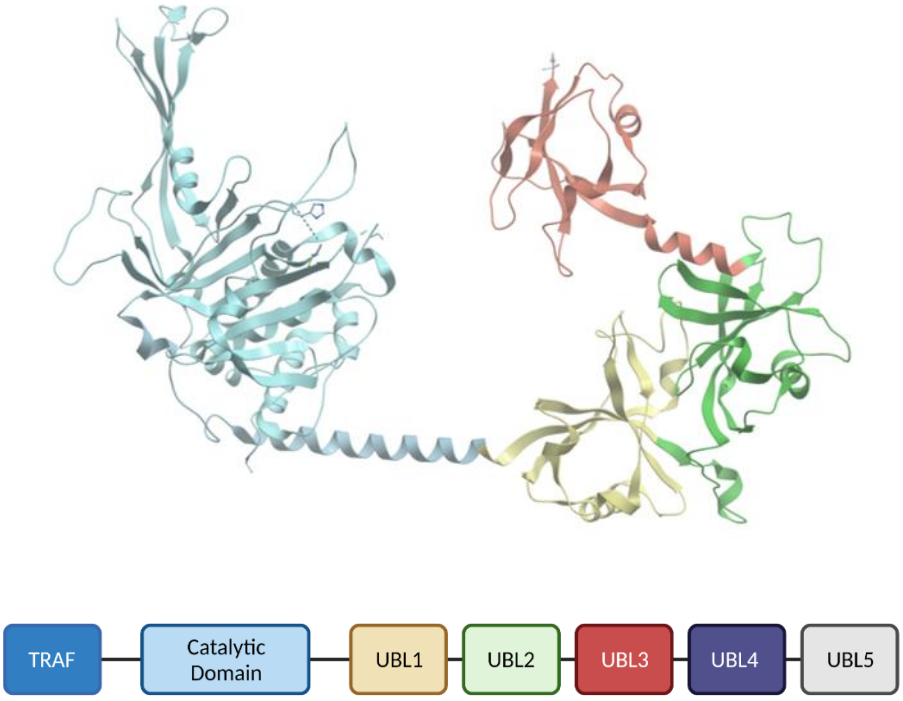

Figure 3.2. Crystal structure of the USP7 catalytic domain (cyan) and UBL1-3 (yellow, green, red, respectively), with accompanying domain map (PDB: 5FWI).

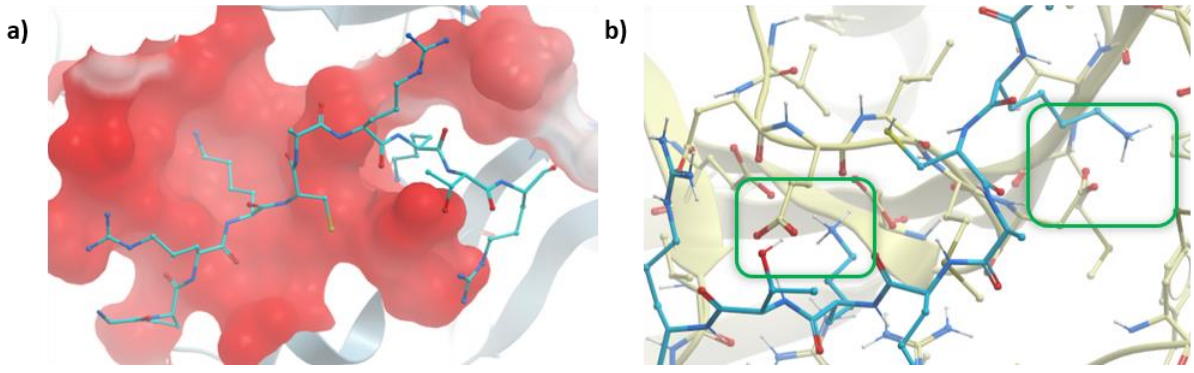

Figure 3.3. **a)** Crystal structure of the interaction of ICP0 with USP7, showing K620 and K624 extending towards the buried aspartate residues; **b)** Specific interactions of K620 and K624 of ICP0 with D762 and D764 of USP7 (highlighted in green) (PDB: 4WPI).

3.1.2 Targeting a POI

Small molecule drug discovery has largely focused on the development of inhibitors, which is in part a reason why the PROTAC field has been able to expand so rapidly: inhibition and degradation work synergistically, and so there is no shortage of ligands from which to develop PROTACs. By contrast, the same cannot necessarily be said for a DUBTAC: whilst an inhibitory ligand may help target a DUB to a POI, continued inhibition would be antagonistic to the desired effect of induced stabilisation. As a result, it may be necessary to focus on the development of allosteric binders for any putative POIs. This may not be the case however, particularly given the mechanisms by which PROTACs exert their effects.[355] Firstly, as the PROTAC is not itself degraded by the proteasome, they can operate sub-stoichiometrically and exert their effect on multiple POI equivalents.[356] DUBTACs could work in a similar manner given binding affinity to the POI may be affected by ubiquitination status. Secondly, because PROTAC efficacy is event-driven, i.e., by ubiquitination rather than binding affinity, potency is not a concern and non-functional ligands can be used and still exert an effect.[355,357] Therefore weak orthosteric ligands could be used that will induce deubiquitination but not inhibit protein activity. Furthermore, given the rate of proteome turnover is on the timescale of days rather than hours as for small molecules,[358] inhibition of the POI may not be a problem given the DUBTAC will be cleared well before the POI is re-ubiquitinated. The issue then becomes one of dosing rather than mechanism of action. Finally, many proteins perform non-enzymatic functions as scaffolding proteins or molecular chaperones, playing central roles in health and disease.[359–361] DUBTACs could be targeted towards these in the first instance as questions around mechanism are investigated.

Research into the structure of frataxin has identified potentially druggable surfaces including the region of K147, frataxin's main ubiquitination site.[362] A series of small molecules that compete with this binding site and induce frataxin accumulation have been described, however require high cellular concentrations (10-45 μM) for efficacy (Figure 3.4).[363] Optimisation of these scaffolds could yield a ligand with improved potency which would then work in concert with the deubiquitinase preventing ubiquitination at other sites.

Failing this, a small molecule screen against frataxin would yield potential ligands amenable for optimisation and eventual use as one end of the DUBTAC. Alternatively, for initial proof of concept studies the ligand for USP7 could be appended to a nanobody specific for frataxin, permitting targeting of the POI in the absence of a suitable small molecule binder. The use of HaloTag technology to append the USP7 ligand to frataxin would also be a convenient means of ensuring induced proximity.[364]

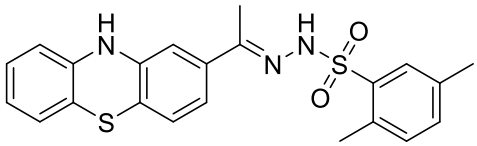

93

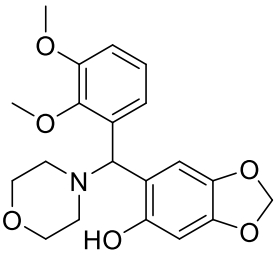

94

Figure 3.4. Reported small molecule binders of the frataxin ubiquitination site.

3.1.3 Linker Design and Other Mechanistic Considerations

In the case of PROTACs, there is not always a correlation between target binding affinity and the efficiency of degradation. Compound design is often centred on the interactions of the respective ligands with their proteins, however as a greater mechanistic understanding has

emerged it has become clear that beyond just conjugating ligands together, linkers play a key role in mediating degradation efficiency.[365,366]

Degradation efficiency is driven by the formation of the ternary complex, which is in turn governed by the strength of cooperativity, a metric used to describe the newly formed PPI.[365] Positive cooperativity occurs when interactions between the E3 ligase and POI enhance ternary complex formation; negative cooperativity describes poor complex formation as a result of repulsive interactions between the two proteins. With respect to linkers, various factors can influence the degree of cooperativity. Linkers are traditionally formed of repeating polyethylene glycol (PEG) units,[365] however purely alky linkers and those formed by click reactions have also proved effective.[367,368] Changes in linker length also influence efficacy with a high degree of sensitivity, for example the introduction of a single ethylene glycol unit into a human epidermal growth factor receptor 2 (HER2) PROTAC led to an almost complete loss of degradative ability.[369] Mechanistic studies have demonstrated the importance of the PROTAC being able to "fold on itself" in order to bury extended surface areas and enable the productive PPI of the protein targets, which can be heavily influenced by linker length.[370] Finally, the vector along which the linker is bonded to either ligand can affect efficacy as well as selectivity for different targets,[366] for example selective degradation of different members of the BET family of bromodomains could be achieved with the same triazolodiazepine ligand by modulating the point of linker attachment.[371]

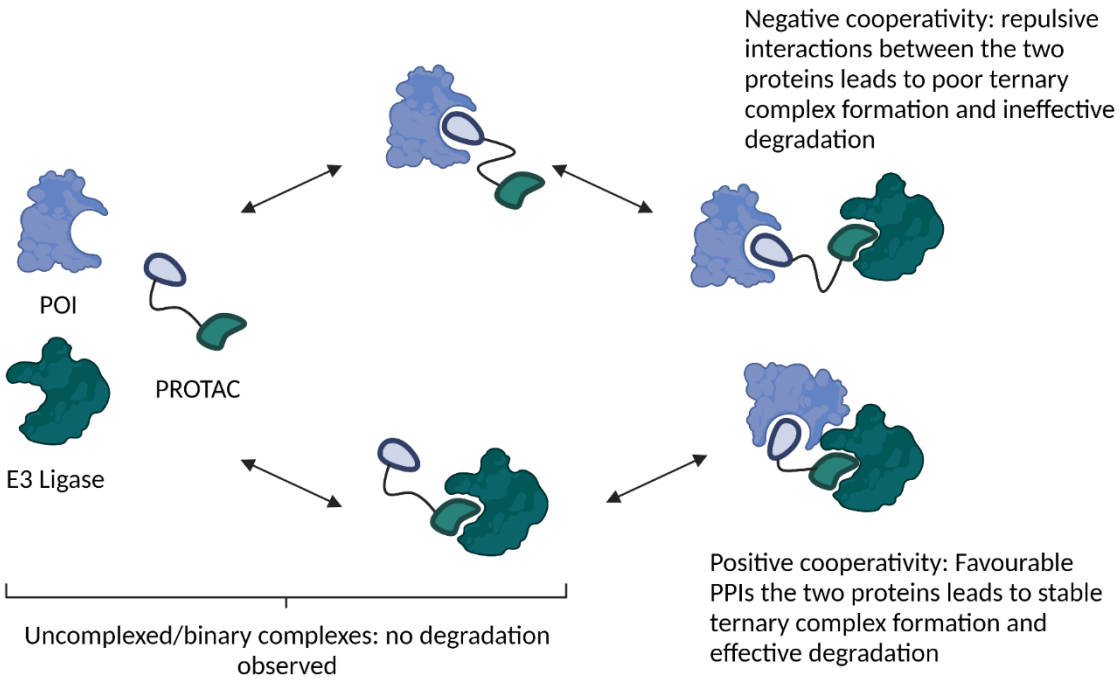

Figure 3.5. The influence of cooperativity on ternary complex formation.

DUBs are of course different from E3 ligases and thus the formation of a ternary complex may not be as important for a DUBTAC, particularly given their efficacy may depend on binding a ubiquitin substrate as opposed to the POI. Nevertheless, USP7 substrate recognition is to some degree dependent on interactions of its TRAF-like domain with the target protein, and so it is expected that ternary complex formation will be a key driver of efficacy.[348] Prototype DUBTACs that recruit a POI using a nanobody or HaloTag technology may be useful as a means of elucidating the necessary ternary structure to subsequently guide linker design, however the impact of the linker on PROTAC efficacy still remains poorly understood, and as such various iterations of linker type and length will likely need to be evaluated.

3.2 TOWARDS AN ALLOSTERIC USP7 LIGAND

3.2.1 Peptide Design and Synthesis

*Biolayer interferometry was carried out by the author with the aid of **Dr James Bennett, Dr Franziska Guenther,** and **Amber Truepenny** of the Target Discovery Institute, University of Oxford.*

The USP7 binding region of ICP0 is found between residues 594-633, which comprises the key ^{620}KCARK^{624} motif.[354] The peptide binds to an acidic region on UBL2 (^{758}DELMDGD^{764}), forming key salt-bridge interactions between the two lysine residues (K620 and K624) and two buried aspartate residues (D762 and D764) on UBL2 (Figure 3.6). A backbone-backbone hydrogen bond is formed between the nitrogen of ICP0 C621 and the oxygen of UBL2 L760, along with a further hydrogen bond between ICP0 T625 and UBL2 E759. R619 and R626 of ICP0 are in proximity to D682 and D758 of UBL2 and may interact weakly, whilst the side chain of R623 (ICP0) points away from the interface and doesn't contribute to binding. Pfoh *et al* evaluated the binding affinity of a 13-amino acid long section of ICP0 comprising the key *KxxxK* motif (^{615}PRGPRKCARKTRH^{627}).[354] It bound to the UBL domains of USP7 with a K_D of 400 nM, and a complete loss of affinity was observed with mutation of either K620 or K624, highlighting the importance of these residues.

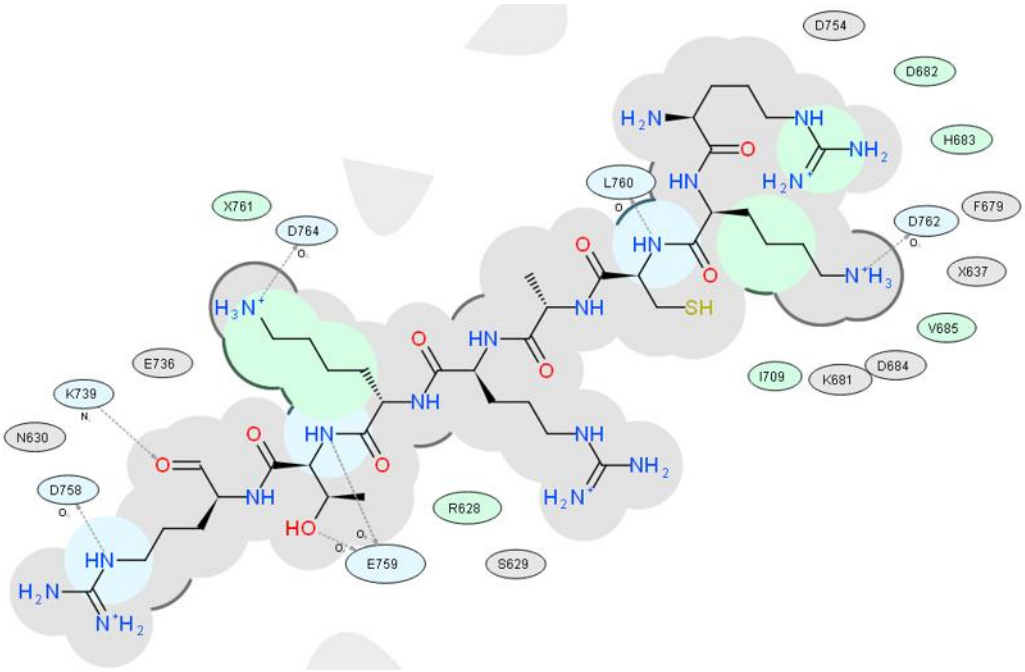

Figure 3.6. Key binding interactions between ICP0 and the UBL domains. Green represents hydrophobic regions of the protein, and grey represents generic van der Waals protein contacts. A blue residue or shading and dashed arrow indicates a hydrogen bonding interaction. X761 corresponds to M761 of the binding site (PDB: 4WPI).

The 13-mer peptide described by Pfoh *et al* provides an ideal starting point for the development of allosteric peptide ligands for USP7.[354] Due to the notoriously poor cellular permeability of peptides,[372] initial efforts were centred around shortening the peptide and evaluating whether the binding affinity could be recapitulated with just the *KxxxK* motif (**95**). Given R623 is not involved in any binding interactions, mutations were introduced in an attempt to engage the proximal M761 of UBL2 in either hydrogen bonding or Met-aromatic interactions (**96** and **97**). Systematic extension beyond the core motif was then evaluated, given concerns that the proline residue may be necessary to induce the optimal binding conformation (**98** and **99**). The peptides were synthesised using standard fluorenylmethyloxycarbonyl (Fmoc)-based solid-phase peptide synthesis (SPPS), employing *N*-*N'*-diisopropylcarbodiimide (DIC) and hydroxybenzotriazole (HOBt) as coupling reagents.

Table 3.1. Binding affinity of ICP0-based peptides **95**-**99** against UBL1-5 of USP7. [a]As determined by biolayer interferometry (BLI): peptides were tested at 1 and 10 μM.

Peptide	Sequence	K_D[a] (μM)
95	Ac-KCARK-COOH	>10
96	Ac-KCSRK-COOH	>10
97	Ac-KCFRK-COOH	>10
98	Ac-RKCARKT-COOH	>10
99	Ac-PRKCARKT-COOH	>10

No appreciable binding was observed at either 1 or 10 μM for the peptides tested in a biolayer interferometry (BLI) assay (Table 3.1). BLI measures the optical interference pattern of white light reflected from two surfaces: a sensor with a layer of immobilised protein, and an internal reference layer. Any ligand biding to the protein will cause an increase in the thickness of this layer, changing the interference pattern and allowing binding to be measured as a function of the change in thickness. Clearly the core *KxxxK* motif alone is not sufficient for binding to USP7, and the peptide requires contributions from the surrounding resides. As such, a further set of peptides were designed that grew the peptide iteratively in both directions in order to ascertain both the shortest length of peptide that could be used for binding as well as the key residues beyond the core motif (Table 3.2). The peptide described by Pfoh *et al* was also evaluated (**107**),[354] along with a longer section of the ICP0 binding region (**108**). Instead of free acids, the peptides were evaluated as C-terminus amides, in order to avoid potentially unfavourable interactions with the acidic UBL2 binding region and to mimic the native protein more closely. Again, the peptides were synthesised using standard Fmoc-SPPS, with DIC and HOBt as coupling reagents. Rink amide resins were used to derive C-terminus amides.

Three of the peptides (**100**, **107**, **108**) initially showed binding to USP7 at both 1 and 10 μM, however this signal was also observed in the absence of the protein, indicating non-specific binding to the biosensor. Apart from this, no binding was observed at either concentration for the remaining peptides. Further assessments of affinity could make use of blocking reagents in order to reduce non-specific interactions to background levels. Failing this, an assay such as isothermal titration calorimetry (ITC) could be used which would circumvent the need for sensors.

Table 3.2. Binding affinity of a second series of ICP0-based peptides **100**-**108** against UBL1-5 of USP7.

Peptide	Sequence	K_D (μM)
100	Ac-PRKCARKTR-NH_2	N/A
101	Ac-GPRKCARKT-NH_2	>10
102	Ac-PRKCARKTRH-NH_2	>10
103	Ac-RGPRKCARKT-NH_2	>10
104	Ac-PRGPRKCARKT-NH_2	>10
105	Ac-PRGPRKCARKTR-NH_2	>10
106	Ac-RGPRKCARKTRH-NH_2	>10
107	Ac-PRGPRKCARKTRH-NH_2	N/A
108	Ac-SGPRGPRKCARKTRHAE-NH_2	N/A

3.2.2 Next Steps

Before further progress can be made, the concerns surrounding the assay need to be addressed, specifically the issue of non-specific binding. This may be an inherent problem with the use of cationic peptides and biosensors, and therefore ITC would offer a convenient solution. However, ITC requires relatively large amounts of protein per experiment which

would limit the potential throughput. The use of blocking reagents would enable the use of BLI which is far higher throughput, following which ITC could be used a means of validating any observed hits. Once suitable assay conditions have been chosen, the above peptides can be re-tested and details of the SAR surrounding the ICP0-USP7 binding interaction can be elucidated, particularly with respect to the importance of the residues either side of the core *KxxxK* motif.

The ultimate goal of the development of this technology is to incorporate a small molecule recruiter of a DUB, and so once a suitable peptide has been found, it can serve as a reporter molecule for a screening campaign against the UBL domains of USP7. The surface of the UBL2 binding domain provides numerous opportunities for covalent modification, the tractability of which could be evaluated using targeted mutation of a model peptide. The incorporation of covalent warheads, for example sulfonyl fluorides to target lysines or serines, or an oxaziridine to target the binding site methionine, could pave the way for their use in an eventual small molecule binder.

3.3 Conclusions and Future Work

Whilst this work was ongoing, two separate reports were published detailing the development of technologies aimed at the targeted stabilisation of proteins. One described the development of engineered deubiquitinases (enDUBs) that consisted of the catalytic domain of a deubiquitinase fused to an antibody for yellow fluorescent protein (YFP).[373] When this was co-expressed with a cystic fibrosis transmembrane regulator (CFTR)-YFP fusion protein, the enDUB was recruited and able to stabilise CFTR mutants associated with cystic fibrosis, rescuing the disease phenotype. The second report was a pre-print that also concerned the rescue of CFTR mutants however this time described a small molecule DUBTAC

that recruited the DUB OTUB1 via a covalent ligand for an allosteric cysteine.[374] This was linked to the CFTR-targeting small molecule **lumacaftor** and was shown to stabilise the mutant protein and increase its levels in a concentration and time-dependent manner.

Both of these reports provide encouragement and demonstrate that the concept of protein stabilisation via induced deubiquitination is feasible. However, there is little by way of mechanistic understanding: for the small molecule DUBTAC, only two linker lengths are evaluated and there are no structural insights as to their differences in efficacy. Similarly, there is no information regarding a potential ternary complex formed between the enDUB and its target, so this remains an area requiring further investigation. As well as this, the OTUB1 recruiting ligand of the DUBTAC shows poor selectivity for the DUB, which is of particular concern given it contains a covalent warhead. Alongside potential issues with permeability, this may explain why cellular high concentrations of the DUBTAC (10 μM) are required to elicit the desired response. As such, there remains a need for a more potent and specific DUB recruiter. The natural role of the ICP0 protein highlights its suitability as inspiration for this:[352] it acts as a DUBTAC for HSV-1 and specifically targets USP7 via its UBL domains, increasing its catalytic activity in the process. A small molecule that could recapitulate this interaction would be of value not least because of its specificity, but also due to the promiscuous nature of USP7's deubiquitinase activity, both with respect to the substrate protein and its degree and type of ubiquitination.[348] Work has begun in earnest on the development of allosteric peptide ligands for USP7 and is ongoing. A suitable peptide will enable a small molecule screen and accelerate DUBTAC development.

With respect to its application in FRDA, any DUBTAC would require a suitable ligand for frataxin. This would form part of a parallel development strategy with a ligand for USP7. The

applications of DUBTAC technology are not limited to FRDA: currently work is ongoing to develop a ligand for phenylalanine hydroxylase (PAH), deficiencies in which cause the metabolic disorder phenylketonuria.[375] The applications in cystic fibrosis have already been discussed,[373,374] and beyond this there are various diseases that could benefit from targeted stabilisation and induced up-regulation of proteins. For example, tumour suppressors p53 and p27 are regulated by the UPS and actively degraded to enable tumour cell proliferation.[376] Smad7 is degraded by the UPS and regulates transforming growth factor-β (TGF-β) signalling in progressive renal fibrosis; its upregulation has been shown to be protective in various disease models.[377] BCL2-associated athanogene 3 (BAG3) is constitutively expressed in the heart and skeletal muscle and its levels are significantly decreased in cases of dilated cardiomyopathy and late-stage heart failure.[378] Finally, intracellular amyloid-beta accumulation and impaired proteasome function in Alzheimer's disease (AD) can be reversed by the ubiquitin E3 ligase parkin, whose expression is downregulated in diseased brains.[379] These are but a fraction of the 80-90% of proteins whose levels are regulated by the UPS,[343] and therefore very much not the only diseases in which DUBTACs may find applications.

Outside of therapeutic applications, DUBTACs could be used to probe the role of non-degradative ubiquitin signalling in a variety of cellular processes. For example, K63-linked polyubiquitination (regulated by DUBs such as cylindromatosis (CYLD)) modulates protein trafficking, kinase activation, phosphatase activation, DNA repair, NF-κB activation, chromatin dynamics, and plays an essential role in the signal transduction of inflammation.[380,381] As well as this, histone ubiquitination has been linked to both transcriptional activation and repression, along with the DNA damage response.[382] A DUBTAC could interrogate these processes and provide valuable insights into complex cellular biology.

4 THESIS CONCLUSIONS AND FUTURE PLANS

Friedreich's ataxia is a rare, autosomal recessive neurodegenerative disorder that leads to progressive loss of the sensory neurons of the dorsal root ganglia. The damage results in awkward, unsteady movements and impaired sensory functions, leaving sufferers wheelchair bound and eventually incapacitated. It is caused by the expansion of a trinucleotide repeat region within the first intron of the *FXN* gene, which leads to reduced expression of the essential mitochondrial protein frataxin. The resulting mitochondrial defects can lead to cardiomyopathy alongside neurodegeneration, with heart disease the eventual cause of death for sufferers. Currently, there is no available treatment.

The work in this thesis describes two approaches to the treatment of FRDA. Genetic ablation and small molecule inhibition of the H4K20 methyltransferase SUV4-20 has been shown to reverse the heterochromatin-induced pathological reduction in *FXN* gene expression. Chapter 2 builds on these discoveries and describes efforts to develop a small molecule SUV4-20 inhibitor suitable for *in vivo* evaluation. **A-196** is a potent and selective inhibitor however suffers from very poor metabolic stability, a result of extensive oxidation on the lipophilic cyclopentyl substituent. Numerous analogues were designed and synthesised that attempted to address the metabolic liabilities of **A-196** whilst also further probing SAR around the scaffold.

The SUV4-20 binding pocket was found to be incredibly sensitive to both steric and electronic factors. Traditional strategies for improving metabolic stability, such as fluorination or the introduction of heteroatoms, were not tolerated. Changes in the size of the cyclopentyl substituent led to large losses of activity: only the introduction of bridging atoms in the form

of bicyclic analogues maintained potency. The solvent exposed pyridyl moiety was more amenable to modification; aryl-based hydrogen bonding substituents were well tolerated, with an *N*-difluoromethylpyrazole-based analogue (**39**) displaying improved potency over the parent compound. Modulation of the central phthalazine core substituents was synthetically challenging and not extensively explored, however conversion to a dimethoxy-substituted scaffold led to complete loss of potency. The analogues were also evaluated in a reporter cell model of FRDA that expressed a frataxin-luciferase fusion protein and used luciferase intensity as a proxy for frataxin expression. The cells were treated with compounds at 5 µM for six days, and many compounds restored the levels of frataxin expression to those of the healthy control. There were some discrepancies between on-target potency and efficacy in the reporter model, which may have been due to issues of cell permeability or compound solubility, however raised questions about the reproducibility and fidelity of the assay. Work addressing these concerns is currently ongoing.

The eventual strategy pursued to improve metabolic stability was to constrain labile sites in such a way as to be unfavourable to metabolic enzymes. Introducing a bicyclopentane substituent maintained potency, and further derivatisation to include a pyrazole substituent yielded compound **76**, with an IC_{50} of 0.4 µM against SUV4-20 and EC_{50} of 3.3 µM in the reporter cell model of FRDA. The modifications increased the half-life in human hepatocytes nine-fold over **A-196**, from 19 to 180 minutes, and when dosed subcutaneously in mice at 1 mg/kg **76** displayed a half-life of approximately two hours and caused no adverse effects. CNS MPO evaluation gave a score of 4.78 out of 6, suggesting that the compound would cross the blood-brain barrier. There are still some issues to address: both on-target and cellular potency need to improve, and further gains in stability are needed. Target selectivity and compound safety assays need to be carried out, as well as the evaluation of physiochemical properties

such as solubility and permeability. Alongside these, prior to *in vivo* assessment the extent of plasma protein binding and CNS penetrance need to be established to aid decisions on dosing.

Work is ongoing to address the concerns with cellular potency, and to build on the gains already made in metabolic stability. Efforts will focus on reducing the lipophilicity of the compounds and the evaluation of new core scaffolds that might provide improvements in stability. Nevertheless, **76** is a promising candidate for *in vivo* assessment of a SUV4-20 inhibitor for the treatment of FRDA.

The second section explores the conceptualisation and early efforts towards the development of a heterobifunctional molecule for induced protein stabilisation via deubiquitination, a deubiquitinase targeting chimera or DUBTAC. The pathological basis of FRDA is the reduction in frataxin levels; a DUBTAC would act to prevent the degradation of frataxin by the UPS and lead to its accumulation in cells. USP7 was chosen as the preferred DUB target due to its well-studied interaction with the E3 ligase ICP0, a protein that plays a key role in protecting HSV-1 from host cell innate immune responses. ICP0 recruits USP7 via its UBL domains and hijacks its deubiquitinase activity, preventing autoubiquitination. Previous mapping of the interaction between ICP0 and USP7 identified a core peptide motif essential for binding and provided inspiration for an allosteric USP7 recruiter. Initial work focused on exploring the SAR of the interaction between the peptide and USP7, however issues with the chosen assay conditions hampered progress this area. Nevertheless, work is ongoing to address these and develop a suitable peptide-based ligand that will allow initial proof-of-concept studies, as well as act as a reporter molecule for a screen of small molecules against the UBL domains of USP7.

An effective DUBTAC will likely find myriad applications in the worlds of disease treatment and chemical biology. There are numerous diseases where loss-of-function mutations and

reduced protein expression play pathological roles; analogous to PROTACs, which challenged traditional, affinity-driven notions of drug discovery, DUBTACs could offer a novel route to disease treatment not limited by requirements of potency and selectivity. As well as this, they would enable interrogation of the complex cellular pathways governed by ubiquitination and provide insight into the numerous roles it plays.

It is hoped that the progress made in developing a SUV4-20 inhibitor to treat FRDA will continue, enabling evaluation in animal models of the disease and accelerating preclinical development. Despite progress in the development of other therapies, there remains no approved drug for this devastating disease, leaving almost two million people with no recourse to treatment. More broadly, it has highlighted the utility of epigenetic probe libraries to enable drug discovery and should inspire similar approaches in other diseases. DUBTACs offer a complementary means of treating FRDA, and recent similar work has exemplified their potential. Although very much still in its infancy, the project has enormous potential and could cause a paradigm shift in the fields of disease treatment and chemical biology.

5 APPENDIX

5.1 CHAPTER 2

Supplementary Table 2.1. Full metabolic stability for **A-196** in human and mouse liver microsomes. [a]SE = standard error of the mean.

	Metabolic Stability (Human)				Metabolic Stability (Mouse)			
Compound	**CL_{int} (µL/min/mg protein)**	**SE[a] CL_{int}**	**$t_{1/2}$ (min)**	**n**	**CL_{int} (µL/min/mg protein)**	**SE CL_{int}**	**$t_{1/2}$ (min)**	**n**
A-196	191	5.88	7.28	5	239	4.66	5.79	5

Supplementary Table 2.2. Full metabolic stability data for **A-196, 39, 76,** and **77** in human and mouse hepatocytes. [a]CV = coefficient of variation, the ratio of the standard deviation to the mean.

	Metabolic Stability (Human)				Metabolic Stability (Mouse)			
Compound	**CL_{int} (µL/min/x10^6 cells)**	**CV[a] CL_{int} (%)**	**$t_{1/2}$ (min)**	**n**	**CL_{int} (µL/min/x10^6 cells)**	**CV CL_{int} (%)**	**$t_{1/2}$ (min)**	**n**
A-196	72	13.0	19	2	60	9.7	23	2
39	56	13.0	25	2	248	13.4	6	2
76	9	7.0	179	2	41	15.0	34	2
77	13	13.7	103	2	193	13.4	7	2

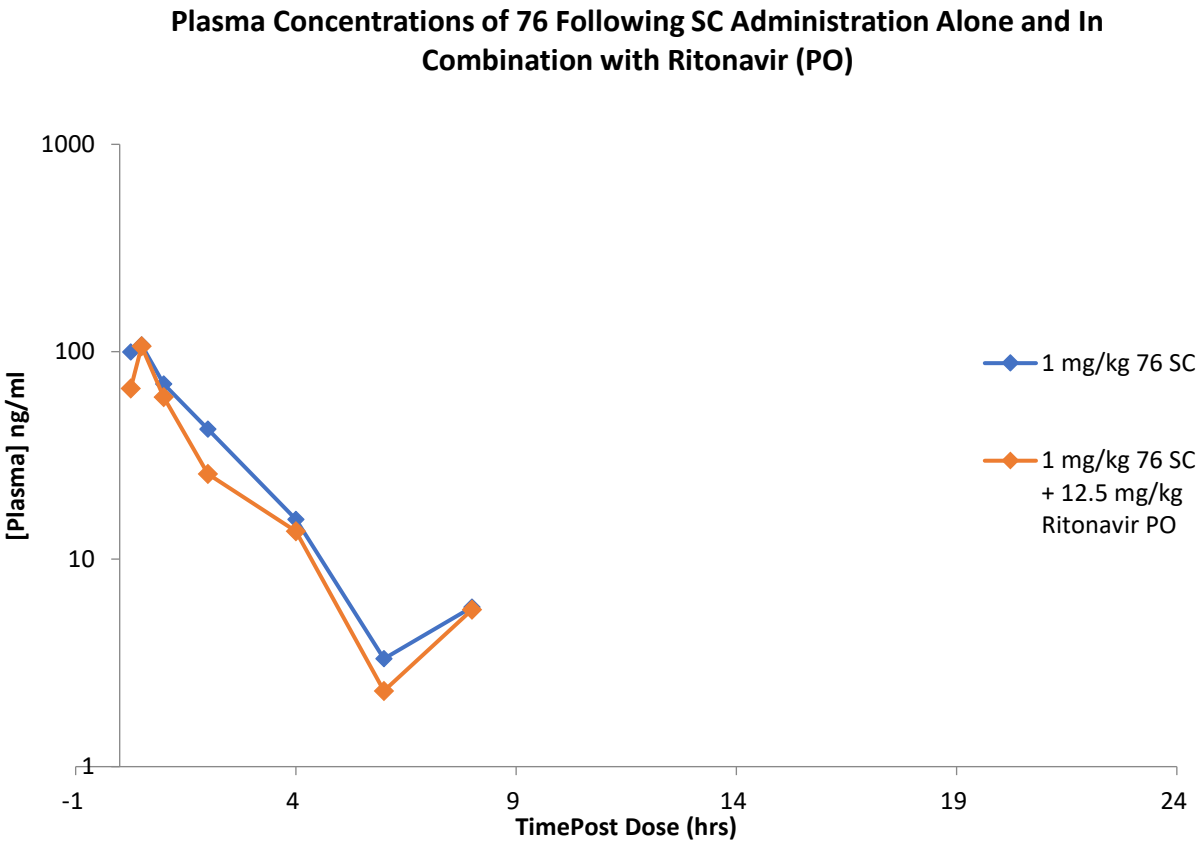

Supplementary Figure 2.1. Plasma concentrations of compound **76** following 1 mg/kg SC administration alone and in combination with CYP3A4 inhibitor **ritonavir** (12.5 mg/kg PO). The study was carried out in male CD1 mice (n = 3). **76** was formulated as a solution in DMSO (10%) and hydroxypropyl-β-cyclodextrin (HP-β-CD, 90%). **Ritonavir** was formulated as a solution in DMSO (10%), cremaphor (10%), and water (80%), and was dosed 30 minutes before **76**.

5.2 CHAPTER 3

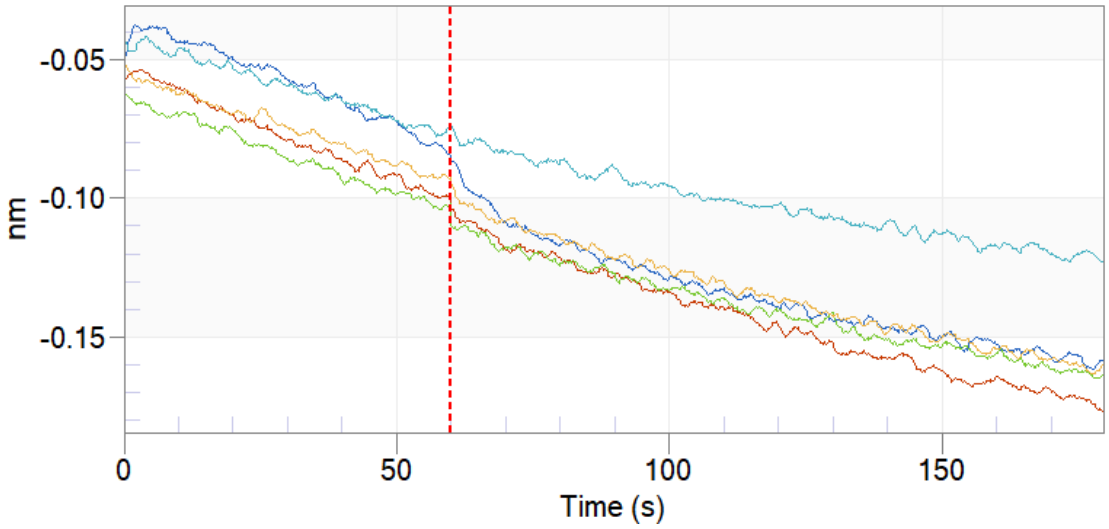

Supplementary Figure 3.1. BLI plot mapping the interaction of peptides **95**-**99** (10 µM) with USP7 (immobilised on an anti-His (HIS2) biosensor). Binding is measured as a function of the change in the wavelength of light observed upon binding.

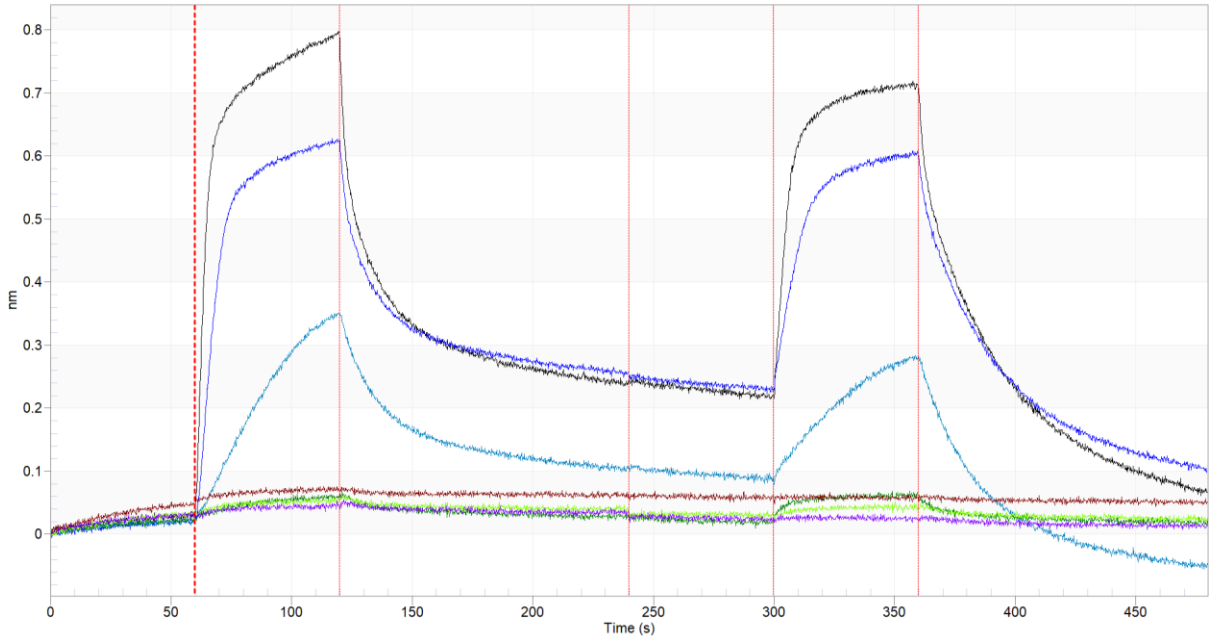

Supplementary Figure 3.2. BLI plot mapping the interaction of peptides **100-108** at 1 (50s) and 10 (300s) µM with USP7 (immobilised on an anti-His (HIS2) biosensor).

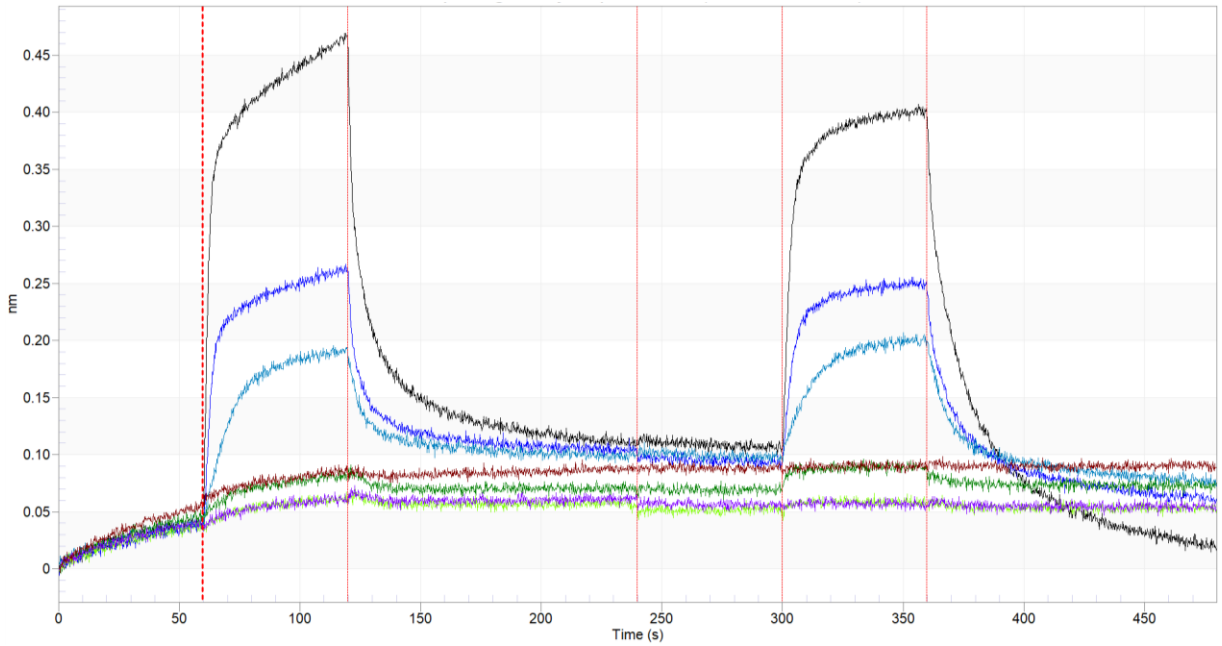

Supplementary Figure 3.3. BLI plot mapping the interaction of peptides **100-108** at 1 (50s) and 10 (300s) µM with a reference anti-His (HIS2) biosensor, indicating the binding observed in Supplementary Figure 3.2 is the result of non-specific binding to the sensor.

6 BIBLIOGRAPHY

1 Jack Klugman's Secret, Lifesaving Legacy https://www.washingtonpost.com/news/wonk/wp/2012/12/25/jack-klugmans-secret-lifesaving-legacy/?variant=116ae929826d1fd3, (accessed April 7, 2021).

2 S. Thomas and A. Caplan, *JAMA - Journal of the American Medical Association*, 2019, **321**, 833–834.

3 K. Mikami, *Social History of Medicine*, 2019, **32**, 609–630.

4 M. E. Haffner, *Clinical Pharmacology and Therapeutics*, 2016, **100**, 342–343.

5 M. J. Finkel, *New England Journal of Medicine*, 1980, **302**, 643–644.

6 M. H. van Woert, *New England Journal of Medicine*, 1978, **298**, 903–906.

7 The Story Behind the Orphan Drug Act, https://www.fda.gov/industry/orphan-products-development-events/story-behind-orphan-drug-act, (accessed April 7, 2021).

8 Jack Klugman's Other Amazing Legacy, https://www.medpagetoday.com/blogs/celebritydiagnosis/36643, (accessed April 11, 2021).

9 House Told for Need for "Orphan Drugs", https://www.nytimes.com/1981/03/10/us/house-told-of-need-for-orphan-drugs.html, (accessed April 7, 2021).

10 Electronic Code of Federal Regulations (eCFR): Title 21, Chapter I, Subchapter D, Part 316, Subpart C – Designation of an Orphan Drug, https://www.ecfr.gov/cgi-bin/retrieveECFR?gp=&SID=718f6fcbc20f2755bd1f5a980eb5eecd&mc=true&n=sp21.5.316.c&r=SUBPART&ty=HTML#se21.5.316_120, (accessed April 11, 2021).

11 M. E. Haffner, J. Whitley and M. Moses, *Nature Reviews Drug Discovery*, 2002, **1**, 821–825.

12 S. Aymé, A. Kole and S. Groft, *The Lancet*, 2008, **371**, 2048–2051.

13 O. Wellman-Labadie and Y. Zhou, *Health Policy*, 2010, **95**, 216–228.

14 W. Yin, *Journal of Health Economics*, 2008, **27**, 1060–1077.

15 M. E. Haffner and P. D. Maher, *Expert Opinion on Drug Discovery*, 2006, **1**, 521–524.

16 E. Tambuyzer, B. Vandendriessche, C. P. Austin, P. J. Brooks, K. Larsson, K. I. Miller Needleman, J. Valentine, K. Davies, S. C. Groft, R. Preti, T. I. Oprea and M. Prunotto, *Nature Reviews Drug Discovery*, 2020, **19**, 93–111.

17 M. Haendel, N. Vasilevsky, D. Unni, C. Bologa, N. Harris, H. Rehm, A. Hamosh, G. Baynam, T. Groza, J. McMurry, H. Dawkins, A. Rath, C. Thaxon, G. Bocci, M. P. Joachimiak, S. Köhler, P. N. Robinson, C. Mungall and T. I. Oprea, *Nature Reviews Drug Discovery*, 2020, **19**, 77–78.

18 K. M. Boycott, M. R. Vanstone, D. E. Bulman and A. E. MacKenzie, *Nature Reviews Genetics*, 2013, **14**, 681–691.

19 A. M. Issa, *Nature Reviews Drug Discovery*, 2002, **1**, 300–308.

20 M. Hay, D. W. Thomas, J. L. Craighead, C. Economides and J. Rosenthal, *Nature Biotechnology*, 2014, **32**, 40–51.

21 M. J. Waring, J. Arrowsmith, A. R. Leach, P. D. Leeson, S. Mandrell, R. M. Owen, G. Pairaudeau, W. D. Pennie, S. D. Pickett, J. Wang, O. Wallace and A. Weir, *Nature Reviews Drug Discovery*, 2015, **14**, 475–486.

22 M. C. Parrish, Y. J. Tan, K. v. Grimes and D. Mochly-Rosen, *Annual Review of Pharmacology and Toxicology*, 2019, **59**, 405–421.

23 A. A. Seyhan, *Translational Medicine Communications*, 2019, **4**, 1–19.

24 J. D. Hughes, J. Blagg, D. A. Price, S. Bailey, G. A. DeCrescenzo, R. v. Devraj, E. Ellsworth, Y. M. Fobian, M. E. Gibbs, R. W. Gilles, N. Greene, E. Huang, T. Krieger-Burke, J. Loesel, T. Wager, L. Whiteley and Y. Zhang, *Bioorganic and Medicinal Chemistry Letters*, 2008, **18**, 4872–4875.

25 J. J. Sutherland, J. W. Raymond, J. L. Stevens, T. K. Baker and D. E. Watson, *Journal of Medicinal Chemistry*, 2012, **55**, 6455–6466.

26 T. T. Wager, B. L. Kormos, J. T. Brady, Y. Will, M. D. Aleo, D. B. Stedman, M. Kuhn and R. Y. Chandrasekaran, *Journal of Medicinal Chemistry*, 2013, **56**, 9771–9779.

27 D. Muthas, S. Boyer and C. Hasselgren, *Medicinal Chemistry Communications*, 2013, **4**, 1058–1065.

28 D. Cook, D. Brown, R. Alexander, R. March, P. Morgan, G. Satterthwaite and M. N. Pangalos, *Nature Reviews Drug Discovery*, 2014, **13**, 419–431.

29 A. King, *Nature Reviews Cardiology*, 2010, **7**, 602.

30 T. Tralau and A. Luch, *Trends in Pharmacological Sciences*, 2012, **33**, 353–364.

31 M. E. Bunnage, *Nature Chemical Biology*, 2011, **7**, 335–339.

32 P. Morgan, P. H. van der Graaf, J. Arrowsmith, D. E. Feltner, K. S. Drummond, C. D. Wegner and S. D. A. Street, *Drug Discovery Today*, 2012, **17**, 419–424.

33 K. D. Davis, N. Aghaeepour, A. H. Ahn, M. S. Angst, D. Borsook, A. Brenton, M. E. Burczynski, C. Crean, R. Edwards, B. Gaudilliere, G. W. Hergenroeder, M. J. Iadarola, S. Iyengar, Y. Jiang, J. T. Kong, S. Mackey, C. Y. Saab, C. N. Sang, J. Scholz, M. Segerdahl, I. Tracey, C. Veasley, J. Wang, T. D. Wager, A. D. Wasan and M. A. Pelleymounter, *Nature Reviews Neurology*, 2020, **16**, 381–400.

34 D. B. Fogel, *Contemporary Clinical Trials Communications*, 2018, **11**, 156–164.

35 M. R. Nelson, H. Tipney, J. L. Painter, J. Shen, P. Nicoletti, Y. Shen, A. Floratos, P. C. Sham, M. J. Li, J. Wang, L. R. Cardon, J. C. Whittaker and P. Sanseau, *Nature Genetics*, 2015, **47**, 856–860.

36 A. Wendler and M. Wehling, *Current Opinion in Pharmacology*, 2010, **10**, 601–606.

37 M. Jucker, *Nature Medicine*, 2010, **16**, 1210–1214.

38 K. M. Boycott and D. Ardigó, *Nature Reviews Drug Discovery*, 2018, **17**, 151–152.

39 E. Tambuyzer, *Nature Reviews Drug Discovery*, 2010, **9**, 921–929.

40 B. M. Buckley, *The Lancet*, 2008, **371**, 2051–2055.

41 W. Sun, W. Zheng and A. Simeonov, *American Journal of Medical Genetics Part A*, 2017, **173**, 2307–2322.

42 A. J. Carter, O. Kraemer, M. Zwick, A. Mueller-Fahrnow, C. H. Arrowsmith and A. M. Edwards, *Drug Discovery Today*, 2019, **24**, 2111–2115.

43 C. H. Arrowsmith, J. E. Audia, C. Austin, J. Baell, J. Bennett, J. Blagg, C. Bountra, P. E. Brennan, P. J. Brown, M. E. Bunnage, C. Buser-Doepner, R. M. Campbell, A. J. Carter, P. Cohen, R. A. Copeland, B. Cravatt, J. L. Dahlin, D. Dhanak, A. M. Edwards, S. v. Frye, N. Gray, C. E. Grimshaw, D. Hepworth, T. Howe, K. V. M. Huber, J. Jin, S. Knapp, J. D. Kotz, R. G. Kruger, D. Lowe, M. M. Mader, B. Marsden, A. Mueller-Fahrnow, S. Müller, R. C. O'Hagan, J. P. Overington, D. R. Owen, S. H. Rosenberg, B. Roth, R. Ross, M. Schapira, S. L. Schreiber, B. Shoichet, M. Sundström, G. Superti-Furga, J. Taunton, L. Toledo-Sherman, C. Walpole, M. A.

Walters, T. M. Willson, P. Workman, R. N. Young and W. J. Zuercher, *Nature Chemical Biology*, 2015, **11**, 536–541.

44 P. Workman and I. Collins, *Chemistry and Biology*, 2010, **17**, 561–577.

45 S. V. Frye, *Nature Chemical Biology*, 2010, **6**, 159–161.

46 D. M. C. Schwarz and J. E. Gestwicki, *ACS Chemical Biology*, 2018, **13**, 1109–1110.

47 R. M. Garbaccio and E. R. Parmee, *Cell Chemical Biology*, 2016, 23, 10–17.

48 R. B. A. Quinlan and P. E. Brennan, *RSC Chemical Biology*, 2021, **2**, 759-795.

49 M. Beltramo, *Mini-Reviews in Medicinal Chemistry*, 2008, **9**, 11–25.

50 P. J. Manley, A. Zartman, D. v. Paone, C. S. Burgey, D. A. Henze, K. della Penna, R. Desai, M. D. Leitl, W. Lemaire, R. B. White, S. Yeh, M. O. Urban, S. A. Kane, G. D. Hartman, M. T. Bilodeau and B. W. Trotter, *Bioorganic and Medicinal Chemistry Letters*, 2011, **21**, 2359–2364.

51 B. W. Trotter, K. K. Nanda, C. S. Burgey, C. M. Potteiger, J. Z. Deng, A. I. Green, J. C. Hartnett, N. R. Kett, Z. Wu, D. A. Henze, K. della Penna, R. Desai, M. D. Leitl, W. Lemaire, R. B. White, S. Yeh, M. O. Urban, S. A. Kane, G. D. Hartman and M. T. Bilodeau, *Bioorganic and Medicinal Chemistry Letters*, 2011, **21**, 2354–2358.

52 N. Thornberry and A. Weber, *Current Topics in Medicinal Chemistry*, 2007, **7**, 557–568.

53 R. A. Pederson, H. A. White, D. Schlenzig, R. P. Pauly, C. H. S. McIntosh and H. U. Demuth, *Diabetes*, 1998, **47**, 1253–1258.

54 Dooseop Kim, Liping Wang, Maria Beconi, George J. Eiermann, Michael H. Fisher, Huaibing He, Gerard J. Hickey, Jennifer E. Kowalchick, Barbara Leiting, Kathryn Lyons, Frank Marsilio, Margaret E. McCann, Reshma A. Patel, Aleksandr Petrov, Giovanna Scapin, Sangita B. Patel, Ranabir Sinha Roy, Joseph K. Wu, Matthew J. Wyvratt, Bei B. Zhang, Lan Zhu, Nancy A. Thornberry and A. E. Weber, *Journal of Medicinal Chemistry*, 2004, **48**, 141–151.

55 A. J. Roecker, C. D. Cox and P. J. Coleman, *Journal of Medicinal Chemistry*, 2016, **59**, 504–530.

56 T. C. Thannickal, R. Y. Moore, R. Nienhuis, L. Ramanathan, S. Gulyani, M. Aldrich, M. Cornford and J. M. Siegel, *Neuron*, 2000, **27**, 469–474.

57 R. M. Chemelli, J. T. Willie, C. M. Sinton, J. K. Elmquist, T. Scammell, C. Lee, J. A. Richardson, S. Clay Williams, Y. Xiong, Y. Kisanuki, T. E. Fitch, M. Nakazato, R. E. Hammer, C. B. Saper and M. Yanagisawa, *Cell*, 1999, **98**, 437–451.

58 L. Lin, J. Faraco, R. Li, H. Kadotani, W. Rogers, X. Lin, X. Qiu, P. J. de Jong, S. Nishino and E. Mignot, *Cell*, 1999, **98**, 365–376.

59 J. M. Bergman, A. J. Roecker, S. P. Mercer, R. A. Bednar, D. R. Reiss, R. W. Ransom, C. Meacham Harrell, D. J. Pettibone, W. Lemaire, K. L. Murphy, C. Li, T. Prueksaritanont, C. J. Winrow, J. J. Renger, K. S. Koblan, G. D. Hartman and P. J. Coleman, *Bioorganic and Medicinal Chemistry Letters*, 2008, **18**, 1425–1430.

60 A. Basavapathruni, L. Jin, S. R. Daigle, C. R. A. Majer, C. A. Therkelsen, T. J. Wigle, K. W. Kuntz, R. Chesworth, R. M. Pollock, M. P. Scott, M. P. Moyer, V. M. Richon, R. A. Copeland and E. J. Olhava, *Chemical Biology and Drug Design*, 2012, **80**, 971–980.

61 W. Yu, E. J. Chory, A. K. Wernimont, W. Tempel, A. Scopton, A. Federation, J. J. Marineau, J. Qi, D. Barsyte-Lovejoy, J. Yi, R. Marcellus, R. E. Iacob, J. R. Engen, C. Griffin, A. Aman, E. Wienholds, F. Li, J. Pineda, G. Estiu, T. Shatseva, T. Hajian, R. Al-Awar, J. E. Dick, M. Vedadi, P. J. Brown, C. H. Arrowsmith, J. E. Bradner and M. Schapira, *Nature Communications*, 2012, **3**, 1–12.

62 Q. Feng, H. Wang, H. H. Ng, H. Erdjument-Bromage, P. Tempst, K. Struhl and Y. Zhang, *Current Biology*, 2002, **12**, 1052–1058.

63 L. Godfrey, N. T. Crump, R. Thorne, I. J. Lau, E. Repapi, D. Dimou, A. L. Smith, J. R. Harman, J. M. Telenius, A. M. Oudelaar, D. J. Downes, P. Vyas, J. R. Hughes and T. A. Milne, *Nature Communications*, 2019, **10**, 2803.

64 C. W. Chen, R. P. Koche, A. U. Sinha, A. J. Deshpande, N. Zhu, R. Eng, J. G. Doench, H. Xu, S. H. Chu, J. Qi, X. Wang, C. Delaney, K. M. Bernt, D. E. Root, W. C. Hahn, J. E. Bradner and S. A. Armstrong, *Nature Medicine*, 2015, **21**, 335–343.

65 D. J. Steger, M. I. Lefterova, L. Ying, A. J. Stonestrom, M. Schupp, D. Zhuo, A. L. Vakoc, J.-E. Kim, J. Chen, M. A. Lazar, G. A. Blobel and C. R. Vakoc, *Molecular and Cellular Biology*, 2008, **28**, 2825–2839.

66 J. L. Hess, *Trends in Molecular Medicine*, 2004, **10**, 500–507.

67 A. V. Krivtsov and S. A. Armstrong, *Nature Reviews Cancer*, 2007, **7**, 823–833.

68 A. V. Krivtsov, Z. Feng, M. E. Lemieux, J. Faber, S. Vempati, A. U. Sinha, X. Xia, J. Jesneck, A. P. Bracken, L. B. Silverman, J. L. Kutok, A. L. Kung and S. A. Armstrong, *Cancer Cell*, 2008, **14**, 355–368.

69 A. T. Nguyen, O. Taranova, J. He and Y. Zhang, *Blood*, 2011, **117**, 6912–6922.

70 Y. Okada, Q. Feng, Y. Lin, Q. Jiang, Y. Li, V. M. Coffield, L. Su, G. Xu and Y. Zhang, *Cell*, 2005, **121**, 167–178.

71 S. R. Daigle, E. J. Olhava, C. A. Therkelsen, C. R. Majer, C. J. Sneeringer, J. Song, L. D. Johnston, M. P. Scott, J. J. Smith, Y. Xiao, L. Jin, K. W. Kuntz, R. Chesworth, M. P. Moyer, K. M. Bernt, J. C. Tseng, A. L. Kung, S. A. Armstrong, R. A. Copeland, V. M. Richon and R. M. Pollock, *Cancer Cell*, 2011, **20**, 53–65.

72 A. E. Conway, J. M. Haldeman, D. S. Wechsler and C. P. Lavau, *Leukemia*, 2015, **29**, 423–432.

73 M. Wong, A. E. L. Tee, G. Milazzo, J. L. Bell, R. C. Poulos, B. Atmadibrata, Y. Sun, D. Jing, N. Ho, D. Ling, P. Y. Liu, X. D. Zhang, S. Hüttelmaier, J. W. H. Wong, J. Wang, P. Polly, G. Perini, C. J. Scarlett and T. Liu, *Cancer Research*, 2017, **77**, 2522–2533.

74 K. Ishiguro, H. Kitajima, T. Niinuma, T. Ishida, R. Maruyama, H. Ikeda, T. Hayashi, H. Sasaki, H. Wakasugi, K. Nishiyama, T. Shindo, E. Yamamoto, M. Kai, Y. Sasaki, T. Tokino, H. Nakase and H. Suzuki, *Haematologica*, 2019, **104**, 155–165.

75 T. D. D. Somerville and C. R. Vakoc, *Cancer Cell*, 2016, **30**, 9–10.

76 S. R. Daigle, E. J. Olhava, C. A. Therkelsen, A. Basavapathruni, L. Jin, P. A. Boriack-Sjodin, C. J. Allain, C. R. Klaus, A. Raimondi, M. P. Scott, N. J. Waters, R. Chesworth, M. P. Moyer, R. A. Copeland, V. M. Richon and R. M. Pollock, *Blood*, 2013, **122**, 1017–1025.

77 N. J. Waters, *European Journal of Drug Metabolism and Pharmacokinetics*, 2017, **42**, 891–901.

78 E. M. Stein, G. Garcia-Manero, D. A. Rizzieri, R. Tibes, J. G. Berdeja, M. Jongen-Lavrencic, J. K. Altman, H. Dohner, B. Thomson, S. J. Blakemore, S. Daigle, G. Fine, N. J. Waters, A. v Krivstov, R. Koche, S. A. Armstrong, P. T. Ho, B. Lowenberg and M. S. Tallman, *Blood*, 2015, **126**, 2547–2547.

79 N. Shukla, M. M. O'Brien, L. B. Silverman, M. Pauly, C. Wetmore, M. L. Loh, J. A. Whitlock, P. Brown, B. Thomson, S. J. Blakemore, S. Daigle, P. Pimentel, N. J. Waters, A. v Krivstov, R. Koche, S. A. Armstrong, P. T. Ho and L. Gore, *Blood*, 2015, **126**, 3792–3792.

80 K. Menghrajani, S. F. Cai, S. M. Devlin, S. A. Armstrong, R. Piekarz, M. Rudek, M. S. Tallman and E. M. Stein, *Blood*, 2019, **134**, 2655–2655.

81 G. van Mierlo, G. J. C. Veenstra, M. Vermeulen and H. Marks, *Trends in Cell Biology*, 2019, **29**, 660–671.

82 R. Margueron and D. Reinberg, *Nature*, 2011, **469**, 343–349.

83 B. Schuettengruber, D. Chourrout, M. Vervoort, B. Leblanc and G. Cavalli, *Cell*, 2007, **128**, 735–745.

84 J. A. Simon and C. A. Lange, *Mutation Research - Fundamental and Molecular Mechanisms of Mutagenesis*, 2008, **647**, 21–29.

85 S. K. Knutson, T. J. Wigle, N. M. Warholic, C. J. Sneeringer, C. J. Allain, C. R. Klaus, J. D. Sacks, A. Raimondi, C. R. Majer, J. Song, M. P. Scott, L. Jin, J. J. Smith, E. J. Olhava, R. Chesworth, M. P. Moyer, V. M. Richon, R. A. Copeland, H. Keilhack, R. M. Pollock and K. W. Kuntz, *Nature Chemical Biology*, 2012, **8**, 890–896.

86 M. T. McCabe, H. M. Ott, G. Ganji, S. Korenchuk, C. Thompson, G. S. van Aller, Y. Liu, A. della Pietra, L. v. LaFrance, M. Mellinger, C. Duquenne, X. Tian, R. G. Kruger, C. F. McHugh, W. H. Miller, D. Dhanak, S. K. Verma, P. J. Tummino, C. L. Creasy, A. P. Graves and E. Diaz, *Nature*, 2012, **492**, 108–112.

87 S. K. Verma, X. Tian, L. v. Lafrance, C. Duquenne, D. P. Suarez, K. A. Newlander, S. P. Romeril, J. L. Burgess, S. W. Grant, J. A. Brackley, A. P. Graves, D. A. Scherzer, A. Shu, C. Thompson, H. M. Ott, G. S. van Aller, C. A. MacHutta, E. Diaz, Y. Jiang, N. W. Johnson, S. D. Knight, R. G. Kruger, M. T. McCabe, D. Dhanak, P. J. Tummino, C. L. Creasy and W. H. Miller, *ACS Medicinal Chemistry Letters*, 2012, **3**, 1091–1096.

88 E. Diaz, C. A. MacHutta, S. Chen, Y. Jiang, C. Nixon, G. Hofmann, D. Key, S. Sweitzer, M. Patel, Z. Wu, C. L. Creasy, R. G. Kruger, L. Lafrance, S. K. Verma, M. B. Pappalardi, B. Le, G. S. van Aller, M. T. McCabe, P. J. Tummino, A. J. Pope, S. H. Thrall, B. Schwartz and M. Bandt, *Journal of Biomolecular Screening*, 2012, **17**, 1279–1292.

89 R. G. Vaswani, V. S. Gehling, L. A. Dakin, A. S. Cook, C. G. Nasveschuk, M. Duplessis, P. Iyer, S. Balasubramanian, F. Zhao, A. C. Good, R. Campbell, C. Lee, N. Cantone, R. T. Cummings, E. Normant, S. F. Bellon, B. K. Albrecht, J. C. Harmange, P. Trojer, J. E. Audia, Y. Zhang, N. Justin, S. Chen, J. R. Wilson and S. J. Gamblin, *Journal of Medicinal Chemistry*, 2016, **59**, 9928–9941.

90 K. W. Kuntz, J. E. Campbell, H. Keilhack, R. M. Pollock, S. K. Knutson, M. Porter-Scott, V. M. Richon, C. J. Sneeringer, T. J. Wigle, C. J. Allain, C. R. Majer, M. P. Moyer, R. A. Copeland and R. Chesworth, *Journal of Medicinal Chemistry*, 2016, **59**, 1556–1564.

91 S. M. Hoy, *Drugs*, 2020, **80**, 513–521.

92 FDA granted accelerated approval to tazemetostat for follicular lymphoma, https://www.fda.gov/drugs/fda-granted-accelerated-approval-tazemetostat-follicular-lymphoma, (accessed December 3, 2020).

93 S. K. Knutson, N. M. Warholic, T. J. Wigle, C. R. Klaus, C. J. Allain, A. Raimondi, M. P. Scott, R. Chesworth, M. P. Moyer, R. A. Copeland, V. M. Richon, R. M. Pollock, K. W. Kuntz and H. Keilhack, *Proceedings of the National Academy of Sciences of the United States of America*, 2013, **110**, 7922–7927.

94 J. G. Moffat, F. Vincent, J. A. Lee, J. Eder and M. Prunotto, *Nature Reviews Drug Discovery*, 2017, **16**, 531–543.

95 F. Cong, A. K. Cheung and S.-M. A. Huang, *The Annual Review of Pharmacology and Toxicology*, 2011, **52**, 57–78.

96 J. A. Lee, M. T. Uhlik, C. M. Moxham, D. Tomandl and D. J. Sall, *Journal of Medicinal Chemistry*, 2012, **55**, 4527–4538.

97 D. C. Swinney and J. Anthony, *Nature Reviews Drug Discovery*, 2011, **10**, 507–519.

98 J. A. Lee and E. L. Berg, *Journal of Biomolecular Screening*, 2013, **18**, 1143–1155.

99 L. H. Jones and M. E. Bunnage, *Nature Reviews Drug Discovery*, 2017, **16**, 285–296.

100 M. Bredel and E. Jacoby, *Nature Reviews Genetics*, 2004, **5**, 262–275.

101 P. R. Caron, M. D. Mullican, R. D. Mashal, K. P. Wilson, M. S. Su and M. A. Murcko, *Current Opinion in Chemical Biology*, 2001, **5**, 464–470.

102 J. M. Elkins, V. Fedele, M. Szklarz, K. R. Abdul Azeez, E. Salah, J. Mikolajczyk, S. Romanov, N. Sepetov, X. P. Huang, B. L. Roth, A. al Haj Zen, D. Fourches, E. Muratov, A. Tropsha, J. Morris, B. A. Teicher, M. Kunkel, E. Polley, K. E. Lackey, F. L. Atkinson, J. P. Overington, P. Bamborough, S. Müller, D. J. Price, T. M. Willson, D. H. Drewry, S. Knapp and W. J. Zuercher, *Nature Biotechnology*, 2016, **34**, 95–103.

103 M. Boettcher and M. T. McManus, *Molecular Cell*, 2015, **58**, 575–585.

104 Epigenetics Probes Collection, https://www.thesgc.org/chemical-probes/epigenetics, (accessed May 21, 2021).

105 S. Scheer, S. Ackloo, T. S. Medina, M. Schapira, F. Li, J. A. Ward, A. M. Lewis, J. P. Northrop, P. L. Richardson, H. Ü. Kaniskan, Y. Shen, J. Liu, D. Smil, D. McLeod, C. A. Zepeda-Velazquez, M. Luo, J. Jin, D. Barsyte-Lovejoy, K. V. M. Huber, D. D. de Carvalho, M. Vedadi, C. Zaph, P. J. Brown and C. H. Arrowsmith, *Nature Communications*, 2019, **10**, 1–14.

106 Q. Wu, D. Heidenreich, S. Zhou, S. Ackloo, A. Krämer, K. Nakka, E. Lima-Fernandes, G. Deblois, S. Duan, R. N. Vellanki, F. Li, M. Vedadi, J. Dilworth, M. Lupien, P. E. Brennan, C. H. Arrowsmith, S. Müller, O. Fedorov, P. Filippakopoulos and S. Knapp, *Nature Communications*, 2019, **10**, 1–14.

107 C. H. Arrowsmith, C. Bountra, P. v. Fish, K. Lee and M. Schapira, *Nature Reviews Drug Discovery*, 2012, **11**, 384–400.

108 T. B. Nicholson, N. Veland and T. Chen, in *Epigenetic Cancer Therapy*, ed. S. G. Gray, Elsevier, Amsterdam,1st edn, 2015, ch. 3, 31–66.

109 T. K. Kelly, D. D. de Carvalho and P. A. Jones, *Nature Biotechnology*, 2010, **28**, 1069–1078.

110 I. M. Adcock, K. Ito and P. J. Barnes, *COPD: Journal of Chronic Obstructive Pulmonary Disease*, 2005, **2**, 445–455.

111 B. M. Javierre, A. F. Fernandez, J. Richter, F. Al-Shahrour, J. Ignacio Martin-Subero, J. Rodriguez-Ubreva, M. Berdasco, M. F. Fraga, T. P. O'Hanlon, L. G. Rider, F. v. Jacinto, F. Javier Lopez-Longo, J. Dopazo, M. Forn, M. A. Peinado, L. Carreño, A. H. Sawalha, J. B. Harley, R. Siebert, M. Esteller, F. W. Miller and E. Ballestar, *Genome Research*, 2010, **20**, 170–179.

112 L. M. Villeneuve and R. Natarajan, *American Journal of Physiology - Renal Physiology*, 2010, **299**, 14–25.

113 R. G. Urdinguio, J. v. Sanchez-Mut and M. Esteller, *The Lancet Neurology*, 2009, **8**, 1056–1072.

114 L. M. Williams, F. E. McCann, M. A. Cabrita, T. Layton, A. Cribbs, B. Knezevic, H. Fang, J. Knight, M. Zhang, R. Fischer, S. Bonham, L. M. Steenbeek, N. Yang, M. Sood, C. Bainbridge, D. Warwick, L. Harry, D. Davidson, W. Xie, M. Sundström, M. Feldmann and J. Nanchahal, *Proceedings of the National Academy of Sciences of the United States of America*, 2020, **117**, 20753–20763.

115 L. S. Verjee, K. Midwood, D. Davidson, D. Essex, A. Sandison and J. Nanchahal, *Journal of Hand Surgery*, 2009, **34**, 1785–1794.

116 D. A. Hay, O. Fedorov, S. Martin, D. C. Singleton, C. Tallant, C. Wells, S. Picaud, M. Philpott, O. P. Monteiro, C. M. Rogers, S. J. Conway, T. P. C. Rooney, A. Tumber, C. Yapp, P. Filippakopoulos, M. E. Bunnage, S. Müller, S. Knapp, C. J. Schofield and P. E. Brennan, *Journal of the American Chemical Society*, 2014, **136**, 9308–9319.

117 A. Hammitzsch, C. Tallant, O. Fedorov, A. O'Mahony, P. E. Brennan, D. A. Hay, F. O. Martinez, M. H. Al-Mossawi, J. de Wit, M. Vecellio, C. Wells, P. Wordsworth, S. Müller, S. Knapp and P. Bowness, *Proceedings of the National Academy of Sciences of the United States of America*, 2015, **112**, 10768–10773.

118 N. Brooks, M. Raja, B. W. Young, G. J. Spencer, T. C. Somervaille and N. A. Pegg, *Blood*, 2019, **134**, 2560–2560.

119 J. Welti, A. Sharp, N. Brooks, W. Yuan, C. McNair, S. N. Chand, A. Pal, I. Figueiredo, R. Riisnaes, B. Gurel, J. Rekowski, D. Bogdan, W. West, B. Young, M. Raja, A. Prosser, J. Lane, S. Thomson, J. Worthington, S. Onions, J. Shannon, S. Paoletta, R. Brown, D. Smyth, G. W. Harbottle, V. S. Gil, S. Miranda, M. Crespo, A. Ferreira, R. Pereira, N. Tunariu, S. Carreira, A. J. Neeb, J. Ning, A. Swain, D. Taddei, S. U. to C.-P. International Dream Team, M. J. Schiewer, K. E. Knudsen, N. Pegg and J. S. de Bono, *Cancer Discovery*, **2021**, CD-20-0751.

120 N. Grinshtein, C. C. Rioseco, R. Marcellus, D. Uehling, A. Aman, X. Lun, O. Muto, L. Podmore, J. Lever, Y. Shen, M. D. Blough, G. J. Cairncross, S. M. Robbins, S. J. Jones, M. A. Marra, R. Al-awar, D. L. Senger and D. R. Kaplan, *Oncotarget*, 2016, **7**, 59360–59376.

121 M. Lim, Y. Xia, C. Bettegowda and M. Weller, *Nature Reviews Clinical Oncology*, 2018, **15**, 422–442.

122 P. Zhang, M. C. de Gooijer, L. C. M. Buil, J. H. Beijnen, G. Li and O. van Tellingen, *International Journal of Cancer*, 2015, **137**, 2007–2018.

123 G. Franci, V. Folliero, M. Cammarota, C. Zannella, F. Sarno, C. Schiraldi, A. R. de Lera, L. Altucci and M. Galdiero, *Scientific Reports*, 2018, **8**, 13117.

124 K. Ren, W. Zhang, X. Chen, Y. Ma, Y. Dai, Y. Fan, Y. Hou, R. X. Tan and E. Li, *PLoS Pathogens*, 2016, **12**, e1005950.

125 K. C. L. Whatley, G. Padalino, H. Whiteland, K. K. Geyer, B. J. Hulme, I. W. Chalmers, J. Forde-Thomas, S. Ferla, A. Brancale and K. F. Hoffmann, *PLoS Neglected Tropical Diseases*, 2019, **13**, e0007693.

126 D. P. McManus, D. W. Dunne, M. Sacko, J. Utzinger, B. J. Vennervald and X. N. Zhou, *Nature Reviews Disease Primers*, 2018, **4**, 1–19.

127 A. Cabezas-Cruz, J. Lancelot, S. Caby, G. Oliveira and R. J. Pierce, *Frontiers in Genetics*, 2014, **5**, 317.

128 V. C. Carneiro, I. C. de Abreu da Silva, E. J. L. Torres, S. Caby, J. Lancelot, M. Vanderstraete, S. D. Furdas, M. Jung, R. J. Pierce and M. R. Fantappié, *PLoS Pathogens*, 2014, **10**, e1004116.

129 F. Sams-Dodd, *Drug Discovery Today*, 2005, **10**, 139–147.

130 G. Vilema-Enríquez, R. Quinlan, P. Kilfeather, R. Mazzone, S. Saqlain, I. del Molino del Barrio, A. Donato, G. Corda, F. Li, M. Vedadi, A. H. Németh, P. E. Brennan and R. Wade-Martins, *Journal of Biological Chemistry*, 2020, **295**, 17973–17985.

131 A. E. Harding, *Brain*, 1981, **104**, 589–620.

132 N. Friedreich, *Archiv für Pathologische Anatomie und Physiologie und für Klinische Medicin*, 1863, **26**, 391–419.

133 N. Friedreich, *Archiv für Pathologische Anatomie und Physiologie und für Klinische Medicin*, 1863, **26**, 433–459.

134 N. Friedreich, *Archiv für Pathologische Anatomie und Physiologie und für Klinische Medicin*, 1863, **27**, 1–26.

135 N. Friedreich, *Archiv für Pathologische Anatomie und Physiologie und für Klinische Medicin*, 1876, **68**, 145–245.

136 N. Friedreich, *Archiv für Pathologische Anatomie und Physiologie und für Klinische Medicin*, 1877, **70**, 140–152.

137 A. H. Koeppen, *Journal of Neurochemistry*, 2013, **126**, 4–10.

138 A. H. Koeppen and J. E. Mazurkiewicz, *Journal of Neuropathology & Experimental Neurology*, 2013, **72**, 78–90.

139 A. H. Koeppen, *Journal of the Neurological Sciences*, 2011, **303**, 1–12.

140 R. Virchow, *Archiv für Pathologische Anatomie und Physiologie und für Klinische Medicin*, 1882, **90**, 213–220.

141 F. Fanon, *Alienation and Freedom*, Bloomsbury, London, 2018.

142 P. R. Ladame, *Brain*, 1890, **13**, 467–537.

143 M. B. Delatycki, R. Williamson and S. M. Forrest, *Journal of Medical Genetics*, 2000, **37**, 1–8.

144 F. W. Mott, *Archives of Neurology and Psychiatry London*, 1907, **3**, 180–200.

145 H. Urich, R. M. Norman and C. Lloyd, *Stereotactic and Functional Neurosurgery*, 1957, **17**, 360–371.

146 D. R. Oppenheimer, *Canadian Journal of Neurological Sciences / Journal Canadien des Sciences Neurologiques*, 1979, **6**, 173–176.

147 A. H. Koeppen, A. N. Davis and J. A. Morral, *Acta Neuropathologica*, 2011, **122**, 323–330.

148 G. Geoffroy, A. Barbeau, G. Breton, B. Lemieux, M. Aube, C. Leger and J. P. Bouchard, *Canadian Journal of Neurological Sciences / Journal Canadien des Sciences Neurologiques*, 1976, **3**, 279–286.

149 A. Barbeau, *Canadian Journal of Neurological Sciences / Journal Canadien des Sciences Neurologiques*, 1984, **11**, 646–660.

150 A. Filla, G. DeMichele, G. Caruso, R. Marconi and G. Campanella, *Journal of Neurology*, 1990, **237**, 345–351.

151 A. Filla, G. de Michele, G. Coppola, A. Federico, G. Vita, A. Toscano, A. Uncini, P. Pisanelli, P. Barone, V. Scarano, A. Perretti, L. Santoro, A. Monticelli, F. Cavalcanti, G. Caruso and S. Cocozza, *Movement Disorders*, 2000, **15**, 1255–1258.

152 D. S. Russell, *The Journal of Pathology and Bacteriology*, 1946, **58**, 739–748.

153 W. Evans and G. Wright, *Heart*, 1942, **4**, 91–102.

154 A. S. Nadas, M. M. Alimurung and L. A. Sieracki, *New England Journal of Medicine*, 1951, **244**, 239–244.

155 S. H. Boyer, A. W. Chisolm and V. A. McKusick, *Circulation*, 1962, **25**, 493–505.

156 G. Sanchez-Casis, M. Cote and A. Barbeau, *Canadian Journal of Neurological Sciences / Journal Canadien des Sciences Neurologiques*, 1976, **3**, 349–354.

157 T. N. James and C. Fisch, *American Heart Journal*, 1963, **66**, 164–175.

158 W. W. Ellwood, *California medicine*, 1948, **68**, 296–8.

159 M. R. Hejtmancik, J. Y. Bradfield and G. v. Miller, *American Heart Journal*, 1949, **38**, 757–765.

160 G. W. Manning, *American Heart Journal*, 1950, **39**, 799–816.

161 R. L. Hewer, *British Medical Journal*, 1968, **3**, 649–652.

162 J. B. Lamarche, M. Côté and B. Lemieux, *Canadian Journal of Neurological Sciences / Journal Canadien des Sciences Neurologiques*, 1980, **7**, 389–396.

163 S. Michael, S. v Petrocine, J. Qian, J. B. Lamarche, M. D. Knutson, M. D. Garrick and A. H. Koeppen, *The Cerebellum*, 2006, **5**, 257.

164 R. Fujita, Y. Agid, P. Trouillas, A. Seck, C. Tommasi-Davenas, A. J. Driesel, K. Olek, K. H. Grzeschik, Y. Nakamura, J. L. Mandel and A. Hanauer, *Genomics*, 1989, **4**, 110–111.

165 A. Hanauer, M. Chery, R. Fujita, A. J. Driesel, S. Gilgenkrantz and J. L. Mandel, *American Journal of Human Genetics*, 1990, **46**, 133–7.

166 V. Campuzano, L. Montermini, M. D. Moltò, L. Pianese, M. Cossée, F. Cavalcanti, E. Monros, F. Rodius, F. Duclos, A. Monticelli, F. Zara, J. Cañizares, H. Koutnikova, S. I. Bidichandani, C. Gellera, A. Brice, P. Trouillas, G. de Michele, A. Filla, R. de Frutos, F. Palau, P. I. Patel, S. di Donato, J. L. Mandel, S. Cocozza, M. Koenig and M. Pandolfo, *Science*, 1996, **271**, 1423–1427.

167 S. Chamberlain, J. Shaw, A. Rowland, J. Wallis, S. South, Y. Nakamura, A. von Gabain, M. Farrall and R. Williamson, *Nature*, 1988, **334**, 248–250.

168 C. Sandi, M. Sandi, S. Anjomani Virmouni, S. Al-Mahdawi and M. A. Pook, *Frontiers in Genetics*, 2014, **5**, 165.

169 J. B. Schulz and M. Pandolfo, *Journal of Neurochemistry*, 2013, **126**, 1–3.

170 G. Romeo, P. Menozzi, A. Ferlini, S. Fadda, S. di Donato, G. Uziel, B. Lucci, L. Capodaglio, A. Filla and G. Campanella, *American Journal of Human Genetics*, 1983, **35**, 523–9.

171 A. E. Harding and K. J. Zilkha, *Journal of Medical Genetics*, 1981, **18**, 285–287.

172 M. Cossée, M. Schmitt, V. Campuzano, L. Reutenauer, C. Moutou, J. L. Mandel and M. Koenig, *Proceedings of the National Academy of Sciences of the United States of America*, 1997, **94**, 7452–7457.

173 A. Dürr, M. Cossee, Y. Agid, V. Campuzano, C. Mignard, C. Penet, J.-L. Mandel, A. Brice and M. Koenig, *New England Journal of Medicine*, 1996, **335**, 1169–1175.

174 F. Weidemann, C. Rummey, B. Bijnens, S. Störk, R. Jasaityte, J. Dhooge, A. Baltabaeva, G. Sutherland, J. B. Schulz, T. Meier and Mitochondrial Protection with Idebenone in Cardiac or Neurological Outcome (MICONOS) study group, *Circulation*, 2012, **125**, 1626–34.

175 S. R. Regner, S. J. Lagedrost, T. Plappert, E. K. Paulsen, L. S. Friedman, M. L. Snyder, S. L. Perlman, K. D. Mathews, G. R. Wilmot, K. A. Schadt, M. S. J. Sutton and D. R. Lynch, *American Journal of Cardiology*, 2012, **109**, 401–405.

176 M. Cnop, H. Mulder and M. Igoillo-Esteve, *Journal of Neurochemistry*, 2013, **126**, 94–102.

177 M. Pandolfo, *Journal of Neurology*, 2009, **256**, 3–8.

178 C. M. Gomes and R. Santos, *Oxidative Medicine and Cellular Longevity*, 2013, 487534.

179 R. Santos, S. Lefevre, D. Sliwa, A. Seguin, J. M. Camadro and E. Lesuisse, *Antioxidants and Redox Signaling*, 2010, **13**, 651–690.

180 T. J. Gibson, E. v. Koonin, G. Musco, A. Pastore and P. Bork, *Trends in Neurosciences*, 1996, **19**, 465–468.

181 H. Koutnikova, V. Campuzano, F. Foury, P. Dollé, O. Cazzalini and M. Koenig, *Nature Genetics*, 1997, **16**, 345–351.

182 V. Campuzano, L. Montermini, Y. Lutz, L. Cova, C. Hindelang, S. Jiralerspong, Y. Trottier, S. J. Kish, B. Faucheux, P. Trouillas, F. J. Authier, A. Dürr, J.-L. Mandel, A. Vescovi, M. Pandolfo and M. Koenig, *Human Molecular Genetics,* 1997, **6**, 1771-1780

183 N. G. Fox, X. Yu, X. Feng, H. J. Bailey, A. Martelli, J. F. Nabhan, C. Strain-Damerell, C. Bulawa, W. W. Yue and S. Han, *Nature Communications*, 2019, **10**, 1–8.

184 E. Clark, J. Johnson, Y. N. Dong, E. Mercado-Ayon, N. Warren, M. Zhai, E. McMillan, A. Salovin, H. Lin and D. R. Lynch, *Neuronal Signaling*, 2018, **2**, NS20180060.

185 S. Schmucker, A. Martelli, F. Colin, A. Page, M. Wattenhofer-Donzé, L. Reutenauer and H. Puccio, *PLoS ONE*, 2011, **6**, e16199.

186 R. Lill, *Nature*, 2009, **460**, 831–838.

187 R. Lill and U. Mühlenhoff, *Annual Review of Cell and Developmental Biology*, 2006, **22**, 457–486.

188 C. W. Lin, J. W. McCabe, D. H. Russell and D. P. Barondeau, *Journal of the American Chemical Society*, 2020, **142**, 6018–6029.

189 N. G. Fox, A. Martelli, J. F. Nabhan, J. Janz, O. Borkowska, C. Bulawa and W. W. Yue, *Biochimie*, 2018, **152**, 211–218.

190 H. Puccio, D. Simon, M. Cossée, P. Criqui-Filipe, F. Tiziano, J. Melki, C. Hindelang, R. Matyas, P. Rustin and M. Koenig, *Nature Genetics*, 2001, **27**, 181–186.

191 M. Babcock, D. de Silva, R. Oaks, S. Davis-Kaplan, S. Jiralerspong, L. Montermini, M. Pandolfo and J. Kaplan, *Science*, 1997, **276**, 1709–1712.

192 F. Foury and O. Cazzalini, *FEBS Letters*, 1997, **411**, 373–377.

193 S. Shcmucker and H. Puccio, *Human Molecular Genetics*, 2010, **19**, 103–110.

194 N. Sakamoto, P. D. Chastain, P. Parniewski, K. Ohshima, M. Pandolfo, J. D. Griffith and R. D. Wells, *Molecular Cell*, 1999, **3**, 465–475.

195 K. Ohshima, L. Montermini, R. D. Wells and M. Pandolfo, *Journal of Biological Chemistry*, 1998, **273**, 14588–14595.

196 R. D. Wells, *The FASEB Journal*, 2008, **22**, 1625–1634.

197 A. Savellev, C. Everett, T. Sharpe, Z. Webster and R. Festenstein, *Nature*, 2003, **422**, 909–913.

198 N. Dillon and R. Festenstein, *Trends in Genetics*, 2002, **18**, 252–258.

199 M. Groh, M. M. P. Lufino, R. Wade-Martins and N. Gromak, *PLOS Genetics*, 2014, **10**, e1004318.

200 Y. Li, Y. Lu, U. Polak, K. Lin, J. Shen, J. Farmer, L. Seyer, A. D. Bhalla, N. Rozwadowska, D. R. Lynch, J. S. Butler and M. Napierala, *Human Molecular Genetics*, 2015, **24**, 6932–6943.

201 K. D. Robertson, *Oncogene*, 2001, **20**, 3139–3155.

202 E. Li and Y. Zhang, *Cold Spring Harbor Perspectives in Biology*, 2014, **6**, a019133.

203 M. C. Lorincz, D. R. Dickerson, M. Schmitt and M. Groudine, *Nature Structural and Molecular Biology*, 2004, **11**, 1068–1075.

204 M. V. C. Greenberg and D. Bourc'his, *Nature Reviews Molecular Cell Biology*, 2019, **20**, 590–607.

205 Y. Yin, E. Morgunova, A. Jolma, E. Kaasinen, B. Sahu, S. Khund-Sayeed, P. K. Das, T. Kivioja, K. Dave, F. Zhong, K. R. Nitta, M. Taipale, A. Popov, P. A. Ginno, S. Domcke, J. Yan, D. Schübeler, C. Vinson and J. Taipale, *Science*, 2017, **502**, eaaj2239.

206 E. Greene, L. Mahishi, A. Entezam, D. Kumari and K. Usdin, *Nucleic Acids Research*, 2007, **35**, 3383–3390.

207 S. Al-Mahdawi, R. M. Pinto, O. Ismail, D. Varshney, S. Lymperi, C. Sandi, D. Trabzuni and M. Pook, *Human Molecular Genetics*, 2008, **17**, 735-746.

208 I. Castaldo, M. Pinelli, A. Monticelli, F. Acquaviva, M. Giacchetti, A. Filla, S. Sacchetti, S. Keller, V. E. Avvedimento, L. Chiariotti and S. Cocozza, *Journal of Medical Genetics*, 2008, **45**, 808–812.

209 M. v. Evans-Galea, N. Carrodus, S. M. Rowley, L. A. Corben, G. Tai, R. Saffery, J. C. Galati, N. C. Wong, J. M. Craig, D. R. Lynch, S. R. Regner, A. F. D. Brocht, S. L. Perlman, K. O. Bushara, C. M. Gomez, G. R. Wilmot, L. Li, E. Varley, M. B. Delatycki and J. P. Sarsero, *Annals of Neurology*, 2012, **71**, 487–497.

210 J. U. Guo, Y. Su, C. Zhong, G. L. Ming and H. Song, *Cell*, 2011, **145**, 423–434.

211 M. Tahiliani, K. P. Koh, Y. Shen, W. A. Pastor, H. Bandukwala, Y. Brudno, S. Agarwal, L. M. Iyer, D. R. Liu, L. Aravind and A. Rao, *Science*, 2009, **324**, 930–935.

212 K. E. Szulwach, X. Li, Y. Li, C. X. Song, H. Wu, Q. Dai, H. Irier, A. K. Upadhyay, M. Gearing, A. I. Levey, A. Vasanthakumar, L. A. Godley, Q. Chang, X. Cheng, C. He and P. Jin, *Nature Neuroscience*, 2011, **14**, 1607–1616.

213 S. Al-Mahdawi, C. Sandi, R. Mouro Pinto and M. A. Pook, *PLoS ONE*, 2013, **8**, e74956.

214 T. Kouzarides, *Cell*, 2007, **128**, 693–705.

215 K. Luger, A. W. Mäder, R. K. Richmond, D. F. Sargent and T. J. Richmond, *Nature*, 1997, **389**, 251–260.

216 C. Sandi, S. Al-Mahdawi and M. A. Pook, *Genetics Research International*, 2013, **2013**, 12.

217 D. E. Sterner and S. L. Berger, *Microbiology and Molecular Biology Reviews*, 2000, **64**, 435–459.

218 S. C. R. Elgin and S. I. S. Grewal, *Current Biology*, 2003, **13**, R895–R898.

219 D. Herman, K. Jenssen, R. Burnett, E. Soragni, S. L. Perlman and J. M. Gottesfeld, *Nature Chemical Biology*, 2006, **2**, 551–558.

220 I. de Biase, Y. K. Chutake, P. M. Rindler and S. I. Bidichandani, *PLoS ONE*, 2009, **4**, e7914.

221 P. K. Chan, R. Torres, C. Yandim, P. P. Law, S. Khadayate, M. Mauri, C. Grosan, N. Chapman-Rothe, P. Giunti, M. Pook and R. Festenstein, *Human Molecular Genetics*, 2013, **22**, 2662-2675.

222 E. Greene, L. Mahishi, A. Entezam, D. Kumari and K. Usdin, *Nucleic Acids Research*, 2007, **35**, 3383–3390.

223 J. C. Black, C. van Rechem and J. R. Whetstine, *Molecular Cell*, 2012, **48**, 491–507.

224 R. J. Sims, K. Nishioka and D. Reinberg, *Trends in Genetics*, 2003, **19**, 629–639.

225 Y. Zhang and D. Reinberg, *Genes and Development*, 2001, **15**, 2343–2360.

226 M. Tachibana, K. Sugimoto, M. Nozaki, J. Ueda, T. Ohta, M. Ohki, M. Fukuda, N. Takeda, H. Niida, H. Kato and Y. Shinkai, *Genes and Development*, 2002, **16**, 1779–1791.

227 A. H. F. M. Peters, D. O'Carroll, H. Scherthan, K. Mechtler, S. Sauer, C. Schöfer, K. Weipoltshammer, M. Pagani, M. Lachner, A. Kohlmaier, S. Opravil, M. Doyle, M. Sibilia and T. Jenuwein, *Cell*, 2001, **107**, 323–337.

228 J. Ernst and M. Kellis, *Nature Biotechnology*, 2010, **28**, 817–825.

229 A. Shilatifard, *Annual Review of Biochemistry*, 2006, **75**, 243–269.

230 E. Smith and A. Shilatifard, *Molecular Cell*, 2010, **40**, 689–701.

231 T. Jenuwein, *FEBS Journal*, 2006, **273**, 3121–3135.

232 N. Kourmouli, P. Jeppesen, S. Mahadevhaiah, P. Burgoyne, R. Wu, D. M. Gilbert, S. Bongiorni, G. Prantera, L. Fanti, S. Pimpinelli, W. Shi, R. Fundele and P. B. Singh, *Journal of Cell Science*, 2004, **117**, 2491–2501.

233 D. Kumari, R. E. Biacsi and K. Usdin, *Journal of Biological Chemistry*, 2011, **286**, 4209–4215.

234 E. Kim, M. Napierala and S. Y. R. Dent, *Nucleic Acids Research*, 2011, **39**, 8366-8377.

235 C. Strawser, K. Schadt, L. Hauser, A. McCormick, M. Wells, J. Larkindale, H. Lin and D. R. Lynch, *Expert Review of Neurotherapeutics*, 2017, **17**, 895–907.

236 FARA - Research Pipeline, https://www.curefa.org/pipeline#mib-626, (accessed June 17, 2021).

237 S. Zhang, M. Napierala and J. S. Napierala, *Trends in Pharmacological Sciences*, 2019, **40**, 229–233.

238 D. Herman, K. Jenssen, R. Burnett, E. Soragni, S. L. Perlman and J. M. Gottesfeld, *Nature Chemical Biology*, 2006, **2**, 551–558.

239 M. Rai, E. Soragni, C. J. Chou, G. Barnes, S. Jones, J. R. Rusche, J. M. Gottesfeld and M. Pandolfo, *PLoS ONE*, 2010, **5**, e8825.

240 C. Sandi, R. M. Pinto, S. Al-Mahdawi, V. Ezzatizadeh, G. Barnes, S. Jones, J. R. Rusche, J. M. Gottesfeld and M. A. Pook, *Neurobiology of Disease*, 2011, **42**, 496–505.

241 E. Soragni and J. M. Gottesfeld, *Expert Opinion on Orphan Drugs*, 2016, **4**, 961–970.

242 V. Libri, C. Yandim, S. Athanasopoulos, N. Loyse, T. Natisvili, P. P. Law, P. K. Chan, T. Mohammad, M. Mauri, K. T. Tam, J. Leiper, S. Piper, A. Ramesh, M. H. Parkinson, L. Huson, P. Giunti and R. Festenstein, *The Lancet*, 2014, **384**, 504–513.

243 E. Soragni, W. Miao, M. Iudicello, D. Jacoby, S. de Mercanti, M. Clerico, F. Longo, A. Piga, S. Ku, E. Campau, J. Du, P. Penalver, M. Rai, J. C. Madara, K. Nazor, M. O'Connor, A. Maximov, J. F. Loring, M. Pandolfo, L. Durelli, J. M. Gottesfeld and J. R. Rusche, *Annals of Neurology*, 2014, **76**, 489–508.

244 M. Rai, E. Soragni, K. Jenssen, R. Burnett, D. Herman, G. Coppola, D. H. Geschwind, J. M. Gottesfeld and M. Pandolfo, *PLOS ONE*, 2008, **3**, e1958.

245 G. Coppola, R. Burnett, S. Perlman, R. Versano, F. Gao, H. Plasterer, M. Rai, F. Saccá, A. Filla, D. R. Lynch, J. R. Rusche, J. M. Gottesfeld, M. Pandolfo and D. H. Geschwind, *Annals of Neurology*, 2011, **70**, 790–804.

246 G. S. Erwin, M. P. Grieshop, A. Ali, J. Qi, M. Lawlor, D. Kumar, I. Ahmad, A. McNally, N. Teider, K. Worringer, R. Sivasankaran, D. N. Syed, A. Eguchi, M. Ashraf, J. Jeffery, M. Xu, P. M. C. Park, H. Mukhtar, A. K. Srivastava, M. Faruq, J. E. Bradner and A. Z. Ansari, *Science*, 2017, **358**, 1617–1622.

247 Design Therapeutics – Designing a New Class of Genomic Medicines, https://www.designtx.com/, (accessed July 13, 2021).

248 P. Filippakopoulos, J. Qi, S. Picaud, Y. Shen, W. B. Smith, O. Fedorov, E. M. Morse, T. Keates, T. T. Hickman, I. Felletar, M. Philpott, S. Munro, M. R. McKeown, Y. Wang, A. L. Christie, N. West, M. J. Cameron, B. Schwartz, T. D. Heightman, N. la Thangue, C. A. French, O. Wiest, A. L. Kung, S. Knapp and J. E. Bradner, *Nature*, 2010, **468**, 1067–1073.

249 Q. Zhou, T. Li and D. H. Price, *Annual Reviews in Biochemistry*, 2012, **81**, 119–143.

250 G. M. Burslem and C. M. Crews, *Cell*, 2020, **181**, 102–114.

251 T. K. Neklesa, J. D. Winkler and C. M. Crews, *Pharmacology & Therapeutics*, 2017, **174**, 138–144.

252 L. Li, M. Matsui and D. R. Corey, *Nature Communications*, 2016, **7**, 1–8.

253 L. Li, X. Shen, Z. Liu, M. Norrbom, T. P. Prakash, D. O'Reilly, V. K. Sharma, M. J. Damha, J. K. Watts, F. Rigo, D. R. Corey, *Nucleic Acid Therapeutics*, 2018, **28**, 23–33.

254 X. Shen, J. Wong, T. P. Prakash, F. Rigo, Y. Li, M. Napierala and D. R. Corey, *Bioorganic & Medicinal Chemistry*, 2020, **28**, 115472.

255 V. Prakash, *Gene Therapy*, 2017, **24**, 497–497.

256 T. A. Zesiewicz, J. Hancock, S. D. Ghanekar, S. H. Kuo, C. A. Dohse and J. Vega, *Expert Review of Neurotherapeutics*, 2020, **20**, 1215–1228.

257 D. R. Lynch, S. M. Willi, R. B. Wilson, M. G. Cotticelli, K. W. Brigatti, E. C. Deutsch, O. Kucheruk, W. Shrader, P. Rioux, G. Miller, A. Hawi and T. Sciascia, *Movement Disorders*, 2012, **27**, 1026–1033.

258 T. Zesiewicz, J. L. Salemi, S. Perlman, K. L. Sullivan, J. D. Shaw, Y. Huang, C. Isaacs, C. Gooch, D. R. Lynch and M. B. Klein, *Neurodegenerative Disease Management*, 2018, **8**, 233–242.

259 G. M. Enns, S. L. Kinsman, S. L. Perlman, K. M. Spicer, J. E. Abdenur, B. H. Cohen, A. Amagata, A. Barnes, V. Kheifets, W. D. Shrader, M. Thoolen, F. Blankenberg and G. Miller, *Molecular Genetics and Metabolism*, 2012, **105**, 91–102.

260 T. Zesiewicz, S. Perlman, K. Sullivan, Y. Huang, J. Salemi, M. Klein, C. Isaacs, C. Gooch, J. Shaw and D. Lynch, *Neurology*, 2017, **88**, supplement 16

261 M. C. Fahey, L. Corben, V. Collins, A. J. Churchyard and M. B. Delatycki, *Journal of Neurology, Neurosurgery & Psychiatry*, 2007, **78**, 411–413.

262 N. Esteras, A. T. Dinkova-Kostova and A. Y. Abramov, *Biological Chemistry*, 2016, **397**, 383–400.

263 V. Paupe, E. P. Dassa, S. Goncalves, F. Auchère, M. Lönn, A. Holmgren and P. Rustin, *PLOS ONE*, 2009, **4**, e4253.

264 R. Abeti, A. Baccaro, N. Esteras and P. Giunti, *Frontiers in Cellular Neuroscience*, 2018, **12**, 188.

265 B. C. Creelan, D. I. Gabrilovich, J. E. Gray, C. C. Williams, T. Tanvetyanon, E. B. Haura, J. S. Weber, G. T. Gibney, J. Markowitz, J. W. Proksch, S. A. Reisman, M. D. McKee, M. P. Chin, C. J. Meyer and S. J. Antonia, *OncoTargets and Therapy*, 2017, **10**, 4239–4250.

266 D. R. Lynch, M. P. Chin, M. B. Delatycki, S. H. Subramony, M. Corti, J. C. Hoyle, S. Boesch, W. Nachbauer, C. Mariotti, K. D. Mathews, P. Giunti, G. Wilmot, T. Zesiewicz, S. Perlman, A. Goldsberry, M. O'Grady and C. J. Meyer, *Annals of Neurology*, 2021, **89**, 212–225.

267 D. R. Lynch, J. Farmer, L. Hauser, I. A. Blair, Q. Q. Wang, C. Mesaros, N. Snyder, S. Boesch, M. Chin, M. B. Delatycki, P. Giunti, A. Goldsberry, C. Hoyle, M. G. McBride, W. Nachbauer, M. O'Grady, S. Perlman, S. H. Subramony, G. R. Wilmot, T. Zesiewicz and C. Meyer, *Annals of Clinical and Translational Neurology*, 2019, **6**, 15–26.

268 Reata Pharmaceuticals Inc. - Reata Pharmaceuticals, Inc. Announces Fourth Quarter and Full Year 2020 Financial Results and Provides an Update on Clinical Development Programs, https://www.reatapharma.com/investors/news/news-details/2021/Reata-Pharmaceuticals-Inc-Announces-Fourth-Quarter-and-Full-Year-2020-Financial-Results-and-Provides-an-Update-on-Clinical-Development-Programs/default.aspx, (accessed July 14, 2021).

269 P. M. Vyas, W. J. Tomamichel, P. M. Pride, C. M. Babbey, Q. Wang, J. Mercier, E. M. Martin and R. M. Payne, *Human Molecular Genetics*, 2012, **21**, 1230–1247.

270 E. Britti, F. Delaspre, A. Feldman, M. Osborne, H. Greif, J. Tamarit and J. Ros, *Journal of Cellular and Molecular Medicine*, 2018, **22**, 834–848.

271 M. J. Kim, D. W. Kim, H. J. Jeong, E. J. Sohn, M. J. Shin, E. H. Ahn, S. W. Kwon, Y. N. Kim, D. S. Kim, J. Park, W. S. Eum, H. S. Hwang and S. Y. Choi, *Biochimie*, 2012, **94**, 2448–2456.

272 Larimar Therapeutics Reports Positive Topline Phase 1 Clinical Trial Data Showing Dose-Dependent Increases in Frataxin Levels in Patients with Friedreich's Ataxia - Larimar Therapeutics, Inc., https://investors.larimartx.com/news-releases/news-release-

details/larimar-therapeutics-reports-positive-topline-phase-1-clinical, (accessed July 15, 2021).

273 Larimar Therapeutics Reports FDA Clinical Hold on CTI-1601 and Termination of Recently Announced Private Placement Funding – Larimar Therapeutics, Inc., https://investors.larimartx.com/node/10676/pdf, (accessed July 15, 2021).

274 K. D. Bromberg, T. R. H. Mitchell, A. K. Upadhyay, C. G. Jakob, M. A. Jhala, K. M. Comess, L. M. Lasko, C. Li, C. T. Tuzon, Y. Dai, F. Li, M. S. Eram, A. Nuber, N. B. Soni, V. Manaves, M. A. Algire, R. F. Sweis, M. Torrent, G. Schotta, C. Sun, M. R. Michaelides, A. R. Shoemaker, C. H. Arrowsmith, P. J. Brown, V. Santhakumar, A. Martin, J. C. Rice, G. G. Chiang, M. Vedadi, D. Barsyte-Lovejoy and W. N. Pappano, *Nature Chemical Biology*, 2017, **13**, 317–324.

275 S. Jorgensen, G. Schotta and C. S. Sorensen, *Nucleic Acids Research*, 2013, **41**, 2797–2806.

276 J. I. Lai, D. Nachun, L. Petrosyan, B. Throesch, E. Campau, F. Gao, K. K. Baldwin, G. Coppola, J. M. Gottesfeld and E. Soragni, *Journal of Biological Chemistry*, 2019, **294**, 1846–1859.

277 H. M. Herz, A. Garruss and A. Shilatifard, *Trends in Biochemical Sciences*, 2013, **38**, 621–639.

278 C. Plass, S. M. Pfister, A. M. Lindroth, O. Bogatyrova, R. Claus and P. Lichter, *Nature Reviews Genetics 2013 14:11*, 2013, **14**, 765–780.

279 R. van Nuland and O. Gozani, *Molecular & Cellular Proteomics*, 2016, **15**, 755–764.

280 D. B. Beck, A. Burton, H. Oda, C. Ziegler-Birling, M.-E. Torres-Padilla and D. Reinberg, *Genes & Development*, 2012, **26**, 2580–2589.

281 M. Shoaib, D. Walter, P. J. Gillespie, F. Izard, B. Fahrenkrog, D. Lleres, M. Lerdrup, J. V. Johansen, K. Hansen, E. Julien, J. J. Blow and C. S. Sørensen, *Nature Communications,* 2018, **9**, 1–11.

282 G. Schotta, R. Sengupta, S. Kubicek, S. Malin, M. Kauer, E. Callén, A. Celeste, M. Pagani, S. Opravil, I. A. D. la Rosa-Velazquez, A. Espejo, M. T. Bedford, A. Nussenzweig, M. Busslinger and T. Jenuwein, *Genes & Development*, 2008, **22**, 2048–2061.

283 G. Schotta, M. Lachner, K. Sarma, A. Ebert, R. Sengupta, G. Reuter, D. Reinberg and T. Jenuwein, *Genes & Development*, 2004, **18**, 1251–1262.

284 S. Fioriniello, D. Marano, F. Fiorillo, M. D'Esposito and F. della Ragione, *Genes*, 2020, **11**, 595.

285 D. A. Smith, C. Allerton, A. S. Kalgutkar, H. van de Waterbeemd and D. K. Walker, in *Pharmacokinetics and Metabolism in Drug Design*, ed. R. Mannhold, H. Kubinyi, G. Folkers, John Wiley & Sons Inc., New Jersey, 3rd edn., 2012, ch. 3, pp. 41-59.

286 H. van de Waterbeemd, D. A. Smith, K. Beaumont and D. K. Walker, *Journal of Medicinal Chemistry*, 2001, **44**, 1313–1333.

287 C. A. Lipinski, F. Lombardo, B. W. Dominy and P. J. Feeney, *Advanced Drug Delivery Reviews*, 1997, **23**, 3–25.

288 H. Suzuki and Y. Sugiyama, *European Journal of Pharmaceutical Sciences*, 2000, **12**, 3–12.

289 Y. Kim and J. Chen, *Science*, 2018, **359**, 915–919.

290 P. v. Desai, T. J. Raub and M. J. Blanco, *Bioorganic & Medicinal Chemistry Letters*, 2012, **22**, 6540–6548.

291 D. A. Smith, C. Allerton, A. S. Kalgutkar, H. van de Waterbeemd and D. K. Walker, in *Pharmacokinetics and Metabolism in Drug Design*, ed. R. Mannhold, H. Kubinyi, G. Folkers, John Wiley & Sons Inc., New Jersey, 3rd edn., 2012, ch. 4, pp. 61-79.

292 Y. Kwon, *Handbook of Essential Pharmacokinetics, Pharmacodynamics and Drug Metabolism for Industrial Scientists*, Springer US, New York, 2002.

293 D. A. Smith, K. Beaumont, T. S. Maurer and L. Di, *Journal of Medicinal Chemistry*, 2015, **58**, 5691–5698.

294 D. A. Smith, K. Beaumont, T. S. Maurer and L. Di, *Journal of Medicinal Chemistry*, 2017, **61**, 4273–4282.

295 D. A. Smith, K. Beaumont, T. S. Maurer and L. Di, *Journal of Medicinal Chemistry*, 2018, **62**, 2245–2255.

296 J. Faulkner, D. McGibney, L. Chasseaud, J. Perry and I. Taylor, *British Journal of Clinical Pharmacology*, 1986, **22**, 21–25.

297 D. R. Abernethy and J. B. Schwartz, *Clinical Pharmacokinetics*, 2012, **15**, 1–14.

298 P. M. Manoury, J. L. Binet, J. Rousseau, F. M. Lefevre-Borg and I. G. Cavero, *Journal of Medicinal Chemistry*, 2002, **30**, 1003–1011.

299 R. Daneman and A. Prat, *Cold Spring Harbor Perspectives in Biology*, 2015, **7**, a020412.

300 N. J. Abbott, A. A. K. Patabendige, D. E. M. Dolman, S. R. Yusof and D. J. Begley, *Neurobiology of Disease*, 2010, **37**, 13–25.

301 J. McAinsh and J. M. Cruickshank, *Pharmacology & Therapeutics*, 1990, **46**, 163–197.

302 T. T. Wager, X. Hou, P. R. Verhoest and A. Villalobos, *ACS Chemical Neuroscience*, 2016, **7**, 767–775.

303 T. T. Wager, X. Hou, P. R. Verhoest and A. Villalobos, *ACS Chemical Neuroscience*, 2010, **1**, 435–449.

304 K. S. Pang and M. Rowland, *Journal of Pharmacokinetics and Biopharmaceutics*, 2015, **5**, 625–653.

305 D. A. Smith, C. Allerton, A. S. Kalgutkar, H. van de Waterbeemd and D. K. Walker, in *Pharmacokinetics and Metabolism in Drug Design*, ed. R. Mannhold, H. Kubinyi, G. Folkers, John Wiley & Sons Inc., New Jersey, 3rd edn., 2012, ch. 5, pp. 81-102.

306 D. A. Smith, C. Allerton, A. S. Kalgutkar, H. van de Waterbeemd and D. K. Walker, in *Pharmacokinetics and Metabolism in Drug Design*, ed. R. Mannhold, H. Kubinyi, G. Folkers, John Wiley & Sons Inc., New Jersey, 3rd edn., 2012, ch. 7, pp. 111-158.

307 J. Rittle and M. T. Green, *Science*, 2010, **330**, 933–937.

308 M. Ingelman-Sundberg, *Trends in Pharmacological Sciences*, 2004, **25**, 193–200.

309 T. N. Thompson, *Medicinal Research Reviews*, 2001, **21**, 412–449.

310 Jr. David J. St. Jean and C. Fotsch, *Journal of Medicinal Chemistry*, 2012, **55**, 6002–6020.

311 N. A. Meanwell, *Journal of Medicinal Chemistry*, 2011, **54**, 2529–2591.

312 C. Barillari and N. Brown, in *Bioisosteres in Medicinal Chemistry*, ed. N. Brown, John Wiley & Sons Inc., New Jersey, 1st edn., 2012, ch. 2, pp. 15-29.

313 S. K. Bardal, J. E. Waechter and D. S. Martin, *Applied Pharmacology*, Elsevier, Amsterdam, 2011.

314 G. Ghibellini, E. M. Leslie and K. L. R. Brouwer, *Molecular Pharmaceutics*, 2006, **3**, 198–211.

315 M. S. Roberts, B. M. Magnusson, F. J. Burczynski and M. Weiss, *Clinical Pharmacokinetics 2002 41:10*, 2012, **41**, 751–790.

316 D. A. Smith, C. Allerton, A. S. Kalgutkar, H. van de Waterbeemd and D. K. Walker, in *Pharmacokinetics and Metabolism in Drug Design*, ed. R. Mannhold, H. Kubinyi, G. Folkers, John Wiley & Sons Inc., New Jersey, 3rd edn., 2012, ch. 6, pp. 103-110**.**

317 N. Manevski, L. King, W. R. Pitt, F. Lecomte and F. Toselli, *Journal of Medicinal Chemistry*, 2019, **62**, 10955-10994.

318 S. Ma, R. Subramanian, Y. Xu, M. Schrag and M. Shou, *Drug Metabolism and Disposition*, 2008, **36**, 2414–2418.

319 V. Berthelier, J. M. Tixier, H. Muller-Steffner, F. Schuber and P. Deterre, *Biochemical Journal*, 1998, **330**, 1383–1390.

320 Y. Dai, M. Michaelides, WO2016123796A1, 2016.

321 T. G. Gant, *Journal of Medicinal Chemistry*, 2013, **57**, 3595–3611.

322 K. Parcella, K. Eastman, K.-S. Yeung, K. A. Grant-Young, J. Zhu, T. Wang, Z. Zhang, Z. Yin, D. Parker, K. Mosure, H. Fang, Y.-K. Wang, J. Lemm, X. Zhuo, U. Hanumegowda, M. Liu, K. Rigat, M. Donoso, M. Tuttle, T. Zvyaga, Z. Haarhoff, N. A. Meanwell, M. G. Soars, S. B. Roberts and J. F. Kadow, *ACS Medicinal Chemistry Letters*, 2017, **8**, 771–774.

323 W. H. Brooks, W. C. Guida and K. G. Daniel, *Current Topics in Medicinal Chemistry*, 2011, **11**, 760–770.

324 F. F. Fleming, L. Yao, P. C. Ravikumar, L. Funk and B. C. Shook, *Journal of Medicinal Chemistry*, 2010, **53**, 7902–7917.

325 Y.-H. Zhang, B.-F. Shi and J.-Q. Yu, *Angewandte Chemie International Edition*, 2009, **48**, 6097–6100.

326 G. M. A. III, P. A. Kollman, L. N. Domelsmith and K. N. Houk, *Journal of the American Chemical Society*, 2002, **101**, 2344–2352.

327 M. M. P. Lufino, A. M. Silva, A. H. Németh, J. Alegre-Abarrategui, A. J. Russell and R. Wade-Martins, *Human Molecular Genetics*, 2013, **22**, 5173–5187.

328 V. Myrianthopoulos, N. Gaboriaud-Kolar, C. Tallant, M.-L. Hall, S. Grigoriou, P. M. Brownlee, O. Fedorov, C. Rogers, D. Heidenreich, M. Wanior, N. Drosos, N. Mexia, P. Savitsky, T. Bagratuni, E. Kastritis, E. Terpos, P. Filippakopoulos, S. Müller, A.-L. Skaltsounis, J. A. Downs, S. Knapp and E. Mikros, *Journal of Medicinal Chemistry*, 2016, **59**, 8787–8803.

329 C. Lu, P. Li, R. Gallegos, V. Uttamsingh, C. Q. Xia, G. T. Miwa, S. K. Balani and L.-S. Gan, *Drug Metabolism and Disposition*, 2006, **34**, 1600-1605

330 L. Di, C. Keefer, D. O. Scott, T. J. Strelevitz, G. Chang, Y. A. Bi, Y. Lai, J. Duckworth, K. Fenner, M. D. Troutman and R. S. Obach, *European Journal of Medicinal Chemistry*, 2012, **57**, 441–448.

331 M. Martignoni, G. M. M. Groothuis and R. de Kanter, *Expert Opinion on Drug Metabolism and Toxicology*, 2006, **2**, 875–894.

332 W. F. Richter and B. Jacobsen, *Drug Metabolism and Disposition*, 2014, **42**, 1881–1889.

333 K. M. Sakamoto, K. B. Kim, A. Kumagai, F. Mercurio, C. M. Crews and R. J. Deshaies, *Proceedings of the National Academy of Sciences*, 2001, **98**, 8554–8559.

334 X. Sun, H. Gao, Y. Yang, M. He, Y. Wu, Y. Song, Y. Tong and Y. Rao, *Signal Transduction and Targeted Therapy 2019 4:1*, 2019, **4**, 1–33.

335 M. Schneider, C. J. Radoux, A. Hercules, D. Ochoa, I. Dunham, L.-P. Zalmas, G. Hessler, S. Ruf, V. Shanmugasundaram, M. M. Hann, P. J. Thomas, M. A. Queisser, A. B. Benowitz, K. Brown and A. R. Leach, *Nature Reviews Drug Discovery,* 2021, **20**, 789-797.

336 S. M. Banik, K. Pedram, S. Wisnovsky, G. Ahn, N. M. Riley and C. R. Bertozzi, *Nature 2020 584:7820*, 2020, **584**, 291–297.

337 M. G. Costales, Y. Matsumoto, S. P. Velagapudi and M. D. Disney, *Journal of the American Chemical Society*, 2018, **140**, 6741–6744.

338 S. Yamazoe, J. Tom, Y. Fu, W. Wu, L. Zeng, C. Sun, Q. Liu, J. Lin, K. Lin, W. J. Fairbrother and S. T. Staben, *Journal of Medicinal Chemistry*, 2019, **63**, 2807–2813.

339 D. Takahashi, J. Moriyama, T. Nakamura, E. Miki, E. Takahashi, A. Sato, T. Akaike, K. Itto-Nakama and H. Arimoto, *Molecular Cell*, 2019, **76**, 797-810.

340 M. Reynders, B. S. Matsuura, M. Bérouti, D. Simoneschi, A. Marzio, M. Pagano and D. Trauner, *Science Advances*, 2020, **6**, eaay5064.

341 W. W. Wang, L.-Y. Chen, J. M. Wozniak, A. M. Jadhav, H. Anderson, T. E. Malone and C. G. Parker, *Journal of the American Chemical Society*, 2021, doi: 10.1021/jacs.1c07850

342 D. Komander, M. J. Clague and S. Urbé, *Nature Reviews Molecular Cell Biology*, 2009, **10**, 550–563.

343 D. H. Lee, *Trends in Cell Biology*, 1998, **8**, 397–403.

344 M. Benini, S. Fortuni, I. Condò, G. Alfedi, F. Malisan, N. Toschi, D. Serio, D. S. Massaro, G. Arcuri, R. Testi and A. Rufini, *Cell Reports*, 2017, **18**, 2007–2017.

345 T. E. T. Mevissen and D. Komander, *Annual Reviews in Biochemistry*, 2017, **86**, 159–192.

346 J. A. Harrigan, X. Jacq, N. M. Martin and S. P. Jackson, *Nature Reviews Drug Discovery*, 2017, **17**, 57–78.

347 A. P. Turnbull, S. Ioannidis, W. W. Krajewski, A. Pinto-Fernandez, C. Heride, A. C. L. Martin, L. M. Tonkin, E. C. Townsend, S. M. Buker, D. R. Lancia, J. A. Caravella, A. v. Toms, T. M. Charlton, J. Lahdenranta, E. Wilker, B. C. Follows, N. J. Evans, L. Stead, C. Alli, V. v. Zarayskiy, A. C. Talbot, A. J. Buckmelter, M. Wang, C. L. McKinnon, F. Saab, J. F. McGouran, H. Century, M. Gersch, M. S. Pittman, C. G. Marshall, T. M. Raynham, M. Simcox, L. M. D. Stewart, S. B. McLoughlin, J. A. Escobedo, K. W. Bair, C. J. Dinsmore, T. R. Hammonds, S. Kim, S. Urbé, M. J. Clague, B. M. Kessler and D. Komander, *Nature*, 2017, **550**, 481–486.

348 A. Pozhidaeva and I. Bezsonova, *DNA Repair*, 2019, **76**, 30–39.

349 A. C. Faesen, A. M. G. Dirac, A. Shanmugham, H. Ovaa, A. Perrakis and T. K. Sixma, *Molecular Cell*, 2011, **44**, 147–159.

350 M. Canning, C. Boutell, J. Parkinson and R. D. Everett, *Journal of Biological Chemistry*, 2004, **279**, 38160–38168.

351 M. Meredith, A. Orr and R. Everett, *Virology*, 1994, **200**, 457–469.

352 M. P. Lanfranca, H. H. Mostafa and D. J. Davido, *Cells*, 2014, **3**, 438–454.

353 A. Georges, E. Marcon, J. Greenblatt and L. Frappier, *Scientific Reports*, 2018, **8**, 1–12.

354 R. Pfoh, I. K. Lacdao, A. A. Georges, A. Capar, H. Zheng, L. Frappier and V. Saridakis, *PLOS Pathogens*, 2015, **11**, e1004950.

355 S. L. Paiva and C. M. Crews, *Current Opinion in Chemical Biology*, 2019, **50**, 111–119.

356 D. P. Bondeson, A. Mares, I. E. D. Smith, E. Ko, S. Campos, A. H. Miah, K. E. Mulholland, N. Routly, D. L. Buckley, J. L. Gustafson, N. Zinn, P. Grandi, S. Shimamura, G. Bergamini, M. Faelth-Savitski, M. Bantscheff, C. Cox, D. A. Gordon, R. R. Willard, J. J. Flanagan, L. N. Casillas, B. J. Votta, W. den Besten, K. Famm, L. Kruidenier, P. S. Carter, J. D. Harling, I. Churcher and C. M. Crews, *Nature Chemical Biology*, 2015, **11**, 611–617.

357 L. N. Gechijian, D. L. Buckley, M. A. Lawlor, J. M. Reyes, J. Paulk, C. J. Ott, G. E. Winter, M. A. Erb, T. G. Scott, M. Xu, H.-S. Seo, S. Dhe-Paganon, N. P. Kwiatkowski, J. A. Perry, J. Qi, N. S. Gray and J. E. Bradner, *Nature Chemical Biology*, 2018, **14**, 405–412.

358 S. B. Cambridge, F. Gnad, C. Nguyen, J. L. Bermejo, M. Krüger and M. Mann, *Journal of Proteome Research*, 2011, **10**, 5275–5284.

359 J. E. Kung and N. Jura, *Structure*, 2016, **24**, 7–24.

360 D. Garbett and A. Bretscher, *Molecular Biology of the Cell*, 2017, **25**, 2315–2319.

361 F. U. Hartl, A. Bracher and M. Hayer-Hartl, *Nature*, 2011, **475**, 324–332.

362 A. Rufini, S. Fortuni, G. Arcuri, I. Condò, D. Serio, O. Incani, F. Malisan, N. Ventura and R. Testi, *Human Molecular Genetics*, 2011, **20**, 1253–1261.

363 A. Rufini, F. Cavallo, I. Condò, S. Fortuni, G. de Martino, O. Incani, A. di Venere, M. Benini, D. S. Massaro, G. Arcuri, D. Serio, F. Malisan and R. Testi, *Neurobiology of Disease*, 2015, **75**, 91–99.

364 G. v. Los, L. P. Encell, M. G. McDougall, D. D. Hartzell, N. Karassina, C. Zimprich, M. G. Wood, R. Learish, R. F. Ohana, M. Urh, D. Simpson, J. Mendez, K. Zimmerman, P. Otto, G. Vidugiris, J. Zhu, A. Darzins, D. H. Klaubert, R. F. Bulleit and K. v. Wood, *ACS Chemical Biology*, 2008, **3**, 373–382.

365 R. L. M. van Montfort, P. Workman, S. J. Hughes and A. Ciulli, *Essays in Biochemistry*, 2017, **61**, 505–516.

366 D. P. Bondeson, B. E. Smith, G. M. Burslem, A. D. Buhimschi, J. Hines, S. Jaime-Figueroa, J. Wang, B. D. Hamman, A. Ishchenko and C. M. Crews, *Cell Chemical Biology*, 2018, **25**, 78-87.

367 R. P. Wurz, K. Dellamaggiore, H. Dou, N. Javier, M.-C. Lo, J. D. McCarter, D. Mohl, C. Sastri, J. R. Lipford and V. J. Cee, *Journal of Medicinal Chemistry*, 2017, **61**, 453–461.

368 G. E. Winter, D. L. Buckley, J. Paulk, J. M. Roberts, A. Souza, S. Dhe-Paganon and J. E. Bradner, *Science*, 2015, **348**, 1376–1381.

369 G. M. Burslem, B. E. Smith, A. C. Lai, S. Jaime-Figueroa, D. C. McQuaid, D. P. Bondeson, M. Toure, H. Dong, Y. Qian, J. Wang, A. P. Crew, J. Hines and C. M. Crews, *Cell Chemical Biology*, 2018, **25**, 67-77.

370 M. S. Gadd, A. Testa, X. Lucas, K.-H. Chan, W. Chen, D. J. Lamont, M. Zengerle and A. Ciulli, *Nature Chemical Biology*, 2017, **13**, 514–521.

371 K.-H. Chan, M. Zengerle, A. Testa and A. Ciulli, *Journal of Medicinal Chemistry*, 2017, **61**, 504–513.

372 N. J. Yang and M. J. Hinner, in *Site Specific Protein Labelling,* ed. A. Gautier and M. J. Hinner, Springer US, New Jersey, 1st edn., 2015, ch. 3, pp. 29-53.

373 S. A. Kanner, Z. Shuja, P. Choudhury, A. Jain and H. M. Colecraft, *Nature Methods*, 2020, **17**, 1245–1253.

374 N. J. Henning, L. Boike, J. N. Spradlin, C. C. Ward, B. Belcher, S. M. Brittain, M. Hesse, D. Dovala, L. M. McGregor, J. M. McKenna, J. A. Tallarico, M. Schirle and D. K. Nomura, *bioRxiv*, 2021, 2021.04.30.441959.

375 F. Fusetti, H. Erlandsen, T. Flatmark and R. C. Stevens, *Journal of Biological Chemistry*, 1998, **273**, 16962–16967.

376 A. M. Burger and A. K. Seth, *European Journal of Cancer*, 2004, **40**, 2217–2229.

377 X.-M. Meng, P. M.-K. Tang, J. Li and H. Y. Lan, *Frontiers in Physiology*, 2015, **0**, 82.

378 T. Knezevic, V. D. Myers, J. Gordon, D. G. Tilley, T. E. Sharp, J. Wang, K. Khalili, J. Y. Cheung and A. M. Feldman, *Heart Failure Reviews*, 2015, **20**, 423–434.

379 Q. Zheng, T. Huang, L. Zhang, Y. Zhou, H. Luo, H. Xu and X. Wang, *Frontiers in Aging Neuroscience*, 2016, **0**, 303.

380 H. Hu and S.-C. Sun, *Cell Research,* 2016, **26**, 457–483.

381 Z. J. Chen, *Nature Cell Biology,* 2005, **7**, 758–765.

382 J. Cao and Q. Yan, *Frontiers in Oncology*, 2012, **0**, 26.

7 EXPERIMENTAL PROCEDURES

7.1 GENERAL EXPERIMENTAL

7.1.1 Solvents and reagents

All solvents were purchased from commercial sources and used without purification (HPLC or analytical grade). Anhydrous solvents were purchased from Acros Organics stored under a nitrogen atmosphere with activated molecular sieves. Standard vacuum line techniques were used, and glassware was flame dried prior to use. Deionised water was sourced using an Elga DV 25 system. Organic solvents were dried during workup using anhydrous Na_2SO_4.

7.1.2 Purification and chromatography

Thin Layer Chromatography (TLC) was carried out using aluminium plates coated with 60 F_{254} silica gel. Plates were visualised using UV light (254 or 365 nm) or staining with Ninhydrin (1 M, EtOH) or 1% aq. $KMnO_4$. Normal-phase, silica gel column chromatography was carried out using Biotage Isolera One flash column chromatography system. Compound analytical HPLC and low resolution mass spectrometry were carried out on a waters LCMS system (Waters 2767 sample manager, Waters SFO System Fluidics organizer, Waters 2545 binary gradient module, 2 × Waters 515 HPLC pumps, Waters 2998 photodiode array detector, Waters 2424 ELS detector, Waters SQ detector 2). Analytical separation used a Kinetex 5 µM EVO C18 column (100 mm × 3.0 mm, 100 A) with a flow rate of 2 mL/min along a 3 minute gradient elution. The mobile phase consisted of solvent A (93% water, 5% MeCN, and 2% 0.5 M ammonium acetate adjusted to pH 6 with glacial acetic acid) and solvent B (18% water, 80% MeCN, and 2% of 0.5 M ammonium acetate adjusted to pH 6 with glacial acetic acid). The

elution gradient was: 95:5 (A/B) 0.35 min, 95:5 (A/B) to 5:95 (A/B) over 1 min, 5:95 (A/B) over 0.75 min, and then reversion back to 95:5 (A/B) over 0.1 min and 95:5 (A/B) over 0.8 min.

7.1.3 Characterisation

Melting points were recorded using a Stuart SMP40 instrument. Infrared spectroscopy was carried out with a Thermo Scientific Nicolet iS5 FTIR spectrometer fitted with an iD7IATR accessory, selected absorption maxima (ν_{max}) recorded in wavenumbers (cm^{-1}). NMR spectra were recorded using a Bruker Avance 400 MHz spectrometer using the deuterated solvent stated. Chemical shifts (δ) are quoted in parts per million (ppm) and referenced to the residual solvent peak. The data are presented as chemical shift, multiplicity (s = singlet, d = doublet, t = triplet, q = quartet, quin = quintet, sext = sextet, dd = doublet of doublets, dt = doublet of triplets, m = multiplet, br = broad resonance peak, and derivatives thereof), coupling constant (recorded in Hz and rounded to the nearest 0.1), and signal area integration. Two-dimensional NMR experiments (COSY, HSQC, HMBC) were used to aid the assignment of ^{1}H and ^{13}C spectra. Low Resolution mass spectra (LR-ESI-MS) were recorded on a Waters SQ Detector 2 (LC-MS) and the data processed using Waters FractionLynx software. High Resolution mass spectra (HR-ESI-MS) were recorded on a RapidFire 360 High Throughput MS system and processing was performed using Agilent MassHunter Workstation software. Compound names were generated using ChemBioDraw Ultra v20.1.1 systematic naming. Atom numbering in structures does not reflect IUPAC numbering conventions and is for the purpose of assignment.

7.2 CHAPTER 2

7.2.1 Chemical Synthesis

Synthesis of *tert*-butyl (3,3-difluorocyclopentyl)carbamate (9)

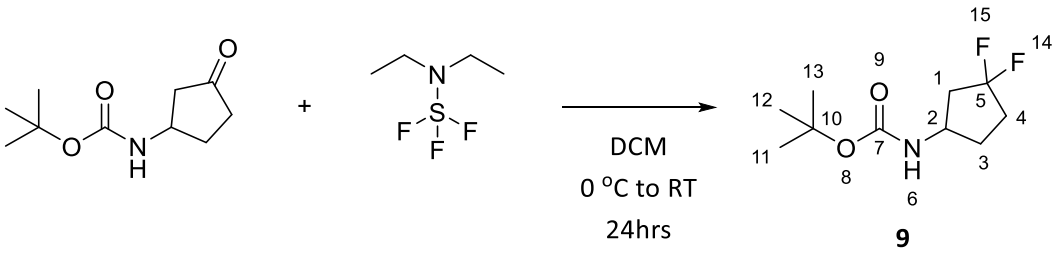

9

A 2-necked RBF equipped with stirrer bar and septum was backfilled with N_2 and charged with *tert*-butyl *N*-(3-oxocyclopentyl)carbamate) (235.0 mg, 1.179 mmol, 1.0 eq.). Dry dichloromethane (7 mL) was added, and the solution cooled to 0 °C. Diethylaminosulfur trifluoride (0.234 mL, 1.769 mmol, 1.5 eq.) was added dropwise with stirring, keeping the reaction at 0 °C. Once addition was complete, the reaction was allowed to warm to room temperature and left stirring overnight.

The reaction mixture was poured slowly into ice-cold, saturated $NaHCO_3$ solution and the organic layer extracted 3 times with DCM. The combined organic extracts were dried over sodium sulfate and the remaining solvent removed in vacuo. The crude product was purified using column chromatography (DCM:MeOH 95:5) to yield the title compound as a brown solid (159 mg, 61% yield). **M.P. =** 105-108 °C; **ν_{max} (cm^{-1})** 1742 (C=O), 1456 (C-F), 1161 (C-O); **^{1}H NMR (400 MHz, $CDCl_3$)** δ 4.85 (br, 1H, 6), 4.18 (br, 1H, 2), 2.56 (dd, *J* = 18.3, 7.4 Hz, 1H), 2.40 – 2.23 (m, 2H), 2.23 – 2.14 (m, 1H), 2.14 – 2.02 (dd, *J* = 18.3, 7.4 Hz, 1H), 1.82 (m, 1H), 1.40 (s, 9H); **^{13}C NMR (101 MHz, $CDCl_3$)** δ 155.44 (7), 132.07 (t, *J* = 248.8 Hz, 5) 79.81 (10), 48.96 (5),

45.39 (1), 37.14 (1), 29.97 (3), 28.43 (11, 12, 13); **LR-ESI-MS:** $C_{10}H_{17}F_2NO_2$ [M+H$^+$] *m/z* found: 221.43, calc.: 221.25; **HR-ESI-MS:** $C_{10}H_{17}F_2NO_2$ [M+H$^+$] *m/z* found: 222.0299, calc.: 222.1306;

Synthesis of (3,4-$^2H_2$)cyclopentan-1-aminium chloride (10)

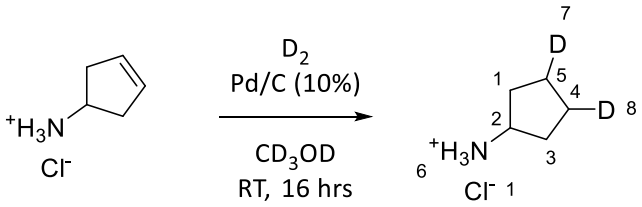

10

In an RBF equipped with stirrer bar and septum, cyclopent-3-en-1-aminium chloride (200.0 mg, 2.00 mmol, 1.00 eq.) was dissolved in methanol. 10% palladium on carbon (200.0 mg) was added and the mixture then underwent sequential cycles of nitrogen bubbling and vacuum degassing. Once the mixture had been fully degassed, a deuterium balloon was introduced with the reaction still under vacuum. The vacuum was turned off and the mixture left stirring under deuterium overnight.

The reaction mixture was filtered through celite and washed with ethyl acetate, with care taken to prevent the celite from drying out. The solvent was then removed in vacuo to yield (3,4-$^2H_2$)cyclopentan-1-aminium chloride (205.0 mg, quant.) as a white solid. **M.P. =** 192-195 °C; **^{1}H NMR (400 MHz, DMSO)** δ 8.14 (s, 3H, 6), 3.42 (p, *J* = 6.0 Hz, 1H, 2), 1.87-1.81 (m, 2H, 1, 3), 1.76 – 1.50 (m, 2H, 1, 3), 1.49-1.41 (m, 2H, 4, 5); **^{13}C NMR (101 MHz, DMSO)** δ 51.12 (2), 30.59 (1, 3), 23.42 (4, 5); **LR-ESI-MS:** $C_5H_9{}^2H_2N$ [M+H$^+$] *m/z* found: 87.27, calc.: 87.16; **HR-ESI-MS:** $C_5H_9{}^2H_2N$ [M+H$^+$] *m/z* found: 88.0094, calc.: 88.1095.

Synthesis of 1,4,6,7-tetrachlorophthalazine (Int 1)

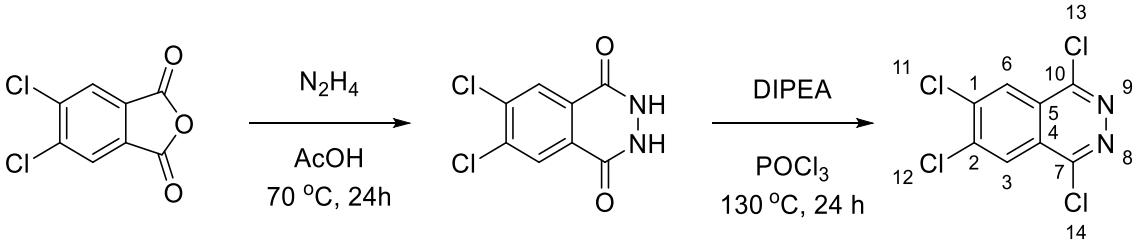

To a solution of 5,6-dichloroisobenzofuran-1,3-dione (5 g, 23.04 mmol, 1.00 eq.) in acetic acid (20 ml) at room temp was added hydrazine (78% in H_2O, 1.5 mL, 32.26 mmol, 1.4 eq.) dropwise. The solution was stirred overnight at 70 °C under nitrogen. The excess acetic acid was removed *in vacuo* and the resultant 6,7-dichloro-2,3-dihydrophthalazine-1,4-dione (5.32 g, 23.03 mmol, quantitative) was dissolved in $POCl_3$ (21.46 ml, 230 mmol, 10 eq.) immediately without further purification. N-ethyl-N-isopropylpropan-2-amine (4.01 ml, 23.03 mmol) was added dropwise, and the mixture was heated overnight at 130 °C.

The reaction mixture was poured into ice water (400 mL) and left stirring for one hour. The crude product was extracted using dichloromethane (DCM, 3 x 300 mL) and washed with sat. bicarbonate solution (5 x 100 mL) until pH = 7, followed by brine (3 x 50 mL). The combined organic extracts were dried over sodium sulfate and the excess solvent removed *in vacuo*. The crude product was purified using column chromatography (cyclohexane:EtOAc, 9:1) to yield 1,4,6,7-tetrachlorophthalazine (3.8 g, 14.18 mmol, 61.6 % yield) as white, crystalline solid. **^{1}H NMR (400 MHz, $CDCl_3$)** δ 8.42 (s, 2H, 3, 6); ^{13}C **NMR (101 MHz, $CDCl_3$)** δ 153.29 (7, 10), 140.10 (1, 2), 127.23 (4, 5), 125.90 (3, 6); **LR-ESI-MS:** $C_8H_2Cl_4N_2$ [M+H$^+$] *m/z* found: 268.11, calc.: 267.92.

General Procedure A

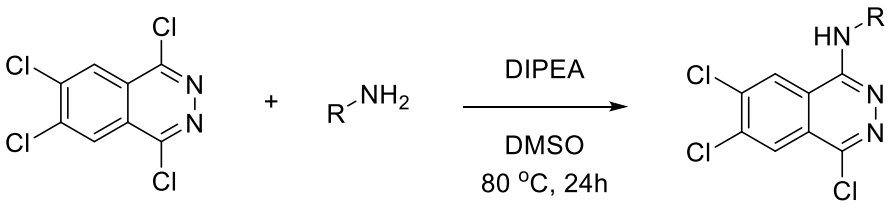

To a solution of 1,4,6,7-tetrachlorophthalazine (**Int 1,** 1 equiv.) and DIPEA (1.2 equiv) in DMSO in a 22 mL vial at 80 °C was added amine (1 equiv.) in DMSO. The reaction was stirred at 80 °C overnight. Upon completion (as determined by LCMS), the reaction was cooled to room temperature and extracted with DCM (3 x 10 mL). The combined organic extracts were washed with water (5 x 10 mL), dried over sodium sulfate and the excess solvent removed *in vacuo*. The crude product was purified using column chromatography (DCM:MeOH, 100:0 to 98:2) to yield the desired compound.

General Procedure B

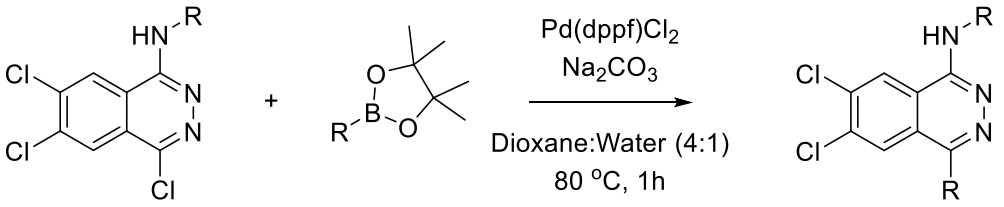

4,6,7-trichlorophthalazine-1-amine (1 equiv.), boronic ester (1 equiv.), $Pd(dppf)Cl_2$ (0.1 equiv.), and Na_2CO_3 (3 equiv.) were placed in a dry 22 mL vial equipped with stirrer bar. The vial was backfilled with N_2 and the contents dissolved in a degassed mixture of dioxane and water (4:1 ratio). The reaction was heated at 80 °C under N_2 for 1 hour before being cooled

to room temperature and filtered through celite. The mixture was extracted with ethyl acetate (3 x 10 mL) and the combined organic phases washed with water (3 x 10 mL) and brine (1 x 10 mL) before being dried over sodium sulfate. The residual solvent was removed *in vacuo* and the crude product purified using column chromatography (cyclohexane:ethyl acetate, 8:2 to 1:1).

6,7-dichloro-*N*-(3,3-difluorocyclopentyl)-4-(pyridin-4-yl)phthalazin-1-amine (11)

Step 1: 3,3-difluorocyclopentan-1-aminium chloride

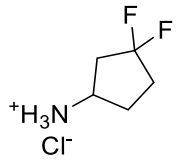

9 (xx mg, xx mmol, 1.0 eq.) was dissolved in dioxane and HCl added (4M in dioxane, x mL, xx eq.). The solution was left stirring for 2 hours and the residual solvent removed *in vacuo* to yield 3,3-difluorocyclopentan-1-aminium chloride (xx mg, quantitative), which was engaged directly in the next step without further purification. **LR-ESI-MS:** $C_5H_{10}ClF_2N$ [M+H$^+$] *m/z* found: 157.21, calc.: 157.59.

Step 2: 4,6,7-trichloro-*N*-(3,3-difluorocyclopentyl)phthalazin-1-amine

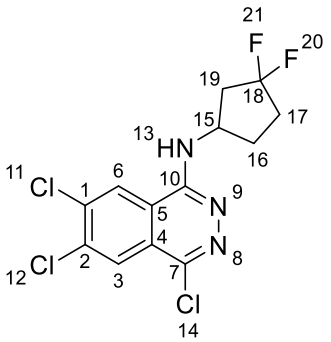

To a 4 mL vial containing 3,3-difluorocyclopentan-1-aminium chloride (58.8 mg, 0.373 mmol, 1.0 eq.) was added DMSO (1 mL) and diisopropylethylamine (DIPEA, 0.078 mL, 0.448 mmol,

1.0 eq.). The resulting solution was reacted with **Int 1** (100 mg, 0.373 mmol, 1.0 eq) according to **general procedure A** to yield 4,6,7-trichloro-N-(3,3-difluorocyclopentyl)phthalazin-1-amine (85.4 mg, 64.9%) as a brown solid. **^{1}H NMR (400 MHz, $CDCl_3$)** δ 8.25 (s, 1H, 6), 8.20 (s, 1H, 3), 6.29 (d, *J* = 6.6 Hz, 1H, 13), 4.81 (h, *J* = 7.0 Hz, 1H, 15), 2.77-2.66 (m, 1H, 19), 2.47-2.35 (m, 1H, 17), 2.35 – 1.96 (m, 3H, 17, 19, 16), 1.97 – 1.84 (m, 1H, 16); **^{13}C NMR (101 MHz, $CDCl_3$)** δ 152.45 (10), 144.51 (7), 137.53 (1), 137.16 (2), 131.35 (t, *J* = 248.9 Hz, 18), 127.16 (6), 125.60 (4), 124.36 (3), 119.37 (5), 50.07 (t, *J* = 4.7 Hz, 15), 42.28 (t, *J* = 24.8 Hz, 19) 34.52 (t, *J* = 25.1 Hz, 17), 30.12 (t, *J* = 3.4 Hz, 16); **LR-ESI-MS:** $C_{13}H_{10}Cl_3F_2N_3$ [M+H$^+$] *m/z* found: 352.53, calc.: 352.59

Step 3: 6,7-dichloro-*N*-(3,3-difluorocyclopentyl)-4-(pyridin-4-yl)phthalazin-1-amine (**11**)

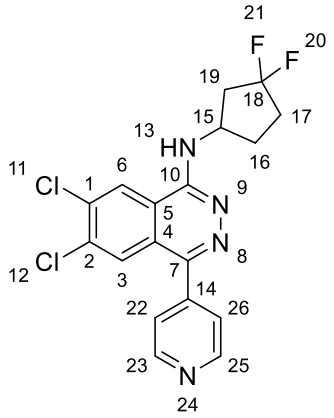

11

4,6,7-trichloro-*N*-(3,3-difluorocyclopentyl)phthalazin-1-amine (50 mg, 0.142 mmol, 1.0 eq) was reacted with 4-pyridinylboronic acid (17.4 mg, 0.142 mmol, 1.0 eq.) according to **general procedure B** to yield **11** (49.2 mg, 87.8%) as a brown solid. **M.P.** = 277-279 °C; **ν_{max} (cm^{-1})** 3189 (NH), 2979, 2890 (CH), 1651 (C=N), 1297 (C-F); **^{1}H NMR (400 MHz, $CDCl_3$)** δ 8.81 (d, *J* = 4.8 Hz, 2H, 23, 25), 8.01 (d, 2H, 6, 3), 7.61 (dd, *J* = 4.5, 1.4 Hz, 2H, 22, 26), 5.46 (d, *J* = 6.7 Hz, 1H, 13), 4.98 (sext., *J* = 6.8 Hz, 1H, 15), 2.82 (ddt, *J* = 22.8, 14.6, 8.0 Hz, 1H, 19), 2.52 (dt, *J* = 13.2, 5.9

Hz, 1H, 17), 2.43 – 2.29 (m, 1H, 19), 2.29 – 2.11 (m, 2H, 17, 16), 2.01 – 1.89 (m, 1H, 16); **^{13}C NMR (101 MHz, $CDCl_3$)** δ 151.60 (10), 150.38 (23, 25), 149.60 (7), 143.89 (14), 137.24 (1), 136.62 (2), 131.45 (t, *J* = 249.2 Hz, 18), 127.47 (6), 125.03 (4), 124.37 (22, 26), 123.22 (3), 117.43 (5), 50.26 (dd, *J* = 5.9, 3.6, 15), 42.78 (t, *J* = 24.5 Hz, 19), 34.48 (t, *J* = 25.2 Hz, 17), 30.58 (dd, *J* = 4.5, 2.3 Hz, 16); **LR-ESI-MS:** $C_{18}H_{14}Cl_2F_2N_4$ [M+H$^+$] *m/z* found: 395.43, calc.: 395.23; **HR-ESI-MS:** $C_{18}H_{14}Cl_2F_2N_4$ [M+H$^+$] *m/z* found: 394.9541, calc.: 395.06419

6,7-dichloro-*N*-(cyclopentyl-3,4-$^2H_2$)-4-(pyridin-4-yl)phthalazin-1-amine (12)

Step 1: 4,6,7-trichloro-*N*-(cyclopentyl-3,4-$^2H_2$)phthalazin-1-amine

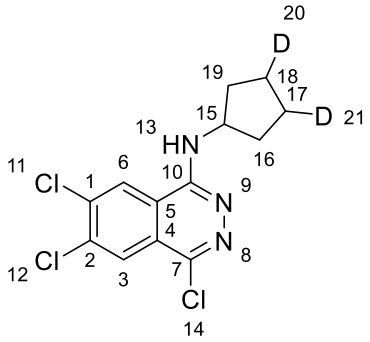

To a 4 mL vial containing **10** (46.1 mg, 0.373 mmol, 1.0 eq.) was added DMSO (1 mL) and diisopropylethylamine (DIPEA, 0.78 mL, 0.448 mmol, 1.2 eq.). The resulting solution was reacted with **Int 1** (100 mg, 0.373 mmol, 1.0 eq.) according to **general procedure A** to yield 4,6,7-trichloro-N-(cyclopentyl-3,4-$^2H_2$)phthalazin-1-amine (84.2 mg, 70.8%) as an off-white solid. **^{1}H NMR (400 MHz, $CDCl_3$)** δ 8.24 (s, 1H, 6), 7.89 (s, 1H, 3), 5.12 (d, *J* = 6.5 Hz, 1H, 13), 4.60 (sext, *J* = 6.5 Hz, 1H, 15), 2.26-2.17 (m, 1H, 16), 1.82 – 1.70 (m, 2H 16, 19), 1.74-1.65 (m, 1H, 19), 1.63 – 1.49 (m, 2H, 17, 18); **^{13}C NMR (101 MHz, $CDCl_3$)** δ 152.28 (10), 144.08 (7), 137.39 (1), 137.06 (2), 127.47 (6), 125.60 (4), 123.26 (3), 119.21 (5), 53.72 (15), 33.40 (16, 19), 24.10 (17, 18); **LR-ESI-MS:** $C_{13}H_{10}D_2Cl_3N_3$ [M+H$^+$] *m/z* found: 318.30, calc.: 318.62Step 2: 6,7-dichloro-*N*-(cyclopentyl-3,4-$^2H_2$)-4-(pyridin-4-yl)phthalazin-1-amine (**12**)

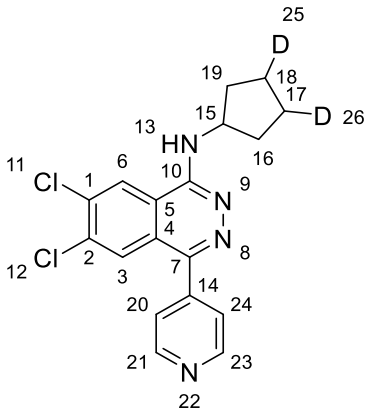

12

4,6,7-trichloro-*N*-(cyclopentyl-3,4-$^{2}H_2$)phthalazin-1-amine (50 mg, 0.157 mmol, 1.0 eq.) was reacted with 4-pyridinylboronic acid (19.3 mg, 0.157 mmol, 1.0 eq.) according to **general procedure B** to yield **12** (31.2 mg, 55.0%) as a white solid. **M.P. =** 249-251 °C; **ν_{max} (cm^{-1})** 3213 (NH), 2960, 2867 (CH), 1651 (C=N); **^{1}H NMR (400 MHz, $CDCl_3$)** δ 8.83 (dd, *J* = 4.4, 1.6 Hz, 2H, 21, 23), 8.04 (s, 1H, 6), 7.97 (s, 1H, 3), 7.69 – 7.61 (dd, *J* = 4.4, 1.6 Hz, 2H, 20, 24), 5.18 (d, *J* = 6.5 Hz, 1H, 13), 4.77 (sext, *J* = 6.3 Hz, 1H, 15), 2.38-2.28 (m, 1H, 16), 1.88-1.70 (m, 3H, 16, 19 (2)), 1.69-1.57 (m, 2H, 17, 18); **^{13}C NMR (101 MHz, $CDCl_3$)** δ 151.91 (10), 150.37 (21, 23), 148.70 (7), 144.16 (14), 136.80 (1), 136.14 (2), 127.36 (6), 124.99 (4), 124.37 (3), 123.11 (20, 24), 117.43 (5), 55.88 (15), 33.62 (16, 19), 24.15 (17, 18); **LR-ESI-MS:** $C_{18}H_{14}D_2Cl_2N_4$ [M+H^+] *m/z* found: 361.09, calc.: 361.27; **HR-ESI-MS:** $C_{18}H_{14}D_2Cl_2N_4$ [M+H^+] *m/z* found: 360.99110, calc.: 361.09559

6,7-dichloro-4-(pyridin-4-yl)-*N*-(tetrahydrofuran-3-yl)phthalazin-1-amine (13)

Step 1: 4,6,7-trichloro-*N*-(tetrahydrofuran-3-yl)phthalazin-1-amine

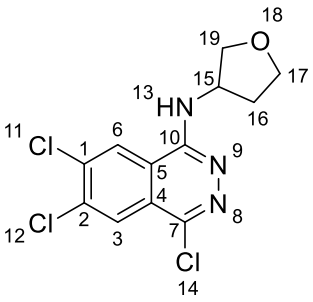

3-Aminotetrahydrofuran (32.5 mg, 0.373 mmol, 1.0 eq.) was reacted with **Int 1** (100 mg, 0.373 mmol, 1.0 eq.) according to **general procedure A** to yield 4,6,7-trichloro-N-(tetrahydrofuran-3-yl)phthalazin-1-amine (94 mg, 79 % yield) as a yellow solid. **^{1}H NMR (400 MHz, $CDCl_3$)** δ 8.27 (s, 1H, 6), 7.93 (s, 1H, 6), 5.34 (d, *J* = 6.7 Hz, 1H, 13), 4.97-4.90 (m, 1H, 15), 4.06 (td, *J* = 8.2, 6.6 Hz, 1H, 19), 4.00 (dd, *J* = 9.7, 5.1 Hz, 1H, 17), 3.92 (dd, *J* = 9.7, 2.4 Hz, 1H, 17), 3.87 (td, *J* = 8.7, 5.9 Hz, 1H, 19), 2.52-2.42 (m, 1H, 16), 2.09 – 1.98 (m, 1H, 16); **^{13}C NMR (101 MHz, $CDCl_3$)** δ 152.10 (10), 144.90 (7), 137.75 (1), 137.44 (2), 127.51 (6), 125.61 (4), 123.44 (3), 119.20 (5), 73.83 (19), 67.26 (17), 52.95 (15), 33.46 (16); **LR-ESI-MS:** $C_{12}H_{10}Cl_3N_3O$ [M+H$^+$] *m/z* found: 318.34, calc.: 318.58

Step 2: 6,7-dichloro-4-(pyridin-4-yl)-*N*-(tetrahydrofuran-3-yl)phthalazin-1-amine (**13**)

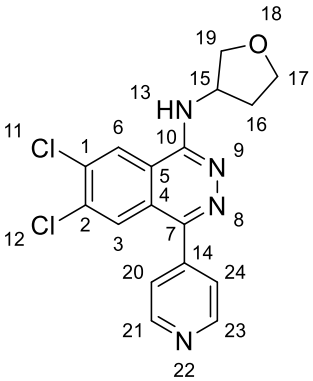

13

4,6,7-trichloro-*N*-(tetrahydrofuran-3-yl)phthalazin-1-amine (50 mg, 0.157 mmol, 1.0 eq.) and 4-pyridinylboronic acid (19.29 mg, 0.157 mmol, 1.0 eq.) were reacted together according to

general procedure B to yield **13** (42.0 mg, 74 % yield) as a white solid. **M.P. =** 260-263 °C; **ν_{max} (cm^{-1})** 3194 (NH), 3062, 2920, 2845 (CH), 1730, 1596 (C=N), 1161 (C-O); **^{1}H NMR (400 MHz, $CDCl_3$)** δ 8.81 (dd, *J* = 4.4, 1.6 Hz, 2H, 21, 23), 8.01 (d, *J* = 5.8 Hz, 2H, 6, 3), 7.61 (dd, *J* = 4.4, 1.6 Hz, 2H, 20, 24), 5.44 (d, *J* = 6.6 Hz, 1H, 13), 5.09-5.01 (m, 1H, 15), 4.14 – 4.07 (m, 1H, 19), 4.05 (dd, *J* = 9.9, 5.2 Hz, 1H, 17), 3.98 (dd, *J* = 9.7, 2.5 Hz, 1H, 17), 3.90 (td, *J* = 8.7, 5.9 Hz, 1H, 19), 2.57-2.47 (m, 1H, 16), 2.15 – 2.03 (m, 1H, 16); **^{13}C NMR (101 MHz, $CDCl_3$)** δ 151.68 (10), 150.39 (21, 23), 149.45 (7), 143.91 (14), 137.18 (1), 136.56 (2), 127.45 (6), 125.00 (5), 124.35 (20, 24), 123.23 (3), 117.49 (4), 74.07 (19), 67.23 (17), 53.00 (15), 33.59 (16)$^{\cdot}$; **LR-ESI-MS:** $C_{17}H_{14}Cl_2N_4O$ [M+H$^+$] *m/z* found: 361.11, calc.: 361.23; **HR-ESI-MS:** $C_{17}H_{14}Cl_2N_4O$ [M+H$^+$] *m/z* found: 360.9615, calc.: 361.0623

(*R*)-6,7-dichloro-4-(pyridin-4-yl)-*N*-(tetrahydrofuran-3-yl)phthalazin-1-amine (14)

Step 1: (*R*)-4,6,7-trichloro-*N*-(tetrahydrofuran-3-yl)phthalazin-1-amine

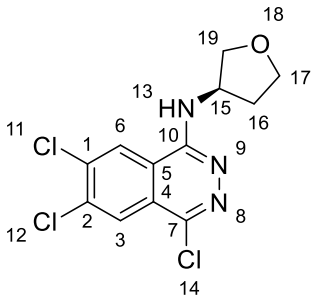

(*R*)-3-Aminotetrahydrofuran (32.5 mg, 0.373 mmol, 0.1 eq.) was reacted with **Int 1** (100 mg, 0.373 mmol, 0.1 eq.) according to **general procedure A** to yield 4,6,7-trichloro-N-(tetrahydrofuran-3-yl)phthalazin-1-amine (91.2 mg, 77.2%) as a yellow solid. **^{1}H NMR (400 MHz, $CDCl_3$)** δ 8.26 (s, 1H, 6), 7.98 (s, 1H, 3), 5.49 (d, *J* = 6.7 Hz, 1H, 13), 4.96-4.90 (m, 1H, 15), 4.09 – 4.02 (m, 1H, 19), 3.99 (dd, *J* = 9.7, 5.1 Hz, 1H, 17), 3.92 (dd, *J* = 9.7, 2.5 Hz, 1H, 17), 3.87 (td, *J* = 8.7, 5.9 Hz, 1H, 19), 2.51-2.42 (m, 1H, 16), 2.08 – 1.99 (m, 1H, 16); **^{13}C NMR (101 MHz, $CDCl_3$)** δ 152.09 (10), 144.92 (7), 137.77 (1), 137.45 (2), 127.53 (6), 125.62 (4), 123.44 (3),

119.21 (5), 73.88 (19), 67.20 (17), 52.93 (15), 33.43 (16); **LR-ESI-MS:** $C_{12}H_{10}Cl_3N_3O$ [M+H$^+$] *m/z* found: 318.46, calc.: 318.58

Step 2: (*R*)-6,7-dichloro-4-(pyridin-4-yl)-*N*-(tetrahydrofuran-3-yl)phthalazin-1-amine **(14)**

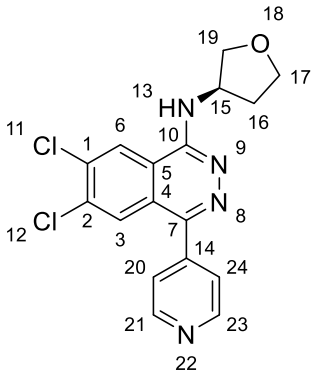

14

(*R*)-4,6,7-trichloro-N-(tetrahydrofuran-3-yl)phthalazin-1-amine (50 mg, 0.158 mmol, 1.0 eq.) and 4-pyridinylboronic acid (19.4 mg, 0.158 mmol, 1.0 eq.) were reacted together according to **general procedure B** to yield **14** (47.3 mg, 82.9%) as a white solid. **M.P. =** 262-264 °C; **ν_{max} (cm^{-1})** 3201 (NH), 3098, 2944, 2855 (CH), 1600 (C=N), 1136 (C-O); **^{1}H NMR (400 MHz, $CDCl_3$)** δ 8.81 (dd, *J* = 4.4, 1.6 Hz, 2H, 21, 23), 8.03 (d, *J* = 11.2 Hz, 2H, 6, 3), 7.61 (dd, *J* = 4.4, 1.6 Hz, 2H, 20, 24), 5.56 (d, *J* = 6.7 Hz, 1H, 13), 5.09-5.03 (m, 1H, 15), 4.14 – 4.07 (m, 1H, 19), 4.05 (dd, *J* = 9.7, 5.1 Hz, 1H, 17), 3.98 (dd, *J* = 9.7, 2.5 Hz, 1H, 17), 3.89 (td, *J* = 8.6, 5.9 Hz, 1H, 19), 2.56-2.48 (m, 1H, 16), 2.12-2.05 (m, 1H, 16); **^{13}C NMR (101 MHz, $CDCl_3$)** δ 151.76 (10), 150.38 (21, 23), 149.42 (7), 143.94 (14), 137.15 (1), 136.52 (2), 127.41 (6), 125.02 (5), 124.36 (20, 24), 123.36 (3), 117.54 (4), 74.05 (19), 67.25 (17), 52.99 (15), 33.57 (16); **LR-ESI-MS:** $C_{17}H_{14}Cl_2N_4O$ [M+H$^+$] *m/z* found: 361.17, calc.: 361.23; **HR-ESI-MS:** $C_{17}H_{14}Cl_2N_4O$ [M+H$^+$] *m/z* found: 360.9617, calc.: 361.0623

(*S*)-6,7-dichloro-4-(pyridin-4-yl)-*N*-(tetrahydrofuran-3-yl)phthalazin-1-amine (15)

Step 1: (*S*)-4,6,7-trichloro-*N*-(tetrahydrofuran-3-yl)phthalazin-1-amine

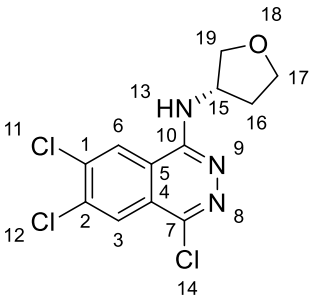

(*S*)-3-Aminotetrahydrofuran (32.5 mg, 0.373 mmol, 1.0 eq.) was reacted with **Int 1** (100 mg, 0.373 mmol, 1.0 eq.) according to **general procedure A** to yield 4,6,7-trichloro-N-(tetrahydrofuran-3-yl)phthalazin-1-amine (93.2 mg, 78.4%) as a yellow solid. **^{1}H NMR (400 MHz, $CDCl_3$)** δ 8.25 (s, 1H, 6), 7.99 (s, 1H, 3), 5.53 (d, *J* = 6.7 Hz, 1H, 13), 4.96-4.90 (m, 1H, 15), 4.09 – 4.02 (m, 1H, 19), 3.99 (dd, *J* = 9.7, 5.1 Hz, 1H, 17), 3.92 (dd, *J* = 9.7, 2.5 Hz, 1H, 17), 3.87 (td, *J* = 8.6, 5.9 Hz, 1H, 19), 2.51-2.42 (m, 1H, 16), 2.09 – 1.99 (m, 1H, 16); ^{13}C NMR (101 MHz, $CDCl_3$) δ 152.11 (10), 144.91 (7), 137.77 (1), 137.44 (2), 127.52 (6), 125.62 (4), 123.47 (3), 119.22 (5), 73.87 (19), 67.21 (17), 52.93 (15), 33.42 (16); **LR-ESI-MS:** $C_{12}H_{10}Cl_3N_3O$ [M+H$^+$] *m/z* found: 318.31, calc.: 318.58

Step 2: (*S*)-6,7-dichloro-4-(pyridin-4-yl)-*N*-(tetrahydrofuran-3-yl)phthalazin-1-amine **(15)**

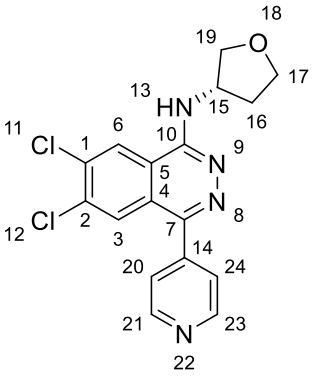

15

(*S*)-4,6,7-trichloro-N-(tetrahydrofuran-3-yl)phthalazin-1-amine (50 mg, 0.157 mmol) and 4-pyridinylboronic acid (19.29 mg, 0.157 mmol) were reacted together according to **general procedure B** to yield **15** (xx) as a white solid. **M.P. =** 260-262 °C; **ν_{max} (cm^{-1})** 3210 (NH), 3002,

2872, 2811 (CH), 1602 (C=N), 1177 (C-O); **^{1}H NMR (400 MHz, $CDCl_3$)** δ 8.80 (br, 2H, 21, 23), 8.03 (d, *J* = 19.3 Hz, 2H, 6, 3), 7.61 (d, *J* = 5.5 Hz, 2H, 20, 24), 5.63 (d, *J* = 6.6 Hz, 1H, 13), 5.09-5.03 (m, 1H, 15), 4.12 – 4.07 (m, 1H, 19), 4.07 – 4.02 (m, 1H, 17), 3.98 (dd, *J* = 9.7, 2.5 Hz, 1H, 17), 3.89 (td, *J* = 8.6, 5.9 Hz, 1H, 19), 2.52 (sext., *J* = 7.1 Hz, 1H, 16), 2.12-2.05 (m, 1H, 16); **^{13}C NMR (101 MHz, $CDCl_3$)** δ 151.79 (10), 150.38 (21, 23), 149.40 (7), 143.94 (14), 137.13 (1), 136.50 (2), 127.39 (6), 125.02 (5), 124.35 (20, 24), 123.41 (3), 117.55 (4), 74.03 (19), 67.25 (17), 52.98 (15), 33.56 (16); **LR-ESI-MS:** $C_{17}H_{14}Cl_2N_4O$ [M+H$^+$] *m/z* found: 361.06, calc.: 361.23; **HR-ESI-MS:** $C_{17}H_{14}Cl_2N_4O$ [M+H$^+$] *m/z* found: 360.9616, calc.: 361.0623

(*R*)-6,7-dichloro-4-(pyridin-4-yl)-*N*-(pyrrolidin-3-yl)phthalazin-1-amine (16)

Step 1: tert-butyl (*R*)-3-((4,6,7-trichlorophthalazin-1-yl)amino)pyrrolidine-1-carboxylate

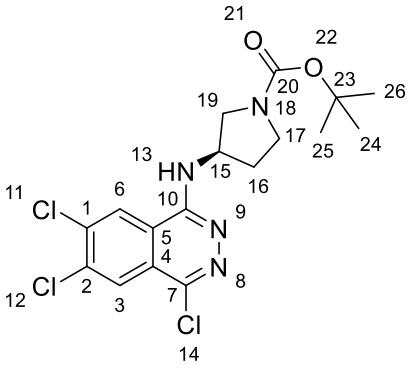

(*R*)-(+)-1-Boc-3-aminopyrrolidine (139.0 mg, 0.746 mmol, 1.0 eq.) was reacted with **Int 1** (200 mg, 0.746 mmol, 1.0 eq.) according to **general procedure A** to yield tert-butyl (*R*)-3-((4,6,7-trichlorophthalazin-1-yl)amino)pyrrolidine-1-carboxylate (212.3 mg, 68.1%) as a white solid. **^{1}H NMR (400 MHz, $CDCl_3$)** δ 8.43 (s, 1H, 6), 8.16 (s, 1H, 3), 6.70 (br d, *J* = 43.9 Hz, 1H, 13), 4.82 (br, 1H, 15), 3.77 (s, 1H, 19), 3.48 (m, 3H, 17 (2), 19), 2.28 (br, 1H, 16), 2.11 (br, 1H, 16), 1.55 – 1.31 (m, 9H, 24, 25, 26); ^{13}C NMR (101 MHz, $CDCl_3$) δ 154.97, 152.39, 144.75, 137.65, 137.28, 127.29, 125.65, 124.04, 119.36, 79.94, 53.56, 52.11, 44.54, 31.76, 28.71 **^{13}C NMR (101 MHz, $CDCl_3$)** δ 154.87 (20), 152.58 (10), 144.27 (7), 137.43 (1), 136.99 (2), 126.97 (6), 125.58 (3),

124.85 (4), 119.50 (5), 79.69 (23), 52.00 (19) , 51.05 (17), 44.51 (15), 31.55 (16), 28.62 (24, 25, 26); **LR-ESI-MS:** $C_{17}H_{19}Cl_3N_4O_2$ [M+H$^+$] *m/z* found: 417.38, calc.: 417.72

Step 2: tert-butyl (*R*)-3-((6,7-dichloro-4-(pyridin-4-yl)phthalazin-1-yl)amino)pyrrolidine-1-carboxylate (**17**)

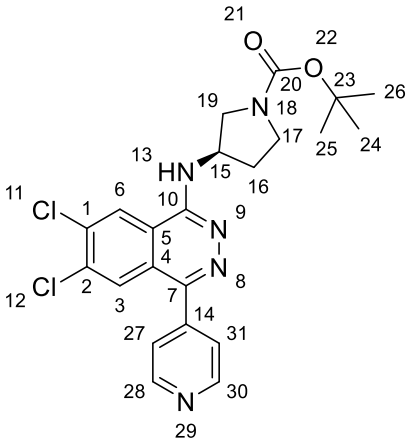

17

tert-Butyl (*R*)-3-((4,6,7-trichlorophthalazin-1-yl)amino)pyrrolidine-1-carboxylate (100 mg, 0.239 mmol, 1.0 eq.) and 4-pyridinylboronic acid (35.3 mg, 0.287 mmol, 1.0 eq.) were reacted together according to **general procedure B** to yield **17** (71.2 mg, 64.6%) as a white solid. **M.P. =** 189-193 °C; **ν_{max} (cm^{-1})** 3268 (NH), 2951, 2919 (CH), 1980 (C=O), 1651 (C=N); **^{1}H NMR** (400 MHz, Chloroform-*d*) δ 8.81 (dd, *J* = 4.5, 1.4 Hz, 2H, 28, 30), 8.34 (s, 1H, 6), 7.99 (s, 1H, 3) 7.62 (dd, *J* = 4.5, 1.6 Hz, 2H, 27, 31), 5.48 (d, *J* = 63.5 Hz, 1H, 13), 5.06 – 4.94 (m, 1H, 15), 3.87 (br, 1H, 19), 3.70 – 3.37 (m, 3H, 17 (2), 19), 2.51 – 2.33 (m, 1H, 16), 2.28 – 2.12 (m, 1H, 16), 1.46 (s, 9H, 24, 25, 26); **^{13}C NMR (101 MHz, $CDCl_3$)** δ 154.96 (20), 152.00 (10), 150.21 (28, 30), 149.25 (7) 143.98 (14), 137.14 (1), 136.44 (2), 127.18 (6), 125.05 (3), 124.69 (27, 31), 124.08 (4), 117.69 (5), 79.91 (23), 60.54 (19), 52.14 (17), 51.58 (1), 28.69 (24, 25, 26); **LR-ESI-MS:** $C_{22}H_{22}Cl_2N_5O_2$ [M+H$^+$] *m/z* found: 460.48, calc.: 460.36; **HR-ESI-MS:** $C_{22}H_{22}Cl_2N_5O_2$ [M+H$^+$] *m/z* found: 460.0022, calc.: 460.1307.

Step 3: (*R*)-6,7-dichloro-4-(pyridin-4-yl)-*N*-(pyrrolidin-3-yl)phthalazin-1-amine (**16**)

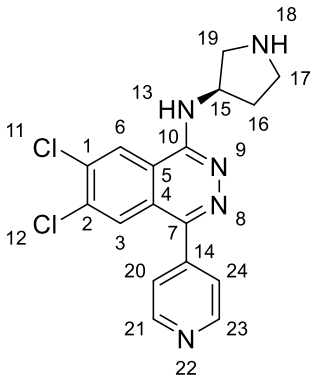

16

17 (30 mg, 0.65 mmol, 1.0 eq.) was dissolved in dioxane (3 mL) and HCl (4.0 M in dioxane, 1.0 mL) was added. The solution was left stirring for four hours after which the solvent was removed *in vacuo*. The resulting solid was taken up in DCM and washed with aq. NaOH (3 x 10 mL). The organic extracts were dried over sodium sulfate and the residual solvent removed *in vacuo* to yield **16** (23 mg, quant.) as a brown oil. **ν_{max} (cm^{-1})** 3273 (NH), 2971, 2866, 2843 (CH), 1612 (C=N); **^{1}H NMR (400 MHz, $CDCl_3$)** δ 8.79 (dd, *J* = 4.4, 1.6 Hz, 2H, 21, 23), 8.27 (s, 1H, 6), 7.97 (s, 1H, 3), 7.60 (dd, *J* = 4.5, 1.6 Hz, 2H, 20, 24), 6.32 (s, 1H. 13), 4.99 (s, 1H, 15), 3.35 (dd, *J* = 11.3, 6.0 Hz, 1H, 19), 3.28-3.18 (m, 2H, 17), 3.13 – 3.00 (m, 1H, 19), 2.93 (br, 1H, 18), 2.48 – 2.27 (m, 1H, 16), 2.12 – 1.78 (m, 1H, 16); **^{13}C NMR (101 MHz, $CDCl_3$)** δ 151.99 (10), 150.83 (21, 23), 150.37 (7), 144.05 (14), 136.93 (1), 136.29 (2), 127.12 (6), 125.02 (3), 124.32 (20, 24), 124.08 (4), 117.74 (5), 53.36 (19), 52.45 (17), 45.45 (15), 33.17 (16); **LR-ESI-MS:** $C_{17}H_{15}Cl_2N_5$ [M+H$^+$] *m/z* found: 360.08, calc.: 360.24; **HR-ESI-MS:** $C_{17}H_{15}Cl_2N_5$ [M+H$^+$] *m/z* found: 359.9975, calc.: 360.0783.

6,7-dichloro-*N*-(cyclopropylmethyl)-4-(pyridin-4-yl)phthalazin-1-amine (18)

Step 1: 4,6,7-trichloro-*N*-(cyclopropylmethyl)phthalazin-1-amine

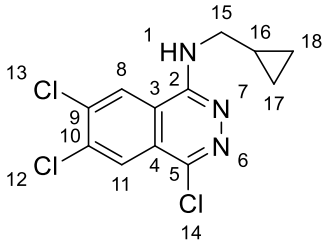

(Aminomethyl)cyclopropane (26.5 mg, 0.373 mmol, 1.0 eq.) was reacted with **Int 1** (100 mg, 0.373 mmol, 1.0 eq.) according to **general procedure A** to yield 4,6,7-trichloro-N-(cyclopropylmethyl)phthalazin-1-amine (102.4 mg, 91%) as an off-white solid**. ^{1}H NMR (400 MHz, $CDCl_3$)** δ 8.26 (s, 1H, 8), 7.97 (s, 1H, 11), 5.30 (br, 1H, 1), 3.52 (dd, *J* = 7.3, 4.6 Hz, 2H, 15), 1.23 (dtt, *J* = 10.5, 7.7, 4.0 Hz, 1H, 16), 0.67 – 0.57 (m, 2H, 17), 0.40-0.29 (m, 2H, 18); **^{13}C NMR (101 MHz, $CDCl_3$)** δ 152.45 (2), 144.39 (5), 137.57 (9), 137.21 (10), 127.56 (8), 125.61 (3), 123.26 (11), 119.10 (4), 47.56 (15), 10.68 (16), 3.91 (17, 18); **LR-ESI-MS:** $C_{12}H_{10}Cl_3N_3$ [M+H$^+$] *m/z* found: 302.37, calc.: 302.58

Step 2: 6,7-dichloro-*N*-(cyclopropylmethyl)-4-(pyridin-4-yl)phthalazin-1-amine (**18**)

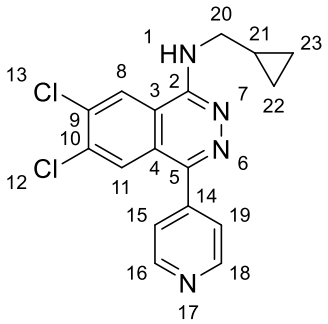

18

4,6,7-trichloro-*N*-(cyclopropylmethyl)phthalazin-1-amine (50 mg, 0.165 mmol, 1.0 eq.) was reacted with 4-pyridinylboronic acid (24.4 mg, 0.198 mmol, 1.2 eq.) according to **general procedure B** to yield **18** (28.2 mg, 49.4%) as an off-white solid. **M.P. =** 221-223 °C; **ν_{max} (cm^{-1})** 3278 (NH), 3074, 2964, 2922 (CH), 1601 (C=N); **^{1}H NMR (400 MHz, $CDCl_3$)** δ 8.81 (s, 2H, 16, 18), 8.22 (s, 1H, 8), 7.99 (s, 1H, 11), 7.60 (s, 2H, 15, 19), 5.95 (s, 1H, 1), 3.65 (d, *J* = 7.1 Hz, 2H, 20), 1.37 – 1.26 (m, 1H, 21), 0.76 – 0.54 (m, 2H, 22), 0.49 – 0.30 (m, 2H, 23); **^{13}C NMR (101**

MHz, $CDCl_3$) δ 151.94 (2), 150.26 (16, 18), 148.87 (5), 143.93 (14), 137.36 (9), 136.60 (10), 127.38 (8), 125.06 (3), 124.39 (15, 19), 123.95 (11), 117.70 (4), 47.63 (20), 10.72 (21), 4.01 (22, 23); **LR-ESI-MS:** $C_{17}H_{14}Cl_2N_4$ [M+H$^+$] *m/z* found: 345.14, calc.: 345.23; **HR-ESI-MS:** $C_{17}H_{14}Cl_2N_4$ [M+H$^+$] *m/z* found: 344.9709, calc.: 345.0674.

6,7-dichloro-*N*-(1-cyclopropylethyl)-4-(pyridin-4-yl)phthalazin-1-amine (19)

Step 1: 4,6,7-trichloro-*N*-(1-cyclopropylethyl)phthalazin-1-amine

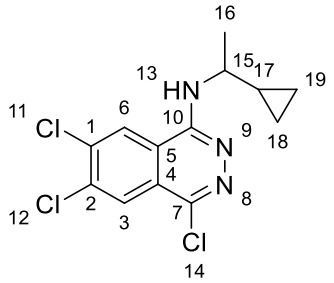

To a 4 mL vial containing 1-cyclopropyl-ethylamine hydrochloride (45.4 mg, 0.373 mmol, 1.0 eq.) was added DMSO (1 mL) and diisopropylethylamine (DIPEA, 0.78 mL, 0.448 mmol, 1.2 eq.). The resulting solution was reacted with **Int 1** (100 mg, 0.373 mmol, 1.0 eq.) according to **general procedure A** to yield 4,6,7-trichloro-*N*-(1-cyclopropylethyl)phthalazin-1-amine (85.3 mg, 72.2%) as an off-white solid. **^{1}H NMR (400 MHz, $CDCl_3$)** δ 8.25 (s, 1H, 6), 7.98 (s, 1H, 3), 5.30 (s, 1H, 13), 3.87 (dp, J = 8.7, 6.5 Hz, 1H, 15), 1.40 (d, J = 6.4 Hz, 3H, 16), 1.07 (qt, J = 8.3, 4.9 Hz, 1H, 17), 0.65 – 0.57 (m, 1H, 18), 0.48-0.56 (m, 1H, 19), 0.49 – 0.40 (m, 1H, 18), 0.40 – 0.31 (m, 1H, 19); **^{13}C NMR (101 MHz, $CDCl_3$)** δ 151.77 (10), 143.85 (7), 137.41 (1), 137.03 (2), 127.36 (6), 125.58 (4), 123.28 (3), 119.07 (5), 52.24 (15), 19.77 (17), 17.63 (16), 3.78 (18), 3.28 (19); **LR-ESI-MS:** $C_{13}H_{12}Cl_3N_3$ [M+H$^+$] *m/z* found: 316.11, calc.: 316.61.

Step 2: 6,7-dichloro-*N*-(1-cyclopropylethyl)-4-(pyridin-4-yl)phthalazin-1-amine **(19)**

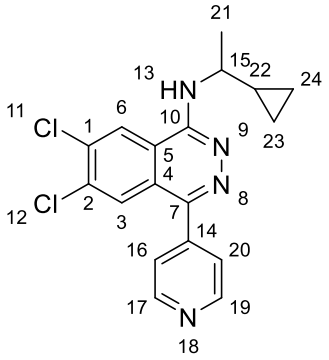

19

4,6,7-trichloro-*N*-(1-cyclopropylethyl)phthalazin-1-amine (50 mg, 0.158 mmol, 1.0 eq.) was reacted with 4-pyridinylboronic acid (23.3 mg, 0.190 mmol, 1.2 eq. according to **general procedure B** to yield **19** (34.1 mg, 60.1%) as an off-white solid. **M.P. =** 107-109 °C; **ν_{max} (cm^{-1})** 3260 (NH), 3075, 2999, 2931 (CH), 1698 (CH ar), 1600 (C=N); **^{1}H NMR (400 MHz, $CDCl_3$)** δ 8.79 (dd, J = 4.4, 1.7, 2H, 17, 19), 8.18 (s, 1H, 6), 7.98 (s, 1H, 3), 7.61 (dd, J = 4.2, 1.5, 2H, 16, 20), 5.75 (s, 1H, 13), 4.03 (br, 1H, 15), 1.46 (d, *J* = 5.8 Hz, 3H, 21), 1.15 (br, 1H, 22), 0.59 (br, 2H, 23), 0.43 (br, 2H, 24); **^{13}C NMR (101 MHz, $CDCl_3$)** δ 151.50 (10), 150.22 (17, 19), 148.53 (7), 144.04 (14), 137.15 (1), 136.37 (2), 127.29 (6), 125.14 (4), 124.39 (3), 123.86 (5), 117.63 (16, 20), 67.23 (15), 20.13 (22), 17.80 (21), 4.01 (23), 3.54 (24); **LR-ESI-MS:** $C_{18}H_{16}Cl_2N_4$ [M+H$^+$] *m/z* found: 359.36, calc.: 359.25; **HR-ESI-MS:** $C_{18}H_{16}Cl_2N_4$ [M+H$^+$] *m/z* found: 358.9827, calc.: 359.08304.

***N*-(bicyclo[1.1.1]pentan-1-yl)-6,7-dichloro-4-(pyridin-4-yl)phthalazin-1-amine (20)**

Step 1: *N*-(bicyclo[1.1.1]pentan-1-yl)-4,6,7-trichlorophthalazin-1-amine

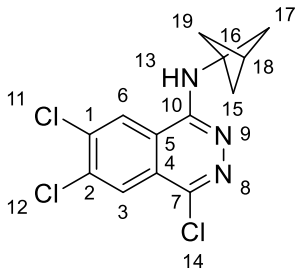

To a 4 mL vial containing 1-Bicyclo[1.1.1]pentylamine hydrochloride (44.6 mg, 0.373 mmol, 1.0 eq.) was added DMSO (1 mL) and diisopropylethylamine (DIPEA, 0.76 mL, 0.448 mmol, 1.2 eq.). The resulting solution was reacted with **Int 1** (100 mg, 0.373 mmol, 1.0 eq.) according to **general procedure A** to yield *N*-(bicyclo[1.1.1]pentan-1-yl)-4,6,7-trichlorophthalazin-1-amine (43.2 mg, 36.8%) as a yellow solid. **^{1}H NMR (400 MHz, $CDCl_3$)** δ 8.26 (s, 1H, 6), 7.85 (s, 1H, 3), 5.56 (s, 1H, 13), 2.58 (s, 1H, 18), 2.29 (s, 6H, 15, 16, 17); **^{13}C NMR (101 MHz, $CDCl_3$)** δ 152.32 (10), 144.78 (7), 138.10 (1), 137.74 (2), 127.55 (6), 125.67 (3), 124.09 (4), 119.23 (5), 52.77 (16), 50.47 (18), 25.52 (15, 17, 19); **LR-ESI-MS:** $C_{13}H_{10}Cl_2N_3$ [M+H$^+$] *m/z* found: 314.23, calc.: 314.59

Step 2: *N*-(bicyclo[1.1.1]pentan-1-yl)-6,7-dichloro-4-(pyridin-4-yl)phthalazin-1-amine (**20**)

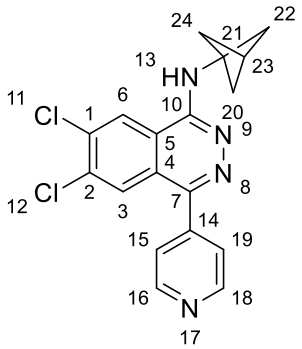

20

N-(bicyclo[1.1.1]pentan-1-yl)-4,6,7-trichlorophthalazin-1-amine (50 mg, 0.159 mmol, 1.0 eq.) was reacted with 4-pyridinylboronic acid (23.4 mg, 0.191 mmol, 1.2 eq.) according to **general procedure B** to yield **20** (38.6 mg, 68%) as a white solid. **M.P =** 253-255 °C; **ν_{max} (cm^{-1})** 3219

(NH), 2966, 2908, 2870 (CH), 1690, 1600 (C=N); **^{1}H NMR (400 MHz, $CDCl_3$)** δ 8.80 (dd, *J* = 5.1, 1.4 Hz, 2H, 16, 18), 8.00 (s, 1H, 6), 7.95 (s, 1H, 3), 7.61 (dd, *J* = 6.0, 1.3 Hz, 2H, 15, 19), 5.76 (s, 1H, 13), 2.61 (s, 1H, 23), 2.35 (s, 6H, 20, 21, 22); **^{13}C NMR (101 MHz, $CDCl_3$)** δ 152.36 (10), 150.35 (16, 18), 149.39 (7), 144.03 (14), 136.94 (1), 136.39 (2), 127.36 (6), 124.99 (4), 124.39 (3), 123.17 (5), 117.23 (15, 19), 52.83 (21), 50.69 (23), 25.47 (20, 22, 24); **LR-ESI-MS:** $C_{18}H_{14}Cl_2N_4$ [M+H$^+$] *m/z* found: 357.17, calc.: 357.24; **HR-ESI-MS:** $C_{18}H_{14}Cl_2N_4$ [M+H$^+$] *m/z* found: 356.9676, calc.: 357.0674

***N*-((1*S*,4*R*)-bicyclo[2.2.1]heptan-2-yl)-6,7-dichloro-4-(pyridin-4-yl)phthalazin-1-amine (21)**

Step 1: *N*-((1*S*,4*R*)-bicyclo[2.2.1]heptan-2-yl)-4,6,7-trichlorophthalazin-1-amine

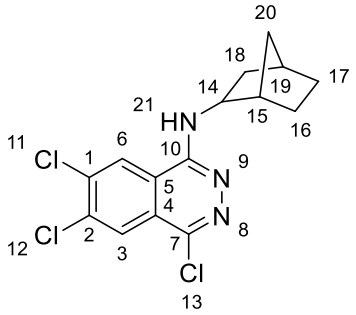

To a 4 mL vial containing 2-aminonorbornane hydrochloride (55.1 mg, 0.373 mmol, 1.0 eq.) was added DMSO (1 mL) and diisopropylethylamine (DIPEA, 0.78 mL, 0.448 mmol, 1.2 eq.). This was reacted with **Int 1** (100 mg, 0.373 mmol, 1.0 eq.) according to **general procedure A** to yield *N*-((1*S*,4*R*)-bicyclo[2.2.1]heptan-2-yl)-4,6,7-trichlorophthalazin-1-amine (93.6 mg, 73.2%) as a white solid. **^{1}H NMR (400 MHz, $CDCl_3$)** δ 8.24 (s, 1H, 6), 8.01 (s, 1H, 3), 5.43 (s, 1H, 21), 4.47 (q, *J* = 5.2 Hz, 1H, 14), 2.78 (p, *J* = 1.9 Hz, 1H, 15), 2.36 – 2.24 (m, 2H), 1.67-1.58 (m, 2H), 1.56-1.51 (m, 1H), 1.51 – 1.44 (m, 1H), 1.42 – 1.37 (m, 1H), 1.37-1.29 (m, 1H), 1.03 – 0.90 (m, 1H); **^{13}C NMR (101 MHz, $CDCl_3$)** δ 152.52 (10), 144.16 (7), 137.59 (1), 137.25 (2), 127.52 (6), 125.59 (4), 123.44 (3), 119.22 (5), 53.88 (14), 39.89 (15), 38.43 (19), 38.36 (20), 36.92 (18), 30.20 (16), 21.83 (17); **LR-ESI-MS:** $C_{15}H_{14}Cl_3N_3$ [M+H$^+$] *m/z* found: 342.31, calc.: 342.65.

Step 2: *N*-((1*S*,4*R*)-bicyclo[2.2.1]heptan-2-yl)-6,7-dichloro-4-(pyridin-4-yl)phthalazin-1-amine **(21)**

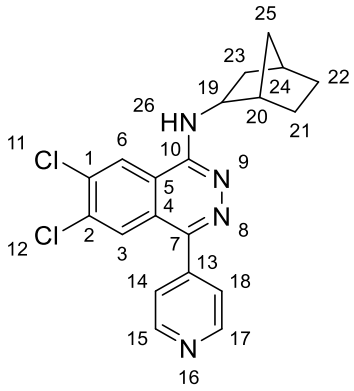

21

N-((1*S*,4*R*)-bicyclo[2.2.1]heptan-2-yl)-4,6,7-trichlorophthalazin-1-amine (50 mg, 0.146 mmol, 1.0 eq.) was reacted with 4-pyridinylboronic acid (21.5 mg, 0.175 mmol, 1.0 eq.) according to **general procedure B** to yield **21** (39.5 mg, 70.3%) as a white solid. **M.P. =** 267-271 °C; **ν_{max} (cm^{-1})** 3192 (NH), 2982, 2923, 2866 (CH), 1685, 1637 (C=N); **^{1}H NMR (400 MHz, $CDCl_3$)** δ 8.80 (d, *J* = 5.0 Hz, 2H, 15, 17), 8.03 (s, 1H, 6), 8.01 (s, 1H, 3), 7.65 – 7.59 (d, *J* = 5.5 Hz, 2H, 14, 18), 5.44 (s, 1H, 26), 4.61 (q, *J* = 5.5 Hz, 1H, 19), 2.85 (t, *J* = 3.7 Hz, 1H), 2.37-2.31 (m, 2H), 1.71-1.61 (m, 2H), 1.61 – 1.56 (m, 2H), 1.56 – 1.48 (m, 1H), 1.44 – 1.34 (m, 2H), 1.00 (dt, *J* = 12.5, 3.7 Hz, 1H); **^{13}C NMR (101 MHz, $CDCl_3$)** δ 152.19 (10), 150.27 (15, 17), 148.72 (7), 144.13 (13), 136.94 (1), 136.26 (2), 127.37 (6), 124.95 (4), 124.37 (3), 123.24 (5), 117.44 (14, 18), 53.87 (19), 40.04 (20), 38.66 (24), 38.40 (25), 36.97 (23), 30.27 (21), 21.87 (22); **LR-ESI-MS:** $C_{20}H_{18}Cl_2N_4$ [M+H$^+$] *m/z* found: 385.22, calc.: 385.29; **HR-ESI-MS:** $C_{20}H_{18}Cl_2N_4$ [M+H$^+$] *m/z* found: 384.9909, calc.: 385.0987.

6,7-dichloro-*N*-(oxetan-3-yl)-4-(pyridin-4-yl)phthalazin-1-amine (22)

Step 1: 4,6,7-trichloro-*N*-(oxetan-3-yl)phthalazin-1-amine

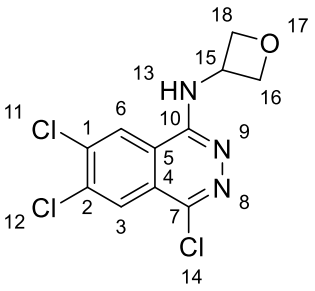

Oxetan-3-amine (27.3 mg, 0.373 mmol) was reacted with **Int 1** (100 mg, 0.373 mmol) according to **general procedure A** to yield 4,6,7-trichloro-N-(oxetan-3-yl)phthalazin-1-amine (75mg, 0.246 mmol, 66.0 % yield) as a yellow solid. **^{1}H NMR (400 MHz, $CDCl_3$)** δ 8.28 (s, 1H, 6), 7.65 (s, 1H, 3), 5.44 (s, 1H, 13), 4.44 – 4.04 (m, 4H, 16, 18), 3.70 (dd, *J* = 12.4, 2.1 Hz, 1H, 15); **^{13}C NMR (101 MHz, $CDCl_3$)** δ 151.56 (10), 137.78 (1), 137.36 (2), 132.88 (7), 127.31 (6), 126.84 (4), 125.54 (3), 123.19 (5), 64.23 (18), 63.13 (16), 51.95 (15); **LR-ESI-MS:** $C_{11}H_8Cl_3N_3O$ [M+H$^+$] *m/z* found: 304.19, calc.: 304.56

Step 2: 6,7-dichloro-*N*-(oxetan-3-yl)-4-(pyridin-4-yl)phthalazin-1-amine **(22)**

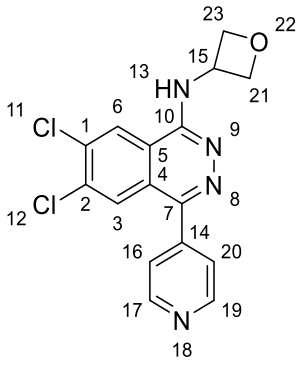

22

4,6,7-trichloro-*N*-(oxetan-3-yl)phthalazin-1-amine (50 mg, 0.164 mmol) and 4-pyridinylboronic acid (20.18 mg, 0.164 mmol) were reacted according to **general procedure B** to yield **22** (44.5 mg, 0.128 mmol, 78 % yield) as a yellow solid. **M.P. =** 251-253 °C; **ν_{max} (cm^{-1})** 3312 (NH), 3024, 2918, 2861 (CH), 1727 (C=N), 1181 (C-O); **^{1}H NMR (400 MHz, $CDCl_3$)** δ 8.76

(dd, *J* = 4.4, 1.1 Hz, 2H, 17, 19), 8.39 (s, 1H, 6), 7.49 (s, 1H, 3), 7.41 (dd, *J* = 4.5, 1.6 Hz, 2H, 16, 20), 4.49 – 4.38 (m, 1H, 15), 4.35 (s, 1H, 21) 4.32 (d, *J* = 4.1 Hz, 1H, 23), 4.11 (dd, *J* = 11.8, 3.1 Hz, 1H, 21), 3.75 (dd, *J* = 11.8, 3.3 Hz, 1H, 23); **^{13}C NMR (101 MHz, $CDCl_3$)** δ 152.11 (10), 150.62 (17, 19), 148.52 (7), 142.16 (14), 137.34 (1), 136.38 (2), 127.95 (6), 127.30 (4), 126.13 (3), 123.91 (5), 123.60 (16, 20), 64.44 (21), 64.30 (23), 52.93 (15); **LR-ESI-MS** $C_{16}H_{12}Cl_2N_4O$ [M+H$^+$] *m/z* found: 347.31, calc.: 347.20; **HR-ESI-MS** $C_{16}H_{12}Cl_2N_4O$ [M+H$^+$] *m/z* found: 346.9067, calc.: 347.0467.

6,7-dichloro-*N*-cyclohexyl-4-(pyridin-4-yl)phthalazin-1-amine (23)

Step 1: 4,6,7-trichloro-*N*-cyclohexylphthalazin-1-amine

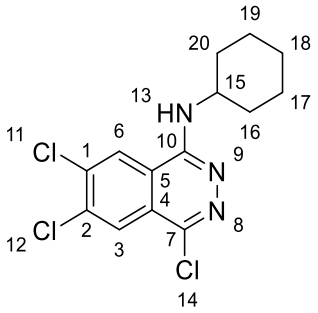

Cyclohexanamine (37.0 mg, 0.373 mmol) was reacted with **Int 1** (100 mg, 0.373 mmol) according to **general procedure A** to yield 4,6,7-trichloro-N-cyclohexylphthalazin-1-amine (101 mg, 0.306 mmol, 82 % yield) as a yellow solid. **^{1}H NMR (400 MHz, $CDCl_3$)** δ 8.16 (s, 1H, 6), 7.83 (s, 1H, 3), 4.97 (d, *J* = 7.5 Hz, 1H, 13), 4.24-4.15 (m, 1H, 15), 2.13 (dd, *J* = 12.0, 3.8 Hz, 2H), 1.71 (dt, *J* = 13.9, 3.8 Hz, 2H), 1.47 – 1.30 (m, 2H), 1.26-1.11 (m, 4H); **^{13}C NMR (101 MHz, $CDCl_3$)** δ 151.80 (10), 143.82 (7), 137.38 (1), 137.00 (2), 127.43 (6), 125.71 (4), 123.25 (3), 119.18 (5), 50.51 (15) 33.09 (16, 20), 25.89 (17, 19), 25.11 (18); **LR-ESI-MS** $C_{14}H_{14}Cl_3N_3$ [M+H$^+$] *m/z* found: 330.27, calc.: 330.64.

Step 2: 6,7-dichloro-*N*-cyclohexyl-4-(pyridin-4-yl)phthalazin-1-amine (**23**)

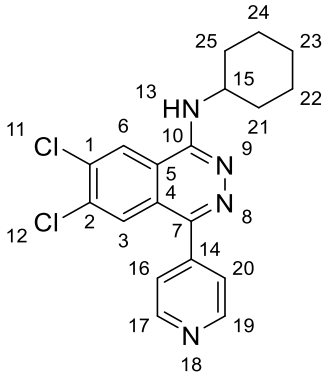

23

4,6,7-trichloro-*N*-cyclohexylphthalazin-1-amine (50 mg, 0.151 mmol) was reacted with 4-pyridinylboronic acid (18.59 mg, 0.151 mmol) according to **general procedure B** to yield **23** (44.0 mg, 0.118 mmol, 78 % yield) as an off-white solid. **M.P. =** 247-251 °C; **ν_{max} (cm^{-1})** 3230 (NH), 3010, 2981, 2924 (CH), 1599 (C=N); **^{1}H NMR (400 MHz, $CDCl_3$)** δ 8.80 (dd, *J* = 4.3, 1.6 Hz, 2H, 17, 19), 8.02 (s, 1H, 6), 7.92 (s, 1H, 3), 7.62 (dd, *J* = 4.4, 1.6 Hz, 2H, 16, 20), 5.00 (d, *J* = 7.5 Hz, 1H, 13), 4.48 – 4.35 (m, 1H, 15), 2.34 – 2.22 (m, 2H), 1.89 – 1.78 (m, 2H), 1.52 – 1.45 (m, 2H), 1.40 – 1.27 (m, 4H); **^{13}C NMR (101 MHz, $CDCl_3$)** δ 151.36 (10), 150.36 (17, 19), 149.02 (7), 143.61 (14), 136.87 (1), 136.12 (2), 126.57 (6), 124.85 (4), 124.35 (3), 123.08 (5), 118.03 (16, 20), 50.21 (15), 32.72 (21, 25), 26.12 (22, 24), 25.05 (23); **LR-ESI-MS** $C_{19}H_{18}Cl_2N_4$ [M+H$^+$] *m/z* found: 373.11, calc.: 373.28; **HR-ESI-MS** $C_{19}H_{18}Cl_2N_4$ [M+H$^+$] *m/z* found: 372.9479, calc.: 373.0987.

6,7-dichloro-4-(pyridin-4-yl)-*N*-(tetrahydro-2H-pyran-4-yl)phthalazin-1-amine (24)

Step 1: 4,6,7-trichloro-*N*-(tetrahydro-2H-pyran-4-yl)phthalazin-1-amine

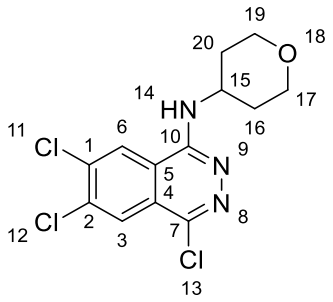

Tetrahydro-2H-pyran-4-amine (37.8 mg, 0.373 mmol) was reacted with **Int 1** (100 mg, 0.373 mmol) according to **general procedure A** to yield 4,6,7-trichloro-N-(tetrahydro-2H-pyran-4-yl)phthalazin-1-amine (98 mg, 0.295 mmol, 79 % yield) as a white solid. **^{1}H NMR (400 MHz, $CDCl_3$)** δ 8.28 (s, 1H, 6), 7.88 (s, 1H, 3), 4.90 (d, *J* = 7.2 Hz, 1H, 14), 4.55-4.46 (m, 1H, 15), 4.16 – 3.94 (m, 2H), 3.59 (td, *J* = 11.8, 2.1 Hz, 2H), 2.22 (ddd, *J* = 12.3, 4.3, 2.1 Hz, 2H), 1.69 – 1.58 (m, 2H); **^{13}C NMR (101 MHz, $CDCl_3$)** δ 151.70 (10), 144.52 (7), 137.70 (1), 137.34 (2), 127.58 (6), 125.73 (4), 123.19 (3), 119.11 (5), 67.06 (17, 19), 48.10 (15), 33.18 (16, 20); **LR-ESI-MS** $C_{13}H_{12}Cl_3N_3O$ [M+H$^+$] *m/z* found: 332.34, calc.: 332.61.

Step 2: 6,7-dichloro-4-(pyridin-4-yl)-*N*-(tetrahydro-2H-pyran-4-yl)phthalazin-1-amine (**24**)

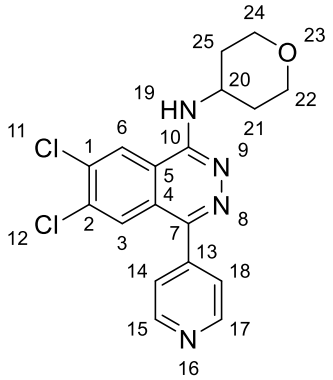

24

4,6,7-trichloro-*N*-(tetrahydro-2H-pyran-4-yl)phthalazin-1-amine (50 mg, 0.150 mmol) was reacted with 4-pyridinylboronic acid (18.48 mg, 0.150 mmol) according to **general procedure B** to yield 6,7-dichloro-4-(pyridin-4-yl)-*N*-(tetrahydro-2H-pyran-4-yl)phthalazin-1-amine,

compound **20** (35 mg, 0.093 mmol, 62.0 % yield) as a brown gum. **ν_{max} (cm^{-1})** 3251 (NH), 2926, 2853 (CH), 1600 (C=N), 1086 (C-O); **^{1}H NMR (400 MHz, $CDCl_3$)** δ 8.80 (dd, *J* = 4.4, 1.3 Hz, 2H, 15, 17), 8.02 (s, 1H, 6), 7.99 (s, 1H, 3), 7.61 (dd, *J* = 4.5, 1.4 Hz, 2H, 14, 18), 5.14 (d, *J* = 7.2 Hz, 1H, 19), 4.70 – 4.57 (m, 1H, 20), 4.12 – 4.01 (m, 2H), 3.61 (td, *J* = 11.8, 2.0 Hz, 2H), 2.32 – 2.21 (m, 2H), 1.71 (dd, *J* = 11.7, 4.5 Hz, 2H); **^{13}C NMR (101 MHz, $CDCl_3$)** δ 151.39 (10), 150.36 (15, 17), 149.12 (7), 143.98 (13), 137.08 (1), 136.40 (2), 127.42 (6), 125.09 (4), 124.33 (3), 123.12 (5), 117.36 (14, 18), 67.12 (22, 24), 48.16 (20), 33.32 (21, 25); **LR-ESI-MS** $C_{18}H_{16}Cl_2N_4O$ [M+H^+] *m/z* found: 375.17, calc.: 375.25; **HR-ESI-MS** $C_{18}H_{16}Cl_2N_4O$ [M+H^+] *m/z* found: 374.9268, calc.: 375.0780.

6,7-dichloro-*N*-(piperidin-3-yl)-4-(pyridin-4-yl)phthalazin-1-amine (25)

Step 1: tert-butyl 3-((4,6,7-trichlorophthalazin-1-yl)amino)piperidine-1-carboxylate

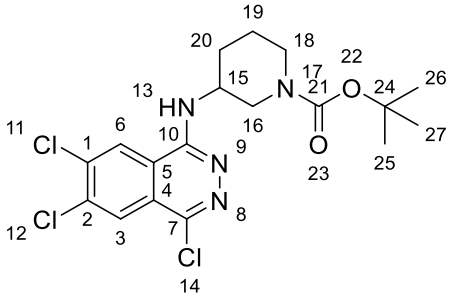

tert-Butyl 3-aminopiperidine-1-carboxylate (0.073 ml, 0.373 mmol) was reacted with **Int 1** (100 mg, 0.373 mmol) according to **general procedure A** to yield *tert*-butyl 3-((4,6,7-trichlorophthalazin-1-yl)amino)piperidine-1-carboxylate (118 mg, 0.272 mmol, 73 % yield) as a white solid. **^{1}H NMR (400 MHz, $CDCl_3$)** δ 8.23 (s, 1H, 6), 7.93 (s, 1H, 3), 6.33 (br, 1H, 13), 4.40 (br, 1H, 15), 4.26 – 2.99 (m, 6H, 16, 18, 20), 2.56 – 1.93 (m, 2H, 19), 1.50 (s, 9H, 25, 26, 27); **^{13}C NMR (101 MHz, $CDCl_3$)** δ 158.28 (21), 152.01 (10), 144.19 (7), 137.61 (1), 137.36 (2), 127.43 (6), 125.65 (4), 123.50 (3), 119.32 (5), 80.53 (24), 48.86 (16), 45.17 (15), 44.32 (18),

42.26 (20), 28.61 (25, 26, 27), 22.17 (19); **LR-ESI-MS** $C_{18}H_{21}Cl_3N_4O_2$ [M+H$^+$] *m/z* found: 431.49, calc.: 431.74

Step 2: 6,7-dichloro-*N*-(piperidin-3-yl)-4-(pyridin-4-yl)phthalazin-1-amine (**25**)

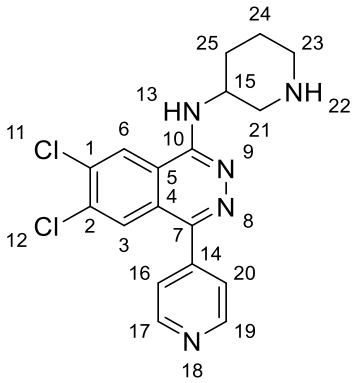

25

tert-Butyl 3-((4,6,7-trichlorophthalazin-1-yl)amino)piperidine-1-carboxylate (50 mg, 0.116mmol) was reacted with 4-pyridinyl boronic acid (14.24 mg, 0.116 mmol) according to **general procedure B** to yield tert-butyl 3-((6,7-dichloro-4-(pyridin-4-yl)phthalazin-1-yl)amino)piperidine-1-carboxylate (**LR-ESI-MS** $C_{23}H_{25}Cl_2N_5O_2$ [M+H$^+$] *m/z* found: 474.11, calc.: 474.39)**.** This was dissolved in dioxane (3 mL) before HCl (4.0 M in dioxane, 1 mL) was added and the solution left stirring overnight. The residual solvent was removed *in vacuo* and the product was re-dissolved in methanol (2 mL) before being applied to an Isolute SCX column that had been equilibrated with methanol. The column was washed with methanol (5 x 10mL) and the product then eluted with ammonia (7.0 M in MeOH, 10 mL), to yield **25** (22.11 mg, 0.059 mmol, 51 % yield) as a brown oil. **ν_{max} (cm^{-1})** 3365, 3197 (NH), 3071, 2956, 2834 (CH), 1602 (C=N); **^{1}H NMR (400 MHz, $CDCl_3$)** δ 8.86 (s, 1H, 6), 8.80 (dd, *J* = 4.4, 1.6 Hz, 2H, 17, 19), 7.97 (s, 1H, 3), 7.60 (dd, *J* = 4.3, 1.9 Hz, 2H, 16, 20), 5.77 (s, 1H, 13), 5.10 (s, 1H, 22), 3.56 – 3.48 (m, 1H, 15), 3.43 (d, *J* = 12.4 Hz, 1H), 3.25 (dd, *J* = 13.3, 3.6 Hz, 1H), 2.99 – 2.86 (m, 1H), 2.40 – 2.27 (m, 1H), 2.24 – 2.12 (m, 2H), 1.88 – 1.72 (m, 2H); **^{13}C NMR (101 MHz, $CDCl_3$)** δ

152.03 (10), 150.15 (17, 19), 149.05 (7), 144.26 (14), 137.06 (1), 136.32 (2), 126.85 (6), 125.37 (4), 125.24 (3), 124.38 (5), 118.16 (16, 20), 47.78 (15), 44.04 (21), 43.62 (23), 26.52 (25), 18.48 (24); **LR-ESI-MS** $C_{18}H_{17}Cl_2N_5$ [M+H$^+$] *m/z* found: 374.01, calc.: 374.27; **HR-ESI-MS** $C_{18}H_{17}Cl_2N_5$ [M+H$^+$] *m/z* found: 373.9892, calc.: 374.0939

6,7-dichloro-*N*-(4,4-difluorocyclohexyl)-4-(pyridin-4-yl)phthalazin-1-amine (26)

Step 1: 4,6,7-trichloro-*N*-(4,4-difluorocyclohexyl)phthalazin-1-amine

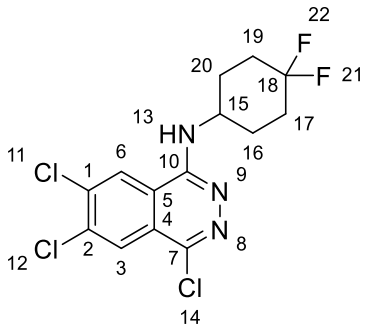

To a 4 mL vial containing 4,4-difluorocyclohexylamine hydrochloride (64.1 mg, 0.373 mmol, 1.0 eq.) was added DMSO (1 mL) and diisopropylethylamine (DIPEA, 0.78 mL, 0.448 mmol, 1.2 eq.). This was reacted with **Int 1** (100 mg, 0.373 mmol, 1.0 eq.) according to **general procedure A** to yield 4,6,7-trichloro-*N*-(4,4-difluorocyclohexyl)phthalazin-1-amine (105.0 mg, 76.7%) as an off-white solid. **^{1}H NMR (400 MHz, $CDCl_3$)** δ 8.27 (s, 1H, 6), 7.89 (s, 1H, 3), 4.97 (d, *J* = 7.2 Hz, 1H, 13), 4.50 – 4.32 (m, 1H, 15), 2.37 – 2.25 (m, 2H, 17, 19), 2.18 (m, 2H, 17, 19), 1.96 (dtt, *J* = 31.3, 13.5, 4.3 Hz, 2H, 16, 20), 1.68 (qd, *J* = 12.8, 3.8 Hz, 2H, 16, 20); **^{13}C NMR (101 MHz, $CDCl_3$)** δ 151.72 (10), 144.72 (7), 137.81 (1), 137.46 (2), 127.68 (6), 125.72 (4), 123.01 (3), 119.05 (5), 48.58 (15), 32.97 – 32.06 (t, *J* = 24.9 Hz, 18), 28.69 (17, 19), 28.60 (16, 20); **LR-ESI-MS** $C_{14}H_{12}Cl_3F_2N_3$ [M+H$^+$] *m/z* found: 366.11, calc.: 366.62;

Step 2: 6,7-dichloro-*N*-(4,4-difluorocyclohexyl)-4-(pyridin-4-yl)phthalazin-1-amine (**26**)

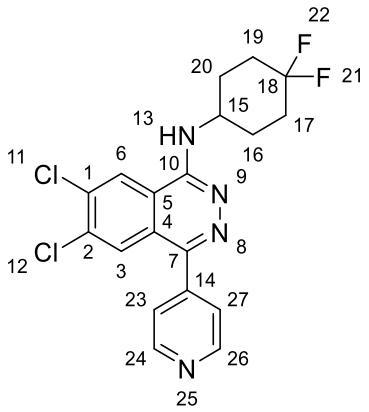

26

4,6,7-trichloro-*N*-(4,4-difluorocyclohexyl)phthalazin-1-amine (50 mg, 0.136 mmol, 1.0 eq.) was reacted with 4-pyridinylboronic acid (20.1 mg, 0.164 mmol, 1.2 eq.) according to **general procedure B** to yield **26** (43.0 mg, 77%) as a white solid. **M.P. =** 241-243 °C; **ν_{max} (cm^{-1})** 3192 (NH), 2952, 2866 (CH), 1597 (C=N), 1214 (C-F); **^{1}H NMR (400 MHz, $CDCl_3$)** δ 8.81 (dd, *J* = 4.4, 1.6 Hz, 2H, 24, 26), 8.03 (s, 1H, 6), 7.95 (s, 1H, 3), 7.62 (dd, *J* = 4.4, 1.6 Hz, 2H, 23, 27), 5.04 (d, *J* = 7.2 Hz, 1H, 13), 4.60 – 4.48 (m, 1H, 15), 2.41-2.31 (m, 2H), 2.27-2.15 (m, 2H), 2.11 – 1.90 (m, 2H), 1.81 – 1.66 (m, 2H); **^{13}C NMR (101 MHz, $CDCl_3$)** δ 151.46 (10), 150.44 (24, 26), 149.32 (7), 143.91 (14), 137.19 (1), 136.53 (2), 127.52 (6), 125.10 (4), 124.32 (3), 123.00 (5), 117.36 (23, 27), 48.67 (15), 32.44 (t, *J* = 24.7 Hz), 28.84 (17, 19), 28.74 (16, 20); **LR-ESI-MS** $C_{19}H_{16}Cl_2F_2N_4$ [M+H$^+$] *m/z* found: 409.09, calc.: 409.26; **HR-ESI-MS** $C_{19}H_{16}Cl_2F_2N_4$ [M+H$^+$] *m/z* found 411.9730 (M+2H$^+$), calc.: 411.0769.

***N*-(adamantan-2-yl)-6,7-dichloro-4-(pyridin-4-yl)phthalazin-1-amine (27)**

Step 1: *N*-(adamantan-2-yl)-4,6,7-trichlorophthalazin-1-amine

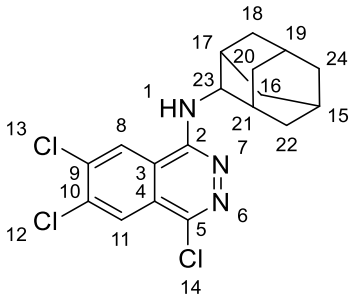

To a 4 mL vial containing 2-adamantylamine hydrochloride (70.1 mg, 0.373 mmol, 1.0 eq.) was added DMSO (1 mL) and diisopropylethylamine (DIPEA, 0.78 mL, 0.448 mmol, 1.2 eq.). This was reacted with **Int 1** (100 mg, 0.373 mmol, 1.0 eq.) according to **general procedure A** to yield *N*-(adamantan-2-yl)-4,6,7-trichlorophthalazin-1-amine (122.3 mg, 85.6%) as a white solid. **^{1}H NMR (400 MHz, $CDCl_3$)** δ 8.25 (s, 1H, 8), 7.86 (s, 1H, 11), 5.31 (d, *J* = 6.9 Hz, 1H, 1), 4.55-4.51 (m, 1H, 23), 2.27 – 2.19 (br, 2H), 2.01-1.86 (m, 8H), 1.80 (s, 2H), 1.74 (d, *J* = 12.7 Hz, 2H); **^{13}C NMR (101 MHz, $CDCl_3$)** δ 151.70 (2), 143.90 (5), 137.43 (9), 137.09 (10), 127.61 (8), 125.73 (3), 122.85 (11), 119.28 (4), 55.35 (23), 37.67, 37.20, 32.30, 31.48, 27.47, 27.40; **LR-ESI-MS** $C_{18}H_{18}Cl_3N_3$ [M+H$^+$] *m/z* found: 382.42, calc.: 382.71;

Step 2: *N*-(adamantan-2-yl)-6,7-dichloro-4-(pyridin-4-yl)phthalazin-1-amine (**27**)

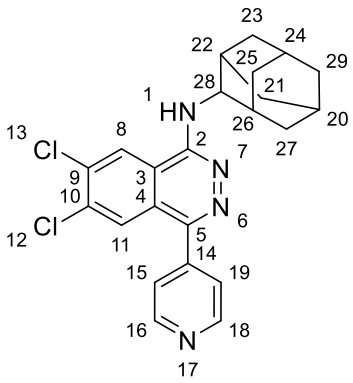

27

N-(adamantan-2-yl)-4,6,7-trichlorophthalazin-1-amine (50.0 mg, 0.131 mmol, 1.0 eq.) was reacted with 4-pyridinylboronic acid (32.1 mg, 0.157 mmol, 1.2 eq.) according to **general procedure B** to yield **27** (36.8 mg, 66.2%) as an off white solid. **M.P.** = 210-213 °C; **ν_{max} (cm^{-1})** 3399 (NH), 3021, 2904, 2848 (CH), 1602 (C=N); **^{1}H NMR (400 MHz, $CDCl_3$)** δ 8.79 (dd, *J* = 4.5, 1.4 Hz, 2H, 16, 18), 8.02 (s, 1H, 8), 7.95 (s, 1H, 11), 7.61 (dd, *J* = 4.4, 1.6 Hz, 2H, 15, 19), 5.47 (d, *J* = 6.9 Hz, 1H, 1), 4.69-4.61 (m, 1H, 28), 2.29 (s, 2H), 2.07 – 1.88 (m, 8H), 1.83 (s, 2H), 1.77 (d, *J* = 12.9 Hz, 2H); **^{13}C NMR (101 MHz, $CDCl_3$)** δ 151.44 (2), 150.36 (16, 18), 148.57 (5), 144.15 (14), 136.83 (9), 136.15 (10), 127.42 (8), 125.10 (3), 124.32 (15, 19), 122.86 (11), 117.51 (4), 55.41 (28), 37.69, 37.26, 32.35, 31.63, 27.51, 27.42; **LR-ESI-MS** $C_{23}H_{22}Cl_2N_4$ [M+H^+] *m/z* found: 425.19, calc.: 425.36; **HR-ESI-MS** $C_{23}H_{22}Cl_2N_4$ [M+H^+] *m/z* found: 425.0112, calc.: 425.1299.

6,7-dichloro-*N*-(2,3-dihydro-1H-inden-2-yl)-4-(pyridin-4-yl)phthalazin-1-amine (28)

Step 1: 4,6,7-trichloro-*N*-(2,3-dihydro-1H-inden-2-yl)phthalazin-1-amine

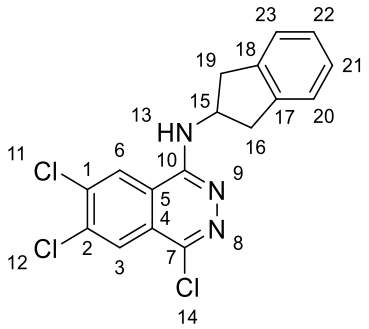

2,3-Dihydro-1H-inden-2-amine (49.7 mg, 0.373 mmol, 1.0 eq.) was reacted with **Int 1** (100 mg, 0.373 mmol, 1.0 eq) according to **general procedure A** to yield 4,6,7-trichloro-*N*-(2,3-dihydro-1H-inden-2-yl)phthalazin-1-amine (87 mg, 64 %) as a yellow solid. **^{1}H NMR (400 MHz, $CDCl_3$)** δ 8.26 (s, 1H, 6), 7.83 (s, 1H, 3), 7.30-7.17 (m, 4H, 20, 21, 22, 23), 5.28 (d, *J* = 7.0 Hz, 1H, 13), 5.16 (dt, *J* = 7.0, 4.0 Hz, 1H, 15), 3.54 (dd, *J* = 16.4, 6.9 Hz, 2H, 16), 3.03 (dd, *J* = 16.4, 3.9 Hz, 2H, 19); **^{13}C NMR (101 MHz, $CDCl_3$)** δ 151.79 (10), 144.35 (7), 140.88 (17, 18), 137.29 (1),

136.92 (2), 127.21 (6), 126.68 (3), 125.33 (4), 124.84 (21, 22), 122.96 (20, 23), 118.85 (5), 52.78 (15), 40.08 (16, 19); **LR-ESI-MS** $C_{17}H_{12}Cl_3N_3$ [M+H$^+$] *m/z* found: 364.07, calc.: 364.65;

Step 2: 6,7-dichloro-*N*-(2,3-dihydro-1H-inden-2-yl)-4-(pyridin-4-yl)phthalazin-1-amine (**28**)

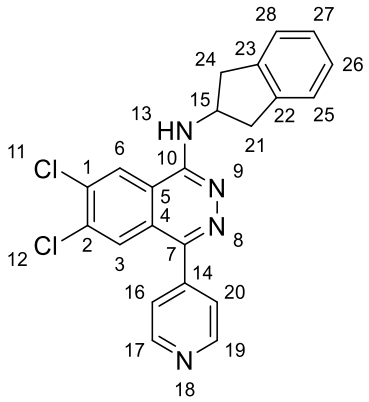

28

4,6,7-trichloro-*N*-(2,3-dihydro-1H-inden-2-yl)phthalazin-1-amine (50 mg, 0.137 mmol, 1.0 eq.) was reacted with 4-pyridinylboronic acid (16.85 mg, 0.137 mmol, 1.0 eq.) according to **general procedure B** to yield **28** (28 mg, 50.1 %) as a brown solid. **M.P. =** 269-271 °C; **ν_{max} (cm^{-1})** 3215 (NH), 3068, 2925, 2868 (CH), 1602 (C=N); **^{1}H NMR (400 MHz, $CDCl_3$)** δ 8.81 (dd, *J* = 4.4, 1.6 Hz, 2H, 17, 19), 8.01 (s, 1H, 6), 7.90 (s, 1H, 3), 7.63 (dd, *J* = 4.4, 1.6 Hz, 2H, 16, 20), 7.30 (dd, *J* = 5.4, 3.4 Hz, 2H, 26, 27), 7.25 – 7.20 (m, 2H, 25, 28), 5.38 (d, *J* = 7.0 Hz, 1H, 13), 5.34 – 5.23 (m, 1H, 15), 3.61 (dd, *J* = 16.4, 6.8 Hz, 2H, 21), 3.09 (dd, *J* = 16.3, 3.9 Hz, 2H, 24); **^{13}C NMR (101 MHz, $CDCl_3$)** δ 151.80 (10), 150.39 (17, 19), 149.20 (7), 144.02 (14), 141.25 (22, 23), 137.00 (1), 136.31 (2), 127.38 (4), 127.04 (6), 125.20 (16, 20), 125.02 (3), 124.37 (26, 27), 123.21 (25, 28), 117.46 (5), 53.16 (15), 40.56 (21, 24); **LR-ESI-MS** $C_{22}H_{16}Cl_2N_4$ [M+H$^+$] *m/z* found: 407.13, calc.: 407.30; **HR-ESI-MS** $C_{22}H_{16}Cl_2N_4$ [M+H$^+$] *m/z* found: 406.9692, calc.: 407.0830.

6,7-dichloro-4-(pyridin-4-yl)-*N*-(1,2,3,4-tetrahydronaphthalen-1-yl)phthalazin-1-amine (29)

Step 1: 4,6,7-trichloro-*N*-(1,2,3,4-tetrahydronaphthalen-1-yl)phthalazin-1-amine

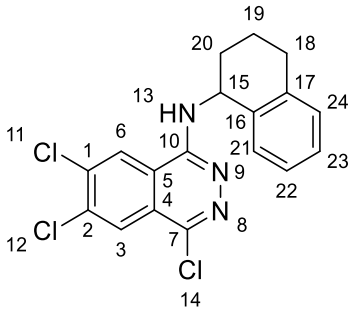

1,2,3,4-tetrahydronaphthalen-1-amine (0.054 ml, 0.373 mmol, 1.0 eq.) was reacted with **Int 1** (100 mg, 0.373 mmol, 1.0 eq.) according to **general procedure A** to yield 4,6,7-trichloro-*N*-(1,2,3,4-tetrahydronaphthalen-1-yl)phthalazin-1-amine (88.0 mg, 62 %) as a white solid. **^{1}H NMR (400 MHz, $CDCl_3$)** δ 8.25 (s, 1H, 6), 7.89 (s, 1H, 6), 7.39 – 7.31 (m, 1H, 22), 7.24 – 7.10 (m, 3H, 21, 23, 24), 5.73-5.66 (m, 1H, 15), 5.41 (d, *J* = 7.6 Hz, 1H, 13), 2.95 – 2.75 (m, 2H, 18), 2.22-2.08 (m, 2H, 20), 1.97 – 1.82 (m, 2H, 19).; **^{13}C NMR (101 MHz, $CDCl_3$)** δ 151.76 (10), 144.34 (7), 140.00 (16), 138.26 (17), 137.57 (4), 137.24 (1), 136.88 (2), 129.48 (6), 129.44 (3), 127.73 (22), 127.46 (23), 126.49 (21), 123.31 (24), 119.14 (5), 49.55 (15), 29.53 (18), 28.97 (20), 19.86 (19); **LR-ESI-MS** $C_{18}H_{14}Cl_3N_3$ [M+H$^+$] *m/z* found: 378.68, calc.: 378.68;

Step 2: 6,7-dichloro-4-(pyridin-4-yl)-*N*-(1,2,3,4-tetrahydronaphthalen-1-yl)phthalazin-1-amine (**29**)

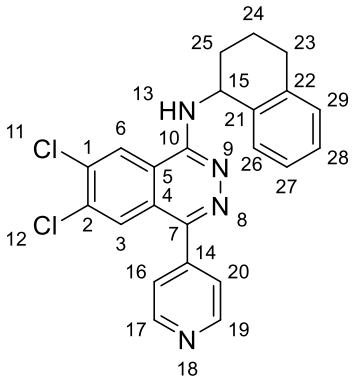

29

4,6,7-trichloro-*N*-(1,2,3,4-tetrahydronaphthalen-1-yl)phthalazin-1-amine (50 mg, 0.132 mmol, 1.0 eq.) was reacted with 4-pyridinylboronic acid (16.23 mg, 0.132 mmol, 1.0 eq) according to **general procedure B** to yield **29** (37.3 mg, 67 %) as an off-white solid. **M.P. =** 274-278 °C ; **ν_{max} (cm^{-1})** 3333 (NH), 3024, 2973, 2862 (CH), 1602 (C=N); **^{1}H NMR (400 MHz, $CDCl_3$)** δ 8.82 (dd, *J* = 4.4, 1.5 Hz, 2H, 17, 19), 8.04 (s, 1H, 6), 7.88 (s, 1H, 3), 7.65 (dd, *J* = 4.5, 1.7 Hz, 2H, 16, 20), 7.41 (d, *J* = 7.6 Hz, 1H, 27), 7.27-7.18 (m, 3H, 26, 28, 29), 5.91-5.83 (m, 1H, 15), 5.37 (d, *J* = 7.5 Hz, 1H, 13), 2.99 – 2.80 (m, 2H, 23), 2.31 – 2.14 (m, 2H, 25), 2.00 – 1.88 (m, 2H, 24); **^{13}C NMR (101 MHz, $CDCl_3$)** δ 151.35 (10), 150.41 (17, 19), 149.12 (7), 144.09 (21), 138.36 (22), 137.01 (4), 136.99 (1), 136.36 (2), 129.62 (6), 129.50 (3), 127.85 (27), 127.40 (28), 126.62 (26), 125.15 (29), 123.07 (16, 20), 117.35 (5), 49.58 (15), 29.58 (23), 29.15 (25), 19.88 (24); **LR-ESI-MS** $C_{23}H_{18}Cl_2N_4$ [M+H^+] *m/z* found: 421.48, calc.: 421.33; **HR-ESI-MS** $C_{23}H_{18}Cl_2N_4$ [M+H^+] *m/z* found: 420.9811, calc.: 421.0987

6,7-dichloro-4-(pyridin-4-yl)-*N*-(2-(pyrrolidin-1-yl)ethyl)phthalazin-1-amine (30)

Step 1: 4,6,7-trichloro-*N*-(2-(pyrrolidin-1-yl)ethyl)phthalazin-1-amine

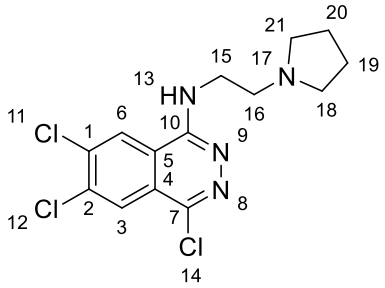

2-(Pyrrolidin-1-yl)ethan-1-amine (0.047 ml, 0.373 mmol, 1.0 eq.) was reacted with **Int 1** (100 mg, 0.373 mmol, 1.0 eq.) according to **general procedure A.** The product was eluted from the column using DCM:(7.0 M NH_3 in MeOH) (90:10) to yield 4,6,7-trichloro-N-(2-(pyrrolidin-1-yl)ethyl)phthalazin-1-amine (93 mg, 0.134 mmol, 72 %) as a yellow solid. **^{1}H NMR (400 MHz, $CDCl_3$)** δ 8.79 (s, 1H, 6), 8.18 (s, 1H, 3), 8.00 (s, 1H, 13), 4.11 (s, 2H, 15), 3.54 – 3.44 (m, 2H, 16), 3.43-3.27 (m, 4H, 18, 21), 2.23 – 2.13 (m, 4H, 19, 20); **^{13}C NMR (101 MHz, $CDCl_3$)** δ 154.93

(10), 144.95 (7), 137.96 (1), 137.87 (2), 126.78 (6), 125.81 (3), 125.56 (4), 119.75 (5), 55.50 (15), 54.64 (18, 21), 38.34 (16), 23.49 (19, 20); **LR-ESI-MS** $C_{14}H_{15}Cl_3N_4$ [M+H$^+$] *m/z* found: 345.29, calc.: 345.65

Step 2: 6,7-dichloro-4-(pyridin-4-yl)-*N*-(2-(pyrrolidin-1-yl)ethyl)phthalazin-1-amine (**30**)

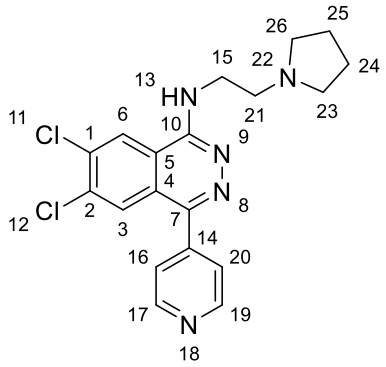

30

4,6,7-trichloro-*N*-(2-(pyrrolidin-1-yl)ethyl)phthalazin-1-amine (50 mg, 0.145 mmol, 1.0 eq.) was reacted with 4-pyridinylboronic acid (17.78 mg, 0.145 mmol, 1.0 eq.) according to **general procedure B.** The product was eluted from the column using DCM:(7.0 M NH_3 in MeOH) (90:10) to yield **30** (34.8 mg, 62 %) as a brown gum. **ν_{max} (cm^{-1})** 3112 (NH), 2996, 2851 (CH), 1588 (C=N); **^{1}H NMR (400 MHz, $CDCl_3$)** δ 8.79 (dd, *J* = 4.4, 1.6 Hz, 2H, 17, 19), 8.45 (s, 1H, 6), 7.95 (s, 1H, 3), 7.60 (dd, *J* = 4.3, 1.6 Hz, 2H, 16, 20), 4.96 (br, 1H, 13) 4.16 – 3.98 (m, 2H, 15), 3.39 – 3.28 (m, 2H, 21), 3.19-3.02 (m, 4H, 23, 26), 2.05-1.98 (m, 4H, 24, 25); **^{13}C NMR (101 MHz, $CDCl_3$)** δ 152.71 (10), 150.32 (17, 19), 148.90 (7), 144.25 (14), 136.93 (1), 136.31 (2), 126.80 (6), 125.14 (3), 125.07 (4), 124.32 (16, 20), 118.14 (5), 54.65 (15), 54.02 (23, 26), 38.83 (21), 23.46 (24, 25); **LR-ESI-MS** $C_{19}H_{19}Cl_2N_5$ [M+H$^+$] *m/z* found: 388.17, calc.: 388.300; **HR-ESI-MS** $C_{19}H_{19}Cl_2N_5$ [M+H$^+$] *m/z* found: 388.0000, calc.: 388.10958

6,7-dichloro-*N*-((1-ethylpyrrolidin-2-yl)methyl)-4-(pyridin-4-yl)phthalazin-1-amine (31)

Step 1: 4,6,7-trichloro-*N*-((1-ethylpyrrolidin-2-yl)methyl)phthalazin-1-amine

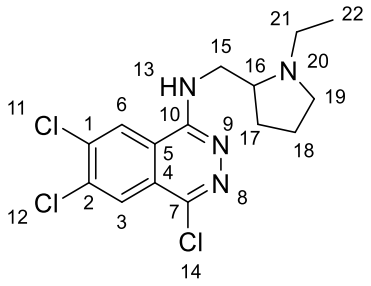

1,4,6,7-tetrachlorophthalazine (100 mg, 0.373 mmol, 1.0 eq.) was reacted with (1-ethylpyrrolidin-2-yl)methanamine (0.054 ml, 0.373 mmol, 1.0 eq.) according to **general procedure A.** The product was eluted from the column using DCM:(7.0M NH_3 in MeOH) (90:10) to yield 4,6,7-trichloro-N-((1-ethylpyrrolidin-2-yl)methyl)phthalazin-1-amine (98 mg, 73 %) as a white solid. **^{1}H NMR (400 MHz, $CDCl_3$)** δ 8.23 (s, 1H, 6), 8.11 (s, 1H, 3), 6.83 (s, 1H, 13), 3.90 (dd, *J* = 13.6, 3.7 Hz, 1H, 15), 3.68 (dd, *J* = 13.8, 3.8 Hz, 1H, 15), 3.43 (p, *J* = 4.8 Hz, 1H, 16), 2.98-2.89 (m, 2H, 21), 2.51-2.41 (m, 2H, 19), 1.83 – 1.72 (m, 4H, 17, 18), 1.19 (t, *J* = 7.2 Hz, 3H, 22); **^{13}C NMR (101 MHz, $CDCl_3$)** δ 153.15 (10), 144.15 (7), 137.63 (1), 137.36 (2), 127.29 (6), 125.59 (4), 124.01 (3), 119.50 (5), 74.95 (16), 63.42 (15), 49.08 (21), 42.21 (19), 28.44 (17), 23.24 (18), 13.32 (22); **LR-ESI-MS** $C_{15}H_{17}Cl_3N_4$ [M+H$^+$] *m/z* found: 359.39, calc.: 359.68

Step 2: 6,7-dichloro-*N*-((1-ethylpyrrolidin-2-yl)methyl)-4-(pyridin-4-yl)phthalazin-1-amine (**31**)

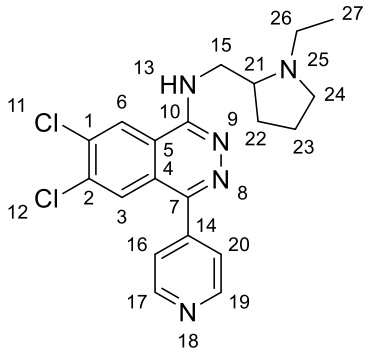

31

4,6,7-trichloro-*N*-((1-ethylpyrrolidin-2-yl)methyl)phthalazin-1-amine (50 mg, 0.139 mmol, 1.0 eq.) was reacted with 4-pyridinylboronic acid (17.09 mg, 0.139 mmol, 1.0 eq.) according to **general procedure B.** The product was eluted from the column using DCM:7.0 M NH_3 in MeOH (90:10) to yield **31** (34.7 mg, 62 %) as a brown gum. **ν_{max} (cm^{-1})** 3290 (NH), 3038, 2968, 2875 (CH), 1600 (C=N); **^{1}H NMR (400 MHz, $CDCl_3$)** δ 8.81 (dd, *J* = 4.4, 1.5 Hz, 2H, 17, 19), 8.68 (s, 1H, 6), 7.96 (s, 1H, 3), 7.63 (dd, *J* = 4.4, 1.7 Hz, 2H, 16, 20), 6.88 (br, 1H, 13), 4.06 (dd, *J* = 14.3, 9.5 Hz, 1H, 15), 3.95 (dd, *J* = 14.3, 9.7 Hz, 1H, 15), 3.89 – 3.75 (m, 1H, 21), 3.30 – 3.14 (m, 1H, 26), 2.96 – 2.82 (m, 2H, 26, 24), 2.38 – 2.23 (m, 1H, 24), 2.03 – 1.86 (m, 4H, 22, 23), 1.23 (t, *J* = 7.2 Hz, 3H, 27); **^{13}C NMR (101 MHz, $CDCl_3$)** δ 152.77 (10), 150.32 (17, 19), 149.45 (7), 144.06 (14), 137.62 (1), 137.22 (2), 126.81 (6), 125.55 (4), 125.10 (3), 124.30 (16, 20), 119.43 (5), 76.13 (21), 64.54 (15), 48.74 (26), 42.56 (24), 28.67 (22), 23.31 (23), 13.37 (27); **LR-ESI-MS** $C_{20}H_{21}Cl_2N_5$ [M+H^+] *m/z* found: 402.13, calc.: 402.32;

6,7-dichloro-*N*-(2-morpholinoethyl)-4-(pyridin-4-yl)phthalazin-1-amine (32)

Step 1: 4,6,7-trichloro-*N*-(2-morpholinoethyl)phthalazin-1-amine

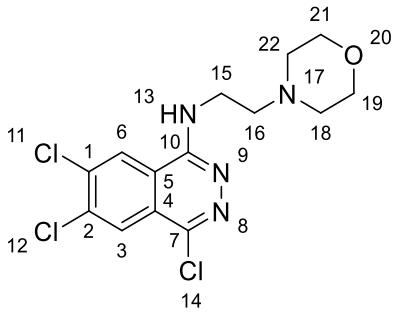

2-Morpholinoethan-1-amine (48.6 mg, 0.373 mmol, 1.0 eq.) was reacted with **Int 1** (100 mg, 0.373 mmol, 1.0 eq.) according to **general procedure A** to yield 4,6,7-trichloro-N-(2-morpholinoethyl)phthalazin-1-amine (88 mg, 65 %) as an off-white solid. **^{1}H NMR (400 MHz, MeOD)** δ 8.48 (s, 1H, 6), 8.24 (s, 1H, 3), 4.56 (s, 1H, 13), 3.78 – 3.68 (m, 6H, 15, 19, 21), 2.65 (t, *J* = 6.5 Hz, 2H, 16), 2.61 – 2.54 (m, 4H, 18, 22); **^{13}C NMR (101 MHz, MeOD)** δ 154.70 (10), 144.19 (7), 138.41 (1), 138.12 (2), 127.84 (6), 126.73 (4), 126.25 (3), 121.02 (5), 67.66 (19, 21), 58.03 (16), 54.76 (18, 22), 39.33 (15).; **LR-ESI-MS** $C_{14}H_{15}Cl_3N_4O$ [M+H$^+$] *m/z* found: 361.30, calc.: 361.65

Step 2: 6,7-dichloro-*N*-(2-morpholinoethyl)-4-(pyridin-4-yl)phthalazin-1-amine (**32**)

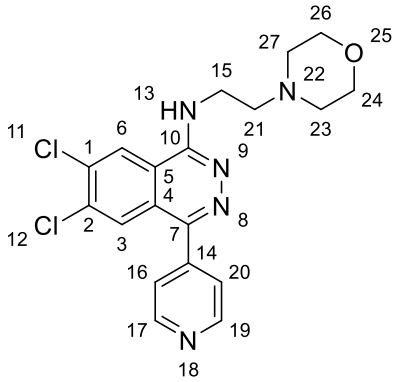

32

4,6,7-trichloro-*N*-(2-morpholinoethyl)phthalazin-1-amine (50 mg, 0.138 mmol, 1.0 eq.) was reacted with 4-pyridinylboronic acid (16.99 mg, 0.138 mmol, 1.0 eq.) according to **general**

procedure B to yield **32** (43.0 mg, 77 %) as a yellow gum. **ν_{max} (cm^{-1})** 3248 (NH), 3060, 2964, 2875 (CH), 1602 (C=N), 1116 (C-O); **^{1}H NMR (400 MHz, $CDCl_3$)** δ 8.77 (dd, *J* = 4.4, 1.6 Hz, 2H, 17, 19), 8.00 (d, *J* = 2.8 Hz, 2H, 6, 3), 7.56 (dd, *J* = 4.5, 1.6 Hz, 2H, 16, 20), 6.21 (br, 1H, 13), 3.89-3.82 (m, 2H, 15), 3.81-3.75 (m, 4H, 24, 26), 2.80 (t, *J* = 5.9 Hz, 2H, 21), 2.65-2.51 (m, 4H, 23, 27); **^{13}C NMR (101 MHz, $CDCl_3$)** δ 152.29 (10), 150.35 (17, 19), 148.98 (7), 144.08 (14), 136.94 (1), 136.27 (2), 127.31 (6), 124.96 (4), 124.33 (3), 123.40 (16, 20), 117.62 (5), 67.11 (24, 26), 56.63 (21), 53.40 (23, 27), 37.87 (15); **LR-ESI-MS** $C_{19}H_{19}Cl_2N_5O$ [M+H^+] *m/z* found: 404.17, calc.: 404.30; **HR-ESI-MS** $C_{19}H_{19}Cl_2N_5O$ [M+H^+] *m/z* found: 403.9914, calc.: 404.1045.

6,7-dichloro-*N*-(3-morpholinobutan-2-yl)-4-(pyridin-4-yl)phthalazin-1-amine (33)

Step 1: 4,6,7-dichloro-*N*-(3-morpholinobutan-2-yl)phthalazin-1-amine

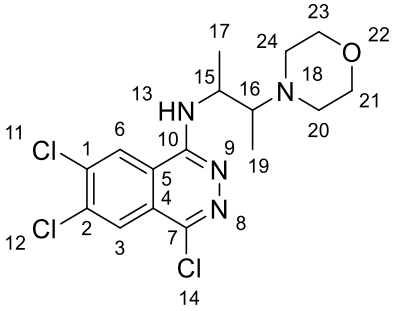

3-Morpholinobutan-2-amine (0.058 ml, 0.373 mmol, 1.0 eq.) was reacted with **Int 1** (100 mg, 0.373 mmol, 1.0 eq.) according to **general procedure A** to yield 4,6,7-trichloro-*N*-(3-morpholinobutan-2-yl)phthalazin-1-amine (95 mg, 65 %) as an off-white solid. **^{1}H NMR (400 MHz, $CDCl_3$)** δ 8.26 (s, 1H, 6), 7.95 (s, 1H, 3), 7.06 (s, 1H, 13), 3.84-3.77 (m, 1H, 15), 3.73-3.68 (m, 2H, 21, 23), 3.61 (br, 2H, 21, 23), 2.72-2.65 (m, 1H, 16), 2.56 (br, 2H, 20, 24), 2.50 (br, 2H, 20, 24), 1.44 (d, *J* = 5.9 Hz, 3H, 19), 1.14 (d, *J* = 6.6 Hz, 3H, 17). **^{13}C NMR (101 MHz, $CDCl_3$)** δ 152.88 (10), 144.44 (7), 137.45 (1), 137.29 (2), 127.58 (6), 125.76 (4), 123.30 (3), 120.15 (5), 67.83 (21, 23), 64.09 (20, 24), 55.31 (16) 49.65 (15), 18.27 (19), 9.37 (17); **LR-ESI-MS** $C_{16}H_{19}Cl_3N_4O$ [M+H^+] *m/z* found: 389.46, calc.: 389.71.

Step 2: 6,7-dichloro-*N*-(3-morpholinobutan-2-yl)-4-(pyridin-4-yl)phthalazin-1-amine (**33**)

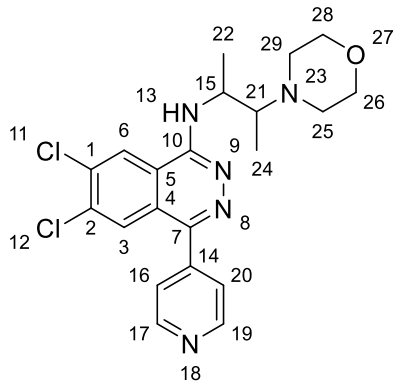

33

4,6,7-dichloro-*N*-(3-morpholinobutan-2-yl)phthalazin-1-amine (50 mg, 0.128 mmol, 1.0 eq.) was reacted with 4-pyridinylboronic acid (15.77 mg, 0.128 mmol, 1.0 eq.) according to **general procedure B** to yield **33** (36.1 mg, 65%) as a brown gum. **ν_{max} (cm^{-1})** 3217 (NH), 2964, 2875 (CH), 1613 (C=N), 1141 (C-O); **^{1}H NMR (400 MHz, $CDCl_3$)** δ 8.81 (dd, *J* = 4.2, 1.7 Hz, 2H, 17, 19), 8.06 (s, 1H, 6), 8.02 (s, 1H, 3), 7.63 (dd, *J* = 4.4, 1.9 Hz, 2H, 16, 20), 4.02 – 3.88 (m, 1H, 21), 3.82 – 3.56 (m, 4H, 26, 28), 2.82 – 2.68 (m, 1H, 15), 2.67 – 2.45 (m, 4H, 25, 29), 1.51 (d, *J* = 5.9 Hz, 3H, 24), 1.17 (d, *J* = 6.6 Hz, 3H, 22); **^{13}C NMR (101 MHz, $CDCl_3$)** δ 152.55 (10), 150.30 (17, 19), 148.92 (7), 136.86 (1), 136.37 (2), 132.30 (14), 127.38 (6), 125.07 (4), 124.35 (3), 123.36 (16, 20), 118.38 (16, 20), 67.80 (26, 28), 64.12 (25, 29), 55.18 (21), 49.72 (15), 18.49 (24), 9.44 (15); **LR-ESI-MS** $C_{21}H_{23}Cl_2N_5O$ [M+H^+] *m/z* found: 432.16, calc.: 432.50; **HR-ESI-MS** $C_{21}H_{23}Cl_2N_5O$ [M+H^+] *m/z* found: 432.0257, calc.: 432.1358.

6,7-dichloro-*N*-((4-methylmorpholin-3-yl)methyl)-4-(pyridin-4-yl)phthalazin-1-amine (34)

Step 1: 4,6,7-trichloro-*N*-((4-methylmorpholin-3-yl)methyl)phthalazin-1-amine

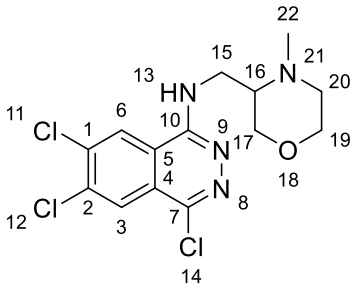

(4-Methylmorpholin-3-yl)methanamine (48.6 mg, 0.373 mmol, 1.0 eq.) was reacted with **Int 1** (100 mg, 0.373 mmol, 1.0 eq.) according to **general procedure B** to yield 4,6,7-trichloro-*N*-((4-methylmorpholin-3-yl)methyl)phthalazin-1-amine (97 mg, 72 %) as a white solid. **^{1}H NMR (400 MHz, $CDCl_3$)** δ 8.22 (s, 1H, 6), 7.97 (s, 1H, 3), 6.20 (s, 1H, 13), 3.90 – 3.80 (m, 2H, 15), 3.77 (br, 1H, 19), 3.71 – 3.61 (m, 2H, 17, 19), 3.52 (br, 1H, 17), 2.92-2.78 (m, 1H, 16), 2.59 – 2.53 (m, 1H, 20), 2.52 – 2.43 (m, 1H, 20), 2.39 (s, 3H, 22); **^{13}C NMR (101 MHz, $CDCl_3$)** δ 152.72 (10), 144.31 (7), 137.53 (1), 137.15 (2), 127.36 (6), 125.48 (4), 123.54 (3), 119.26 (5), 69.26 (19), 66.93 (17), 60.07 (16), 54.95 (20), 42.66 (15), 39.78 (22); **LR-ESI-MS** $C_{14}H_{15}Cl_3N_4O$ [M+H$^+$] *m/z* found: 361.29, calc.: 361.65.

Step 2: 6,7-dichloro-*N*-((4-methylmorpholin-3-yl)methyl)-4-(pyridin-4-yl)phthalazin-1-amine (**34**)

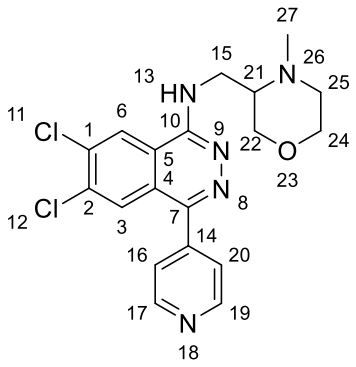

34

4,6,7-trichloro-*N*-((4-methylmorpholin-3-yl)methyl)phthalazin-1-amine (50 mg, 0.138 mmol, 1.0 eq.) was reacted with 4-pyridinylboronic acid (16.99 mg, 0.138 mmol, 1.0 eq.) according to **general procedure B** to yield **34** (36.3 mg, 65% yield) as a brown gum. **ν_{max} (cm^{-1})** 3272 (NH), 3097, 2960, 2852 (CH), 1667 (C=N), 1122 (C-O); **^{1}H NMR (400 MHz, $CDCl_3$)** δ 8.80 (dd, *J* = 4.4, 1.6 Hz, 2H, 17, 19), 8.01 (d, *J* = 6.4 Hz, 2H, 6, 3), 7.60 (dd, *J* = 4.4, 1.5 Hz, 2H, 16, 20), 6.20 (s, 1H, 13), 3.95 – 3.75 (m, 4H, 15 (2), 22, 24), 3.75-3.67 (m, 1H, 24), 3.64-3.59 (m, 1H, 22), 2.87 (m, 1H, 21), 2.67 – 2.58 (m, 1H, 25), 2.55-2.49 (m, 1H, 25), 2.43 (s, 3H, 27); **^{13}C NMR (101 MHz, $CDCl_3$)** δ 152.40 (10), 150.36 (17, 19), 149.14 (7), 144.06 (14), 137.04 (1), 136.33 (2), 127.37 (6), 124.97 (4), 124.35 (3), 123.36 (16, 20), 117.59 (5), 69.21 (24), 66.98 (22), 60.20 (21), 55.05 (25), 42.64 (15), 39.73 (27); **LR-ESI-MS** $C_{19}H_{19}Cl_2N_5O$ [M+H$^+$] *m/z* found: 404.08, calc.: 404.30**;** **HR-ESI-MS** $C_{19}H_{19}Cl_2N_5O$ [M+H$^+$] *m/z* found: 403.9913, calc.: 404.1045**.**

6,7-dichloro-4-(pyridin-4-yl)-*N*-(3-(pyrrolidin-1-yl)propyl)phthalazin-1-amine (35)

Step 1: 4,6,7-trichloro-*N*-(3-(pyrrolidin-1-yl)propyl)phthalazin-1-amine

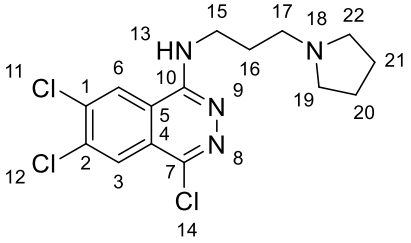

3-(Pyrrolidin-1-yl)propan-1-amine (0.053 ml, 0.373 mmol, 1.0 eq.) was reacted with **Int 1** (100 mg, 0.373 mmol, 1.0 eq.) according to **general procedure A.** The product was eluted from the column using DCM:(7.0 M NH_3 in MeOH) (90:10) to yield 4,6,7-trichloro-N-(3-(pyrrolidin-1-yl)propyl)phthalazin-1-amine (110 mg, 82%) as an off-white solid. **^{1}H NMR (400 MHz, $CDCl_3$)** δ 8.92 (s, 1H, 13), 8.18 (s, 1H, 6), 7.80 (s, 1H, 3), 3.77-3.73 (m, 2H, 15), 2.91 – 2.78 (m, 2H, 19, 22), 2.78 – 2.64 (m, 4H, 17 (2), 19, 22), 2.05 – 1.97 (m, 4H, 20, 21), 1.94 (p, *J* = 5.6 Hz, 2H, 16); **^{13}C NMR (101 MHz, $CDCl_3$)** δ 153.15 (10), 143.12 (7), 137.01 (1), 136.70 (2), 127.16 (6), 125.57

(4), 123.90 (3), 119.82 (5), 56.75 (19, 22), 54.42 (15), 43.72 (17), 25.06 (20, 21), 23.63 (16); **LR-ESI-MS** $C_{15}H_{17}Cl_3N_4$ [M+H$^+$] *m/z* found: 359.30, calc.: 359.68.

Step 2: 6,7-dichloro-4-(pyridin-4-yl)-*N*-(3-(pyrrolidin-1-yl)propyl)phthalazin-1-amine (**35**)

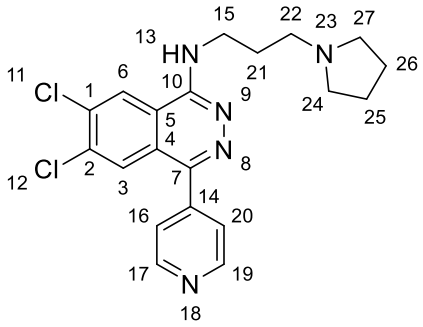

35

4,6,7-trichloro-*N*-(3-(pyrrolidin-1-yl)propyl)phthalazin-1-amine (50 mg, 0.139 mmol, 1.0 eq.) was reacted with 4-pyridinylboronic acid (17.09 mg, 0.139 mmol, 1.0 eq.) according to **general procedure B.** The product was eluted from the column using DCM:(7.0 M NH_3 in MeOH) (90:10) to yield **35** (30.2 mg, 54%) as a brown gum. **ν_{max} (cm^{-1})** 3213 (NH), 3045, 2911, 2801 (CH), 1601 (C=N); **^{1}H NMR (400 MHz, $CDCl_3$)** δ 8.79 (dd, *J* = 4.5, 1.6 Hz 17, 19, 2H), 8.19 (s, 1H, 6), 7.95 (s, 1H, 3), 7.61 (dd, *J* = 4.4, 1.7 Hz, 2H, 16, 20), 3.89 – 3.82 (m, 2H, 15), 3.63-3.51 (m, 2H, 24, 27) 3.13-2.99 (m, 4H, 22 (2), 24, 27), 2.25-2.11 (m, 4H, 25, 26), 1.98-1.91 (m, 2H, 21); **^{13}C NMR (101 MHz, $CDCl_3$)** δ 152.43 (10), 150.43 (17, 19), 149.03 (7), 142.92 (14), 136.45 (1), 136.02 (2), 126.74 (6), 125.02 (4), 124.40 (3), 122.98 (16, 20), 119.03 (5), 57.02 (24, 27), 55.11 (15), 43.24 (22), 25.75 (25, 26), 23.83 (21); **LR-ESI-MS** $C_{20}H_{21}Cl_2N_5$ [M+H$^+$] *m/z* found: 402.13, calc.: 402.32; **HR-ESI-MS** $C_{20}H_{21}Cl_2N_5$ [M+H$^+$] *m/z* found: 402.0245, calc.: 402.1252

***N*^{1}-cyclopentyl-*N*^{1}-(6,7-dichloro-4-(pyridin-4-yl)phthalazin-1-yl)-*N*^{2},*N*^{2}-dimethylethane-1,2-diamine (36)**

Step 1: 4,6,7-trichloro-*N*-cyclopentylphthalazin-1-amine **(37)**

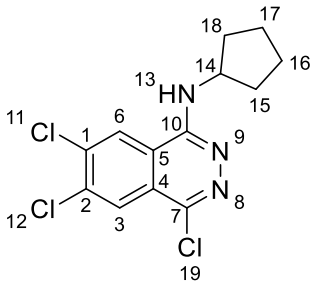

37

Cyclopentylamine (0.037 mL, 0.373 mmol, 1.0 eq.) was reacted with **Int 1** (100 mg, 0.373 mmol, 1.0 eq.) according to **general procedure A** to yield **37** (81.3 mg, 68.8 % yield) as a yellow solid**. ^{1}H NMR (400 MHz, $CDCl_3$)** δ 8.24 (s, 1H, 6), 7.88 (s, 1H, 3), 5.11 (d, *J* = 6.5 Hz, 1H, 13), 4.61 (sext., *J* = 6.7 Hz, 1H, 14), 2.31 – 2.17 (m, 2H, 15, 18), 1.84 – 1.63 (m, 4H, 15, 16, 17, 18), 1.60-1.50 (m, 2H, 16, 17). ; **^{13}C NMR (101 MHz, $CDCl_3$)** δ 152.34 (10), 144.22 (7), 137.51 (1), 137.18 (2), 127.61 (6), 125.71 (4), 123.28 (3), 119.29 (5), 53.88 (14), 33.55 (15, 18), 24.20 (16, 17); **LR-ESI-MS** $C_{13}H_{12}Cl_3N_3$ [M+H$^+$] *m/z* found: 316.17, calc.: 316.61

Step 2: 6,7-dichloro-*N*-cyclopentyl-4-(pyridin-4-yl)phthalazin-1-amine **(A-196)**

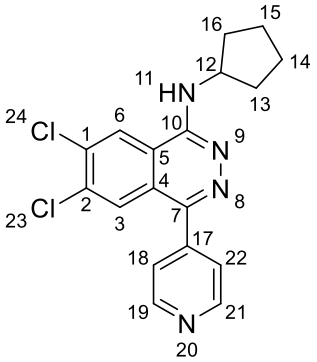

A-196

37 (50 mg, 0.158 mmol, 1.0 eq.) was reacted with 4-pyridinylboronic acid (19.4 mg, 0.158 mmol, 1.0 eq) according to **general procedure B** to yield **A-196** (52.3 mg, 92.2%) as an off-white solid. **^{1}H NMR (400 MHz, $CDCl_3$)** δ 8.78 (dd, *J* = 4.4, 1.6 Hz, 2H, 19, 21), 8.00 (d, *J* = 8.2 Hz, 2H, 6, 3), 7.61 (dd, *J* = 4.3, 1.6 Hz, 2H, 18, 22), 5.41 (d, *J* = 6.5 Hz, 1H, 11), 4.73 (sext., *J* = 6.7 Hz, 1H, 12), 2.32-2.21 (m, 2H, 13, 16), 1.85 – 1.66 (m, 4H, 13, 14, 15, 16), 1.66-1.54 (m, 2H, 14, 15); **^{13}C NMR (101 MHz, $CDCl_3$)** δ 152.03 (10), 150.30 (19, 21), 148.58 (7), 144.17 (17), 136.72 (1), 136.03 (2), 127.22 (6), 124.97 (4), 124.34 (18, 22), 123.39 (3), 117.48 (5), 53.80 (12), 33.49 (13, 16), 24.12 (14, 15); **LR-ESI-MS** $C_{18}H_{16}Cl_2N_4$ [M+H$^+$] *m/z* found: 359.11, calc.: 359.25.

Step 3: *N*^{1}-cyclopentyl-*N*^{1}-(6,7-dichloro-4-(pyridin-4-yl)phthalazin-1-yl)-*N*^{2},*N*^{2}-dimethylethane-1,2-diamine **(36)**

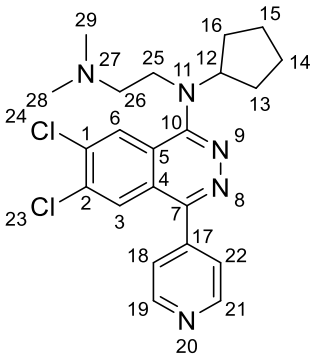

36

To a flame-dried, 50 mL round-bottomed flask that had been evacuated and backfilled with N_2 was added sodium hydride (60 %wt, 6.7 mg, 0.167 mmol, 1.2 eq.). This was suspended in dry THF (2.5 mL) and the mixture cooled to 0 °C and left stirring under nitrogen for 30 minutes. **A-196** (50.0 mg, 0.139 mmol, 1.0 eq.) was dissolved in THF (2.5 mL) and the solution added to the RBF at 0 °C. The resultant mixture was left stirring at 0 °C for 30 minutes. To a 4 mL vial containing 2-chloro-*N,N*-dimethylethylamine hydrochloride (20 mg, 0.139 mmol, 1.0 eq.) was

added THF (2 mL) and DIPEA (0.024 mL, 0.139 mmol, 1.0 eq). The resultant solution was added to the RBF dropwise and the reaction left stirring overnight.

The reaction was quenched with water at 0 °C and extracted with DCM (3 x 10 mL). The combined organic extracts were washed with water and dried over sodium sulfate, before the residual solvent was removed *in vacuo*. The crude material was purified by column chromatography (DCM:(7M NH_3 in MeOH), 95:5) to yield **36** as a yellow solid. **M.P. =** 191-194 °C; **ν_{max} (cm^{-1})** 3392, 3025, 2941, 2865, 2766, 1618, 1544, 1498, 1375, 1263, 1195, 1162, 1096, 982, 891; **^{1}H NMR (400 MHz, $CDCl_3$)** δ 8.76 – 8.68 (dd, *J* = 4.4, 1.6 Hz 2H, 19, 21), 8.14 (s, 1H, 6), 7.60 (s, 1H, 3), 7.52 – 7.43 (dd, *J* = 4.4, 1.7 Hz 2H, 18, 22), 4.40 (sext., *J* = 6.7 Hz, 1H, 12), 4.32 (t, *J* = 7.0 Hz, 2H, 25), 2.93 (t, *J* = 6.8 Hz, 2H, 26), 2.46 (s, 6H, 28, 29), 2.10 – 1.95 (m, 2H, 13, 16), 1.95 – 1.82 (m, 2H, 13, 16), 1.81 – 1.61 (m, 4H, 14, 15); **^{13}C NMR (101 MHz, $CDCl_3$)** δ 150.65 (10), 150.48 (19, 21), 142.80 (7), 137.33 (17), 135.43 (1), 133.66 (2), 130.22 (6), 128.31 (4), 126.81 (3), 123.89 (5), 123.35 (18, 22), 59.15 (28, 29), 56.42 (12), 50.14 (25), 45.30 (26), 36.56, (13, 16), 24.87 (14, 15); **LR-ESI-MS** $C_{18}H_{16}Cl_2N_4$ [M+H^+] *m/z* found: 430.09, calc.: 430.38; **HR-ESI-MS** $C_{18}H_{16}Cl_2N_4$ [M+H^+] *m/z* found: 430.0363, calc.: 430.1565

6,7-dichloro-*N*-cyclopentyl-4-(1-methyl-1*H*-pyrazol-3-yl)phthalazin-1-amine (38)

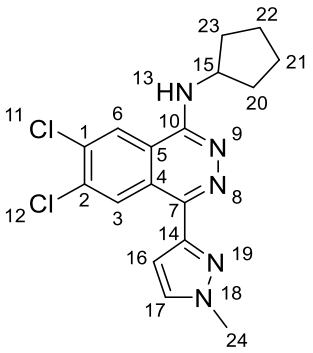

38

37 (50 mg, 0.158 mmol) was reacted with 1-methyl-1*H*-pyrazole-3-boronic acid pinacol ester (32.9 mg, 0.158 mmol) according to **general procedure B** to yield **38** (31 mg, 0.086 mmol, 54.2 % yield) as a white solid. **M.P. =** 238-240 °C; **ν_{max} (cm^{-1})** 3219 (NH), 3068, 2946, 2867 (CH), 1601 (C=N), 1525; **^{1}H NMR (400 MHz, $CDCl_3$)** δ 9.56 (s, 1H, 6), 7.85 (s, 1H, 3), 7.44 (d, *J* = 2.3 Hz, 1H, 17), 7.10 (d, *J* = 2.3 Hz, 1H, 16), 5.02 (d, *J* = 6.4 Hz, 1H, 13), 4.71 (sext., *J* = 6.7 Hz, 1H, 15), 4.04 (s, 3H, 24), 2.36 – 2.21 (m, 2H, 20, 23), 1.85 – 1.74 (m, 2H, 20, 23), 1.74 – 1.67 (m, 2H, 21, 22), 1.67 – 1.54 (m, 2H, 21, 22); **^{13}C NMR (101 MHz, $CDCl_3$)** δ 151.52 (10), 150.40 (7), 143.63 (14), 136.25 (1), 135.37 (2), 130.94 (17), 130.07 (6), 124.97 (4), 122.30 (3), 117.77 (5), 106.74 (16), 53.68 (24), 39.49 (15), 33.63 (20, 23), 24.12 (21,22); **LR-ESI-MS** $C_{17}H_{17}Cl_2N_5$ [M+H$^+$] *m/z* found: 362.47, calc.: 362.26; **HR-ESI-MS** $C_{17}H_{17}Cl_2N_5$ [M+H$^+$] *m/z* found: 361.9925, calc.: 362.0939.

6,7-dichloro-*N*-cyclopentyl-4-(1-(difluoromethyl)-1*H*-pyrazol-4-yl)phthalazin-1-amine (39)

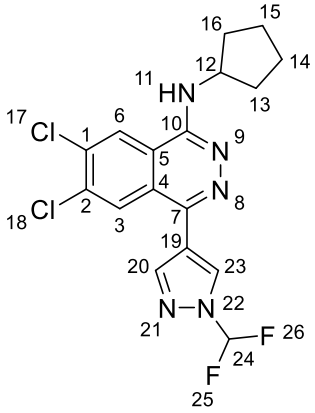

39

37 (50 mg, 0.158 mmol, 1.2 eq.) was reacted with 1-(difluoromethyl)pyrazole-4-boronic acid pinacol ester (46.2 mg, 0.190 mmol, 1.2 eq.) according to **general procedure B** to yield **39** (46.1 mg, 73.3%) as an off-white solid. **M.P. =** 224-226 °C; **ν_{max} (cm^{-1})** 3224 (NH), 2957, 2866 (CH), 1686, 1612 (C=N), 1187 (C-F); **^{1}H NMR (400 MHz, $CDCl_3$)** δ 8.28 (s, 1H, 23), 8.14 (d, *J* = 12.4 Hz, 2H, 6, 3), 7.96 (s, 1H, 20), 7.29 (t, *J* = 60.4 Hz, 1H, 24) 5.18 (s, 1H, 11), 4.69 (sext., *J* =

6.6 Hz, 1H, 12), 2.34 – 2.20 (m, 2H, 13, 16), 1.84-1.77 (m, 2H, 13, 16), 1.74-1.65 (m, 2H, 14, 15), 1.66-1.57 (m, 2H, 14, 15); **^{13}C NMR (101 MHz, $CDCl_3$)** δ 151.55 (10), 142.77 (7), 141.85 (23), 136.87 (1), 136.04 (2), 127.02 (6), 126.28 (20), 125.37 (4), 123.29 (3), 121.28 (19), 117.52 (5), 111.15 (t, *J* = 251 Hz, 24), 33.55 (12), 27.05 (13, 16), 24.13 (14, 15); **LR-ESI-MS** $C_{17}H_{15}Cl_2F_2N_5$ [M+H$^+$] *m/z* found: 398.13, calc.: 398.24; **HR-ESI-MS** $C_{17}H_{15}Cl_2F_2N_5$ [M+H$^+$] *m/z* found: 397.9186, calc.: 398.0673.

6,7-dichloro-*N*-cyclopentyl-4-(1-isopropyl-1*H*-pyrazol-5-yl)phthalazin-1-amine (40)

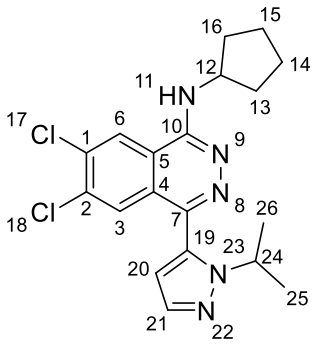

40

37 (50 mg, 0.158 mmol, 1.2 eq.) was reacted with 1-isopropyl-1*H*-pyrazole-5-boronic acid pinacol ester (37.3 mg, 0.158 mmol, 1.0 eq.) according to **general procedure B** to yield **40** (42.1 mg, 68.3%) as an off-white solid. **M.P. =** 245-247 °C; **ν_{max} (cm^{-1})** 3230 (NH), 3041, 2975, 2864 (CH), 1700, 1602 (C=N); **^{1}H NMR (400 MHz, $CDCl_3$)** δ 7.96 (d, *J* = 2.2 Hz, 2H, 6, 3), 7.69 (d, *J* = 1.9 Hz, 1H, 21), 6.43 (d, *J* = 1.9 Hz, 1H, 20), 5.28 (d, *J* = 6.7 Hz, 1H, 11), 4.89 – 4.68 (m, 2H, 12, 24), 2.40 – 2.20 (m, 2H, 13, 16), 1.86 – 1.74 (m, 2H, 13, 16), 1.75 – 1.65 (m, 2H, 14, 15), 1.65 – 1.54 (m, 2H, 14, 15), 1.46 (d, *J* = 6.6 Hz, 6H, 25, 26); **^{13}C NMR (101 MHz, $CDCl_3$)** δ 151.72 (10), 142.74 (7), 138.52 (21), 136.84 (19), 136.16 (1), 135.54 (2), 127.68 (6), 126.59 (4), 122.90 (3), 117.25 (5), 108.42 (20), 50.91 (24), 33.54 (12), 27.04 (13, 16), 24.05 (14, 15), 23.11 (25,

26); **LR-ESI-MS** $C_{19}H_{21}Cl_2N_5$ [M+H$^+$] *m/z* found: 390.07, calc.: 390.31; **HR-ESI-MS** $C_{19}H_{21}Cl_2N_5$ [M+H$^+$] *m/z* found: 390.0159, calc.: 390.1252.

(1-(6,7-dichloro-4-(cyclopentylamino)phthalazin-1-yl)piperidin-4-yl)methanol (41)

Step 1: 4-(((*tert*-butyldimethylsilyl)oxy)methyl)piperidine

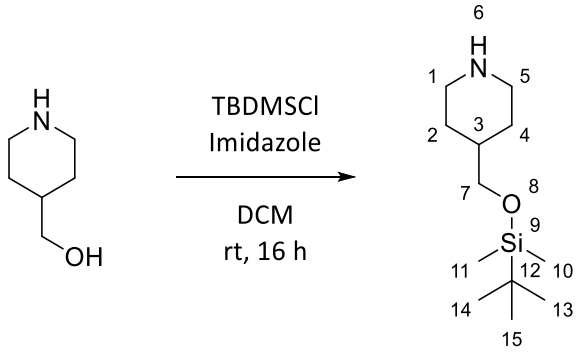

To a solution of 4-piperidinemethanol (330 mg, 2.865 mmol, 1.0 eq.) in DCM (10 mL) in a 50 mL RBF was added imidazole (780.2 mg, 11.461 mmol, 4.0 eq.) and the solution stirred at room temperature for 30 minutes. *tert*-Butyldimethylsilyl chloride (1.0 mL, 5.730 mmol, 2.0 eq.) was added and the reaction left stirring at room temperature for 16 hours.

The reaction mixture was diluted with water (10 mL) and extracted with DCM (3 x 10 mL). The combined organic extracts were washed with brine, dried over sodium sulfate and the residual solvent removed *in vacuo.* The crude product was purified using column chromatography (DCM:(7.0 M NH_3 in MeOH), 95:5) to yield 4-(((*tert*-butyldimethylsilyl)oxy)methyl)piperidine (405.1 mg, 61.6%) as a yellow solid. **^{1}H NMR (400 MHz, $CDCl_3$)** δ 3.54 – 3.43 (m, 4H, 7 (2), 1, 5), 2.85 (td, *J* = 12.7, 3.0 Hz, 2H, 1, 5), 1.93 (d, *J* = 13.6 Hz, 2H, 2, 4), 1.78 – 1.53 (m, 3H, 2, 3, 4), 0.87 (s, 9H, 13, 14, 15), 0.06 (s, 6H, 10, 11); **^{13}C NMR (101 MHz, $CDCl_3$)** δ 66.87 (7), 43.97 (1, 5), 37.07 (3), 26.01 (2, 4), 25.72 (12), 18.41 (13, 14, 15), -5.31 (10, 11); **LR-ESI-MS** $C_{12}H_{27}NOSi$ [M+H$^+$] *m/z* found: 229.24, calc.: 229.44

Step 2: (1-(6,7-dichloro-4-(cyclopentylamino)phthalazin-1-yl)piperidin-4-yl)methanol (**41**)

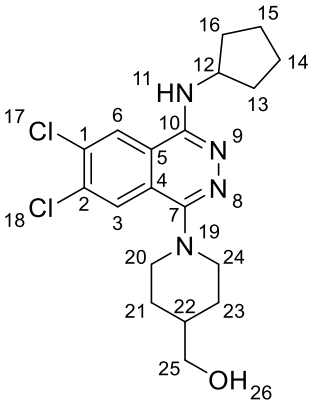

41

4-(((*tert*-butyldimethylsilyl)oxy)methyl)piperidine (87.0 mg, 0.379 mmol, 1.2 eq.) was reacted with **37** according to **general procedure A** to yield **41** as a brown oil. **ν_{max} (cm^{-1})** 3686 (br, OH), 3260 (NH), 2930, 2867 (CH), 1711 (C=N), 1103 (C-O); **^{1}H NMR (400 MHz, $CDCl_3$)** δ 8.05 (s, 1H, 6), 7.85 (s, 1H, 3), 4.84 (d, *J* = 6.2 Hz, 1H, 11), 4.54 (sext., *J* = 6.4 Hz, 1H, 12), 3.61 (d, *J* = 6.2 Hz, 2H, 25), 3.58 – 3.46 (m, 2H, 20, 24), 2.98 (td, *J* = 12.4, 2.4 Hz, 2H, 20, 24), 2.29 – 2.13 (m, 2H, 21, 23), 1.82 – 1.69 (m, 4H, 21, 23, 13, 16), 1.69 – 1.62 (m, 3H, 13, 16, 22), 1.59-1.48 (m, 4H, 14, 15); **^{13}C NMR (101 MHz, $CDCl_3$)** δ 154.84 (7), 150.47 (10), 135.56 (1), 135.31 (2), 126.92 (3), 123.44 (6), 123.03 (4), 120.11 (5), 67.88 (25), 51.88 (20, 24), 41.06 (22), 38.88 (21, 23), 33.60 (12), 29.15 (13, 16), 24.11 (14, 14); **LR-ESI-MS** $C_{19}H_{24}Cl_2N_4O$ [M+H$^+$] *m/z* found: 395.15, calc.: 395.33; **HR-ESI-MS** $C_{19}H_{24}Cl_2N_4O$ [M+H$^+$] *m/z* found: 395.0299, calc.: 395.1406.

4-(6,7-dichloro-4-(cyclopentylamino)phthalazin-1-yl)thiomorpholine 1,1-dioxide (42)

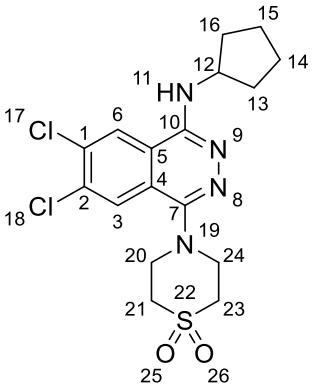

42

37 (50.0 mg, 0.158 mmol, 1.0 eq.) was reacted with thiomorpholine 1,1-dioxide (25.6 mg, 0.190 mmol, 1.2 eq.) according to **general procedure A** to yield **42** (23.1 mg, 35.2%) as a yellow gum. **ν_{max} (cm^{-1})** 3292 (NH), 3054, 2977, 2843 (CH), 1610 (C=N), 1343 (S=O); **^{1}H NMR (400 MHz, $CDCl_3$)** δ 8.02 (s, 1H, 6), 7.86 (s, 1H, 3), 4.86 (d, *J* = 6.5 Hz, 1H, 11), 4.59 (h, *J* = 6.6 Hz, 1H, 12), 3.95 – 3.82 (m, 4H, 21, 23), 3.38 – 3.19 (m, 4H, 20, 24), 2.31 – 2.20 (m, 2H, 13, 16), 1.86 – 1.75 (m, 2H, 13, 16), 1.75 – 1.64 (m, 2H, 14, 15), 1.61 – 1.50 (m, 2H, 14, 15); **^{13}C NMR (101 MHz, $CDCl_3$)** δ 152.45 (7), 151.02 (10), 136.57 (1), 136.29 (2), 126.19 (3), 123.68 (6), 122.29 (4), 120.02 (5), 51.16 (21, 23), 49.71 (20, 24), 33.66 (12), 27.06 (13, 16), 24.08 (14, 15); **LR-ESI-MS** $C_{17}H_{20}Cl_2N_4O_2S$ [M+H$^+$] *m/z* found: 415.09, calc.: 415.33; **HR-ESI-MS** $C_{17}H_{20}Cl_2N_4O_2S$ [M+H$^+$] *m/z* found: 414.9602, calc.: 414.0763.

4-(6,7-dichloro-4-(cyclopentylamino)phthalazin-1-yl)benzonitrile (43)

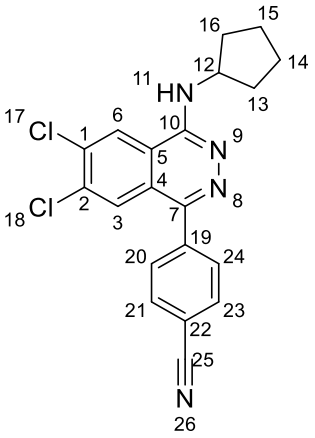

43

37 (50.0 mg, 0.158 mmol, 1.0 eq.) was reacted with 4-cyanophenylboronic acid (27.8 mg, 0.190 mmol, 1.2 eq.) according to **general procedure B** to yield **43** as an off-white solid (48.5 mg, 80.1%). **M.P.** = 253-257 °C; **ν_{max} (cm^{-1})** 3071 (NH), 2958 (CH), 2231 (C≡N), 1601 (C=N); **^{1}H NMR (400 MHz, $CDCl_3$)** δ 7.95 (d, *J* = 4.8 Hz, 2H, 6, 3), 7.87 – 7.77 (m, 4H, 20, 21, 23, 24), 5.21 (d, *J* = 6.5 Hz, 1H, 11), 4.73 (sext., *J* = 6.7 Hz, 1H, 12), 2.34-2.26 (m, 2H, 13, 16), 1.87 – 1.76 (m, 2H, 13, 16), 1.76 – 1.67 (m, 2H, 14, 15), 1.66-1.57 (m, 2H, 14, 15); **^{13}C NMR (101 MHz, $CDCl_3$)** δ 151.83 (10), 149.30 (7), 140.99 (22), 136.78 (1), 136.13 (2), 132.59 (21, 23), 130.50 (20, 24), 127.37 (6), 125.10 (5), 123.22 (3), 118.72 (19), 117.50 (4), 112.77 (25), 33.58 (12), 29.85 (13, 16), 24.14 (14, 15); **LR-ESI-MS** $C_{20}H_{16}Cl_2N_4$ [M+H$^+$] *m/z* found: 383.21, calc.: 383.28; **HR-ESI-MS** $C_{20}H_{16}Cl_2N_4$ [M+H$^+$] *m/z* found: 382.93200, calc.: 383.0752.

6,7-dichloro-*N*-cyclopentyl-4-(4-(trifluoromethyl)phenyl)phthalazin-1-amine (44)

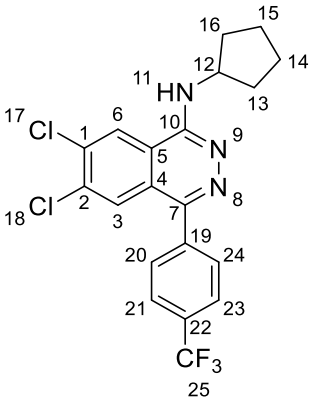

44

37 (50.0 mg, 0.158 mmol, 1.0 eq.) was reacted with 4-(trifluoromethyl)phenylboronic acid (36.0 mg, 0.190 mmol, 1.2 eq.) according to **general procedure B** to yield **44** (30.9 mg, 45.9%) as an off-white solid. **M.P. =** 199-201 °C; **ν_{max} (cm^{-1})** 3316 (NH), 2954, 2867 (CH), 1604 (C=N), 1216 (C-F); **^{1}H NMR (400 MHz, $CDCl_3$)** δ 8.09 (s, 1H, 6), 7.93 (s, 1H, 3), 7.76 (s, 4H, 20, 21, 23, 24), 5.60 (s, 1H, 11), 4.71 (sext., *J* = 6.5 Hz, 1H, 12), 2.35 – 2.15 (m, 2H, 13, 16), 1.84 – 1.72 (m, 2H, 13, 16), 1.70 – 1.54 (m, 4H, 14, 15); **^{13}C NMR (101 MHz, $CDCl_3$)** δ 151.92 (10), 149.65 (7), 139.91 (19), 136.52 (1), 135.84 (2), 130.12 (20, 24), 127.50 (6), 125.69 (t, *J* = 3.7 Hz, 25), 125.44 (21, 23) 125.31 (4), 124.59 (3), 122.81 (22), 117.70 (5), 33.36 (12), 27.00 (13, 16), 24.11 (14, 15); **LR-ESI-MS** $C_{20}H_{16}Cl_2F_3N_3$ [M+H$^+$] *m/z* found: 426.08, calc.: 426.26; **HR-ESI-MS** $C_{20}H_{16}Cl_2F_3N_3$ [M+H$^+$] *m/z* found: 426.0752, calc.: 425.9560.

4-(6,7-dichloro-4-(cyclopentylamino)phthalazin-1-yl)phenol (45)

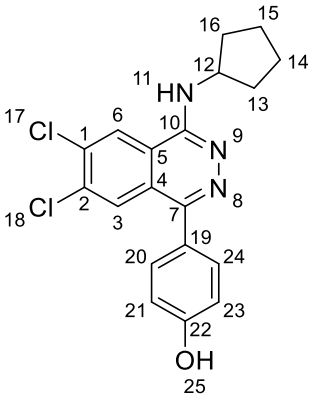

45

37 (50.0 mg, 0.158 mmol, 1.0 eq.) was reacted with 4-hydroxyphenylboronic acid pinacol ester (41.7 mg, 0.190 mmol, 1.2 eq.) according to **general procedure B** to yield **45** (34.1 mg, 57.7%) as a yellow gum. **ν_{max} (cm^{-1})** 3331 (br, OH) 2924, 2852 (CH), 1718, 1654 (CH ar), 1608 (C=N), 1237 (C-O); **^{1}H NMR (400 MHz, MeOD)** δ 8.62 (s, 1H, 6), 7.93 (s, 1H, 3), 7.46 – 7.36 (m, 2H, 21, 23), 7.01 – 6.91 (m, 2H, 20, 24), 4.56 (sext., *J* = 6.5 Hz, 1H, 12), 2.24 – 2.10 (m, 2H, 13, 16), 1.90 – 1.77 (m, 2H, 13, 16), 1.74-1.6 (m, 4H, 14, 15); **^{13}C NMR (101 MHz, MeOD)** δ 159.81 (22), 153.54 (10), 151.93 (7), 137.22 (1), 136.84 (2), 132.07 (20, 24), 129.27 (6), 127.80 (19), 126.06 (3), 119.92 (4), 116.78 (5), 116.57 (20, 24), 54.61 (12), 33.53 (13, 16), 25.02 (14, 15); **LR-ESI-MS** $C_{19}H_{17}Cl_2N_3O$ [M+H$^+$] *m/z* found: 374.13, calc.: 374.27; **HR-ESI-MS** $C_{19}H_{17}Cl_2N_3O$ [M+H$^+$] *m/z* found: 373.9357, calc.: 374.0748

(4-(6,7-dichloro-4-(cyclopentylamino)phthalazin-1-yl)phenyl)methanol (46)

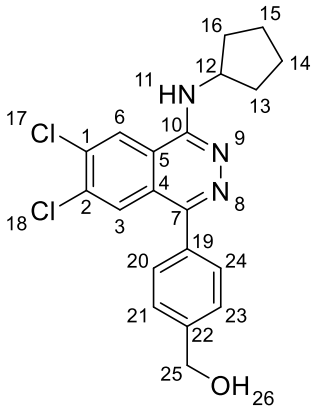

46

37 (50.0 mg, 0.158 mmol, 1.0 eq.) was reacted with 4-(hydroxymethyl)phenylboronic acid (28.8 mg, 0.190 mmol, 1.20 eq.) according **general procedure B** to yield **46** (35.5 mg, 57.9%) as a white solid. **M.P. =** 155-157 °C; **ν_{max} (cm^{-1})** 3389 (br, OH), 3092, 2944, 2864 (CH), 1602 (C=N), 1099 (C-O); **^{1}H NMR (400 MHz, $CDCl_3$)** δ 8.02 (s, 1H, 6), 7.97 (s, 1H, 3p), 7.61 (d, *J* = 8.2 Hz, 2H, 21, 23), 7.50 (d, *J* = 8.0 Hz, 2H, 20, 24), 5.21 (s, 1H, 11), 4.80 (s, 2H, 25), 4.72 (sext., *J* = 6.7 Hz, 1H, 12), 2.33 – 2.19 (m, 2H, 13, 16), 1.85 – 1.73 (m, 2H, 13, 16), 1.73 – 1.66 (m, 2H, 14, 15), 1.66 – 1.52 (m, 2H, 14, 15); **^{13}C NMR (101 MHz, $CDCl_3$)** δ 151.61 (10), 150.98 (22), 141.92 (7), 136.22 (19), 135.67 (1), 135.43 (2), 129.98 (20, 24), 128.32 (6), 127.19 (21, 23), 125.67 (4), 123.06 (3), 117.81 (5), 65.03 (25), 53.73 (12), 33.58 (13, 16), 24.15 (14, 15); **LR-ESI-MS** $C_{20}H_{19}Cl_2N_3O$ [M+H$^+$] *m/z* found: 388.12, calc.: 388.29; **HR-ESI-MS** $C_{20}H_{19}Cl_2N_3O$ [M+H$^+$] *m/z* found: 387.9458, calc.: 388.0905

3-(6,7-dichloro-4-(cyclopentylamino)phthalazin-1-yl)phenol (47)

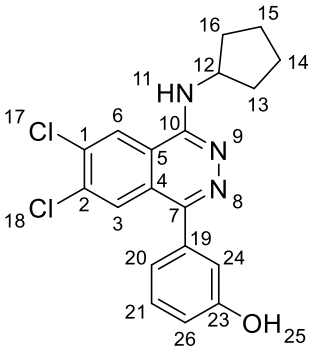

47

37 (50.0 mg, 0.158 mmol, 1.0 eq.) was reacted with 3-hydroxyphenylboronic acid pinacol ester (41.7 mg, 0.190 mmol, 1.20 eq.) according **general procedure B** to yield **47** (18.8 mg, 31.8%) as a white solid. **M.P. =** 149-151 °C; **ν_{max} (cm^{-1})** 3568 (br, OH), 3268 (NH), 3094, 2952, 2866 (CH), 1724, 1701 (CH ar), 1598 (C=N), 1287 (C-O); **^{1}H NMR (400 MHz, MeOD)** δ 8.65 (s, 1H, 6), 7.94 (s, 1H, 3), 7.63-7.54 (m, 1H, 21), 7.52-7.43 (m, 1H, 20), 7.40-7.32 (m, 1H, 26), 7.29-7.24 (m, 1H, 24), 6.26 (d, *J* = 7.4 Hz, 1H, 11), 4.60 (br, 1H, 12), 2.19 (br, 2H, 13, 16), 1.84 (br, 2H, 14, 15), 1.70 (br, 4H, 13, 14, 15, 16); **^{13}C NMR (101 MHz, MeOD)** δ 158.97 (23), 153.91 (10), 147.46 (7), 137.10 (19), 130.85 (1), 130.62 (2), 129.03 (21), 128.43 (6), 127.94 (20), 125.99 (5), 123.02 (26), 121.84 (22), 117.16 (5), 111.71 (24), 52.96 (12), 33.56 (13, 16), 25.02 (14, 15); **LR-ESI-MS** $C_{20}H_{19}Cl_2N_3O$ [M+H^+] *m/z* found: 374.11, calc.: 374.27; **HR-ESI-MS** $C_{20}H_{19}Cl_2N_3O$ [M+H^+] *m/z* found: 373.9355, calc.: 374.0748

2-chloro-5-(6,7-dichloro-4-(cyclopentylamino)phthalazin-1-yl)benzoic acid (48)

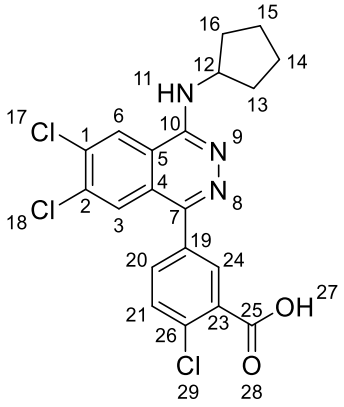

48

37 (50.0 mg, 0.158 mmol, 1.0 eq.) was reacted with 5-borono-2-chlorobenzoic acid (38.0 mg, 0.190 mmol, 1.20 eq.) according **general procedure B** to yield **48** (23.1 mg, 33.5%) as a yellow foam. **ν_{max} (cm^{-1})** 2972 (br, OH), 1714 (C=O); **^{1}H NMR (400 MHz, MeOD)** δ 8.76 (s, 1H, 6), 7.97 (s, 1H, 3), 7.87 – 7.83 (m, 1H, 24), 7.65 – 7.55 (m, 2H, 20, 21), 4.52 (sext., *J* = 6.5 Hz, 1H, 12), 2.24-2.19 (m, 2H, 13, 16), 1.91 – 1.81 (m, 2H, 13, 16), 1.81 – 1.66 (m, 4H, 14, 15); **^{13}C NMR (101 MHz, MeOD)** δ 159.72 (25), 153.38 (10), 148.59 (7), 138.41 (1), 137.61 (2), 135.04 (11) 133.64 (19), 132.32 (26), 131.67 (6), 128.99 (4), 126.62 (3), 121.95 (20), 120.18 (24), 116.24 (5), 54.97 (12), 33.34 (13, 16), 24.99 (14, 15). **LR-ESI-MS** $C_{20}H_{16}Cl_3N_3O_2$ [M+H$^+$] *m/z* found: 436.43, calc.: 436.72; **HR-ESI-MS** $C_{20}H_{16}Cl_3N_3O_2$ [M+H$^+$] *m/z* found: 435.9166, calc.: 436.0387.

5-(6,7-dichloro-4-(cyclopentylamino)phthalazin-1-yl)pyridin-3-ol (49)

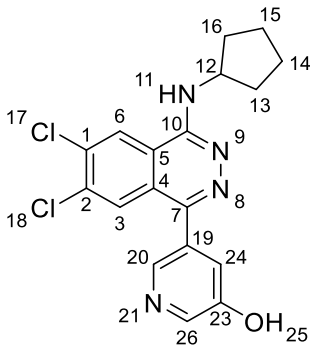

49

37 (50.0 mg, 0.158 mmol, 1.0 eq.) was reacted with 5-(4,4,5,5-Tetramethyl-1,3,2-dioxaborolan-2-yl)pyridin-3-ol (41.9 mg, 0.190 mmol, 1.20 eq.) according **general procedure B** to yield **49** (53.2 mg, 89.8%) as a brown solid. **M.P. =** 299-301 °C; **ν_{max} (cm^{-1})** 3608 (br, OH), 2962, 2862 (CH), 1682, 1633 (C=N); **^{1}H NMR (400 MHz, MeOD)** δ 8.68 (s, 1H, 6), 8.27 (br, 2H, 24, 26), 7.91 (s, 1H, 3), 7.49 (s, 1H, 20), 4.58 (sext., *J* = 6.9 Hz, 1H, 12), 2.24-2.16 (m, 2H, 13, 16), 1.92 – 1.78 (m, 2H, 13, 16), 1.76-1.8 (m, 4H, 14, 15); **^{13}C NMR (101 MHz, MeOD)** δ 156.01 (23), 152.48 (10), 140.54 (7), 137.70 (1), 137.15 (2), 133.38 (19), 129.48 (26), 128.31 (20), 126.27 (6), 125.12 (3), 122.77 (4), 119.58 (5), 113.51 (24) 54.68 (12), 33.51 (13, 16), 25.04 (14, 15); **LR-ESI-MS** $C_{18}H_{16}Cl_2N_4O$ [M+H^+] *m/z* found: 375.11, calc.: 375.25; **HR-ESI-MS** $C_{18}H_{16}Cl_2N_4O$ [M+H^+] *m/z* found: 374.9727, calc.: 375.0780.

6,7-dichloro-*N*-cyclopentyl-4-(6-methoxypyridin-3-yl)phthalazin-1-amine (50)

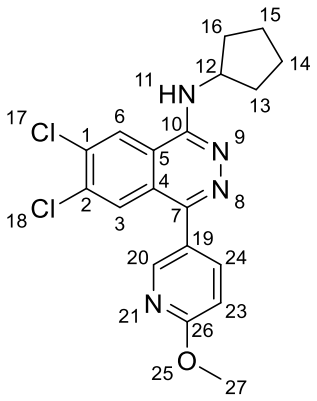

50

37 (50.0 mg, 0.158 mmol, 1.0 eq.) was reacted with 2-methoxy-5-pyridineboronic (29.0 mg, 0.190 mmol, 1.2 eq.) acid according **general procedure B** to yield **50** (54.4 mg, 88.5%) as a brown gum. **ν_{max} (cm^{-1})** 3238 (NH), 3062, 2962, 2879 (CH), 1701, 1607 (C=N); **^{1}H NMR (400 MHz, DMSO)** δ 12.84 (s, 1H, 11), 8.88 (s, 1H, 6), 7.89 (s, 1H, 3), 7.85 (d, *J* = 8.2 Hz, 1H, 23), 7.49 (d, *J* = 6.5 Hz, 1H, 24), 7.29 (dd, *J* = 8.2, 1.4 Hz, 1H, 20), 4.60 (sext., *J* = 6.6 Hz, 1H, 12), 2.55 (s, 3H, 27), 2.15 – 2.03 (m, 2H, 13, 16), 1.85 – 1.72 (m, 2H, 14, 15), 1.72-1.61 (m, 4H, 13, 14, 15, 16); **^{13}C NMR (101 MHz, DMSO)** δ 151.75 (26), 149.87 (10), 141.17 (7), 134.34 (1), 134.00 (2), 133.69 (19), 127.12 (20), 125.38 (6), 125.16 (23), 122.05 (4), 121.33 (24), 120.00 (3), 117.33 (5), 52.72 (27), 32.18 (12), 23.80 (13, 16), 11.76 (14, 15); **LR-ESI-MS** $C_{19}H_{18}Cl_2N_4O$ [M+H^+] *m/z* found: 389.46, calc.: 389.28; **HR-ESI-MS** $C_{19}H_{18}Cl_2N_4O$ [M+H^+] *m/z* found: 388.9846, calc.: 389.0936.

4-(6,7-dichloro-4-(cyclopentylamino)phthalazin-1-yl)-1-methylpyridin-2(1*H*)-one (51)

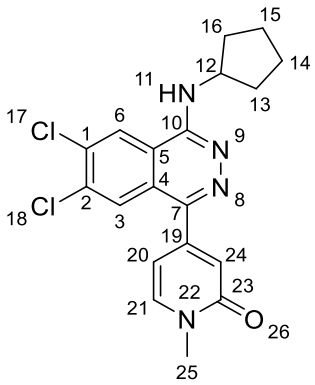

51

37 (50.0 mg, 0.158 mmol, 1.0 eq.) was reacted with (1-methyl-2-oxo-1,2-dihydropyridin-4-yl)boronic acid (29.0 mg, 0.190 mmol, 1.20 eq.) according **general procedure B** to yield **51** (40.3 mg, 65.6%) as a brown solid. **M.P. =** 278-282 °C; **ν_{max} (cm^{-1})** 3308 (NH), 2948, 2864 (CH), 1651 (C=O), 1563 (C=N); **^{1}H NMR (400 MHz, MeOD)** δ 8.70 (s, 1H, 6), 8.06 (s, 1H, 3), 7.84 (d, *J* = 6.9 Hz, 1H, 21), 6.79 (d, *J* = 1.9 Hz, 1H, 24), 6.67 (dd, *J* = 6.9, 1.9 Hz, 1H, 20), 4.61 (sext., *J* = 6.4 Hz, 1H, 12), 3.68 (s, 3H, 25), 2.28 – 2.11 (m, 2H, 13, 16), 1.89-1.81 (m, 2H, 13, 16), 1.78-1.66 (m, 4H, 14, 15); **^{13}C NMR (101 MHz, $CDCl_3$)** δ 162.81 (23), 152.06 (10), 147.75 (7), 138.72 (21), 136.86 (1), 136.14 (2), 131.84 (19), 127.21 (6), 124.75 (4), 123.52 (24), 120.80 (3), 117.52 (5), 107.74 (2), 53.83 (25), 37.82 (12), 33.43 (13, 16), 24.12 (14, 15); **LR-ESI-MS** $C_{19}H_{18}Cl_2N_4O$ [M+H$^+$] *m/z* found: 389.39, calc.: 389.28; **HR-ESI-MS** $C_{19}H_{18}Cl_2N_4O$ [M+H$^+$] *m/z* found: 388.9405, calc.: 389.0858.

6,7-dichloro-*N*-cyclopentyl-4-(1-methyl-1,2,3,6-tetrahydropyridin-4-yl)phthalazin-1-amine (52)

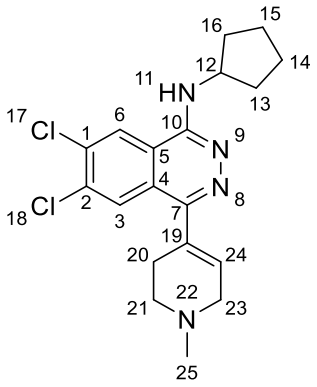

52

37 (50.0 mg, 0.158 mmol, 1.0 eq.) was reacted with 1-methyl-1,2,3,6-tetrahydropyridine-4-boronic acid pinacol ester (42.3 mg, 0.190 mmol, 1.20 eq.) according **general procedure B** to yield **52** 19.2 mg, 32.2%) as a brown gum. **ν_{max} (cm^{-1})** 3293 (NH), 3024 (C=C-H), 2949, 2866 (CH), 1600 (C=N), 1566 (C=C); **^{1}H NMR (400 MHz, $CDCl_3$)** δ 8.29 (s, 1H, 6), 7.85 (s, 1H, 3), 5.92 (h, *J* = 1.7 Hz, 1H, 24), 5.00 (d, *J* = 6.4 Hz, 1H, 11), 4.66 (sext., *J* = 6.7 Hz, 12H), 3.27 (q, *J* = 3.0 Hz, 2H, 23), 2.87-2.82 (m, 2H, 20), 2.81-2.76 (m, 2H, 21), 2.50 (s, 3H, 25), 2.33 – 2.20 (m, 2H, 13, 16), 1.82-1.72 (m, 2H, 14, 15), 1.73 – 1.64 (m, 2H, 14, 15), 1.64 – 1.47 (m, 2H, 13, 16); **^{13}C NMR (101 MHz, $CDCl_3$)** δ 151.38 (br, 2C, 10, 7), 136.06 (1), 135.51 (2), 132.55 (19), 128.28 (6), 128.01 (24), 125.27 (4), 122.75 (3), 117.82 (5), 54.62 (23), 53.65 (25), 52.35 (21), 50.96, 45.66 (12), 33.59 (13, 16), 29.38 (20), 24.12 (14, 15); **LR-ESI-MS** $C_{19}H_{22}Cl_2N_4$ [M+H$^+$] *m/z* found: 377.39, calc.: 377.31; **HR-ESI-MS** $C_{19}H_{22}Cl_2N_4$ [M+H$^+$] *m/z* found: 377.0203, calc.: 377.1299.

6,7-dichloro-*N*-cyclopentyl-4-(3-methyl-1*H*-indazol-6-yl)phthalazin-1-amine (53)

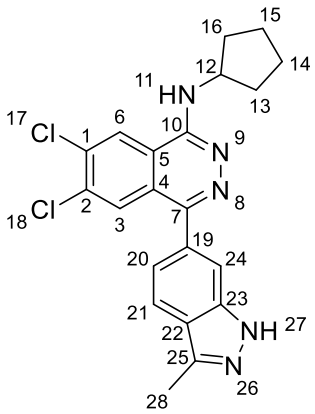

53

37 (50.0 mg, 0.158 mmol, 1.0 eq.) was reacted with 3-methyl-1*H*-indazol-6-yl-6-boronic acid (27.8 mg, 0.190 mmol, 1.20 eq.) according **general procedure B** to yield **53** (14.3 mg, 22.0 %) as a yellow oil. **ν_{max} (cm^{-1})** 3315, 3209 (NH), 2976, 2851 (CH), 1692, 1614 (C=N); **^{1}H NMR (400 MHz, DMSO)** δ 12.84 (s, 1H, 27), 8.88 (s, 1H, 6), 7.89 (s, 1H, 3), 7.85 (d, *J* = 8.2 Hz, 1H, 21), 7.66 (d, *J* = 1.2 Hz, 1H, 24), 7.49 (d, *J* = 6.5 Hz, 1H, 11), 7.29 (dd, *J* = 8.2, 1.4 Hz, 1H, 20), 4.60 (h, *J* = 6.6 Hz, 1H, 12), 2.55 (s, 3H, 28) 2.15 – 1.99 (m, 2H, 13, 16), 1.81-1.76 (m, 2H, 14, 15), 1.71 – 1.60 (m, 4H, 13, 14 15, 16); **^{13}C NMR (101 MHz, DMSO)** δ 151.75 (10), 149.87 (7), 141.20 (23), 140.81 (25), 134.34 (19), 134.00 (1), 133.69 (2), 127.12 (6), 125.38 (20), 125.16 (4), 122.05 (22), 121.33 (21), 120.00 (3), 117.33 (5), 111.00 (24), 52.72 (12), 32.18 (13, 16), 23.80 (14, 15), 11.76 (28); **LR-ESI-MS** $C_{21}H_{19}Cl_2N_5$ [M+H$^+$] *m/z* found: 412.45, calc.: 412.32; **HR-ESI-MS** $C_{21}H_{19}Cl_2N_5$ [M+H$^+$] *m/z* found: 411.9941, calc.: 412.1096

4-(benzo[*d*]thiazol-5-yl)-6,7-dichloro-*N*-cyclopentylphthalazin-1-amine (54)

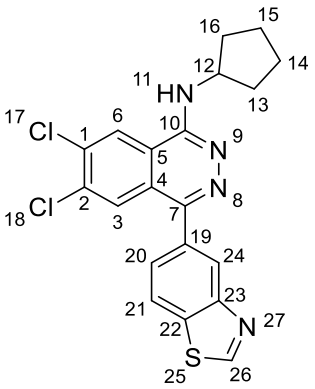

54

37 (50.0 mg, 0.158 mmol, 1.0 eq.) was reacted with benzothiazole-5-boronic acid pinacol ester (49.5 mg, 0.190 mmol, 1.20 eq.) according **general procedure B** to yield **54** (37.8 mg, 57.6%) as a yellow solid. **M.P. =** 268-270 °C; **ν_{max} (cm^{-1})** 3251 (NH), 3013, 2956, 2865 (CH), 1602 (C=N); **^{1}H NMR (400 MHz, $CDCl_3$)** δ 9.09 (s, 1H, 26), 8.39 (d, *J* = 1.6 Hz, 1H, 24), 8.12 (d, *J* = 8.3 Hz, 1H, 21), 8.08 (s, 1H, 6), 7.96 (s, 1H, 3), 7.81 (dd, *J* = 8.3, 1.7 Hz, 1H, 20), 5.17 (d, *J* = 6.2 Hz, 1H, 11), 4.75 (sext., *J* = 6.7 Hz, 1H, 12), 2.36 – 2.23 (m, 2H, 13, 16), 1.85-1.78 (m, 2H, 14, 15), 1.77 – 1.65 (m, 4H, 13, 14, 15, 16); **^{13}C NMR (101 MHz, $CDCl_3$)** δ 155.10 (26), 153.45 (23), 151.69 (10), 150.55 (7), 136.40 (1), 135.80 (2), 134.83 (22), 134.43 (19), 128.13 (24), 127.47 (6), 125.65 (4), 124.81 (21), 123.04 (3), 122.40 (20), 117.74 (5), 33.61 (12), 27.05 (13, 16), 24.15 (14, 15); **LR-ESI-MS** $C_{20}H_{16}Cl_2N_4S$ [M+H$^+$] *m/z* found: 415.38, calc.: 415.34; **HR-ESI-MS** $C_{20}H_{16}Cl_2N_4S$ [M+H$^+$] *m/z* found: 414.9388, calc.: 415.0473.

4-(benzo[*d*]thiazol-6-yl)-6,7-dichloro-*N*-cyclopentylphthalazin-1-amine (55)

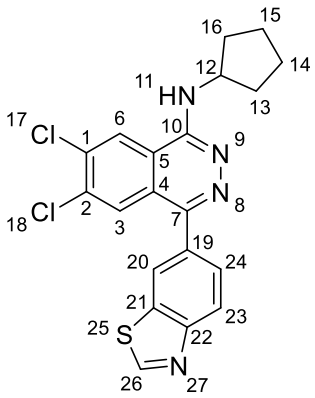

55

37 (50.0 mg, 0.158 mmol, 1.0 eq.) was reacted with benzo[*d*]thiazol-6-ylboronic acid (33.9 mg, 0.190 mmol, 1.20 eq.) according **general procedure B** to yield **55** (44.6 mg, 68.0%) as a yellow solid. **M.P. =** 266-267 °C; **ν_{max} (cm^{-1})** 3245 (NH), 3074, 2953, 2864 (CH), 1600 (C=N); **^{1}H NMR (400 MHz, $CDCl_3$)** δ 9.09 (s, 1H, 26), 8.27 (d, *J* = 1.7 Hz, 1H, 20), 8.25 (s, 1H, 6), 8.07 (br, 1H, 23), 8.01 (s, 1H, 3), 7.77 (dd, *J* = 8.4, 1.7 Hz, 1H, 24), 5.49 (br, 1H, 11), 4.75 (sext., *J* = 6.5 Hz, 1H, 12), 2.35-2.26 (m, 2H, 13, 1), 1.86-1.75 (m, 2H, 14, 15), 1.74-1.66 (m, 4H, 13, 14, 15, 16); **^{13}C NMR (101 MHz, $CDCl_3$)** δ 155.28 (26), 153.57 (22), 151.67 (10), 150.47 (7), 136.46 (1), 135.85 (2), 134.47 (21), 133.96 (19), 128.10 (20), 128.06 (6), 125.67 (4), 123.65 (23), 123.35 (3), 123.22 (24), 117.74 (5), 33.56 (12), 27.05 (13, 16), 24.16 (14, 15); **LR-ESI-MS** $C_{20}H_{16}Cl_2N_4S$ [M+H^+] *m/z* found: 415.36, calc.: 415.34; **HR-ESI-MS** $C_{20}H_{16}Cl_2N_4S$ [M+H^+] *m/z* found: 414.8923, calc.: 415.0473.

4-(benzo[*c*][1,2,5]thiadiazol-5-yl)-6,7-dichloro-*N*-cyclopentylphthalazin-1-amine (56)

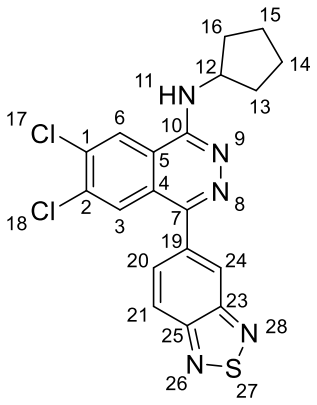

56

37 (50.0 mg, 0.158 mmol, 1.0 eq.) was reacted with benzo[*c*][1,2,5]thiadiazole-5-boronic acid pinacol ester (49.7 mg, 0.190 mmol, 1.2 eq.) according **general procedure B** to yield **56** (47.0 mg, 71.6%) as a yellow solid. **M.P. =** 263-266 °C; **ν_{max} (cm^{-1})** 3252 (NH), 3065, 2957, 2864 (CH), 1676, 1602 (C=N), 1564, 1461, 1312, 1257, 1138, 1060, 982, 905, 851, 705; **^{1}H NMR (400 MHz, $CDCl_3$)** δ 8.25 (br, 1H, 24), 8.13 (d, *J* = 8.8 Hz, 1H, 21), 8.06 (s, 1H, 6), 8.01 – 7.95 (m, 2H, 3, 20), 5.35 (d, *J* = 6.5 Hz, 1H, 11), 4.75 (sext., *J* = 6.7 Hz, 1H, 12), 2.33-2.22 (m, 2H, 13, 16), 1.86 – 1.73 (m, 2H, 14, 15), 1.73-1.66 (m, 2H, 14, 15), 1.67-1.58 (m, 2H, 13, 16); **^{13}C NMR (101 MHz, $CDCl_3$)** δ 154.87 (23), 154.80 (22), 151.83 (10), 149.56 (7), 137.67 (19), 136.71 (1), 136.04 (2), 131.73 (24), 127.62 (6), 125.37 (4), 123.28 (3), 122.25 (21), 121.88 (20), 117.63 (5), 53.81 (12), 33.55 (13, 16), 24.14 (14, 15); **LR-ESI-MS** $C_{19}H_{15}Cl_2N_5S$ [M+H$^+$] *m/z* found: 416.39, calc.: 416.32; **HR-ESI-MS** $C_{19}H_{15}Cl_2N_5S$ [M+H$^+$] *m/z* found: 415.88720, calc.: 416.04253

6,7-dichloro-*N*-cyclopentyl-4-(pyrimidin-5-yl)phthalazin-1-amine (57)

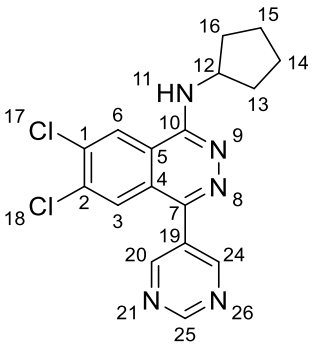

57

37 (50.0 mg, 0.158 mmol, 1.0 eq.) was reacted with 5-pyrimidinylboronic acid (23.5 mg, 0.190 mmol, 1.2 eq.) according **general procedure B** to yield **57** (51.2 mg, 90.0%) as a yellow solid. **M.P. =** 176-178 °C; **ν_{max} (cm^{-1})** 3257 (NH), 3051, 2955, 2866 (CH), 1698, 1602 (C=N); **^{1}H NMR (400 MHz, $CDCl_3$)** δ 9.35 (s, 1H, 25), 9.10 (s, 2H, 20, 24), 7.98 (s, 1H, 6), 7.95 (s, 1H, 3), 5.26 (d, *J* = 6.5 Hz, 1H, 11), 4.75 (sext., *J* = 6.7 Hz, 1H, 12), 2.36 – 2.24 (m, 2H, 13, 16), 1.88 – 1.76 (m, 2H, 14, 15), 1.76 – 1.68 (m, 2H, 14, 15), 1.67 – 1.56 (m, 2H, 13, 16); **^{13}C NMR (101 MHz, $CDCl_3$)** δ 158.74 (25), 157.23 (20, 24), 151.97 (10), 145.29 (7), 137.25 (1), 136.46 (2), 130.67 (19), 126.71 (6), 125.20 (4), 123.36 (3), 117.34 (5), 53.87 (12), 33.57 (13, 16), 24.12 (14, 15); **LR-ESI-MS** $C_{17}H_{15}Cl_2N_5$ [M+H$^+$] *m/z* found: 360.29, calc.: 360.24; **HR-ESI-MS** $C_{17}H_{15}Cl_2N_5$ [M+H$^+$] *m/z* found: 359.9326, calc.: 360.0783

General Procedure C

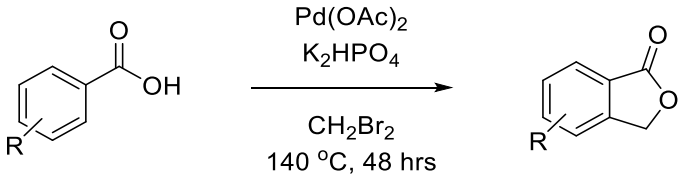

In a 100 mL Ace pressure tube equipped with stirrer bar was placed benzoic acid (1.0 eq.), $Pd(OAc)_2$ (0.1 eq.), and K_2HPO_4 (2.5 eq.). The dry reactants were suspended in CH_2Br_2 (30.0 eq) and the mixture thoroughly degassed using the freeze-pump-thaw method. The reaction

was placed under N_2 and the pressure tube quickly sealed. It was then heated at 140 °C with stirring for 48 hours.

The reaction was allowed to cool, diluted with DCM (25 mL) and the mixture filtered through celite. The filtrate was washed with brine, dried over sodium sulfate and the residual solvent removed *in vacuo.* The resultant crude compound was purified by column chromatography (cyclohexane:EtOAc, 1:0 - 1:1).

General Procedure D

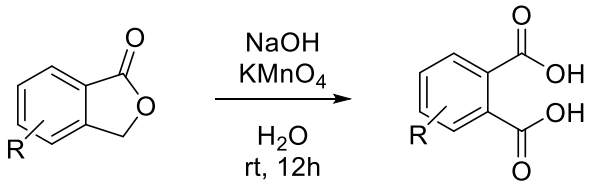

To a 100 mL RBF equipped with stirrer bar was added isobenzofuranone (1.0 eq.), which was subsequently suspended in water (5 mL). A solution of NaOH (19.0 M, 3.0 eq) and $KMnO_4$ (2.2 eq.) in water (10 mL) was added to the suspension dropwise with stirring. The reaction was left stirring at room temperature overnight.

The basic aqueous layer was extracted with Et_2O (3 × 50 mL), and the brown precipitate that had formed filtered through a celite pad. The filtrate was acidified with conc. HCl (aq) and the solvent was removed *in vacuo* to give the desired product.

General Procedure E

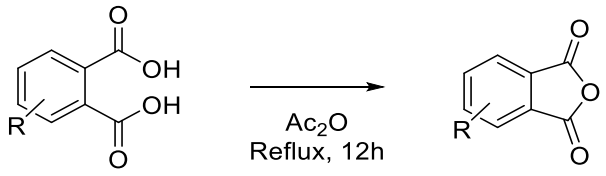

Phthalic acid (1.0 eq.) was suspended in acetic anhydride (30.0 eq) and the mixture heated to reflux for 12 hours. The reaction was allowed to cool and the residual solvent removed *in vacuo* to yield the desired product.

General Procedure F

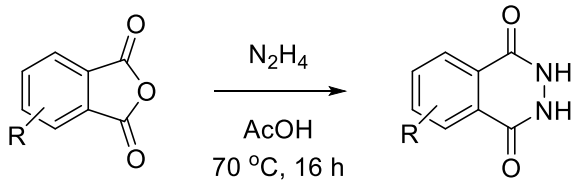

In a two-necked flask equipped with stirrer bar and condenser, isobenzofuran-1,3-dione (1.0 eq) was suspended in acetic acid (15 mL) under N_2. The mixture was stirred for 30 mins at room temperature. Hydrazine (78 %wt, 1.4 eq.) was added dropwise and the reaction then heated with stirring to 70 °C overnight. The residual solvent was removed *in vacuo* to yield the desired product.

General Procedure G

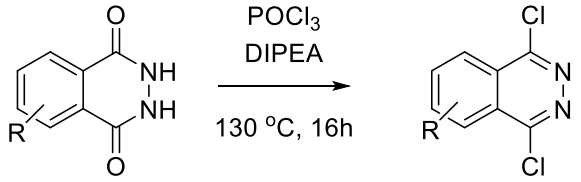

In a two-necked RBF equipped with stirrer bar, dihydrophthalazine-1,4-dione (1.0 eq.) was suspended in $POCl_3$ (10.0 eq.). The mixture was stirred at room temperature for 30 minutes. DIPEA (3.0 eq.) was added dropwise and the reaction heated to 130 °C overnight.

The residual solvent was removed *in vacuo* and the remaining crude product diluted with DCM (10 mL). This solution was poured slowly into ice water and the mixture left stirring at 0 °C for one hour. The acidic mixture was brought to pH 7 with NaOH (50% wt) and then extracted with DCM (3 x 50 mL). The combined organic extracts were washed with brine, dried over sodium sulfate and the residual solvent removed *in vacuo.* The crude product was purified by column chromatography (cyclohexane:EtOAc, 1:0 – 0:1).

1,4-dichloro-6,7-dimethoxyphthalazine (67)

Step 1: 1,4-dichloro-6,7-dimethoxyphthalazine

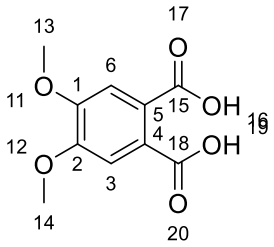

5,6-dimethoxyisobenzofuran-1(3H)-one (**58**) (1.500 g, 7.725 mmol, 1.0 eq.) was reacted according to **general procedure D** to yield 4,5-dimethoxyphthalic acid (1.720 g, quant.) as a white powder. **^{1}H NMR (400 MHz, MeOD)** δ 7.30 (s, 2H, 6, 3), 3.91 (s, 6H, 13, 14); **^{13}C NMR (101 MHz, MeOD)** δ 177.84 (15, 18), 159.38 (1, 2), 135.29 (4, 5), 120.73 (3, 6), 65.28 (13, 14); **LR-ESI-MS** $C_{10}H_{10}O_6$ [M+H$^+$] *m/z* found: 225.140, calc.: 226.184.

Step 2: 5,6-dimethoxyisobenzofuran-1,3-dione (**61**)

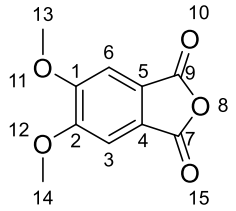

61

4,5-dimethoxyphthalic acid (1.500 g, 6.332 mmol, 1.0 eq.) was reacted according to **general procedure E** yield **61** (1.35 g, quant.) as a white solid. **^{1}H NMR (400 MHz, $CDCl_3$)** δ 7.36 (s, 2H, 6, 3), 4.03 (s, 6H, 13, 14); **^{13}C NMR (101 MHz, $CDCl_3$)** δ 163.22 (7, 9), 155.94 (1, 2), 125.10 (4, 5), 106.26 (3, 6), 57.02 (13, 14); **LR-ESI-MS** $C_{10}H_8O_5$ [M+H$^+$] *m/z* found: 208.110, calc.: 208.169.

Step 3: 6,7-dimethoxy-2,3-dihydrophthalazine-1,4-dione (**64**)

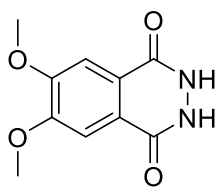

64

61 (1.00 g, 4.804 mmol, 1.0 eq) was reacted according to **general procedure F** to yield **64** (1.05 g, quant.) as a brown solid, which was engaged in the next step without further purification (**LR-ESI-MS** $C_{10}H_{10}N_2O_4$ [M+H$^+$] *m/z* found: 223.24, calc.: 222.200).

Step 4: 1,4-dichloro-6,7-dimethoxyphthalazine (**67**)

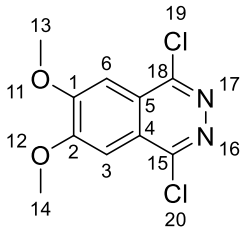

64

64 (1.0 g, 4.500 mmol, 1.0 eq.) was reacted according to **general procedure F** to yield **67** (0.45 g, 39%) as an off-white solid. **M.P. =** 210-214 °C; **ν_{max} (cm^{-1})** 1740 (C=N), 1258 (C-O); **^{1}H NMR (400 MHz, $CDCl_3$)** δ 7.46 (s, 2H, 3, 6), 4.12 (s, 6H, 13, 14); **^{13}C NMR (101 MHz, $CDCl_3$)** δ 155.53 (1, 2), 153.22 (15, 18), 123.76 (4, 5), 104.23 (3, 6), 56.94 (13, 14); **LR-ESI-MS** $C_{10}H_8Cl_2N_2O_2$ [M+H$^+$] *m/z* found: 259.19, calc.: 259.09; **HR-ESI-MS** $C_{10}H_8Cl_2N_2O_2$ [M+H$^+$] *m/z* found: 258.8996, calc.: 259.0041

5,8-dichloro-[1,3]dioxolo[4,5-*g*]phthalazine (68)

Step 1: [1,3]dioxolo[4,5-*f*]isobenzofuran-5(7*H*)-one (**59**)

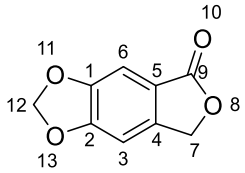

59

1,3-Benzodioxole-5-carboxylic acid (2.0 g, 12.039 mmol, 1.0 eq.) was reacted according to **general procedure C** to yield **59** (0.58 g, 27.0%) as an off-white solid. **M.P. =** 161-164 °C; **ν_{max} (cm^{-1})** 1736 (C=O), 1257 (C-O); **^{1}H NMR (400 MHz, $CDCl_3$)** δ 7.23 (s, 1H, 6), 6.84 (s, 1H, 3), 6.13 (s, 2H, 12), 5.19 (s, 2H, 7); **^{13}C NMR (101 MHz, $CDCl_3$)** δ 170.82 (9), 153.88 (1), 149.38 (2),

143.24 (4), 119.60 (5), 104.59 (6), 102.78 (3), 101.91 (12), 69.27 (7); **LR-ESI-MS** $C_9H_6O_4$ [M+H$^+$] *m/z* found: 179.15, calc.: 178.143; **HR-ESI-MS** $C_9H_6O_4$ [M+H$^+$] *m/z* found: 178.9337, calc.: 179.0345.

Step 2: Benzo[*d*][1,3]dioxole-5,6-dicarboxylic acid

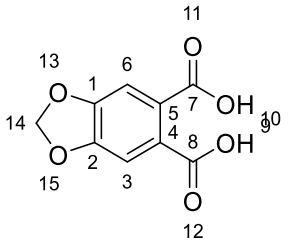

59 (500.0 mg, 2.807 mmol, 1.0 eq.) was reacted according to **general procedure D** to yield benzo[*d*][1,3]dioxole-5,6-dicarboxylic acid (572.0 mg, quant.) as a white solid**. ^{1}H NMR (400 MHz, DMSO)** δ 7.13 (s, 2H), 6.15 (s, 2H); **^{13}C NMR (101 MHz, DMSO)** δ 161.13 (7, 8), 153.67 (1, 2), 127.87 (4, 5), 103.31 (3, 6), 102.82 (14); **LR-ESI-MS** $C_9H_6O_6$ [M+H$^+$] *m/z* found: 209.230, calc.: 210.141

Step 3: [1,3]dioxolo[4,5-*f*]isobenzofuran-5,7-dione (**62**)

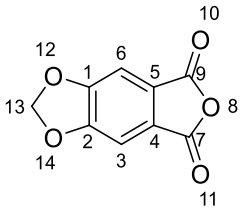

62

Benzo[*d*][1,3]dioxole-5,6-dicarboxylic acid (500.0 mg, 2.379 mmol, 1.0 eq.) was reacted according to **general procedure E** to yield **62** (424.0 mg, quant.) as a white solid. **^{1}H NMR (400 MHz, $CDCl_3$)** δ 7.28 (s, 2H, 3, 6), 6.26 (s, 2H, 13); **^{13}C NMR (101 MHz, $CDCl_3$)** δ 162.45 (7, 9), 154.84 (1, 2), 127.27 (4, 5), 104.87 (3, 6), 104.06 (13); **LR-ESI-MS** $C_9H_6O_6$ [M+H$^+$] *m/z* found: 193.07, calc.: 192.13

Step 4: 6,7-dihydro-[1,3]dioxolo[4,5-*g*]phthalazine-5,8-dione (**65**)

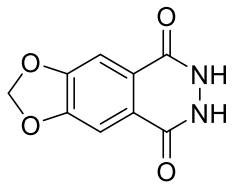

65

62 (300.0 mg, 1.561 mmol, 1.0 eq.) was reacted according to **general procedure F** to yield **65** (314.4 mg, quant.) as a brown solid. This was engaged directly in the next step without further purification (**LR-ESI-MS** $C_9H_6N_2O_4$ [M+H$^+$] *m/z* found: 207.10, calc.: 206.16).

Step 5: 5,8-dichloro-[1,3]dioxolo[4,5-*g*]phthalazine (**68**)

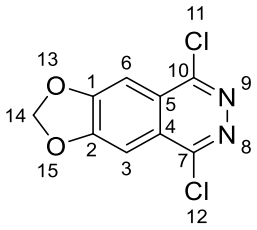

68

65 (250.0 mg, 1.213 mmol, 1.0 eq.) was reacted according to **general procedure G** to yield **68** (37.6 mg, 12.8%) as a yellow solid. **M.P. =** 219-223 °C; **ν_{max} (cm^{-1})** 2633 (CH ar), 1623 (C=N), 1217 (C-O); **^{1}H NMR (400 MHz, $CDCl_3$)** δ 7.55 (s, 2H, 3, 6), 6.29 (s, 2H, 14); **^{13}C NMR (101 MHz, $CDCl_3$)** δ 153. 94 (1, 2), 153.75 (7, 10), 125.72 (4, 5), 103.49 (3, 6), 102.76 (14); **LR-ESI-MS** $C_9H_4Cl_2N_2O_2$ [M+H$^+$] *m/z* found: 243.11, calc.: 243.04; **HR-ESI-MS** $C_9H_4Cl_2N_2O_2$ [M+H$^+$] *m/z* found: 242.8721, calc.: 242.9728.

5,8-dichloro-2,2-difluoro-[1,3]dioxolo[4,5-*g*]phthalazine (69)

Step 1: 2,2-difluoro-[1,3]dioxolo[4,5-*f*]isobenzofuran-5(7*H*)-one (**60**)

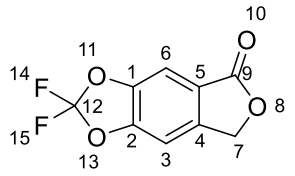

60

2,2-Difluoro-1,3-benzodioxole-5-carboxylic acid (2.0 g, 9.895 mmol) was reacted according to **general procedure C** to yield **60** (0.29 g, 13.6%) as a white solid. **M.P. =** 153-155 °C; **ν_{max} (cm^{-1})** 1773 (C=O), 1363 (C-O), 1113 (C-F); **^{1}H NMR (400 MHz, $CDCl_3$)** δ 7.55 (s, 1H), 7.17 (s, 1H, 3), 5.30 (s, 2H, 7); **^{13}C NMR (101 MHz, $CDCl_3$)** δ 169.71 (9), 148.73 (1), 144.90 (2), 143.66 (4), 131.86 (t, *J* = 258.3 Hz, 12), 121.67 (5), 106.64 (6), 103.64 (3), 69.32 (7); **LR-ESI-MS** $C_9H_4Cl_2N_2O_2$ [M+H$^+$] *m/z* found: 215.120, calc.: 214.124; **HR-ESI-MS** $C_9H_4Cl_2N_2O_2$ [M+H$^+$] *m/z* found: 214.9150, calc.: 215.0156.

Step 2: 2,2-difluorobenzo[*d*][1,3]dioxole-5,6-dicarboxylic acid

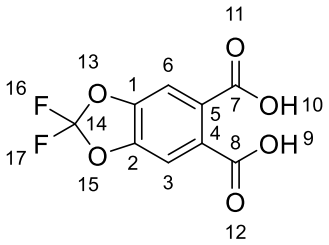

60 (250.0 mg, 1.168 mmol, 1.0 eq) was reacted according to **general procedure D** to yield 2,2-difluorobenzo[*d*][1,3]dioxole-5,6-dicarboxylic acid (267.4 mg, 93.1%) as a white solid. **^{1}H NMR (400 MHz, DMSO)** δ 7.72 (s, 2H, 3, 6); **^{13}C NMR (101 MHz, DMSO)** δ 167.13 (7, 8), 143.85 (1, 2), 130.23 (4, 5), 110.36 (3, 6); **LR-ESI-MS** $C_9H_4F_2O_6$ [M+H$^+$] *m/z* found: 245.16, calc.: 246.12

Step 3: 2,2-difluoro-[1,3]dioxolo[4,5-*f*]isobenzofuran-5,7-dione (**63**)

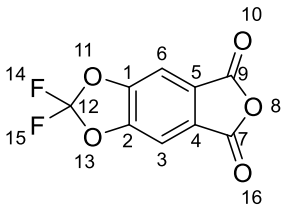

63

2,2-difluorobenzo[*d*][1,3]dioxole-5,6-dicarboxylic acid (250.0 mg, 1.016 mmol, 1.0 eq.) was reacted according to **general procedure E** to yield **63** (227.0 mg, quant.) as a brown solid. **^{1}H NMR (400 MHz, $CDCl_3$)** δ 7.66 (s, 2H, 3, 6); **^{13}C NMR (101 MHz, $CDCl_3$)** δ 161.33 (7, 9), 149.46 (1, 2), 131.94 (t, *J* = 262.2 Hz, 12), 128.45 (4, 5), 106.87 (3, 6); **LR-ESI-MS** $C_9H_4F_2O_5$ [M+H$^+$] *m/z* found: 229.240, calc.: 228.107.

Step 4: 2,2-difluoro-6,7-dihydro-[1,3]dioxolo[4,5-*g*]phthalazine-5,8-dione (**66**)

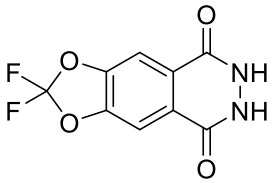

66

63 (200.0 mg, 0.877 mmol, 1.0 eq.) was reacted according to **general procedure F** to yield **66** (204.3 mg, quant.) as a brown solid. This was engaged directly in the next step without further purification (**LR-ESI-MS** $C_9H_4F_2N_2O_4$ [M+H$^+$] *m/z* found: 242.96, calc.: 242.138).

Step 5: 5,8-dichloro-2,2-difluoro-[1,3]dioxolo[4,5-*g*]phthalazine (**69**)

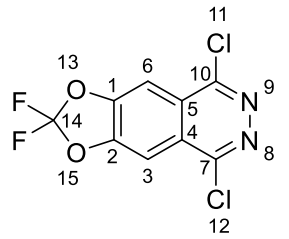

69

66 (200.0 mg, 0.826 mmol, 1.0 eq.) was reacted according to **general procedure G** to yield **69** (23.4 mg, 10.2%) as a yellow solid. **M.P. =** 199-202 °C; **ν_{max} (cm^{-1})** 1655 (C=N), 1430 (C-F), 1294 (C-O); **^{1}H NMR (400 MHz, $CDCl_3$)** δ 7.95 (s, 2H, 3, 6); **^{13}C NMR (101 MHz, $CDCl_3$)** δ 154.19 (7, 10), 148.45 (1, 2), 131.73 (t, *J* = 262.0 Hz, 14), 125.68 (4, 5), 105.32 (3, 6); **LR-ESI-MS** $C_9H_2Cl_2F_2N_2O_2$ [M+H$^+$] *m/z* found: 279.13, calc.: 279.02; **HR-ESI-MS** $C_9H_2Cl_2F_2N_2O_2$ [M+H$^+$] *m/z* found: 278.8532, calc.: 278.9540

***N*-cyclopentyl-6,7-dimethoxy-4-(pyridin-4-yl)phthalazin-1-amine (70)**

Step 1: 4-chloro-*N*-cyclopentyl-6,7-dimethoxyphthalazin-1-amine

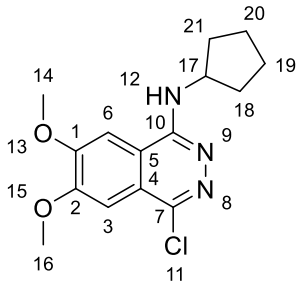

Cyclopentylamine (42.7 mg, 0.502 mmol, 1.3 eq.) was reacted with **67** (100.0 mg, 0.386 mmol, 1.0 eq.) according to **general procedure A** to yield 4-chloro-N-cyclopentyl-6,7-dimethoxyphthalazin-1-amine (41.2 mg, 34.7%) as an off-white solid. **^{1}H NMR (400 MHz, $CDCl_3$)** δ 7.40 (s, 1H, 6), 6.92 (s, 1H, 3), 4.81 (d, *J* = 6.4 Hz, 1H, 12), 4.61 (sext., *J* = 6.8 Hz, 1H, 17), 4.06 (d, 6H, 14, 16), 2.33 – 2.18 (m, 2H, 18, 21), 1.82 – 1.71 (m, 2H, 19, 20), 1.71 – 1.61 (m, 2H, 19, 20), 1.61 – 1.47 (m, 2H, 18, 21); **^{13}C NMR (101 MHz, $CDCl_3$)** δ 153.51 (10), 153.38 (1), 153.23 (2), 145.20 (7), 122.43 (4), 115.56 (5), 105.05 (6), 100.50 (3), 56.70 (14), 56.64 (16), 56.54 (17), 33.63 (18, 21), 24.17 (19, 20); **LR-ESI-MS** $C_{15}H_{18}ClN_3O_2$ [M+H$^+$] *m/z* found: 308.18, calc.: 307.78.

Step 2: *N*-cyclopentyl-6,7-dimethoxy-4-(pyridin-4-yl)phthalazin-1-amine (**70**)

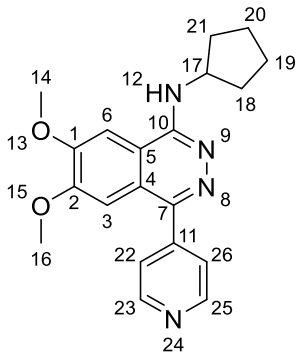

70

4-chloro-N-cyclopentyl-6,7-dimethoxyphthalazin-1-amine (30.0 mg, 0.097 mmol, 1.0 eq.) was reacted with 4-pyridinylboronic acid (14.4 mg, 0.117 mmol, 1.2 eq.) according to **general procedure B** to yield **70** (16.2 mg, 47.4%) as an off-white solid. **M.P. =** 228-232 °C; **ν_{max} (cm^{-1})** 3195 (NH), 2967, 2859 (CH), 1622 (C=N), 1289 (C-O); **^{1}H NMR (400 MHz, $CDCl_3$)** δ 8.76 (dd, *J* = 4.4, 1.6 Hz, 2H, 23, 25), 7.67 (dd, *J* = 4.5, 1.6 Hz, 2H, 22, 26), 7.20 (s, 1H, 6), 7.03 (s, 1H, 3), 5.03 (br, 1H, 12), 4.72 (sext., *J* = 7.0 Hz, 1H, 17), 4.08 (s, 3H, 14), 3.91 (s, 3H, 13), 2.39 – 2.23 (m, 2H, 18, 21), 1.87 – 1.75 (m, 2H, 19, 20), 1.75 – 1.66 (m, 2H, 19, 20), 1.66-1.54 (m, 2H, 18, 21); **^{13}C NMR (101 MHz, $CDCl_3$)** δ 152.95 (10), 152.92 (1), 152.88 (2), 150.11 (23, 25), 149.21 (7), 145.65 (11), 124.46 (16, 20), 121.89 (4), 113.84 (5), 104.85 (6), 100.40 (3), 56.57 (14), 56.30 (16), 53.70 (17), 33.72 (18, 21), 24.20 (19, 20); **LR-ESI-MS** $C_{20}H_{22}N_4O_2$ [M+H$^+$] *m/z* found: 351.47, calc.: 350.422; **HR-ESI-MS** $C_{20}H_{22}N_4O_2$ [M+H$^+$] *m/z* found: 351.0837, calc.: 351.1821.

6,7-dichloro-4-(1-methyl-1*H*-pyrazol-3-yl)-*N*-(tetrahydrofuran-3-yl)phthalazin-1-amine (71)

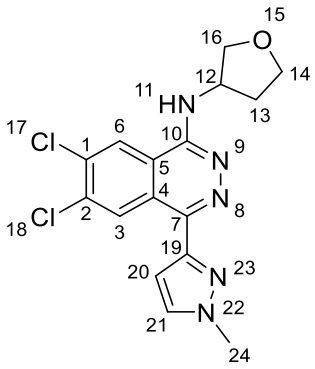

71

4,6,7-Trichloro-*N*-(tetrahydrofuran-3-yl)phthalazin-1-amine (50.0 mg, 0.157 mmol, 1.0 eq.) was reacted with 1-methyl-1*H*-pyrazole-3-boronic acid pinacol ester (39.2 mg, 0.188 mmol, 1.2 eq) according to **general procedure B** to yield **71** (44.5 mg, 77.8%) as an off-white solid. **M.P. =** 231-234 °C; **ν_{max} (cm^{-1})** 3320 (NH), 3088, 2924, 2873 (CH), 1600 (C=N), 1132 (C-O); **^{1}H NMR (400 MHz, $CDCl_3$)** δ 9.57 (s, 1H, 6), 7.91 (s, 1H, 3), 7.44 (d, *J* = 2.3 Hz, 1H, 21), 7.09 (d, *J* = 2.3 Hz, 1H, 20), 5.31 (d, *J* = 6.6 Hz, 1H, 11), 5.14 – 4.89 (m, 1H, 12), 4.12 – 4.06 (m, 2H, 14, 16), 4.04 (s, 3H), 3.99 – 3.92 (m, 1H, 16), 3.88 (td, *J* = 8.6, 5.8 Hz, 1H, 14), 2.54-2.45 (m, 1H, 13), 2.12 – 2.01 (m, 1H, 13); **^{13}C NMR (101 MHz, $CDCl_3$)** δ 151.32 (10), 150.12 (7), 144.34 (19), 136.58 (1), 135.76 (2), 131.02 (21), 130.16 (6), 124.99 (4), 122.45 (3), 117.87 (5), 106.81 (2), 74.16 (16), 67.26 (14), 52.90 (24), 39.52 (12), 33.65 (13); **LR-ESI-MS** $C_{16}H_{15}Cl_2N_5O$ [M+H^+] *m/z* found: 364.40, calc.: 364.230; **HR-ESI-MS** $C_{16}H_{15}Cl_2N_5O$ [M+H^+] *m/z* found: 363.9712, calc.: 364.0732.

6,7-dichloro-*N*-(cyclopropylmethyl)-4-(1-methyl-1*H*-pyrazol-3-yl)phthalazin-1-amine (72)

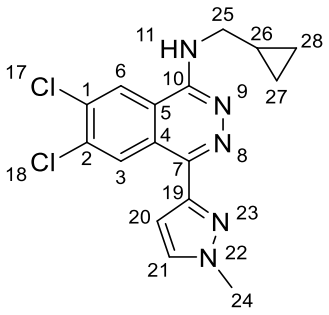

72

4,6,7-trichloro-N-(cyclopropylmethyl)phthalazin-1-amine (50 mg, 0.165 mmol, 1.0 eq.) was reacted with 1-methyl-1*H*-pyrazole-3-boronic acid pinacol ester (41.3 mg, 0.198 mmol, 1.2 eq.) according to **general procedure B** to yield **72** (30.1 mg, 52.3%) as a yellow solid. **M.P. =** 209-211 °C; **ν_{max} (cm^{-1})** 3240 (NH), 3063, 2979, 2862 (CH), 1698 (C=N); **^{1}H NMR (400 MHz, $CDCl_3$)** δ 9.52 (s, 1H, 6), 7.99 (s, 1H, 3), 7.43 (d, *J* = 2.3 Hz, 1H, 21), 7.05 (d, *J* = 2.3 Hz, 1H, 20), 5.44 (s, 1H, 11), 4.03 (s, 3H, 24), 3.58 (d, *J* = 7.1 Hz, 2H, 25), 2.09 (s, 1H, 26), 0.73 – 0.47 (m, 2H, 27, 28), 0.47 – 0.28 (m, 2H, 27, 28); **^{13}C NMR (101 MHz, $CDCl_3$)** δ 151.75 (10), 150.15 (7), 143.82 (19), 136.44 (1), 135.54 (2), 130.96 (21), 130.01 (6), 125.01 (4), 122.70 (3), 117.81 (5), 106.78 (20), 47.47 (25), 10.80 (26), 3.88 (27, 28); **LR-ESI-MS** $C_{16}H_{15}Cl_2N_5$ [M+H$^+$] *m/z* found: 348.35, calc.: 348.230; **HR-ESI-MS** $C_{16}H_{15}Cl_2N_5$ [M+H$^+$] *m/z* found: 347.9410, calc.: 348.0705.

6,7-dichloro-*N*-(1-cyclopropylethyl)-4-(1-methyl-1*H*-pyrazol-3-yl)phthalazin-1-amine (73)

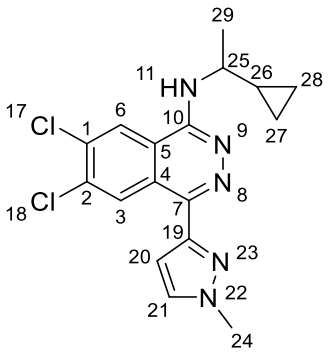

73

4,6,7-trichloro-N-(1-cyclopropylethyl)phthalazin-1-amine (50 mg, 0.158 mmol, 1.0 eq.) was reacted with 1-methyl-1*H*-pyrazole-3-boronic acid pinacol ester (39.4 mg, 0.190 mmol, 1.2 eq. according to **general procedure B** to yield **73** (49.2 mg, 86.0%) as a yellow solid. **M.P. =** 119-124 °C; **ν_{max} (cm^{-1})** 3319 (NH), 3091, 2969, 2929 (CH), 1602 (C=N); **^{1}H NMR (400 MHz, $CDCl_3$)** δ 9.52 (s, 1H, 6), 7.98 (s, 1H, 3), 7.41 (d, *J* = 2.2 Hz, 1H, 21), 7.05 (d, *J* = 2.3 Hz, 1H, 20), 5.36 (br, 1H, 11), 4.02 (s, 3H, 24), 1.40 (d, *J* = 6.4 Hz, 3H, 29), 1.07 (qt, *J* = 8.3, 4.9 Hz, 1H, 25), 0.62-0.54 (m, 1H, 27), 0.54 – 0.48 (m, 1H, 28), 0.48 – 0.40 (m, 1H, 27), 0.39 – 0.29 (m, 1H, 28); **^{13}C NMR (101 MHz, $CDCl_3$)** δ 151.30 (10), 150.20 (7), 143.54 (19), 136.29 (1), 135.38 (2), 130.91 (21), 129.94 (6), 125.09 (4), 122.67 (3), 117.79 (5), 106.67 (20), 52.08 (24), 39.43 (25), 24.97 (26), 17.82 (29), 3.82 (27), 3.43 (28); **LR-ESI-MS** $C_{16}H_{15}Cl_2N_5$ [M+H$^+$] *m/z* found: 362.39, calc.: 362.26; **HR-ESI-MS** $C_{16}H_{15}Cl_2N_5$ [M+H$^+$] *m/z* found: 361.9925, calc.: 362.0939.

6,7-dichloro-*N*-(1-cyclopropylethyl)-4-(1-(difluoromethyl)-1*H*-pyrazol-4-yl)phthalazin-1-amine (74)

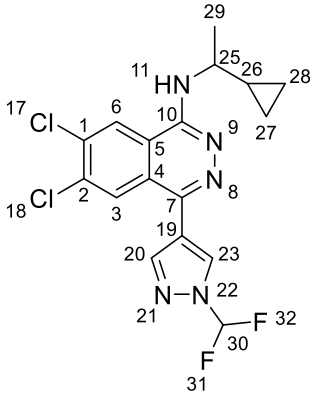

74

4,6,7-trichloro-N-(1-cyclopropylethyl)phthalazin-1-amine (50 mg, 0.158 mmol, 1.0 eq.) was reacted with 1-(difluoromethyl)pyrazole-4-boronic acid pinacol ester (46.2 mg, 0.190 mmol, 1.2 eq. according to **general procedure B** to yield **74** (39.6 mg, 63.0%) as an off-white solid. **M.P. =** 124-127 °C; **ν_{max} (cm^{-1})** 3329 (NH), 3077, 2999, 2931 (CH), 1602 (C=N), 1254 (C-F); **^{1}H NMR (400 MHz, $CDCl_3$)** δ 8.27 (s, 1H, 23), 8.14 (s, 1H, 6), 8.10 (s, 1H, 3), 8.04 (s, 1H, 20), 7.29

(t, *J* = 60.5 Hz, 1H, 30) 5.39 (s, 1H, 11), 3.96 (dp, *J* = 8.3, 6.4 Hz, 1H, 25), 1.42 (d, *J* = 6.3 Hz, 3H, 29), 1.17 – 1.03 (m, 1H, 26), 0.65 – 0.56 (m, 1H, 27), 0.57 – 0.50 (m, 1H, 28), 0.50 – 0.42 (m, 1H, 27), 0.42-0.30 (m, 1H, 28); **^{13}C NMR (101 MHz, $CDCl_3$)** δ 151.32 (10), 142.71 (7), 141.82 (t, *J* = 1.8 Hz, 23), 136.89 (1), 136.02 (2), 126.97 (19), 126.27 (6), 125.49 (4), 123.43 (3), 121.23 (20), 117.47 (5), 111.12 (t, *J* = 252.1 Hz, 30), 52.24 (25), 20.07 (26), 17.83 (29), 3.89 (27), 3.45 (28); **LR-ESI-MS** $C_{17}H_{15}Cl_2F_2N_5$ [M+H$^+$] *m/z* found: 398.39, calc.: 398.24; **HR-ESI-MS** $C_{17}H_{15}Cl_2F_2N_5$ [M+H$^+$] *m/z* found: 397.9636, calc.: 398.0751.

(4-(6,7-dichloro-4-((1-cyclopropylethyl)amino)phthalazin-1-yl)phenyl)methanol (75)

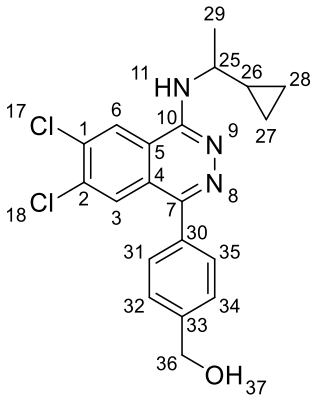

75

4,6,7-trichloro-N-(1-cyclopropylethyl)phthalazin-1-amine (50 mg, 0.158 mmol, 1.0 eq.) was reacted with 4-(hydroxymethyl)phenylboronic acid (28.8 mg, 0.190 mmol, 1.2 eq. according to **general procedure B** to yield **75** (23.6 mg, 38.5%) as a yellow foam. **ν_{max} (cm^{-1})** 3745 (br, OH), 3018 (CH), 1041 (C-O); **^{1}H NMR (400 MHz, $CDCl_3$)** δ 8.01 (d, *J* = 1.4 Hz, 2H, 3, 6), 7.61 (d, *J* = 8.1 Hz, 2H, 32, 34), 7.50 (d, *J* = 8.1 Hz, 2H, 31, 35), 5.29 (s, 1H, 11), 4.79 (s, 2H, 36), 3.98 (dp, *J* = 8.4, 6.4 Hz, 1H, 25), 1.43 (d, *J* = 6.4 Hz, 3H, 29), 1.10 (qt, *J* = 8.1, 4.9 Hz, 1H, 26), 0.65 – 0.57 (m, 1H, 27), 0.57-0.51 (m, 1H, 28), 0.51-0.43 (m, 1H, 27), 0.37 (dq, *J* = 9.4, 4.8 Hz, 1H, 28); **^{13}C NMR (101 MHz, $CDCl_3$)** δ 151.31 (10), 150.97 (33), 141.93 (7), 136.29 (30), 135.72 (1), 135.39 (2), 129.97 (32, 34), 128.32 (6), 127.19 (31, 35), 125.79 (4), 123.13 (3), 117.76 (5),

65.02 (36), 52.17 (25), 20.14 (26), 17.91 (29), 3.90 (27), 3.43 (28); **LR-ESI-MS** $C_{20}H_{19}Cl_2N_3O$ [M+H$^+$] *m/z* found: 388.41, calc.: 388.29; **HR-ESI-MS** $C_{20}H_{19}Cl_2N_3O$ [M+H$^+$] *m/z* found: 387.9895, calc.: 388.0984

***N*-(bicyclo[1.1.1]pentan-1-yl)-6,7-dichloro-4-(1-methyl-1*H*-pyrazol-3-yl)phthalazin-1-amine (76)**

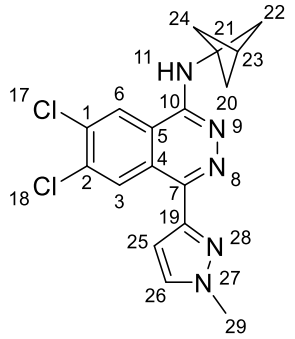

76

N-(bicyclo[1.1.1]pentan-1-yl)-4,6,7-trichlorophthalazin-1-amine (50 mg, 0.159 mmol, 1.0 eq.) was reacted with 1-methyl-1*H*-pyrazole-3-boronic acid pinacol ester (39.7 mg, 0.191 mmol, 1.2 eq.) according to **general procedure B** to yield **76** (43.2 mg, 75.5%) as a yellow solid. **M.P. =** 214-216 °C; **ν_{max} (cm^{-1})** 3299 (NH), 3090, 2988, 2873 (CH), 1601 (C=N); **^{1}H NMR (400 MHz, $CDCl_3$)** δ 9.51 (s, 1H, 6), 7.85 (s, 1H, 3), 7.44 (d, *J* = 2.3 Hz, 1H, 26), 7.11 (d, *J* = 2.3 Hz, 1H, 25), 5.57 (s, 1H, 11), 4.04 (s, 3H, 29), 2.58 (s, 1H, 23), 2.34 (s, 6H, 20, 22, 24); **^{13}C NMR (101 MHz, $CDCl_3$)** δ 151.92 (10), 150.09 (7), 144.41 (19), 136.36 (1), 135.63 (2), 130.97 (26), 130.11 (6), 125.05 (4), 122.36 (3), 117.62 (5), 106.96 (25), 52.85 (29), 50.82 (21), 39.51 (23), 25.35 (20, 22, 24); **LR-ESI-MS** $C_{17}H_{15}Cl_2N_5$ [M+H$^+$] *m/z* found: 360.49, calc.: 360.24; **HR-ESI-MS** $C_{17}H_{15}Cl_2N_5$ [M+H$^+$] *m/z* found: 359.9744, calc.: 360.07828.

***N*-(bicyclo[1.1.1]pentan-1-yl)-6,7-dichloro-4-(1-(difluoromethyl)-1*H*-pyrazol-4-yl)phthalazin-1-amine (77)**

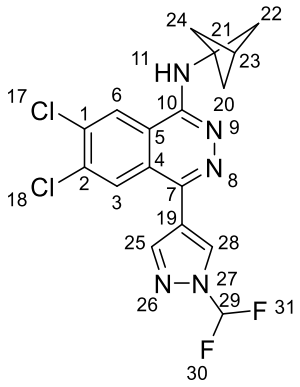

77

N-(bicyclo[1.1.1]pentan-1-yl)-4,6,7-trichlorophthalazin-1-amine (50 mg, 0.159 mmol, 1.0 eq.) was reacted with 1-(difluoromethyl)pyrazole-4-boronic acid pinacol ester (46.5 mg, 0.191 mmol, 1.2 eq.) according to **general procedure B** to yield **77** (48.7 mg, 77.3%) as a yellow solid. **M.P. =** 215-218 °C; **ν_{max} (cm^{-1})** 3240 (NH), 3094, 2989, 2874 (CH), 1673, 1603 (C=N), 1193 (C-F); **^{1}H NMR (400 MHz, $CDCl_3$)** δ 8.31 (s, 1H, 28), 8.14 (s, 1H, 6), 8.11 (s, 1H, 3), 7.99 (s, 1H, 25), 7.29 (t, *J* = 60.4 Hz, 1H, 29) 5.84 (s, 1H, 11), 2.58 (s, 1H, 23), 2.32 (s, 6H, 20, 22, 24); **^{13}C NMR (101 MHz, $CDCl_3$)** δ 151.96 (10), 143.40 (7), 141.79 (t, *J* = 1.9 Hz, 28), 137.00 (1), 136.30 (2), 127.06 (19), 126.50 (6), 125.42 (4), 123.43 (3), 121.06 (25), 117.39 (5), 111.12 (t, *J* = 251.7 Hz, 29), 52.81 (21), 27.05 (23), 25.43 (20, 22, 24); **LR-ESI-MS** $C_{17}H_{13}Cl_2F_2N_5$ [M+H$^+$] *m/z* found: 396.22, calc.: 396.31; **HR-ESI-MS** $C_{17}H_{13}Cl_2F_2N_5$ [M+H$^+$] *m/z* found: 395.9483, calc.: 396.0594

***N*-(bicyclo[1.1.1]pentan-1-yl)-6,7-dichloro-4-(3-methyl-1*H*-indazol-6-yl)phthalazin-1-amine (78)**

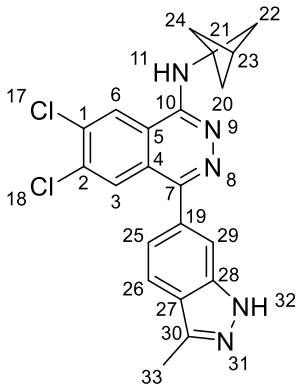

78

N-(bicyclo[1.1.1]pentan-1-yl)-4,6,7-trichlorophthalazin-1-amine (50 mg, 0.159 mmol, 1.0 eq.) was reacted with 3-methyl-1*H*-indazol-6-yl-6-boronic acid (33.6 mg, 0.191 mmol, 1.2 eq.) according to **general procedure B** to yield **78** (30.4 mg, 46.6%) as an off-white solid. **M.P. =** 254-256 °C; **ν_{max} (cm-^{1})** 3646, 3383 (NH), 2980, 2910, 2872 (CH), 1671, 1601 (C=N); **^{1}H NMR (400 MHz, DMSO)** δ 12.81 (s, 1H, 32), 8.78 (s, 1H, 6), 8.26 (s, 1H, 3), 7.90 (s, 1H, 29), 7.86 (d, *J* = 8.2 Hz, 1H, 11), 7.66 (t, *J* = 1.1 Hz, 1H, 26), 7.30 (dd, *J* = 8.3, 1.4 Hz, 1H, 25), 2.57 (s, 1H, 23), 2.56 (s, 3H, 33), 2.26 (s, 6H, 20, 22, 24); **^{13}C NMR (101 MHz, DMSO)** δ 152.19 (10), 150.52 (7), 141.23 (28), 140.72 (30), 134.44 (1), 133.86 (2), 127.21 (19), 125.39 (6), 124.98 (29), 122.11 (26), 121.32 (4), 119.98 (3), 117.12 (5), 110.99 (25), 52.20 (21), 50.47 (23), 25.09 (20, 22, 24), 11.76 (33); **LR-ESI-MS** $C_{17}H_{13}Cl_2F_2N_5$ [M+H$^+$] *m/z* found: 410.16, calc.: 410.30; **HR-ESI-MS** $C_{17}H_{13}Cl_2F_2N_5$ [M+H$^+$] *m/z* found: 409.9762, calc.: 410.0939

General Procedure H

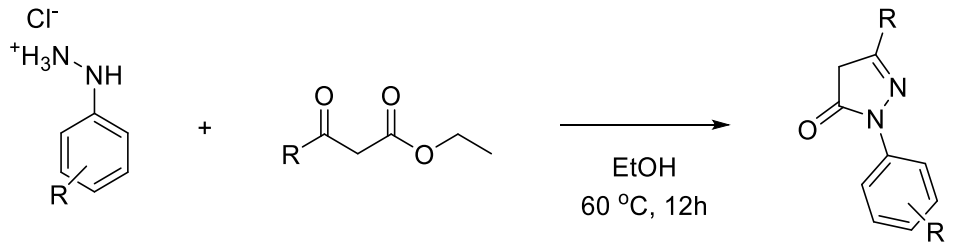

To a solution of β-keto ester (1.0 eq.) in ethanol (2 mL) at 0 °C was added aryl hydrazine hydrochloride (1.0 eq.) as a solution in ethanol (2 mL) and triethylamine (1.0 eq.) The mixture was allowed to reach room temperature and then heated with stirring at 60 °C overnight.

The solvent was removed *in vacuo* and the crude product purified using column chromatography (cyclohexane:EtOAc, 1:0 – 1:1) to yield the desired product.

General Procedure I

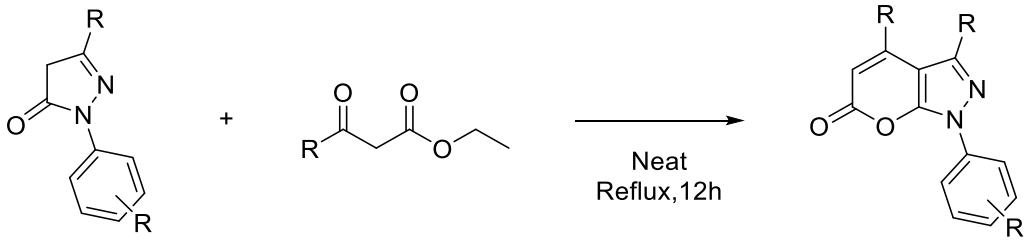

To a 4 mL vial equipped with stirrer bar containing pyrazolone (1.0 eq.) was added β-keto ester (5.0 eq.). The mixture was heated to reflux and left stirring overnight.

The excess β-keto ester was removed *in vacuo* and the crude product taken up in DCM. The organic phase was washed with H_2O (5 x 10 mL) and dried over sodium sulfate. The crude product was purified using column chromatography (cyclohexane:EtOAc, 1:1 – 0:1) to give the desired product.

2-chloro-5-(4-methyl-6-oxo-3-phenylpyrano[2,3-*c*]pyrazol-1(6*H*)-yl)benzoic acid (79)

Step 1: 2-chloro-5-(5-oxo-3-phenyl-4,5-dihydro-1*H*-pyrazol-1-yl)benzoic acid

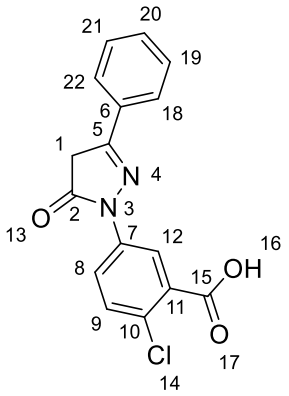

2-Chloro-5-hydrazinylbenzoic acid hydrochloride (200 mg, 0.897 mmol, 1.0 eq.) was reacted with ethyl benzoylacetate (0.155 mL, 0.897 mmol, 1.0 eq.) according to **general procedure H** to yield 2-chloro-5-(5-oxo-3-phenyl-4,5-dihydro-1*H*-pyrazol-1-yl)benzoic acid (211.3 mg, 74.9%) as a yellow solid. **^{1}H NMR (400 MHz, MeOD)** δ 8.33 (d, *J* = 2.7 Hz, 1H, 12), 7.97 (dd, *J* = 8.8, 2.7 Hz, 1H, 8), 7.82 – 7.75 (m, 2H, 18, 22), 7.59 (d, *J* = 8.8 Hz, 1H, 9), 7.45 – 7.39 (m, 2H, 19, 21), 7.38 – 7.33 (m, 1H, 20), 1.45 (s, 2H, 1); **^{13}C NMR (101 MHz, MeOD)** δ 168.30 (2), 157.24 (15), 153.37 (5), 138.43 (7), 133.64 (6), 132.69 (11), 132.55 (9), 129.78 (20), 129.72 (19, 21), 127.39 (10), 126.79 (18, 22), 126.23 (12), 124.94 (8), 27.97 (1); **LR-ESI-MS** $C_{16}H_{11}ClN_2O_3$ [M+H$^+$] *m/z* found: 315.06, calc.: 314.73

Step 2: 2-chloro-5-(4-methyl-6-oxo-3-phenylpyrano[2,3-*c*]pyrazol-1(6*H*)-yl)benzoic acid (**79**)

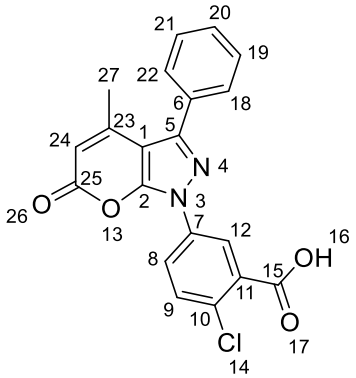

79

2-chloro-5-(5-oxo-3-phenyl-4,5-dihydro-1*H*-pyrazol-1-yl)benzoic acid (100.0 mg, 0.318 mmol, 1.0 eq.) was reacted with ethylacetoacetate (0.201 mL, 1.589 mmol, 5.0 eq.) according to **general procedure I** to yield **79** (99.3 mg, 82.1%) as a brown gum. **ν_{max} (cm^{-1})** 3030 (C=C-H), 2921, 2844 (CH), 1721 (C=O), 1600 (C=N); **^{1}H NMR (400 MHz, $CDCl_3$)** δ 8.60 (d, *J* = 2.7 Hz, 1H, 12), 8.12 (dd, *J* = 8.8, 2.7 Hz, 1H, 8), 7.63 (d, *J* = 8.8 Hz, 1H, 9), 7.60-7.56 (m, 2H, 18-22), 7.54 – 7.48 (m, 3H, 19, 20, 21), 5.96 (s, 1H, 24), 2.20 (s, 3H, 27); **^{13}C NMR (101 MHz, $CDCl_3$)** δ 159.47 (15), 153.89 (25), 150.45 (2), 148.98 (5), 135.57 (7), 133.39 (6), 132.73 (11), 132.65 (9), 132.03 (23), 129.72 (20), 129.63 (19, 21), 128.69 (18, 22), 126.12 (10) 125.26 (12), 124.45 (8), 106.88 (1), 102.69 (24), 20.67 (27); **LR-ESI-MS** $C_{20}H_{13}ClN_2O_4$ [M+H$^+$] *m/z* found: 381.39, calc.: 380.780; **HR-ESI-MS** $C_{20}H_{13}ClN_2O_4$ [M+H$^+$] *m/z* found: 380.9579, calc.: 381.0642.

3-(4-methyl-6-oxo-3-phenylpyrano[2,3-*c*]pyrazol-1(6*H*)-yl)benzoic acid (80)

Step 1: 3-(5-oxo-3-phenyl-4,5-dihydro-1H-pyrazol-1-yl)benzoic acid

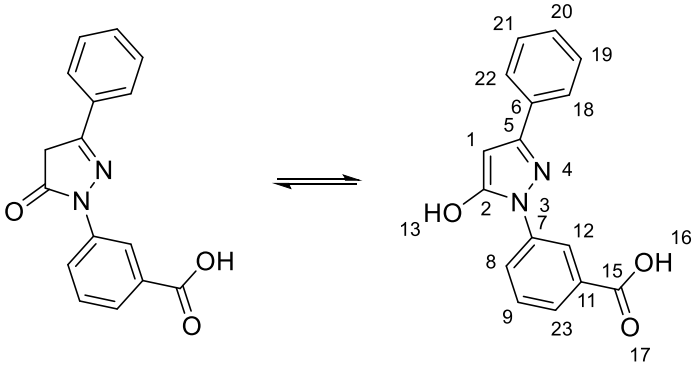

3-hydrazinobenzoic acid hydrochloride (200.0 mg, 1.060 mmol, 1.0 eq.) was reacted with ethyl benzoylacetate (0.183 mL, 1.060 mmol) according to **general procedure H** to yield 3-(5-oxo-3-phenyl-4,5-dihydro-1*H*-pyrazol-1-yl)benzoic acid (189.1 mg, 63.6%) as a white solid. **^{1}H NMR (400 MHz, DMSO)** δ 13.12 (s, 1H, 16), 12.08 (s, 1H, 13), 8.43 (t, *J* = 1.9 Hz, 1H, 12), 8.16 – 8.05 (m, 1H, 23), 7.89 – 7.82 (m, 3H, 18, 22, 8), 7.61 (t, *J* = 8.0 Hz, 1H, 9), 7.47 – 7.39 (m, 2H, 19, 21), 7.37 – 7.30 (m, 1H, 20), 6.05 (s, 1H, 1**); ^{13}C NMR (101 MHz, DMSO**) δ 166.93 (15), 150.04 (5), 139.09 (7), 133.20 (6) 131.59 (11), 129.40 (19, 21), 128.62 (18,22), 128.03 (20),

126.23 (9), 125.19 (23), 124.84 (8), 121.25 (12), 85.34 (1); **LR-ESI-MS** $C_{16}H_{12}N_2O_3$ [M-H$^+$] *m/z* found: 279.04, calc.: 279.23

Step 2: 3-(4-methyl-6-oxo-3-phenylpyrano[2,3-*c*]pyrazol-1(6*H*)-yl)benzoic acid (**80**)

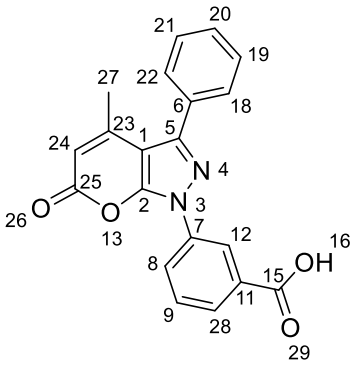

80

3-(5-oxo-3-phenyl-4,5-dihydro-1*H*-pyrazol-1-yl)benzoic acid (100.0 mg, 0.357 mmol, 1.0 eq.) was reacted with ethyl acetoacetate (0.226 mL, 1.784 mmol, 5.0 eq.) according to **general procedure I** to yield **80** (87.6 mg, 70.9%) as an off-white foam. **ν_{max} (cm^{-1})** 3060 (C=C-H), 2961, 2920 (CH), 1717 (C=O), 1688 (C=N); **^{1}H NMR (400 MHz, $CDCl_3$)** δ 8.65 (s, 1H, 12), 8.17 (br, 1H, 28), 8.07 (br, 1H, 8), 7.58 (br, 3H, 9, 18, 22), 7.48 (br, 3H, 19, 20, 21), 5.89 (s, 1H, 24), 2.17 (s, 3H, 27); **^{13}C NMR (101 MHz, $CDCl_3$)** δ 160.90 (15), 159.39 (25), 153.49 (2), 150.50 (5), 150.37 (7), 137.28 (23), 133.39 (6), 132.43 (11), 132.43 (9), 129.68 (19, 21), 129.45 (20), 129.12 (28), 128.59 (18, 22), 125.33 (8), 121.84 (12), 106.73 (24), 103.41 (1) 20.66 (27); **LR-ESI-MS** $C_{20}H_{14}N_2O_4$ [M+H$^+$] *m/z* found: 347.11, calc.: 346.34; **HR-ESI-MS** $C_{20}H_{14}N_2O_4$ [M+H$^+$] *m/z* found: 347.0063, calc.: 347.1032.

3-(6-oxo-3-phenyl-4-(trifluoromethyl)pyrano[2,3-*c*]pyrazol-1(6*H*)-yl)benzoic acid (81)

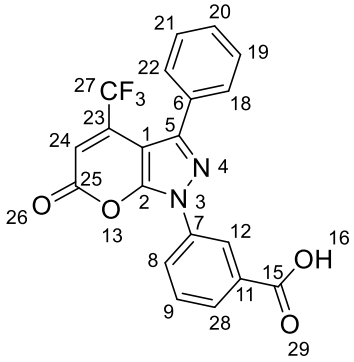

81

3-(5-oxo-3-phenyl-4,5-dihydro-1*H*-pyrazol-1-yl)benzoic acid (100.0 mg, 0.357 mmol, 1.0 eq.) was reacted with ethyl 4,4,4-trifluoroacetoacetate (0.261 mL, 1.784 mmol, 5.0 eq.) according to **general procedure I** to yield **81** (71.1 mg, 49.8%) as a yellow solid. **M.P. =** 217-219 °C; **ν_{max} (cm^{-1})** 3027 (C=C-H), 2891, 2812, (CH), 1756 (C=O), 1601 (C=N), 1257 (C-F); **^{1}H NMR (400 MHz, $CDCl_3$)** δ 8.66 (t, *J* = 1.9 Hz, 1H, 12), 8.26 – 8.10 (m, 2H, 28, 8), 7.67 (t, *J* = 8.0 Hz, 1H, 9), 7.52 (dt, *J* = 7.6, 1.9 Hz, 2H, 18, 22), 7.50 – 7.46 (m, 2H, 19, 21), 7.45 – 7.36 (m, 1H, 20), 6.50 (s, 1H, 24); **^{13}C NMR (101 MHz, $CDCl_3$)** δ 172.18 (15), 170.56 (25), 157.53 (2), 151.21 (5), 148.09 (7), 141.20 (6), 140.84 (11), 136.80 (9), 131.07 (23), 130.03 (28), 129.77 (20), 129.63 (19, 21), 128.23 (18, 22), 127.23 (q, *J* = 346 Hz, 27) 126.31 (8), 123.16 (23), 107.47 (q, *J* = 5.7 Hz, 24), 96.61 (1); **LR-ESI-MS** $C_{20}H_{11}F_3N_2O_4$ [M+H$^+$] *m/z* found: 401.40, calc.: 400.313; **HR-ESI-MS** $C_{20}H_{11}F_3N_2O_4$ [M+H$^+$] *m/z* found: 400.9628, calc.: 401.0749.

4-methyl-3-phenyl-1-(4-(trifluoromethoxy)phenyl)pyrano[2,3-*c*]pyrazol-6(1*H*)-one (82)

Step 1: 5-phenyl-2-(4-(trifluoromethoxy)phenyl)-2,4-dihydro-3*H*-pyrazol-3-one

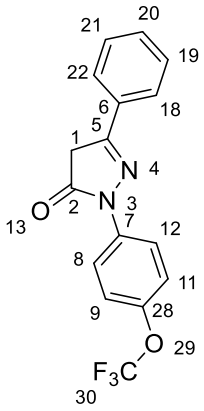

4-(Trifluoromethoxy)phenylhydrazine hydrochloride (200.0 mg, 0.875 mmol, 1.0 eq.) was reacted with ethyl benzoylacetate (0.151 mL, 0.875 mmol, 1.0 eq.) according to **general procedure H** to yield 5-phenyl-2-(4-(trifluoromethoxy)phenyl)-2,4-dihydro-3*H*-pyrazol-3-one (245.0 mg, 87.4%) as an off-white solid. **^{1}H NMR (400 MHz, $CDCl_3$)** δ 8.03 – 7.96 (m, 2H, 9, 11), 7.78 – 7.69 (m, 2H, 19, 21), 7.49 – 7.42 (m, 2H, 8, 12), 7.28 – 7.24 (m, 1H, 20), 7.15-7.05 (m, 2H, 18, 22), 3.79 (s, 2H, 1); **^{13}C NMR (101 MHz, $CDCl_3$)** δ 170.24 (2), 155.11 (28), 149.59 (5), 136.64 (7), 131.01 (6), 130.56 (q, *J* = 227.9 Hz, 30), 129.01 (19, 21), 128.31 (20), 126.04 (18, 22), 121.57 (8, 12), 120.10 (9, 11), 39.60 (1); **LR-ESI-MS** $C_{16}H_{11}F_3N_2O_2$ [M+H$^+$] *m/z* found: 321.120, calc.: 321.12.

Step 2: 4-methyl-3-phenyl-1-(4-(trifluoromethoxy)phenyl)pyrano[2,3-*c*]pyrazol-6(1*H*)-one (**82**)

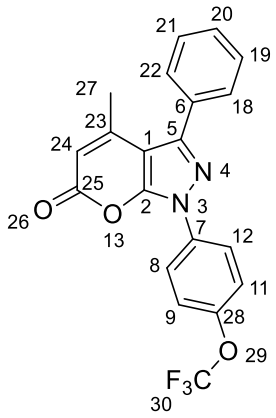

82

5-phenyl-2-(4-(trifluoromethoxy)phenyl)-2,4-dihydro-3*H*-pyrazol-3-one (35.0 mg, 0.109 mmol, 1.0 eq.) was reacted with ethyl acetoacetate (0.138 mL, 1.093 mmol, 5.0 eq.) according to **general procedure I** to yield **82** (17.1 mg, 40.5%) as a brown gum. **ν_{max} (cm^{-1})** 3027 (C=C-H), 2891, 2812, (CH), 1756 (C=O), 1601 (C=N) **^{1}H NMR (400 MHz, $CDCl_3$)** δ 8.07 – 7.96 (m, 2H, 9, 11), 7.62-7.55 (m, 2H, 19, 21), 7.54 – 7.45 (m, 3H, 8, 12, 20), 7.39 – 7.32 (m, 2H, 18, 22), 5.91 (q, *J* = 1.2 Hz, 1H, 24), 2.19 (d, *J* = 1.2 Hz, 3H, 27); **^{13}C NMR (101 MHz, $CDCl_3$)** δ 159.25 (25), 153.51 (28), 150.40 (2), 148.53 (5), 148.01 (7), 135.52 (6), 132.46 (30), 129.64 (19, 21), 129.52 (20), 128.64 (18, 22), 122.43 (8, 12), 122.15 (9, 11), 106.69 (24), 102.37 (1), 20.65 (27); **LR-ESI-MS** $C_{20}H_{13}F_3N_2O_3$ [M+H^+] *m/z* found: 387.48, calc.: 386.330; **HR-ESI-MS** $C_{20}H_{13}F_3N_2O_3$ [M+H^+] *m/z* found: 386.9872, calc.: 387.0966.

3-(3-methoxyphenyl)-4-methyl-1-(4-(trifluoromethoxy)phenyl)pyrano[2,3-*c*]pyrazol-6(1*H*)-one (83)

Step 1: 5-(3-methoxyphenyl)-2-(4-(trifluoromethoxy)phenyl)-2,4-dihydro-3*H*-pyrazol-3-one

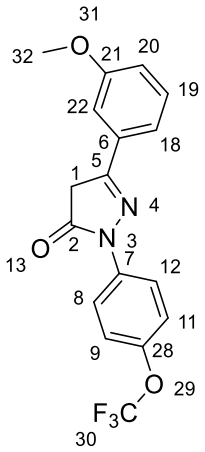

4-(Trifluoromethoxy)phenylhydrazine hydrochloride (200.0 mg, 0.875 mmol, 1.0 eq.) was reacted with 3-(3-methoxyphenyl)-3-oxo-propionic acid methyl ester (0.195 mL, 0.875 mmol, 1.0 eq.) according to **general procedure H** to yield 5-(3-methoxyphenyl)-2-(4-(trifluoromethoxy)phenyl)-2,4-dihydro-3*H*-pyrazol-3-one (278.0 mg, 90.7%) as a white solid. **^{1}H NMR (400 MHz, $CDCl_3$)** δ 8.01 – 7.93 (m, 2H, 9, 11), 7.32 (t, *J* = 7.9 Hz, 1H, 19), 7.26 (br, 1H, 18), 7.24 – 7.20 (m, 3H, 8, 12, 20), 6.96 (ddd, *J* = 8.3, 2.6, 1.0 Hz, 1H, 22), 3.82 (s, 3H, 32), 3.71 (s, 2H, 1); **^{13}C NMR (101 MHz, $CDCl_3$)** δ 170.30 (2), 160.05 (28), 155.06 (21), 146.10 (5), 136.71 (7), 131.91 (6), 130.14 (30), 122.55 (9, 11), 121.61 (19), 120.14 (8, 12), 118.82 (18), 116.83 (20), 111.02 (22), 55.48 (31), 39.72 (1); **LR-ESI-MS** $C_{17}H_{13}F_3N_2O_3$ [M+H$^+$] *m/z* found: 351.120, calc.: 350.297.

Step 2: 3-(3-methoxyphenyl)-4-methyl-1-(4-(trifluoromethoxy)phenyl)pyrano[2,3-*c*]pyrazol-6(1*H*)-one (**83**)

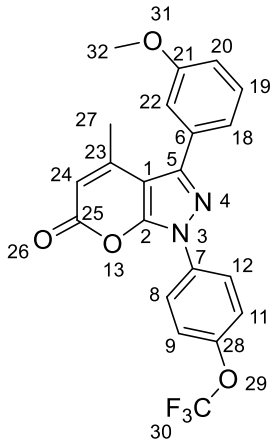

83

5-(3-methoxyphenyl)-2-(4-(trifluoromethoxy)phenyl)-2,4-dihydro-3*H*-pyrazol-3-one (100.0 mg, 0.285 mmol, 1.0 eq.) was reacted with ethyl acetoacetate (0.181 mL, 1.427 mmol, 5.0 eq.) according to **general procedure I** to yield **83** (44.5 mg, 37.4%) as a brown gum. **ν_{max} (cm^{-1})** 3029 (C=C-H), 2919, 2878, 2799 (CH), 1710 (C=O), 1598 (C=N), 1263 (C-O); 1175 (C-F), **^{1}H NMR (400 MHz, $CDCl_3$)** δ 8.07 – 7.97 (m, 2H, 9, 11), 7.43 – 7.38 (m, 1H, 19), 7.38 – 7.32 (m, 2H, 8, 12), 7.15 (dt, *J* = 7.5, 1.2 Hz, 1H, 18), 7.12-7.09 (m, 1H, 20), 7.03 (ddd, *J* = 8.3, 2.7, 1.0 Hz, 1H, 22), 5.91 (q, *J* = 1.2 Hz, 1H, 24), 3.87 (s, 3H, 32), 2.21 (d, *J* = 1.2 Hz, 3H, 27); **^{13}C NMR (101 MHz, $CDCl_3$)** δ 159.67 (25), 159.22 (28), 153.52 (21), 150.35 (2), 148.35 (5), 148.03 (7), 135.49 (6), 133.68 (30), 129.70 (19), 122.44 (9, 11), 122.13 (d, 2C, 18, 20), 122.08 (22), 115.15 (8, 12), 106.71 (24), 102.34 (1), 55.53 (32), 27.05 (27); **LR-ESI-MS** $C_{21}H_{15}F_3N_2O_4$ [M+H^+] *m/z* found: 417.06, calc.: 416.356; **HR-ESI-MS** $C_{21}H_{15}F_3N_2O_4$ [M+H^+] *m/z* found: 416.9900, calc.: 417.1062.

1-(6-chloropyridazin-3-yl)-4-methyl-3-phenylpyrano[2,3-*c*]pyrazol-6(1*H*)-one (84)

Step 1: 2-(6-chloropyridazin-3-yl)-5-phenyl-2,4-dihydro-3*H*-pyrazol-3-one

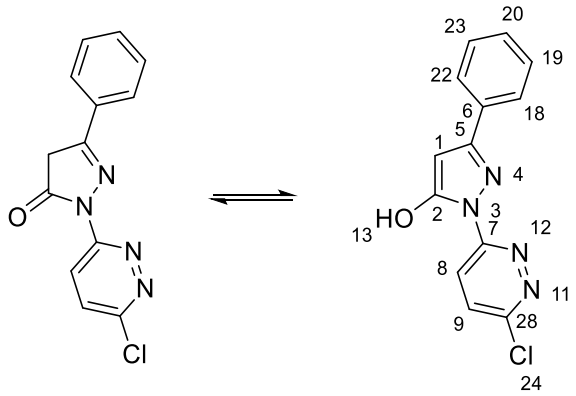

3-Chloro-6-hydrazinopyridazine hydrochloride (200.0 mg, 1.384 mmol, 1.0 eq) was reacted with ethyl benzoylacetate (0.239 mL, 1.384 mmol, 1.0 eq.) according **general procedure H** to yield 2-(6-chloropyridazin-3-yl)-5-phenyl-2,4-dihydro-3*H*-pyrazol-3-one (307.6 mg, 81.5%) as a yellow solid**. ^{1}H NMR (400 MHz, $CDCl_3$)** δ 11.50 (s, 1H, 13), 8.40 – 8.14 (m, 1H, 9), 7.83 (d, *J* = 7.3 Hz, 2H, 18, 22), 7.69 (d, *J* = 9.3 Hz, 1H, 8), 7.51 – 7.33 (m, 3H, 19, 23, 20), 6.02 (s, 1H, 1); **^{13}C NMR (101 MHz, $CDCl_3$)** δ 154.79 (2), 153.14 (28), 136.02 (5) 132.17 (7), 132.06 (6), 129.46 (9), 128.89 (18, 22), 127.61 (20), 126.11 (19, 23), 120.75 (8); **LR-ESI-MS** $C_{13}H_9ClN_4O$ [M+H$^+$] *m/z* found: 273.030, calc.: 272.690.

Step 2: 1-(6-chloropyridazin-3-yl)-4-methyl-3-phenylpyrano[2,3-*c*]pyrazol-6(1*H*)-one (**84**)

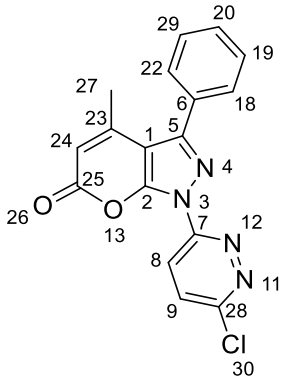

84

2-(6-chloropyridazin-3-yl)-5-phenyl-2,4-dihydro-3*H*-pyrazol-3-one (100.0 mg, 0.367 mmol, 1.0 eq.) was reacted with ethyl acetoacetate (0.232 mL, 1.834 mmol, 5.0 eq.) according to **general procedure I** to yield **84** (77.9 mg, 62.7%) as a yellow solid. **M.P. =** 226-230 °C; **ν_{max} (cm^{-1})** 3058 (C=CH), 2972, 2921, 2865, (CH), 1730 (C=O), 1597, 1579 (C=N); **^{1}H NMR (400 MHz, $CDCl_3$)** δ 8.12 (d, *J* = 9.2 Hz, 1H, 9), 7.68 (d, *J* = 9.2 Hz, 1H, 8), 7.60-7.54 (m, 2H, 18, 22), 7.55 – 7.43 (m, 3H, 19, 20), 5.98 (q, *J* = 1.4 Hz, 1H, 24), 2.17 (d, *J* = 1.3 Hz, 3H, 27); **^{13}C NMR (101 MHz, $CDCl_3$)** δ 158.79 (25), 155.59 (28), 153.55 (2), 152.45 (7), 150.48 (5), 131.94 (6), 130.56 (9), 129.87 (8), 129.57 (18, 22), 128.70 (19, 29), 122.17 (20), 108.17 (24), 103.35 (1), 20.59 (27); **LR-ESI-MS** $C_{17}H_{11}ClN_4O_2$ [M+H^+] *m/z* found: 339.340, calc.: 338.750; **HR-ESI-MS** $C_{17}H_{11}ClN_4O_2$ [M+H^+] *m/z* found: 338.9701, calc.: 339.0649.

4-methyl-1-phenyl-3-(*p*-tolyl)pyrano[2,3-*c*]pyrazol-6(1*H*)-one (85)

Step 1: 2-phenyl-5-(*p*-tolyl)-2,4-dihydro-3*H*-pyrazol-3-one

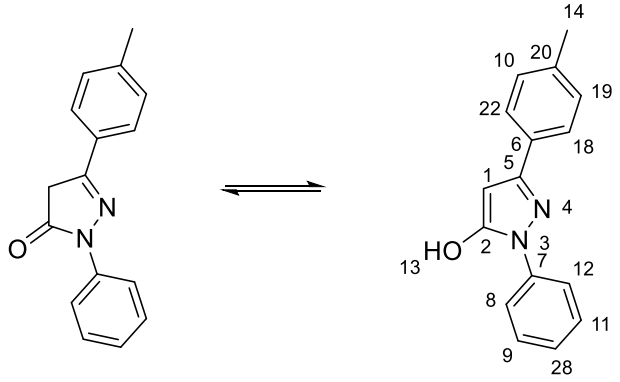

Phenylhydrazine hydrochloride (200.0 mg, 1.383 mmol, 1.0 eq.) was reacted with ethyl (4-methyl)benzoyl acetate (0.297 mL, 1.383 mmol, 1.0 eq.) according to **general procedure H** to yield 2-phenyl-5-(*p*-tolyl)-2,4-dihydro-3*H*-pyrazol-3-one (332.0 mg, 95.9%) as a white solid. **^{1}H NMR (400 MHz, DMSO)** δ 11.75 (s, 1H, 13), 7.81 (dt, *J* = 8.6, 1.7 Hz, 2H, 22, 18), 7.75 – 7.65 (m, 2H, 10, 19), 7.52 – 7.44 (m, 2H, 18, 12), 7.33 – 7.26 (m, 1H, 28), 7.26 – 7.19 (m, 2H, 9, 11), 5.97 (s, 1H, 1), 2.33 (s, 3H, 14); **^{13}C NMR (101 MHz, DMSO)** δ 153.68 (2), 149.60 (5), 138.89

(7), 137.07 (6), 130.64, 129.40, 129.10 (8, 12), 128.87 (18, 22), 125.53 (28), 125.02 (9, 11), 121.01 (19, 10), 118.28 (20), 84.90 (1), 20.86 (14); **LR-ESI-MS** $C_{16}H_{14}N_2O$ [M+H$^+$] *m/z* found: 251.110, calc.: 250.301

Step 2: 4-methyl-1-phenyl-3-(*p*-tolyl)pyrano[2,3-*c*]pyrazol-6(1*H*)-one (**85**)

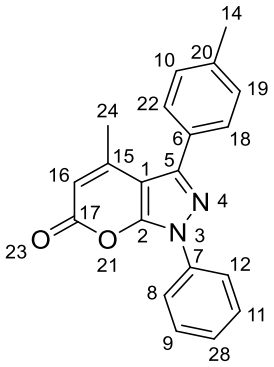

85

2-phenyl-5-(*p*-tolyl)-2,4-dihydro-3*H*-pyrazol-3-one (100.0 mg, 0.400 mmol, 1.0 eq.) was reacted with ethyl acetoacetate (0.253 mL, 2.000 mmol, 5.0 eq.) according to **general procedure I** to yield **85** (82.7 mg, 65.4%) as a brown solid. **M.P. =** 261-263 °C; **ν_{max} (cm^{-1})** 3027 (C=C-H), 2891, 2812, (CH), 1756 (C=O), 1601 (C=N) **^{1}H NMR (400 MHz, $CDCl_3$)** δ 7.99 – 7.92 (m, 2H, 8, 12), 7.53 – 7.46 (m, 4H, 18, 22, 9, 11), 7.36 (tt, *J* = 7.7, 1.2 Hz, 1H, 28), 7.29 (d, *J* = 7.8 Hz, 2H, 10, 19), 5.88 (d, *J* = 1.3 Hz, 1H, 16), 2.43 (s, 3H, 14), 2.20 (d, *J* = 1.2 Hz, 3H, 24); **^{13}C NMR (101 MHz, $CDCl_3$)** δ 159.64 (17), 153.66 (2), 150.33 (5), 148.20 (7), 139.33 (6), 137.06 (28), 129.56 (8, 12), 129.52 (18, 22), 129.25 (9, 11), 127.58 (20), 121.21 (10, 19), 106.37 (16), 102.25 (1), 21.53 (14), 20.66 (24); **LR-ESI-MS** $C_{20}H_{16}N_2O_2$ [M+H$^+$] *m/z* found: 317.38, calc.: 316.360; **HR-ESI-MS** $C_{20}H_{16}N_2O_2$ [M+H$^+$] *m/z* found: 317.0405, calc.: 317.1290.

3-(3-methoxyphenyl)-4-methyl-1-phenylpyrano[2,3-*c*]pyrazol-6(1*H*)-one (86)

Step 1: 5-(3-methoxyphenyl)-2-phenyl-2,4-dihydro-3*H*-pyrazol-3-one

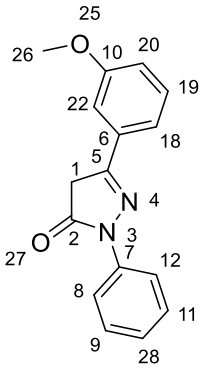

Phenylhydrazine hydrochloride (200.0 mg, 1.383 mmol, 1.0 eq.) was reacted with 3-(3-methoxyphenyl)-3-oxo-propionic acid methyl ester (0.280 mL, 1.383 mmol, 1.0 eq.) according to **general procedure H** to yield 5-(3-methoxyphenyl)-2-phenyl-2,4-dihydro-3*H*-pyrazol-3-one (311.2 mg, 84.5%) as a white solid. **^{1}H NMR (400 MHz, $CDCl_3$)** δ 8.01 – 7.91 (m, 2H), 7.47 – 7.40 (m, 2H, 9, 11), 7.37 – 7.33 (m, 2H, 20, 28), 7.28 (dt, *J* = 7.7, 1.2 Hz, 1H, 19), 7.25 – 7.18 (m, 1H, 18), 7.00 (ddd, *J* = 8.3, 2.5, 1.0 Hz, 1H, 22), 3.87 (s, 3H, 26), 3.82 (s, 2H, 1); **^{13}C NMR (101 MHz, $CDCl_3$)** δ 170.36 (2), 160.09 (10), 154.67 (5), 138.21 (7), 132.28 (6), 130.11 (19), 129.00 (8, 12), 125.48 (18), 119.26 (9, 11), 118.87 (20), 116.80 (22), 110.92 (28), 55.57 (26), 39.87 (1); **LR-ESI-MS** $C_{16}H_{14}N_2O_2$ [M+H$^+$] *m/z* found: 267.110, calc.: 266.300.

Step 2: 3-(3-methoxyphenyl)-4-methyl-1-phenylpyrano[2,3-*c*]pyrazol-6(1*H*)-one (**86**)

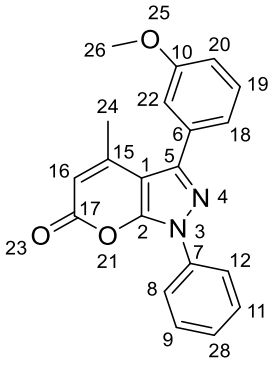

86

5-(3-methoxyphenyl)-2-phenyl-2,4-dihydro-3*H*-pyrazol-3-one (100.0 mg, 0.376 mmol, 1.0 eq.) was reacted with ethyl acetoacetate (0.237 mL, 1.878 mmol, 5.0 eq.) according to **general procedure I** to yield **86** (77.1 mg, 61.8%) as a yellow gum. **ν_{max} (cm^{-1})** 3047 (C=CH), 2921, 2872 (CH), 1715 (C=O), 1584 (C=N), 1231 (C-O); **^{1}H NMR (400 MHz, $CDCl_3$)** δ 7.97 – 7.91 (m, 2H, 8, 12), 7.55 – 7.48 (m, 2H, 9, 11), 7.46 – 7.40 (m, 1H, 28), 7.40 – 7.34 (m, 2H, 19, 20), 7.19 – 7.15 (m, 1H, 18), 7.02 (ddd, *J* = 8.3, 2.6, 1.0 Hz, 2H, 22), 5.90 (q, *J* = 1.2 Hz, 1H, 16), 3.87 (s, 3H, 26), 2.21 (d, *J* = 1.2 Hz, 2H, 24); ^{13}C NMR (101 MHz, $CDCl_3$) δ 159.66 (17), 159.55 (10), 153.51 (2), 150.33 (5), 147.96 (7), 137.03 (6), 133.97 (19), 129.63 (28), 129.54 (8, 12), 127.68 (18), 122.18 (20), 121.28 (9, 11), 115.11 (22), 106.56 (16), 102.24 (1), 55.54 (26), 20.65 (24); **LR-ESI-MS** $C_{20}H_{16}N_2O_3$ [M+H$^+$] *m/z* found: 333.400, calc.: 332.359;**HR-ESI-MS** $C_{20}H_{16}N_2O_3$ [M+H$^+$] *m/z* found: 333.0315, calc.: 332.1239.

7.2.2 CNS MPO Score Calculation

*CNS MPO Scores were calculated with the aid of **Tamas Szommer** at the Target Discovery Institute, University of Oxford.*

Compound structures were represented as a SMILES string and their physiochemical properties calculated using the ChemAxon cxcalc module. Each of the six parameters contributing to the CNS MPO score (clogP, clogD, MW, tPSA, HBD, and pK_a) was given a score between 0-1 based on the scales defined by Wager *et al.*[1] The scores were summed to give an overall CNS MPO score out of 6.

7.2.3 Biological Assays

7.2.3.1 IC_{50} Determination by Scintillation Proximity Assay

*Scintillation proximity assays were carried out by **Dr Fengling Li** and **Professor Masoud Vedadi** at the University of Toronto.*

IC_{50} values were determined for compounds at 30 nM of SUV4-20H1 ((69-335 aa) or 250 nM SUV4-20H2 (2 –248 aa), 3 µM of biotinylated H4(1-24)K20me1 peptide, and 10 µM of [^{3}H]SAM in assay buffer (20 mM Tris pH8.0 , 0.01% Triton X-100, 5 mM DTT). The reaction mixtures were incubated for 1 hr at 23 °C. To stop the enzymatic reactions, 10 µl of 7.5 M Guanidine hydrochloride was added, followed by 180 µl of buffer (20 mM Tris, pH 8.0), mixed and then transferred to a FlashPlate (Cat.# SMP103; Perkin Elmer; www.perkinelmer.com). After mixing, the reaction mixtures in the FlashPlate were incubated for another 2 hrs at 23 °C and the CPM counts measured using Topcount plate reader (Perkin Elmer, www.perkinelmer.com). The CPM counts in the absence of compound for each data set were defined as 100% activity. In the absence of the enzyme, the CPM counts in each data set were defined as background (0%). IC_{50} values were determined using GraphPad Prism 7 software.

7.2.3.2 FXN-Luciferase Co-Expression Assay

*Biological assays were carried out by of **Dr Gabriela Vilema-Enriquez*** and ***Saumya Maheshwari** at the Department of Physiology, Anatomy, and Genetics (DPAG), University of Oxford.*

Cell culture

HEK293 reporter lines transfected with either a pBAC-*FXN-Luc* vector or pBAC-*FXN*-GAA-*Luc* vector were cultured in a 5% CO_2 atmosphere at 37°C in media containing: high glucose Dulbecco's Modified Eagle Medium (DMEM), 10% fetal bovine serum (FBS), 1% L-Glutamine,

1% penicillin-streptomycin, 100 mg/mL hygromycin B (Life Technologies). Sub-culture of adherent cells was performed as follows: cells were rinsed with phosphate buffered saline (PBS) and then incubated for five minutes with trypsin-EDTA. The trypsin was neutralised with media containing FBS before cells were spun (1500 RPM, 5 mins) and re-suspended at the desired concentration in medium. Suspension cells were directly spun (1500 RPM, 5 mins) and seeded accordingly. Cells growing in suspension were regularly passaged by dilution in fresh medium in order to achieve a concentration of 250000 cells/mL.

Assessment of Frataxin-Luciferase Expression

pBAC-*FXN*-GAA-*Luc* cells were seeded in a 96-well plate at a density of 1.5 x 10^3 in duplicate and allowed to recover overnight. Cells were then treated with compounds at 5 µM in media for six days. Cells were washed in PBS and lysed directly onto the plate using the Cell Culture Lysis Reagent from the Luciferase Assay System (Promega). Lysates were transferred to microcentrifuge tubes, vortexed for 15 seconds and then centrifuged (10000 RPM, 15 secs.). 25 µl of supernatant was transferred to a white, opaque 96-well microplate (PerkinElmer). Luciferase activity was determined by measuring luminescence with a PHERAstar FSX microplate reader (BMG LABTECH) equipped with injector pumps using the following program: injection of 100 µl of Luciferase Assay Reagent, shaking of the plate for 3 seconds at 300 RPM and a delay of 2 seconds followed by a 10 second measurement read. Data was normalized to total protein concentration as determined by BCA protein assay (Pierce BCA Protein Assay Kit - Reducing Agent Compatible, Thermo Scientific), carried out following manufacturer's instructions. Significance of results was established relative to the vehicle control using one-way analysis of variance (ANOVA) followed by a Bonferroni correction for multiple comparisons.

7.2.4 Pharmacokinetic Studies

7.2.4.1 Microsomal Stability Assay

*Microsomal stability assays were carried out by **Cyprotex**.*

A-196 (3 µM) was incubated with microsomes at 0.5 mg/mL microsomal protein and 1mM NADPH at 37 °C. Aliquots were taken at 0, 5, 15, 30, and 45 minutes and quenched with methanol containing internal standard. Following centrifugation, the supernatant was analysed using LC-MS/MS. The peak area ratio (compound peak area:internal standard peak area) was plotted against time and the gradient of the line determined to give the elimination rate constant. Negative control incubations in microsomes without NADPH or compound were performed in parallel to eliminate peaks that are not compound related or non-metabolic. Positive control incubations were carried out with dextromethorphan and verapamil for human microsomes and diazepam and diphenhydramine for mouse microsomes.

7.2.4.2 Metabolite Identification

*Metabolite ID studies were carried out by **Sygnature Discovery**.*

A-196 (10 µM) was incubated with mouse liver microsomes at 0.5 mg/mL microsomal protein and 1mM NADPH in a total volume of 300 µL Dulbecco's phosphate buffered saline at 37°C for 60 minutes with shaking at 700 rpm. Aliquots were taken at 0, 10 and 60 minutes and quenched 1:1 (v/v) with ice cold acetonitrile. Negative control incubations in microsomes without NADPH or compound were performed in parallel to eliminate peaks that are not compound related or non-metabolic. Positive control incubations were carried out with verapamil, diphenhydramine and benzydamine to test the metabolic rate of the microsomes. These controls were run both under standard conditions (0.1% (v/v) DMSO) and the modified

conditions (0.5% (v/v) DMSO) and the results did not show a reduced turnover with the additional solvent.

Samples were analysed using a Thermo Q-Exactive Focus mass spectrometer with Thermo Vanquish UPLC system. Mass spectra were run in both positive and negative ion mode, and for each scan, both DDA to acquire MS/MS spectra on the most abundant ions, and AIF to generate non-targeted fragment spectra for all ions were acquired. UV data was recorded at 322nm and 262 nm. Chromatography was performed on an ACQUITY UPLC HSS C18 column (1.8 µm, 2.1 mm X 100 mm), with solvent flow rate of 0.45 mL/min and a column temperature of 40 °C. A water/acetonitrile gradient with 0.1 % (v/v) formic acid was used.

7.2.4.3 Hepatocyte Stability Assay

Hepatocyte stability assays were carried out by ***Sygnature Discovery.***

Compounds (1 µM) were incubated with hepatocytes in buffer and aliquots taken at six time points (0, 5, 10, 20, 40, and 60 minutes). Aliquots were analysed using LCMS and compound peak areas compared to an internal standard to calculate the elimination rate constant, from which CL_{int} and $t_{1/2}$ were calculated. Negative control incubations in hepatocytes without compound were performed in parallel to eliminate peaks that are not compound related or non-metabolic. Positive control incubations were carried out with verapamil and 7-hydroxycoumarin.

7.2.4.4 In Vivo PK Assessment

In vivo studies were carried out by ***Pharmidex Pharmaceutical Services Ltd.***

Male CD1 mice were housed in pre-assigned housing cages until sampling. Mice were dosed subcutaneously with compound **76** (1 mg/kg, solution in 10% DMSO, 90% HP-β-CD) and plasma samples taken at eight time points (0.25, 0.50, 1.0, 2.0, 4.0, 6.0, 8.0, 24 hours).

Samples were stored immediately at -20 °C. Those mice co-dosed orally with **ritonavir** (12.5 mg/kg, solution in 10% DMSO, 10% cremaphor, and 80% water) were treated with **ritonavir** 30 minutes prior to dosing with **76**.

Plasma samples were treated with acetonitrile to induce protein precipitation before being analysed by UHPLC (tandem mass spectrometry using electrospray ionisation). Compound plasma concentration was established in reference to an internal standard.

7.3 CHAPTER 3

7.3.1 Synthetic Peptides

Peptides **95**-**99** were purchased from **GL Biochem** (Shanghai) as *C*-terminal acids with *N*-terminal acetyl capping. Peptides **100**-**108** were purchased from GL Biochem (Shanghai) as *C*-terminal amides with *N*-terminal acetyl capping. Synthesis was performed using standard Fmoc-based solid phase peptide synthesis (SPPS). Purity (>90%) was confirmed by High Performance Liquid Chromatography (HPLC) and the mass verified by LCMS.

95: Ac-Lys-Cys-Ala-Arg-Lys-COOH: **LR-ESI-MS** $C_{26}H_{50}N_{10}O_7S$ $[M+H^+]$ *m/z* found 647.30; calc.: 646.36

96: Ac-Lys-Cys-Ser-Arg-Lys-COOH: **LR-ESI-MS** $C_{26}H_{50}N_{10}O_8S$ $[M+H^+]$ *m/z* found 663.30; calc.: 662.35

97: Ac-Lys-Cys-Phe-Arg-Lys-COOH: **LR-ESI-MS** $C_{32}H_{54}N_{10}O_7S$ $[M+H^+]$ *m/z* found: 723.30; calc.: 722.39

98: Ac-Arg-Lys-Cys-Ala-Arg-Lys-Thr-COOH: **LR-ESI-MS** $C_{36}H_{69}N_{15}O_{10}S$ $[M+H^+]$ *m/z* found 904.55; calc.: 903.51; $[M+2H^+]^{2+}$ *m/z* found: 452.90; calc.: 452.76,

99: Ac-Pro-Arg-Lys-Cys-Ala-Arg-Lys-Thr-COOH: **LR-ESI-MS** $C_{41}H_{76}N_{16}O_{11}S$ $[M+H^+]$ *m/z* found: 1001.90; calc.: 1000.56; $[M+2H^+]^{2+}$ *m/z* found: 501.35; calc.: 501.28

100: Ac-Pro-Arg-Lys-Cys-Ala-Arg-Lys-Thr-Arg-NH_2: **LR-ESI-MS** $C_{47}H_{89}N_{21}O_{11}S$ $[M+2H^+]^{2+}$ *m/z* found: 579.10; calc.: 578.34

101: Ac-Gly-Pro-Arg-Lys-Cys-Ala-Arg-Lys-Thr-NH_2: **LR-ESI-MS** $C_{43}H_{80}N_{18}O_{11}S$ $[M+2H^+]^{2+}$ *m/z* found: 529.50; calc.:529.30

102: Ac-Pro-Arg-Lys-Cys-Ala-Arg-Lys-Thr-Arg-His-NH_2: **LR-ESI-MS** $C_{53}H_{96}N_{24}O_{12}S$ $[M+2H^+]^{2+}$ *m/z* found: 647.50; calc.: 647.37; $[M+3H^+]^{3+}$ *m/z* found: 432.10; calc.: 431.91

103: Ac-Arg-Gly-Pro-Arg-Lys-Cys-Ala-Arg-Lys-Thr-NH_2: **LR-ESI-MS** $C_{49}H_{92}N_{22}O_{12}S$ $[M+2H^+]^{2+}$ *m/z* found: 607.60; calc.: 607.35; $[M+3H^+]^{3+}$ *m/z* found: 405.50; calc.: 405.23

104: Ac-Pro-Arg-Gly-Pro-Arg-Lys-Cys-Ala-Arg-Lys-Thr-NH_2: **LR-ESI-MS** $C_{54}H_{99}N_{23}O_{13}S$ $[M+2H^+]^{2+}$ *m/z* found: 656.10; calc.: 655.88; $[M+3H^+]^{3+}$ *m/z* found: 437.90; calc.:437.58

105: Ac-Pro-Arg-Gly-Pro-Arg-Lys-Cys-Ala-Arg-Lys-Thr-Arg-NH_2: **LR-ESI-MS** $C_{60}H_{111}N_{27}O_{14}S$ $[M+2H^+]^{2+}$ *m/z* found: 734.20; calc.: 733.93; $[M+3H^+]^{3+}$ *m/z* found: 489.80; calc.: 489.62

106: Ac-Arg-Gly-Pro-Arg-Lys-Cys-Ala-Arg-Lys-Thr-Arg-His-NH_2: **LR-ESI-MS** $C_{61}H_{111}N_{29}O_{14}S$ $[M+2H^+]^{2+}$ *m/z* found: 754.20, calc.: 753.93; $[M+3H^+]^{3+}$ *m/z* found: 503.30; calc.: 502.95

107: Ac-Pro-Arg-Gly-Pro-Arg-Lys-Cys-Ala-Arg-Lys-Thr-Arg-His-NH_2: **LR-ESI-MS** $C_{66}H_{118}N_{30}O_{15}S$ $[M+3H^+]^{3+}$ *m/z* found: 535.60; calc.: 535.30; $[M+4H^+]^{4+}$ *m/z* found: 402.00; calc.: 401.73

108: Ac-Ser-Gly-Pro-Arg-Gly-Pro-Arg-Lys-Cys-Ala-Arg-Lys-Thr-Arg-His-Ala-Glu-NH_2: **LR-ESI-MS** $C_{79}H_{138}N_{34}O_{22}S$ $[M+3H^+]^{3+}$ *m/z* found: 650.6; calc.: 650.01; $[M+4H^+]^{4+}$ *m/z* found: 488.10; calc.: 487.76

7.3.2 Biological Assays

7.3.2.1 Biolayer Interferometry

*BLI was carried out with the aid of **Dr James Bennett** and **Dr Franziska Guenther** at the Target Discovery Institute, University of Oxford.*

Full-length, recombinant human His6-USP7 was purchased from R&D Systems.

The direct interaction between peptides and USP7 was measured using a BLI Octet RED384 (FortéBio Inc., Menlo Park, CA). Anti-His (HIS2) biosensors (FortéBio Inc.) were coated in a solution containing 50 µg/mL of his-tagged protein for 5 min at 25 °C. Peptides were made up to 10 mM stock concentrations in DMSO and diluted to 1 and 10 µM in buffer. The peptides were dispensed into alternate wells of a compound plate. Assays were performed at 25°C in a volume of 60 µl in a buffer that was 25 mM HEPES pH 7.5, 150 mM NaCl and 1 mM TCEP. A duplicate set of sensors without protein was used as a background binding control. Association of samples (1 and 10 µM) to coated and uncoated reference sensors was measured over 120 seconds and dissociation over 240 seconds. Data analysis on the FortéBio Octet RED96 instrument was performed using a double reference subtraction (sample and sensor references) in the FortéBio data analysis software, which accounts for nonspecific binding, background, and signal drift and minimizes well-based and sensor variability.

7.4 REFERENCES

1. T. T. Wager, X. Hou, P. R. Verhoest and A. Villalobos, *ACS Chem. Neurosci.,* **2016**, *7*, 767-775.